UNIVERSITY OF BERGEN

GEOPHYSICAL INSTITUTE

Master Thesis in Energy
Electric Power Engineering

Grounding Performance under Lightning Surges in High Voltage Substations

By: Vegard Steinsland

May 2018

Abstract

To achieve electromagnetic compatibility (EMC) and sufficient protection against lighting transients in the power transmission system, understanding of the grounding system transient behavior becomes crucial when deviating from international design standards and recommendations. To consider design deviations the present work is focused towards developing a method of integrating simplified grounding system models in transmission systems and perform lightning transient analysis on both parts to evaluate a particular design case.

Firstly, the grounding system models for substation grounding grids, with a variety of configurations and sizes, is implemented. The characteristic transient response of the grounding system is visualized through simulations to study the sensitivity of configurations and modified soil parameters during current injections. The method of implementation allows for a detailed view and pre-processing of large data-sets from simulations. The advantages of this method is used to extract overall measured values to create a tool for EMC analysis and in addition processing different parameters and functions of the grounding system.
Secondly, the grounding system model is integrated into transmission systems using a newly released interfacing application. The application allows for co-simulation between the development software of the grounding system and a specialized tool for the transmission system. The innovation of this modeling approach is given as a contribution to an international conference by submitting a paper.

Finally, the integrated grounding models and transmission system are studied with two substation design cases; a short and long cable between surge arrester and transformer. The short cable case follows well-known design standards where the long cable case is a design deviation which is common in larger domestic hydropower plants. Even though the long cable case is deviating from design recommendations, the results show a less negative impact on the grounding system compared to the short cable case.

Acknowledgment

On occasion finishing my M.Sc. study, it gives me pleasure to express gratitude to the people which has contributed to my work and for the support along the way.

First, I will thank my supervisor, Assistant Professor Lasse Hugo Sivertsen at the Department of Electrical Engineering, Western Norway University of Applied Sciences (HVL). His skillful guidance and full support have been of great importance for the innovation and outcome of the thesis. Alongside Lasse, I thank Assoc. Prof. Shujun Zhang and Assoc. Prof. Emil Cimpan for academic support and technical guidance, giving me the experience of contributing to international research by together submitting my first conference paper. This process has been a source of great inspiration and given the motivation to consider prolonging my academic career in the field of electrical engineering.

The cooperation with Bergenshalvøens Kommunale Kraftselskap (BKK) has added value in practical considerations and led to the thesis main objective, with appreciation I thank Magne Harkestad and Helge Hekland.
I will also take the opportunity to thank Ann Kristin Hale and Kristian August Mowinckel at HVL IT-department in making a new software application a success factor in this thesis, despite a struggling purchase and installation process. Lastly, I thank Jérôme Cornau and his team at Powersys Solutions for our close cooperation, technical support and rapid implementation of suggestions for improvements in the new software application.

Bergen, 2018

Vegard Steinsland

Table of Contents

List of Figures

List of Tables

List of Equations

List of Symbols

Symbol	Unit	Description	Page(s)
a	m	Grounding conductor radius	22, 23, 26, 40, 44, 84–86
a_e	m	Grounding conductor ionization zone equivalent radius	27
α	$-$	Decay constant of double exponential source	11, 35, 44, 84, 85
β	$-$	Crest constant of double exponential source	11, 35, 44, 84, 85
C	F	General term describing capacitance	12, 13, 23–25, 31
d	m	Grounding conductor burial depth	19, 23, 24, 40, 44, 84, 85
E_c	V/m	Critical electric field for soil ionization	25–27, 68, 86
E_i	V/m	Electric field of the outer ionization zone	27
E_{soil}	V/m	Electric field strenght exerted on the soil	26, 68, 86
G	S	General term describing conductance	12, 13, 23–25, 31
σ_{soil}	S	Conductivity of soil	20
γ	$-$	Propagation constant for the transmission line model	12, 13, 31, 42

Symbol	Unit	Description	Page(s)
I	A	General term describing current	11, 17–20, 27
i_i	A	Current Incident surge wave	14
i_r	A	Current reflected surge wave	14
I_{soil}	A	Current leaked from the ground per-unit lenght conductor to the soil	26, 86
$\hat{I}$	A	Current magnitude of double exponential source	11, 35, 37, 44, 84, 85
J_{soil}	A/m^2	Current density leaked to the soil	26
L	H	General term describing inductance	12, 13, 23–25, 31
l	m	General term describing length	12, 19, 22–27, 35–37, 40, 44, 54, 57, 61, 77, 84
A_0	Ω	MOA Nonlinear element of V–I characteristics	16
A_1	Ω	MOA Nonlinear element of V–I characteristics	16
α_{arr}	$-$	MOA Exponential factor to form the V-I characteristic	15, 36
C_{arr}	F	MOA Capacitive stray effect	15, 16
h_{arr}	m	MOA Height	16
I_{arr}	A	MOA Current during suppression of voltage to form the V-I characteristics	15
k_{seg}	$-$	MOA Voltage segment factor to form the V-I characteristic	15, 36
L_0	H	MOA Magnetic field in immediate vicinity	15, 16
L_1	H	MOA Low-pass filter inductance	15, 16
R_0	Ω	MOA Damp numerical oscillation of model factor	15, 16
R_1	Ω	MOA Low-pass filter resistance	15, 16
U_{arr}	V	MOA Reference voltage for operation	15, 36

Symbol	Unit	Description	Page(s)
μ_0	H/m	Permeability of vacuum: $4\pi \times 10^{-7}$	23, 24
εr_{soil}	$-$	Relative permittivity of the soil	20, 21, 23, 24, 45–53, 58–60, 62–68, 70–72, 75, 76, 78–80, 84–86, 88
ε_0	F/m	Permittivity of vacuum: $\approx 8.8542 \times 10^{-12}$	20, 23, 24
R	Ω	General term describing resitance	17, 19
r	Ω	Resistance of conductor	12, 13, 22, 25
ρ_{cond}	Ωm	Resistivity of conductor	22
ρ_{soil}	Ωm	Resistivity of soil	17, 19, 20, 23, 24, 26, 27, 41–43, 45–53, 58–60, 62–68, 70, 71, 73, 75, 76, 78–80, 84–86, 89
s	m	Grounding conductor spacing	19
t_{half}	s	Half decay time for lightning surge source	11, 37, 103

Symbol	Unit	Description	Page(s)
t_{rise}	s	Rise time for lightning surge source	11, 37, 75, 103
U	V	General term describing voltage	17–20
u_i	V	Voltage incident surge wave	13, 14
u_r	V	Voltage reflected surge wave	13, 14
v_s	m/s	Speed of surge wave	14, 75
Y	S	General term describing admittance	12, 13, 40, 41
Z	Ω	General term describing impedance	12, 13, 24, 41, 42
Z_c	$-$	Characteristic impedance for the transmission line model	12, 13, 31, 36, 43, 57, 61

Abbreviations

Abbreviation	Definition	Page(s)
AWG	American Wire Gauge	85
CIGRE	Conseil International des Grands Réseaux Électriques	4, 6, 10, 11, 26, 35, 37, 57, 61, 74
DC	Direct Current	18
EMC	ElectroMagnetic Compatibility	6, 82, 90
EMF	ElectroMagnetic Field	5, 6, 83, 85, 88
EMI	ElectroMagnetic interference	34, 69, 78, 82
FDTD	Finite Difference Time Domain	88
FEM	Finit Element Method	5, 6
FMI	Functional Mock-up Interface	29, 30, 37, 39, 73, 75
FMU	Functional Mock-up Unit	37
GPR	Ground Potential Rise	6, 16, 17, 34, 79, 82, 89
HVL	Western Norway University of Applied Sciences	73
ICHVE	International Conference on High Voltage Engineering and Application	7, 83
IEC	International Electrotechnical Commission	4, 10

Abbreviation	Definition	Page(s)
IEEE	Institute of Electrical and Electronics Engineers	3, 4, 6, 7, 10, 15, 26, 74, 76–79, 83
KCL	Kirchoff‘s Currrent Law	13
KVL	Kirchoff‘s Voltage Law	13
MOA	Metal-Oxide Arrester	14–16, 74
MTL	Multi-conductor Transmission Line	83, 84
ODE	Ordinary Differential Equation	28, 34, 69
PDE	Partial Differential Equation	28
SI	Système International d’unités	9
TSO	Transmission System Operator	4, 17, 18, 79
V-I	Voltage–Current	14–16, 30, 36, 74
ZnO	Zinc-Oxide	15, 36, 74

1 Introduction

1.1 Background

From early days to the development of modern power transmission system, lightning surges have been a source for troublesome operation of the grid. Faults, which affects the normal sinusoidal power system phases under operation and moreover faults that do permanent damage to equipment and facilities. With short duration, a flash as shown in fig. 1.1, suddenly facilities are experiencing outages, with a varying consequence of a simple restart to days or even months of repairs. Even considering today's understanding and protective measures in design, lightning still represents a source of damage and outages in the power transmission system.

Figure 1.1: Lightning stroke of transmission line, adapted from [1]

More sensitive microprocessor-based equipment has been integrated into the power transmission system, requiring even more protective measures to ensure safe operation. On measure are to provide a proper design of grounding system to discharge an lightning surge efficiently. The grounding system is to be designed such that voltage potential is kept within tolerances, even when high energy and transient faults occur. To secure no damage to facilities and living against the effects of lightning transients, knowledge of its behavior is essential in addition to understand the corresponding grounding system discharges mechanisms. The grounding systems are of fundamental importance in any electrical system. With a wide area of application, the grounding system is designed and optimized for the primary purpose and evaluation of severity.

When considering the high-voltage power transmission grid, a conventional method of power transfer consists of interconnected air insulated transmission lines, which often is terminated to a substation outdoor switchyard in both ends. As function the substation may act as a hub, being the connection points for several transmission lines in a distribution center for factories and cities or serving a power plant as an infeed. Being a central point in the power transmission and distribution chain involves handling high energy and strong electric fields. The main purpose of outdoor switchyard grounding system is to provide a low resistance path, at any point, to discharge high energy fault current at power frequency. The low resistance path ensures the protection of facility and life by

rapidly declare a fault situation and to avoid exceeding limits of voltage potential rise, in the grounding conductor itself and on the ground surface.
This is achieved by a buried grounding grid of copper conductors which covers the switchyard area. Also, the grounding grid is interconnected with the outside grounding system, lowering the total grounding resistance. With a buried grounding grid, the electrical discharge performance is dependent on soil parameters at the location in addition to grid configuration. Chemical compound and type of soil will change slowly and anticipated to be a nearly fixed parameter, while the water content and temperature could change rapidly, affecting the grounding performance. To secure a level of stable and reliable soil resistivity for a switchyard, the construction method includes soil with high drainage factor, as an example consisting of a mix of rocks, clay and moraine gravel. Figure 1.2 shows a 420 kV outdoor switchyard for a hydropower plant under construction which will use soil of this type. This gives high resistivity soil for the local region while securing the safety factors of the overall switchyard area.

Figure 1.2: 300/420 kV outdoor switchyard under construction. Shows a facility of 3200 m^2 with concrete pillars of approx 2-2.5 m heights for equipment. Grounding grid to be buried in soil at 0.6 m depth from top of the pillars to give equipment grounding connection

A second important task for the grounding system is to discharge fast transients overvoltages, originating mainly from an external source of lightning strokes and internal as switching operations. Under fast transients current injections as lightning, the grounding system performs with a significantly different behavior than for current injections at power frequency. While a power frequency current injection will utilize the entire grounding system, the steep front lightning transient will activate inductive effects which will limit the effective area of the grounding system during the steep rise time of the strike. The lightning surge, with fast rise time, will propagate out in the ground grid; which will act as an antenna, inducing a large transient potential in the system. This short-term potential rise could lead to lower performance of protective equipment, and

even malfunction or damage sensitive equipment. For this reason, the term grounding resistance is changed to impedance when describing the grounding system properties under transient conditions.

The ground resistance could be measured accurately by traditional methods to study power frequency performance; which is not the case under transient conditions. Therefore, a study of the grounding system is vital to understand the behavior during lightning current injections. This understanding is especially important when selecting a design which deviates from established standards and recommended construction methods, as unknown negative consequences may not be considered in the design.

A facility case which deviates from design standards is typically found in larger domestic hydropower plants. A typical arrangement composes of one or more generators and transformers located in a rock cavity inside a valley mountain and connected to an outdoor switchyard. The main transformers are connected to a switchyard trough relatively long cables, typically several hundred meters long. A typical infeed for a hydropower generator to an outdoor switchyard is shown in fig. 1.3.

The outdoor switchyard for hydropower facilities is most commonly also located in deep valleys which gives shielding for direct lightning strikes. However, located in remote locations the use of long overhead transmission lines is needed which makes the facility exposed to lightning surge entering from indirect strokes following the line. Protective means for power transmission lines are a shielding design for direct lightning strikes. This is typically performed by having ground wires above the phases in the transmission line towers, to guide a direct strike to ground directly. Also, installation of surge arrester is an effective method to discharge lighting transient to the grounding system. Even with the described protective means, a lighting surge with sufficient low magnitude may follow the transmission line and penetrate deep into a substation facility. And when entering a substation transformer, the magnitude may approximately double due to reflections. Due to space restrictions and fire hazard, surge arresters have traditionally been installed only in the switchyard and not close to the transformer for lager hydropower stations. This is a design deviation where recommendation in standards is a placement of the surge arrester close to the transformer to avoid high voltage build-up caused by indirect lightning transient surge waves reflections. The recommendation is described both in international standards as Institute of

Figure 1.3: Typical infeed arrangement in a outdoor switchyard for a domestic hydropower station

Electrical and Electronics Engineers (IEEE) *"Application Guide for Surge Protection of Electric Generating Plants"* [2] and for domestic installation guidelines described by the Transmission System Operator (TSO) in *"Statnett Earthing Guidelines"* [3]. The voltage build-up when selecting this design is well known and are considered in insulation coordination studies, where the overvoltages withstand level is determined. Moreover, the grounding system will suffer a pulsating current injection from the surge arrester when selecting this design, mainly time-determined by the cable length. The situation of repetitive surge injections, with the fast front exciting the grounding system is not found documented. If the present design is giving an additional factor, which may impact negatively on the switchyard equipment, is left to be discovered in this thesis.

1.2 Literature Review

Lightning has attracted interest by various of groups and research environments for centuries. Evaluated relevant for the power transmission system, Berger and co-workers performed lightning discharge measurements from an observatory on Mount San Salvatore in the Alps, on the borderline between Switzerland and Italy [4]. In the period from the year 1943 to 1963, Berger and his team performed lightning observations were measured and analyzed to increase the understanding of lightning discharge mechanisms. The work performed was later evaluated by the interest organization Conseil International des Grands Réseaux Électriques (CIGRE) for application purpose in electrical installations. In electrical systems, the outer operation boundaries and expected faults stresses, weighted against severity and probability of failure, is one driver in product development, manufacturing, and complete system design. From the analysis of lightning observation, CIGRE defined a standard lightning stroke with properties that stresses the electrical system insulation and discharge abilities. The standard lightning surge waveform characteristics are adopted, with modifications, by the international organization as International Electrotechnical Commission (IEC) and IEEE, making the stroke a factor which is considered in the design of electrical systems and equipment.
By gathering knowledge of lightning characteristics, protective measures could be established. An effective measure is to discharge a lightning current into the soil directly or adapt weaknesses in the transmission system, where a selection of breakdown level can be controlled to wished areas. Even though a lightning surge is following the transmission system or is directly discharged, the main path of discharge is through a grounding system. In understanding the grounding system response during a fast front lightning transient Bewley and co-workers started in 1934 extensive experimental and theoretical work [5]. The primary driver in the assignment was protection against light-

Model concept	Mathematical expression	Visualization	Solution procedure	Computer power needs	Accuracy
Electromagnetic field approach	Complicated	Difficult to understand	Complicated, difficult to include soil ionization, wave propagation delay	Very powerful computer needs, large computing time	Believed to be most accurate
Circuit approach	Simple	Easy to understand	Simple, easy to include soil ionization, can not predict wave propagation delay	Normal PC needs, low computing time	Reasonably accurate
Transmission line approach	The simplest	Very easy to understand	Very simple, can predict wave propagation delay, easy to include soil ionization	Normal PC needs, low computation time	Reasonably accurate
Hybrid approach	Complicated	Not very easy to understand	Slightly complex, can include soil ionization, capability to predict wave propagation delay is not clear	Normal PC needs, low computation time	Reasonably accurate

Table 1.1: Overview of grounding grid modeling approaches [9, p. 33].

ning surges in power transmission system. Form his research he derived the impedance of a counterpoise wire at the injection point when applied to a unit step current. The behavior was clearly deviating from a power frequency injection, where the impedance magnitude during the steep front is considerably larger than when the transient period ended.

In 1941, Bellaschi and co-workers were testing grounding rods during different current injections waveforms and computed the voltage response [6]. From their research, development of the first analytical formula of the voltage response was expressed to describe the transient event. Later in 1949, Sunde presented his work based on the ElectroMagnetic Field (EMF) theory which is considered the most important and classical textbooks covering the grounding systems [7]. His work is still recognized as a foundation for understanding the transient event in the grounding system. With the ground-breaking discovery, he introduces the use of telegraphers equation to connect the soil parameters to the per-unit length grounding wire as a lossy transmission line. In the absence of computers, Gupta attempted to further extend the research of Sunde by expressing the response of complex grounding grids empirically [8]. This was a valid attempt while proven later to give severe inaccuracies for larger grounding grids. Later in the 1980‘s, entering of computers and development of numerical solver methods started which was a breakthrough in the modeling of complex systems. Presently known methods of grounding system models strong suits and limitations are summarized in table 1.1. The modeling method described, which are evaluated of most importance is the EMF and the transmission line approach.

EMF being the most complex modeling method is also believed to be the most accurate. In 1990, Gcrev was the first to implement a full description of the grounding system model based on the EMF and Finit Element Method (FEM) [10]. Since the EMF and

FEM solves the full Maxwell‘s equations in the frequency domain, it has minimum assumptions. However, this modeling approach is complicated and difficult to interface for the use in other systems than performing isolated simulations.
A more applicable modeling method is the transmission line approach. From the first development by Sunde in 1949, Verma and Mukhedkar made a computer model of grounding system using the lossy transmission line approach in 1984 [11]. Later in 2004, Liu further developed this modeling concept to include non-uniform per-unit length parameters to improve the modeling accuracy compared to the results from EMF theory by Gcrev [9]. By this method, the mutual coupling between the grounding grid elements could be more accurately considered and still keep the computer resource needs at an acceptable level for the regular users. Also, the transmission line approach can incorporate the soil ionization phenomenon when performing numerical time-domain simulations. When a high current is conducted through the grounding wire, a strong electric field will arise towards the soil. If the electric field is strong enough, punctuation and arching may occur close to the wire, and the apparent resistivity will be lowered. In reviewed literature and standards, an ionization activity in the soil is evidently present when considering lightning current injection. The critical level of the electric field, to initiate soil ionization, is still a topic of research by IEEE and CIGRE. Another advantage of the transmission line approach, in time-domain simulation, is the ability to predict the surge wave propagation in the grounding system. The voltage distribution, function of time and space, are of great importance when considering ElectroMagnetic Compatibility (EMC) in a switchyard area.
Recent development in the field has been an attempt to determine the soil frequency dependency, which has attracted interests by several researchers in the past. IEEE Senior Member Visacro and co-workers have from 2014 until present developed soil modeling techniques based on own and previous research. With comprehensive analysis, a method to estimate soil characteristics from simple empirical expressions are made available. The developed empirical formulas were first presented in [12] and further applied by the transmission line approach later in [13].

Most of the literature found is treating higher currents, originating from direct lightning strikes and focusing Ground Potential Rise (GPR) in the switchyard area. Therefore more knowledge of the grounding system response when integrated into a transmission system, and injection point through a surge arrester, is needed. This to ensure stable operation and limit the consequences of damage.

1.3 Objective

The objective of this thesis is to verify if the design deviation, with a relatively long cable between the surge arrester and transformer, is presenting additional negative factors when the grounding system is included in lighting transient studies.

- Implement simplified grounding system models for substation grounding grids, with a variety of commonly used configurations and sizes
- Study the characteristic lightning transient response of the grounding system models through simulations with the sensitivity of soil parameters
- Integrate the grounding system models in a simplified transmission system. Perform lightning transient simulation when the grounding system is added as the surge arrester injection point for a:
  - typical transformer infeed, which follows design standards with a relatively short cable between surge arrester and transformer.
  - transformer infeed, where a relatively long cable between surge arrester and transformer exists which deviates from design standards.

  And compare the simulation results to evaluate impacts of the design deviation.

1.4 Limitations/Confidentiality

The targeted reader is holding an M.Sc. degree in electric power engineering or equivalent. Alternatively, have a particular interest in lighting transients in the high voltage grid and grounding systems. Moreover, all interested readers will be given a sense of the lightning transient behavior in the grounding system by reviewing the time-domain simulation in the results chapter.

Due to limitation is given by the local authorities in Norway trough "Forskrift om forebyggende sikkerhet og beredskap i energiforsyningen (beredskapsforskriften)", practical outlines to specific facilities is not included. The original project description, found in Appendix A, are for this reason not fully answered.

The thesis should be treated as confidential until conference paper found in Appendix B is made available on IEEE Xplore trough the persistent link `https://ieeexplore.ieee.org/servlet/opac?punumber=1002613`. The conference, International Conference on High Voltage Engineering and Application (ICHVE) 2018, is planned for September 10-13, 2018.

1.5 Outline of Thesis and Structure

2. **Theory:** The theory chapter aims to build knowledge to implement a simplified grounding system model, which are interconnected in lightning transient study.
   First, a brief introduction of the standardized lightning strike is given and the considered critical properties for the electrical system is weighted. Also, a current source which is commonly used in research, simulating lightning stroke, is presented.
   Following, a description of the fundamental transmission line model is included. This to understand both the surge wave propagation in the transmission system and the behavior of a grounding wire modeled as a lossy transmission line.
   As the surge arrester is a central part of the discharge mechanism between the transmission and grounding system, a full modeling description is presented.
   For the grounding system, the power frequency properties are first described, as a bridge to determine parameters needed in the transient study.
   Secondly, the grounding system is treated with a description of the soil properties, equivalent circuit, parameter determination and significant factors which act on the model accuracy and validity.
   Lastly, the software tools used in the thesis is briefly introduced with key features relevant to the implementation.

3. **Metode:** The method chapter describes the full software implementation of the grounding and transmission system models, separately. Lastly, the custom interface defined between the development software of the grounding system and the specialized tool for the transmission system is described.

   The method chapter is supported by source code, developed models and block descriptions found with specific references to Appendix D to E. For this reason, the description in the method chapter is limited to give a fundamental understanding of the implementation which connects relevant theory, strategies and principles.

4. **Results:** This chapter presents results retrieved from simulations of the implemented models.
   Firstly, the per-unit length grounding wire properties are extracted in the frequency domain to review the characteristic with the sensitivity of soil resistivity.
   Secondly, the grounding system is simulated in time-domain in isolated mode. These simulations were carried out to show the characteristics of the total grounding system under controlled and know conditions of the current injection source.
   Further, results of the per-unit length grounding wire is shown in time-domain to

review the characteristic properties from simulations.
Lastly, the grounding system is integrated into the transmission system. First, the short cable case is simulated. Followed by the design deviation with the long cable case. Also, the electric field distribution exerted on the soil is given for selected simulations.

5. **Discussion:** First, the results from the grounding system in isolated mode is treated to evaluate characteristics.
Secondly, the results from integrated models, grounding and transmission system, are discussed. The main objective of the thesis is concluded, comparing the short cable case with the design deviation of long cable between surge arrester and transformer.
Thirdly, common characteristics are discussed for both the isolated and integrated model.
Finally, model validation against previous work is presented in addition to a discussion of present uncertainties and model limitations.

6. **Conclusion:** Contains the main developments and conclusion of the present work. In addition follows suggestions to improve the accuracy of the grounding system models. Also, the observation which has shown to raise further interesting questions is mentioned.

- **References:** Includes the bibliography that uses IEEE citation style.

- **Appendices:** The appendix chapter consists of supporting documentation of work relevant to the thesis.
First the initial project description is attached (Appendix A).
Secondly, follows a conference paper submitted to IEEE ICHVE 2018 based on the method developed in this thesis (Appendix B).
Thirdly, implementation to illustrate the CIGRE 1.2/50 μs stroke (Appendix C).
Lastly, follows the full implementation of both grounding and transmission systems. Also, a short description of used computer hardware and a detailed list operating system and software packages used is found in (Appendix D to G).
In addition, layout for the refereed switchyard is included (Appendix H)

To support the thesis main content, overviews are generated in an attempt to improve readability. For used symbols and notations there are made a separate overview with a description, corresponding units, and page reference. All units are derived according to Système International d'unités (SI). With the selected approach, the used symbols are only further described in the thesis by the context of an application. For the on-screen reader convenience, symbols are linked to the List of Symbols

2 Theory

First, a brief introduction of the standardized lightning strike is given, and the considered critical properties for the electrical system is weighted. By presenting the lightning strike as a current source with a determined waveform, an unpredictable phenomenon of nature could be integrated as test criteria in electrical systems. Next, a description of the fundamental transmission line model follows. This to understand both the surge wave propagation in the transmission system and the behavior of a grounding wire modeled as a lossy transmission line. As the surge arrester is a central part of the discharge mechanism between the transmission and grounding system, a full modeling description is presented. For the grounding system, the power frequency properties are first described, as a bridge to determine parameters needed in the transient study. Secondly, the grounding system is treated with a description of the soil properties, equivalent circuit, and parameter determination. Also, theory to describe factors which act severely on the model accuracy and validity is included. Lastly, the software tools used in the thesis is briefly introduced with key features relevant to the implementation.

2.1 Characteristic of Lightning Surge

As described in the literature review section 1.2 the lightning phenomenon is formed by nature and is difficult to predict. Based on the measurements by Berger [4] the international, non-profit organization, CIGRE has performed application analysis to collaborate knowledge for their members to advance in the field of lightning studies. From this work an standardized lightning surge waveform was defined; the 1.2/50 μs stroke [14]. The international standards organization, IEC and IEEE, which has an extensive collection standard, covering several areas of engineering interest are unified with the standardized 1.2/50 μs stroke waveform. With the international acceptance (from IEC), the manufacturer of electrical high voltage equipment and systems are considering this as a standardized lightning surge waveform in design [15, p. 54].

By considering a steep front surge in design, the equipment insulation and protective systems (as grounding system) are stressed upon a strict requirement.
From fig. 2.1 the standardized 1.2/50 μs stroke are formed based on CIGRE definitions [16, pp. 67-70]. Characteristics of the 1.2/50 surge wave are a steep front and relatively slow decay of the tail is described by fig. 2.1:

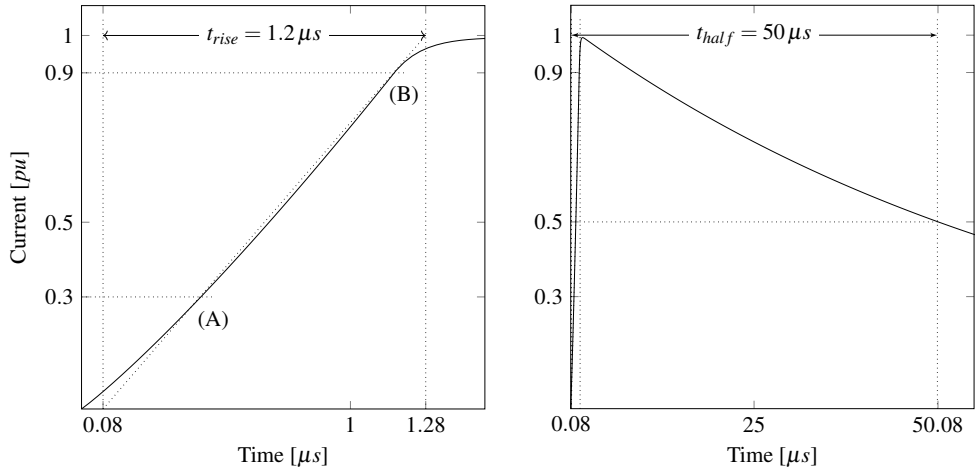

(a) Definition of rise time, t_{rise}.

(b) Definition of half time, t_{half}.

Figure 2.1: Standard lightning impulse, 1.2/50 μs stroke, with definitions of rise (t_{rise}) and half time (t_{half}). Implementation are found in appendix C [16, pp. 67-70]

.

- **fig. 2.1a** are highlighting the surge wave initial crest face.

  From the surge wave, an tangential line from 0 to 1 *pu* are drawn from intersection points "A" at 0.3 and "B" at 0.9 *pu*, resulting Δt defines t_{rise}. In this case t_{rise}=1.28-0.08=1.2 μs

- **fig. 2.1b** are highlighting the surge wave decay.

  From the initial time steep at the surge wave rise until 0.5 *pu* decay gives resulting Δt defines t_{half}. In this case: t_{half}=50.08-0.08= 50 μs.

The waveform of the 1.2/50 μs stroke by CIGRE is complex to implement, both in practical applications and in computer simulations. A common method used in reviewed work is to implement a simplified stroke by a current source which is parameterized by a double exponential function as in eq. (2.1). The stroke magnitude is fitted by parameter $\hat{I}$. The surge waveform is adjusted to fit the desired surge trough α and β. Equation (2.1a) express these parameters as an initial adjustment in relation to t_{half} and t_{rise} [17].

$$\alpha = \frac{0.396}{t_{half}} \qquad \beta = \frac{2.746}{t_{rise}} \tag{2.1a}$$

$$I(t) = \hat{I}(e^{-\alpha t} - e^{-\beta t}) \tag{2.1b}$$

2.2 Fundamental Transmission Line Model

When an impulse is applied, like a lightning stroke, in an electric transmission system far end there will be a time delay and distortion of this impulse before reaching the receiver. The time delay and distortion will be dependent on the transmission system properties like length, insulation material, conductor, and configurations. The lightning impulse is propagating like a high-velocity wave through the transmission system. To evaluate traveling wave characteristics, the fundamental transmission line model is selected to give a presentation with basic electric circuit elements and are shown in fig. 2.2 From the fundamental transmission line, the voltage and current as function of length, l, and time, t, is expressed in eq. (2.2) [18, pp. 8-18].

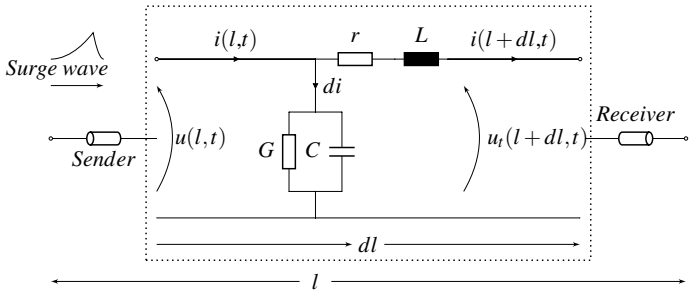

Figure 2.2: Fundamental traveling wave model with distributed circuit equivalent parameters

$$-\frac{\partial u(l,t)}{\partial l} = ri(l,t) + L\frac{\partial i(l,t)}{\partial t} \tag{2.2a}$$

$$-\frac{\partial i(l,t)}{\partial l} = Gu(l,t) + C\frac{\partial u(l,t)}{\partial t} \tag{2.2b}$$

From the per-unit differential length section, dl, the primary properties of the transmission system is given in the form of per-unit series impedance, Z, and shunt admittance, Y.

$$Z = r + j\omega L \qquad\qquad Y = G + j\omega C \tag{2.3}$$

These primary properties gives relations to derive two important characteristics in describing traveling waves, the propagation constant, γ, and surge impedance, Z_c, and follows in eq. (2.4) [19, p. 91]:

- γ: When considering the propagation constant, eq. (2.4a), in complex terms($\gamma = \alpha + j\beta$) the real part are describing the attenuation constant and the imaginary part are giving the phase constant.

- Z_c: The surge impedance is giving a relation between the injected lightning impulse current and the surge wave formation. Also, Z_c describes the relation of the surge wave behavior in boundaries between transmission lines of different surge impedance.

$$\gamma = \sqrt{ZY} = \sqrt{(r + j\omega L)(G + j\omega C)} \tag{2.4a}$$

$$Z_c = \sqrt{\frac{Z}{Y}} = \sqrt{\frac{r + j\omega L}{G + j\omega C}} \tag{2.4b}$$

To evaluate current and voltage as time and place dependent traveling wave on the transmission system further analysis is required. Going back to fig. 2.2 the voltage and current over the per-unit element, $l + dl$, are found by applying Kirchoff's Currrent Law (KCL) and Kirchoff's Voltage Law (KVL) to the circuit. From these terms, the current and voltage are expressed as differential equations with the propagation constant as the main parameter in the frequency domain(s) in eqs. (2.5a) and (2.5b) [20, p. 60].

$$\frac{d^2u(l,s)}{dl^2} = YZu(l,s) = \gamma^2 u(l,s) \tag{2.5a}$$

$$\frac{d^2i(l,s)}{dl^2} = YZi(l,s) = \gamma^2 i(l,s) \tag{2.5b}$$

The general solution by solving the ordinary differential equation for voltage and current, with characteristic roots $\pm\gamma$, are given in eqs. (2.5c) and (2.5d) [19, p. 92]. Interpretation of the two voltage components describes an incident, u_i, and reflected, u_r wave for the general solutions constants c_1 and c_2, respectively.

$$u(l,s) = u_i e^{\gamma l} + u_r e^{-\gamma l} \tag{2.5c}$$

$$i(l,s) = \frac{1}{Z_c}\left(u_i e^{\gamma l} - u_r e^{-\gamma l}\right) \tag{2.5d}$$

When assuming that u_i and u_r is phasors the full expression for the voltage in the frequency domain is given in eq. (2.5e). The time-domain steady-state expression of this equation is defined by eq. (2.5f) [18, pp. 8-18].

$$u(l,s) = u_i e^{j\theta} e^{-\alpha l} e^{-j\beta l} + u_r e^{j\theta} e^{\alpha l} e^{j\beta l} \tag{2.5e}$$

$$u(l,t) = u_i e^{-\alpha l}\cos(\omega t - \beta l + \theta) + u_r e^{\alpha l}\cos(\omega t + \beta l + \theta) \tag{2.5f}$$

The term $e^{\pm\alpha l}$ is the attenuation of amplitudes of the waves. These expressions are the sums of forward (u_i) and backward traveling waves (u_r). A generic time-domain representation is written as eqs. (2.5g) and (2.5h). Where the wave velocity is given by $v_s = \dfrac{\omega}{\beta}$.

$$u(l,t) = u_i(l - v_s t) + u_r(l + v_s t) \tag{2.5g}$$

$$i(l,t) = i_i(l - v_s t) + i_r(l + v_s t) \tag{2.5h}$$

The forward and backward traveling wave concept is interpreted using the illustration in fig. 2.3 for the waveform $u_i(l - v_s t)$. The traveling wave is first shown at $t = 0$ where at $l = a$ it has a value of $u_i(a)$. At any subsequent time, $t = t_l$, it has the same value at $l = a + v_s t_l$ (if considered distortion less) as it formerly had at $l = a$. It means that the voltage distribution has moved in the direction of positive l. A similar explanation is used for u_r(l+v_st) which is traveling in the negative l direction.

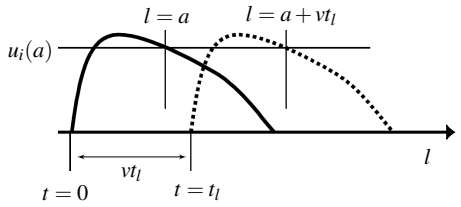

Figure 2.3: Illustration of the traveling wave concept for the transmission line model as function of distance and time (l,t). The wave initial state at $t = 0$ and movement at $t = t_l$

2.3 Lightning Surge in Transmission Systems

2.3.1 Surge Arrester

A surge arrester is connected to the protected equipment. It provides low impedance discharge path to ground if a transient voltage is entering the system that exceeds the threshold voltage, defined by the insulation level. The marked dominating arrester type in high voltage installations are the Metal-Oxide Arrester (MOA) [1], invented in the early 1960s. The operation function of MOA is characterized by highly nonlinear Voltage–Current (V-I) relation around the threshold voltages, described by eq. (2.6) and shown by fig. 2.4. The overvoltage protection region may further be divided into seg-

[1] Metal-Oxide arrester is occasionally named Zink-Oxide arrester due to material properties

ments to improve accuracy in representation, with each segment defining validity for its V-I function [20, p. 17].

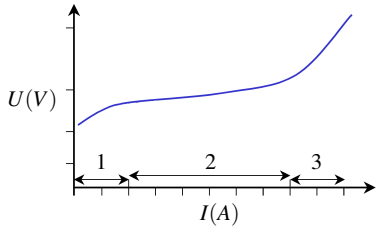

Figure 2.4: Illustration of typical V-I characteristics for a MOA, adopted from [20]. Divided in three regions, where region "1" indicates normal operation area and loss current. Region "2" indicates breakdown characteristic and "3" the full breakdown. The current axis, I, has logarithmic scale

For voltages substantially below U_{arr}, the current being extremely small, a linear representation of the V-I characteristics are used. The surge arrester is then under normal operating conditions and acts closely to an open circuit element: an ideal lossless device. MOA V-I characteristic is realized by design and material properties of varistor valve elements made up mainly of Zinc-Oxide (ZnO). The varistor element forms a disc, with a certain voltage withstands level, which is ceramic molded together in a stack that forms the surge arrester, MOA.

$$I_{arr} = \begin{cases} k_{seg} \dfrac{u}{U_{arr}}^{\alpha_{arr}} & if \quad a < u \leq b \\ \\ k_{seg} \dfrac{u}{U_{arr}}^{\alpha_{arr}} & if \quad b < u \leq c \quad \text{for each segment} \end{cases} \tag{2.6}$$

MOA provides protection against several overvoltages situations that may occur under operation. To describe the MOA electrical properties under lightning strokes, a fast front current surge, there was performed laboratory experiments by D.W Durbak. From this research, he developed a mathematical model that later was adopted as recommended by IEEE in lightning studies [21, p. 112]. The basic idea is to divide the single nonlinear arrester impedance into n parallel elements, which are separated by low pass filter. With two parallel number of n element it was proven sufficient accurate behavior under lightning current injection as illustrated in fig. 2.5. The R_1-L_1 circuit represent the low pass filter which separate the two nonlinear resistance defined by $A_0 = I_0(V_0)$ and $A_1 = I_1(V_1)$. The inductance L_0 represent the magnetic field in the immediate vicinity of the surge arrester, while R_0 purpose is too damp numerical oscillation. The element C_{arr} represents the stray capacitance over the surge arrester.
In determination of the model elements, fig. 2.5, under fast front surge research has ap-

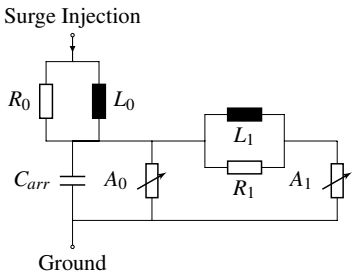

Figure 2.5: IEEE MOA equivalent arrester model for fast front lightning surges [21, p. 113]

proximated the physical arrester properties. From the arrester height, h_{arr}, and number of parallel columns, n, initial element values can be estimated from eq. (2.7). Further the nonlinear varistor elements, A_0 and A_1, are adjusted to correspond to the V-I characteristics under the specific lightning discharge surge [22, pp. 3-6].

$$L_0 = 0.2 \times 10^{-6} \frac{h_{arr}}{n} \qquad R_0 = 100 \frac{h_{arr}}{n} \tag{2.7a}$$

$$L_1 = 15 \times 10^{-6} \frac{h_{arr}}{n} \qquad R_1 = 65 \frac{h_{arr}}{n} \tag{2.7b}$$

$$C_{arr} = 100 \times 10^{-12} \frac{n}{h_{arr}} \tag{2.7c}$$

2.4 Switchyard Grounding System

To ensure the safety of living a stable operation, a sound grounding system is required for a switchyard. Non-live conductive parts and protective systems are interconnected through the switchyard grounding grid, providing an equivalent potential, referred to as true reference. A connection trough ground also applies to the power distribution system, having a neutral path through the grounding. Traditional power systems in normal operation conditions supply close to no current in the ground path. However, a fault situation at power frequency could inject substantial current in the ground return path. Also, surge arresters placed in the switchyard are interconnected through the same grounding grid. Providing a ground path to discharge overvoltages at power frequency in addition to transient originating from lightning or switching operation. Depending on soil properties and grounding structure design, an current injection will rise the local potential in the grounding structure and even at the ground surface, defined as GPR. Consequently, there is a risk of malfunction or also damaging sensitive equipment and/or electrocution

of personnel. To control the GPR, from a grounding design point of view, the terms step and touch voltages are introduced to evaluate safety requirements.
At power frequency, there is great awareness of performance and safety issues concerning the grounding system and well-defined requirements in standards to ensure proper design. From international guides as IEEE Std. 80 [23] and Std.81 [24], detailed recommendation are described. Also, the Norwegian TSO, Statnett, has developed local guidelines, Statnett Earthing Guidelines, Part I. Planning [25], to ensure the law defined safety level set by Norwegian authority for own installations [26]. From examine previous mention guides, there is limited descriptions and recommendations for grounding grid design under fast transient conditions. This impression tends to be a general observation in reviewed litterateur, and is outlined in [27, pp. 394-395]. The soil usually has a very complex composition, and a large number of variables influence its behavior during current injection. Variables such as type, moisture, salt content, size, shape, and arrangement of particles, and temperature, to name a few [28, p. 1163]. Thus, modeling the frequency dependence of soil consists of a significant scientific challenge. To build a bridge between defined standards the following sections will first evaluate soil and grounding system properties at power frequency. From this knowledge and measurement techniques, adaptable models are considered to describe the transient performance during lightning current injections, for switchyard grounding grid structures.

2.4.1 Soil Properties at Power Frequency Current Injection and Measurement

In considering the performance of grounding systems, the soil properties and grounding device design are primary factors. The grounding system resistance is a commonly used measure of performance at power frequency conditions. Grounding resistance is defined as the ratio between the potential rise of the grounding device and impressed current, eq. (2.8a). While the grounding structure is buried in soil, the soil electrical properties are interacting during a current injection by conducting and dispersion of the fault current. With a variety of expected ground fault, both in the magnitude of current and voltage, an approach to evaluate performance are given by the soil resistivity, ρ_{soil}, and a grounding device configuration factor, k, follows in eq. (2.8b) [29].

$$R = \frac{U}{I} \tag{2.8a}$$

$$R = k\rho_{soil} \tag{2.8b}$$

By the interpretation given in eq. (2.8b) the design of grounding device is fitted to the local soil condition, or measures are taken to modify the soil properties to for-fill wished performance. Main factors governing the electrical properties of the soil are the chemical compound, grain size and porosity in additional to variables as temperature and moisture. Known methods in the analysis of soil properties are laboratory sampling and electrical sounding techniques. Some advantage favoring the sampling method is the ability to analyze depth in soil layers, chemical compound and electrical characteristics for the specific sample. However, the cost of geological drilling is high, and ability to represent the entire switchyard area is difficult [30, pp. 31-36]. Also, the soil porosity and water content are challenging to simulate in laboratory analysis, from samples, to give a correct representation. To compensate for the disadvantages of the sampling method an additional analysis exist. By performing electric sounding at the location will provide an improved description of the overall switchyard soil resistivity [30, p. 98]. A commonly used sounding method is based on Wenner measurement principle, which also is recommended by Norwegian TSO (Statnett) through application in [31, p. 4]. The Wenner measurement method is illustrated in fig. 2.6, with four equally spaced measurement rods on a straight line, with an outer current loop and an inner voltage measurement circuit.

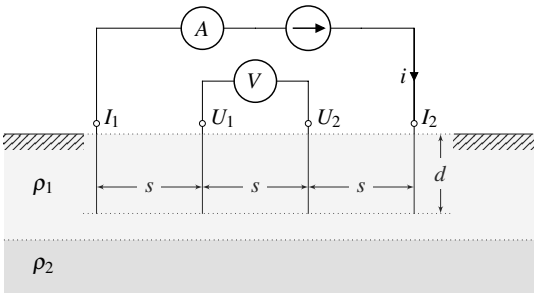

Figure 2.6: Wenner method for soil resistivity, ρ_{soil}, measurement. Illustrated with two-layer soil, ρ_1 and ρ_2 as upper and lower layer, respectively. Measurement rods are equally spaced, s, at depth, d.

The working principle are an calculation of apparent soil resistivity, ρ, from a voltage induction, in points U_1 and U_2 from a injected Direct Current (DC) in loop of point I_1 and I_2. The calculation of soil resistivity is expressed by eq. (2.9). If the burial depth of the four rods are less then 10 % of spacing distance the expression in eq. (2.9a) could be approximated with eq. (2.9b) [23, p. 57]

$$\rho_{soil} = \frac{4\pi s \frac{(U_1 - U_2)}{I}}{1 + \frac{2s}{\sqrt{s^2+4d^2}} \frac{s}{\sqrt{s^2+d^2}}} \tag{2.9a}$$

$$\rho_{soil} = 2\pi s \frac{(U_1 - U_2)}{I} \qquad \text{if} \quad d < 0.1s \tag{2.9b}$$

A single measurement gives the apparent resistivity on the measured horizontal line in the region of the measurement rods (fig. 2.6). The injected current path for small rod spacing tends to flow near the soil surface, whereas more of the current penetrates deeper soils for larger distance [23, p. 57]. The difference in horizontal soil layers is from this approximation possible to discover when performing several measurements with different rod spacing, s and depth, d. With a larger rod spacing, the induced voltage is decreasing and may be out of instrument measurement range in larger distance and high resistivity soils. This leads to a limitation in use of the Wenner method. An categorization of soil resistivity follows in table 2.1 [24, p. 11].

Classification	Range
Low	ρ_{soil}<100 Ωm
Medium	100≤ρ_{soil}<300 Ωm
High	300≤ρ_{soil}<3000 Ωm
Very High	ρ_{soil}≥3000 Ωm

Table 2.1: Categorization of soil resistivity

From the measurements and determination of soil resistivity the grounding system resistance could be estimated, based on the grounding device configuration. The expression is representing the grounding device geometrical factor, k, are expanded from eq. (2.8b). Dwight investigated ground buried structures and resistance based on selected configuration and soil parameters [32]. Later Sunde developed this method as applicable for horizontal buried grounding grid, eq. (2.10), and vertical rod configuration, eq. (2.11) [7].

$$R_{grid} = \frac{\rho_{soil}}{2\pi l} ln \frac{l^2}{sd} \tag{2.10}$$

$$R_{rod} = \frac{\rho_{soil}}{2\pi l} \left(ln \frac{8l}{d} - 1 \right) \tag{2.11}$$

A switchyard grounding grid configuration consists of several interconnected horizontal grids and vertical rods for selected points [25, p. 21]. A power frequency current injection to the grounding system utilizes the large, widespread grounding system area, increasing the overall performance. The total grounding system resistance, at power frequency, is given with application procedure in [23].

2.4.2 Soil Properties under Impulse Current Injection

As described in section 2.4.1 the primary indication of performance at power frequency is the grounding system resistance, which is given by soil resistivity and the grounding structure design. In the evaluation of the grounding system behavior during a fast transient injection impulse, like a lightning surge, the frequency dependent parameter is making a significant contribution. The soil buried grounding structure will, due to the frequency dependent grounding system, respond with inductive and capacitive effects during a lightning current impression. The description of grounding system performance under these conditions are consequently shifted to grounding impedance and described by eq. (2.12).

$$Z(\omega) = \frac{U_T(\omega)}{I_T(\omega)} \tag{2.12}$$

Considering the soil characteristic parameters frequency dependencies, which consisting of [20, p. 488]:

- Magnetic permeability, μ:
  The soil permeability has a constant value similar to the permeability of vacuum, μ_0, in the frequency range of lightning.
- Resistivity, $\rho_{soil}(\frac{1}{\sigma_{soil}})$:
  Experimental research has shown that the soil resistivity is frequency dependent from its value at power frequency.
- Permittivity, $\varepsilon = \varepsilon_0 \times \varepsilon r_{soil}$:
  Experimental research has shown that the soil permittivity is frequency dependent from its value at power frequency.

As described in section 2.4.1 the soil mixture and variable factors as temperature and moisture content are governing the electrical parameters. From the number of elements the soil usually has a very complex composition, thus accurate modeling the frequency dependency consists of a significant scientific challenge [28, p. 1163]. Contrary to the

description given in section 2.4.1, the soil frequency dependent parameters are involved, and measurement techniques are challenging to apply in practical applications. As the list above state, an additional factor in the soil permittivity needs to be introduced. From reviewed literature, the soil relative permittivity, εr_{soil}, is in the range from 4 to 81 and is strongly affected by water content and temperature [33].

The laboratory could analyze the soil properties, however, the accuracy of such representation is expected to be limited for an entire switchyard area. For a grounding arrangement, the standard practice is to use local soil composition, modified by selected construction method and design [25, p. 21]. From this construction method, the soil medium may be controlled to give uniformly distributed soil, of comparable electric properties, over the switchyard area. Visacro[2] and co-workers have in recent years (from 2014) collected a large number of soil measurements under transient conditions, from own work and previous researchers. From the experimental results, Visacro developed a semi-theoretical model to describe the frequency dependence of the soil parameters, first published in [12]. With soil analysis at power frequency conditions, as described in section 2.4.1, a relation to explain the frequency dependent parameters are given in eq. (2.13) which is parameterized by table 2.2. This formulation is described valid from 100 Hz to 4 MHz, which is characterized as the typical frequency range of lightning based on the steep front [20, p. 491].

$$\sigma(f) = \sigma_0 + \sigma_0 \times h(\sigma_0)\left(\frac{f}{1MHz}\right)^{\gamma} \tag{2.13a}$$

$$\varepsilon_r(f) = \frac{\varepsilon'_\infty}{\varepsilon_0} + \frac{tan(\pi\gamma/2)\times 10^{-3}}{2\pi\varepsilon_0(1MHz)^{\gamma}}\sigma_0 \times h(\sigma_0) f^{\gamma-1} \tag{2.13b}$$

	function h(σ_0)	γ	$\frac{\varepsilon'_\infty}{\varepsilon_0}$
mean results	$h_1 = 1.26 \times \sigma_0^{-0.73}$	0.54	12
relatively conservative results	$h_2 = 0.95 \times \sigma_0^{-0.73}$	0.58	8
conservative results	$h_3 = 0.70 \times \sigma_0^{-0.73}$	0.62	4

Table 2.2: Parameter table for frequency dependant soil [12, p. 1169]

[2]Silverio Visacro, Lightning Research Center, Federal University of Minas Gerais (UFMG), Belo Horizonte, Brazil

2.4.3 Grounding Grid Equivalent Circuit

The selected modeling approach for the grounding grid equivalent circuit is based on the transmission line model. From the evaluation made during the literature review in section 1.2, the transmission line approach has several advantages over alternative methods. Building further on the fundamental transmission line described in section 2.2, the circuit parameters is estimated based on the soil properties.

2.4.3.1 Single Horizontal Ground Wire

With reflections on the fundamental traveling model in section 2.2, one side of a grounding grid mesh can be represented by an equivalent electrical circuit as illustrated by fig. 2.7.
The grounding conductor material, radius a and length l governs the per-unit length resistance and inductance, while the conductance and capacitance mainly are governed by surrounding soil. Differing from typical features of cables and transmission lines, where the insulation losses a minimized, the soil conductance and capacitance makes a significant contribution to a current dispersion into the soil.

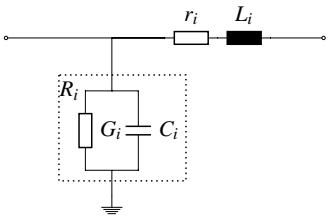

Figure 2.7: Ground grid equivalent circuit for one side

A conductor per-unit length ground wire consists of internal and external impedance. The external impedance is given in relation to the soil, and the internal are given by the grounding wire properties. The conductor internal resistance, r, is given by the length, l, material resistivity, ρ_{cond} and conductor cross-section, a, by eq. (2.14).

$$r_i = r_j = \frac{\rho_{cond}}{\pi a^2} l \tag{2.14}$$

Due to relatively short conductor length and large cross-section, the internal resistance and inductance are significantly smaller than the external self-impedance and are negligible in the frequency range of lightning surge, as described in section 2.4.2. This simplification of the grounding system, under transient conditions, limits the evaluation

to consider the external inductance by eq. (2.15) [34, p. 723].

$$L_i = L_j = \frac{\mu_0}{2\pi}\left(ln\frac{2l}{a} - 1\right) \tag{2.15}$$

From the soil properties, the per-unit length shunt conductance and capacitance is estimated by eq. (2.16) [7, p. 80].

$$G_i = G_j = \frac{\pi}{\rho_{soil}\left[ln\left(\frac{2l}{\sqrt{2ad}} - 1\right)\right]} \tag{2.16a}$$

$$C_i = C_j = G_i\rho_{soil}\left(\varepsilon_0 \times \varepsilon r_{soil}\right) \tag{2.16b}$$

2.4.3.2 Mutual Effects Between Horizontal Ground Wires

For a switchyard grounding system, several interconnected horizontal wires exist in a grid formation. From the past section properties (section 2.4.3.1) for a single horizontal ground wire has been evaluated. When a lightning surge is entering the ground system and excite the wires, mutual effects in the grounding grid arrangement will arise. When defining the equivalent circuit for a horizontal wire, fig. 2.7, as a segment, mutual effects will exist between any two segments which are excited based on the distance, conductor and soil properties [30]. An illustration of the mutual effects between horizontal ground wire segments is given in fig. 2.8.

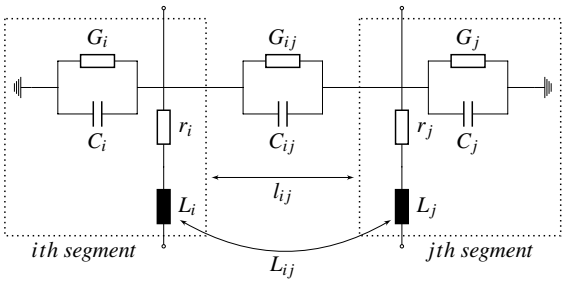

Figure 2.8: Ground buried horizontal wire mutual effects between segments. Consist of two horizontal wires from fig. 2.7, marked as segments, in addition, an illustration of the mutual equivalent parameters

Alipio and co-workers proposed a simplified method of computing the mutual effects in [13]. By modifying the expression in eqs. (2.15) and (2.16) and changing the factor of conductor radius, a, to be the length between the grounding grid segments, l_{ij}.

This simplification is considering the closest grounding grid segments. The simplified grounding grid mutual parameters is estimated by eq. (2.17).

$$L_{ij} = L_{ji} = \frac{\mu_0}{2\pi}\left(ln\frac{2l}{l_{ij}} - 1\right) \tag{2.17a}$$

$$G_{ij} = G_{ji} = \frac{\pi}{\rho_{soil}\left[ln\left(\frac{2l_c}{\sqrt{2l_{ij}d}} - 1\right)\right]} \tag{2.17b}$$

$$C_{ij} = C_{ji} = G_{ij}\rho_{soil}\left(\varepsilon_0 \times \varepsilon r_{soil}\right) \tag{2.17c}$$

A second evaluated method for estimating the mutual effect is through the non-uniform transmission line approach were first introduced by Liu in [9]. The mutual parameter matrix for the grounding grid between each per-unit length grounding wires could be estimated from eqs. (2.18) and (2.19). The mutual inductive coil effect will depend on the distance between segments and are independent of the soil medium, as expressed by eq. (2.18).

$$L_{ij} = \frac{\mu_0}{4\pi}\int_{l_i}\int_{l_j}\frac{1}{l_{ij}}dl_i dl_j \tag{2.18}$$

The mutual parameters related to the soil, conductance G and capacitance C, is also dependent on wire segment spacing. The combined effect is described as the mutual impedance and is expressed in complex terms by eq. (2.19a). Where the mutual conductance and capacitance are expressed in eq. (2.19b) and eq. (2.19c), respectively [30, p. 330].

$$Z_{ij} = \frac{1}{4\pi l_i l_j(\rho_{soil}{}^{-1} + j\omega\varepsilon)}\left[\int_{l_i}\int_{l_j}\frac{1}{l_{ij}}dl_i dl_j + \frac{\rho_{soil}{}^{-1} + j\omega(\varepsilon - \varepsilon_0)}{\rho_{soil}{}^{-1} + j\omega(\varepsilon + \varepsilon_0)}\int_{l_i^{'}}\int_{l_j}\frac{1}{l_{ij}}dl_i^{'}dl_j\right] \tag{2.19a}$$

$$G_{ij} = \frac{1}{ReZ_{ij}} \tag{2.19b}$$

$$C_{ij} = ImZ_{ij} \tag{2.19c}$$

When the per-unit length parameter matrices is determined for the entire grounding grid the modified transmission line model is described in eq. (2.20) for the non-uniform

properties. $V(l,t)$ and $I(l,t)$ are the unknown distributed voltage and current along the grounding conductor, $\mathbf{r}$ the per-unit length grounding wire resistance, $\mathbf{L}(l,t)$, $\mathbf{G}(l,t)$ and $\mathbf{C}(l,t)$ are the effective per-unit length inductance, conductance and capacitance at the position l at the time t[3]. With reference to the classical transmission line model, described in section 2.2 and eq. (2.2), the main difference is the dynamic per-unit length effective parameters.

$$-\frac{\partial u(l,t)}{\partial l} = \mathbf{r}i(l,t) + \mathbf{L}(l,t)\frac{\partial i(l,t)}{\partial t} \tag{2.20a}$$

$$-\frac{\partial i(l,t)}{\partial l} = \mathbf{G}(l,t)u(l,t) + \mathbf{C}(l,t)\frac{\partial u(l,t)}{\partial t} \tag{2.20b}$$

2.4.4 Soil Ionization

A grounding wire conducting a lightning impulse current will exert a time-variant electric field, outwards through the wire and into the surrounding soil. The soil itself, depending on soil resistivity and properties, will conduct a current from the grounding wire, dissipated into the soil. Depending on current density dissipated, a relation of the electric field are given by eq. (2.21a). The surface current density of a round wire is found in eq. (2.21b), which exerts the electric field on the soil [35, p. 1586]. The linear behavior between current density and electric field are valid upon the soil critical breakdown value, E_c. When the current through the conductor is high enough, a soil ionization will start from the wire and surrounding soil. The soil ionization contentious, in length from the wire until the electric field drops below the soil type dependent critical value. In the ionization region and close to the grounding wire, where the electric field is strongest, arcing may occur. The strong electric field produces tracking and leaders on the irregular surface of the soil grains and making soil breakdown to start. The properties of an increased tracking activity will decrease the apparent soil resistivity in the ionization region. If the electric field is increased further spark and even arcing activity may arise, where the arc has punctured the soil. In the soil arcing region the apparent soil resistivity is significantly lowered, also assumed to be close to zero, which is illustrated in fig. 2.9.

[3] Bold notation indicates matrices of the full parameterized grounding grid

$$E_{soil} = J_{soil}\rho_{soil} \tag{2.21a}$$

$$J_{soil} = \frac{I_{soil}}{2\pi al} \tag{2.21b}$$

There have been devoted research effort in the investigation of the properties of soil ionization process and significant influencing factors on the critical breakdown level. An overview of what is anticipated as most important are listed below from the reviewed work.

- Soil grain size and mixture are affecting E_c. Large grains [4] and non-uniformity tends to allow voids and continuous arcing discharge channels from a strong field [30, p. 306]. Larger grains and voids will generally lower E_c.
- Soil compactness and E_c are contrary to the soil resistivity. While a compact soil surrounding the grounding electrode are lowering resistivity, voids to form continuous arcing discharges are reduced. The relation between soil resistivity and E_c have been experimentally investigated in [36]. Approval of research is confirmed as this relation are included and referenced in work by IEEE standard [37].

In addition to the soil properties, variable factors as moisture and temperature are strongly influencing E_c. Correlation is generally given by higher E_c in dry or frozen soil, which is experimentally investigated in [38].
As may be indicated the soil properties and critical breakdown voltage, E_c are complex with several influencing factors. An observation confirming this statement is a missing unified definition of E_c from reviewed standards. IEEE indicates (quoted in standard) a critical breakdown value of E_c=1000 kV/m [37, p. 1263]. This definition gives references to the above mentioned experimental relation between soil resistivity and E_c [36]. Further evaluation of IEEE standards gives a value of E_c=400 kV/m, a level which are referred without reference in [39, p. 38][5]. CIGRE recommends a soil independent generalization to be E_c=400 kV/m [14]. Apparently the defined value of E_c are given without reference to research, however most reviewed referenced work performed in recent years use CIGRE and IEEE recommendations of E_c=400 kV/m.
In modeling the grounding system ionization and include behavior in the transmission

[4] Grain diameter in the range of 0.4-3 mm
[5] Refereed standard is currently under review for update

line model, an effective approach are to relate the grounding wire equivalent radius. When a lightning current is injected from one side of the grounding wire, the transient response through the wire segment follows the traveling wave model as described in section 2.2. If the injected current is raising the electric field on the wire surface per-unit length above a critical level, E_c, an ionization on the segment will be initiated. Following to the wire ionization, the equivalent radius of the conductor will increase outwards in the soil until the electric field intensity falls below E_c.
The field distribution is involved with the various dominating factors as soil properties, grounding system structure and lightning current properties. As a simplification, a modeling technique where the ionization in the soil for a ground wire was introduced in [11], and most of the reviewed work has adopted this approach. Figure 2.9 illustrates the modeling technique, where a grounding wire is injected lightning current. Due to propagation, and inductive effect, the per-unit length distributed electric field is reduced by length, resulting in tree equivalent radius.

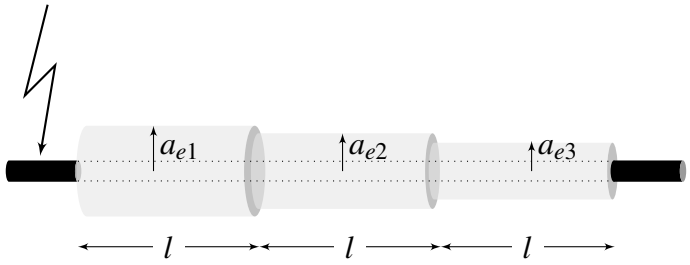

Figure 2.9: Soil ionization around a ground wire when a high impulse current is injected. Illustrated with tree soil breakdown areas, giving corresponding sections l of apparent effective conductor radius a_e

The effective radius of the per-unit length segment and exerted electrical field, is given by eq. (2.22) [35, p. 1587]. The equivalent effective radius during soil ionization does only affect the grounding system shunt conductance and capacitance is as shown by fig. 2.7 [30, p. 327]. For the grounding grid segments, exceeding the critical electric field, the parameters estimated in section 2.4.3.1 and eq. (2.16) and section 2.4.3.2 and eq. (2.17) are a function of the equivalent radius a_e.

$$a_e = \frac{\rho_{soil} I}{2\pi l E_c} \qquad if\ E_i \geq E_c \tag{2.22}$$

2.5 Software Tools

The software tools used in the thesis is briefly introduced with key features relevant for the implementation.

2.5.1 MathWorks Matlab® and Simulink®

MathWorks Matlab® provides a high-level mathematical language and interactive environment for numerical computation, visualization, and programming. With the built-on top accessory Simulink® the functionality of Matlab® are expanded to create models and applications. Simulink® is a block diagram environment for multidomain simulation and Model-Based Design. It supports the system-level design, simulation, automatic code generation, and continuous test and verification. Key features of thesis:

- Matlab® and Simulink® interface for mathematical algorithms integration into own developed models
- Simscape foundation library of electrical elements and properties solver
- Graphical editor for building and managing hierarchical block diagrams
- Simulation engine with fixed-step and variable-step Ordinary Differential Equation (ODE)/Partial Differential Equation (PDE) solvers
- Project and data management tools for managing model files and simulation data
- Post-processing capabilities of simulation data

2.5.2 Powersys EMTP-RV

Powersys EMTP-RV is a full-featured, state-of-the-art and technically advanced simulation and analysis software, specialized for power system transients studies. Main application area for simulation of electromagnetic, electromechanical and control systems transients in multiphase electric power systems. Key features of thesis:

- Comprehensive library of power system components and function blocks
- A powerful and fast computational engine which are optimized for existing component library
- Graphical editor for building and managing hierarchical block diagrams

2.5.3 Co-Simulation Application

In utilizing functionality of both software tools, the flexibility of Matlab®/Simulink® and specialized capabilities of EMTP-RV, co-simulation is performed with a Functional Mock-up Interface (FMI) interface. FMI is a tool-independent standard for model exchange and co-simulation. The first version, FMI 1.0, was published in 2010 followed by FMI 2.0 in July 2014 and developed by the European Consortium Modelisar [40]. The FMI software solution which makes it possible to interface Matlab®/Simulink® and EMTP-RV was released by Powersys Solutions in early 2018. The FMI 2.0 application gives possibilities for co-simulation with information exchange at a per simulation time-step interval (sequentially processed) [41].

3 Method

The method used in this thesis is solely based on computer implementation. From implementing two separate systems, the grounding and the transmission systems, these models are integrated to perform co-simulation. The weighted modeling development and description are given the grounding system in Matlab®/Simulink®. From the foundation of the theory chapter, the grounding system is modeled based on a bottom-up approach, defining the implementation strategy with corresponding utility functions. Secondly, a model of a simplified transmission system is described. The use of specialized software tool, EMTP-RV, allows for utilizing the standard component library for a transmission system, which limits the description by simplicity. As the surge arrester is of significant importance for the injected surge current to the grounding system, the full V-I characteristics is described. Finally, the custom-made FMI interface, which gives options for co-simulation, is defined with the signal exchange and description of the simulation process.

The method chapter is supported by source code, developed models and block descriptions found with specific references to Appendix D to F. For this reason, the description is limited to present an overview which connects relevant theory, implementation strategies and principles.

3.1 Grounding System Model in Matlab®/Simulink®

The grounding system models is implemented by using the general mathematics software tool Matlab® and graphical block development tool and simulation engine Simulink® with add-on features for electrical systems. First, the per-unit length grounding wire is implemented with measurement nodes. Secondly, the grounding wire is defined in a system to build complex grounding grids. With the bottom-up approach of implementation, with a defined strategy, the built simulation log follows with a description which is applicable for all grounding grid models. From the defined simulation log, functions to extract information and map these properties to the physical grounding grid layout is described. These functions are the foundation for three-dimensional visualization.

Followed by a brief description of the numerical solver used by Simulink® in performing the simulation in isolated mode. Lastly, the excitation current source used to perform isolated simulation in Matlab® and Simulink®, is introduced.

3.1.1 Transmission Line Block Modeling of Grounding Wire

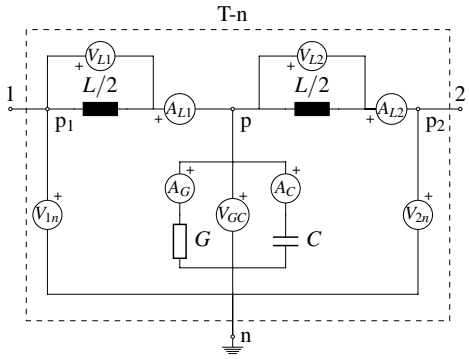

Figure 3.1: Implemented per-unit length grounding wire with measurement nodes

The per-unit length grounding wire are implemented in Matlab® and Simulink® with a t-section form of the fundamental transmission line model, as described in section 2.2. The source code of the t-section implementation, graphical Simulink block element, and variable definition interface are found in Appendix D.1.3. Regarding the source code and Simulink block element connection points, the internal circuit is fully represented with fundamental electrical elements as illustrated in fig. 3.1. Measurement nodes for current and voltage are also defined for each element and branch of the circuit. The transmission line block element has the identification of "T-n", where "T" indicates transmission line block and "n" an increment number when several per-unit grounding wires exist in a segment. To assure a smooth representation of the interconnection between elements and to possibly extend the model functionality of including mutual coupling effect the per-unit T-section represent one meter of ground wire [9, p. 44]. Consequently, the model functionality can be extended to arbitrary lengths. For each length, variables names are defined to connect the surrounding soil to the grounding wire physical properties. From the variable definition, circuit parameters are determined based on the call of function script found in Appendix D.2.1 and D.2.2 for frequency independent and dependent soil, respectively. The horizontal buried grounding wire geometry, per-unit length, soil depth and constants are defined through the variable load script found in Appendix D.1.2. Based on these implementations, an estimation procedure of the circuit elements values are performed. Where the per-unit length inductance, L, conductance, G, and capacitance, C, are estimated by eq. (2.15) and eq. (2.16). In addition, the function scripts found in Appendix D.2.1 and D.2.2 performs a frequency sweep, in range of lightning surges, to determine the individual elements impedance and the characteristics properties (characteristics impedance, Z_c, and propagation constant, γ) of the per-unit length grounding wire, as given by eq. (2.4).

3.1.2 Grounding Grid Formation

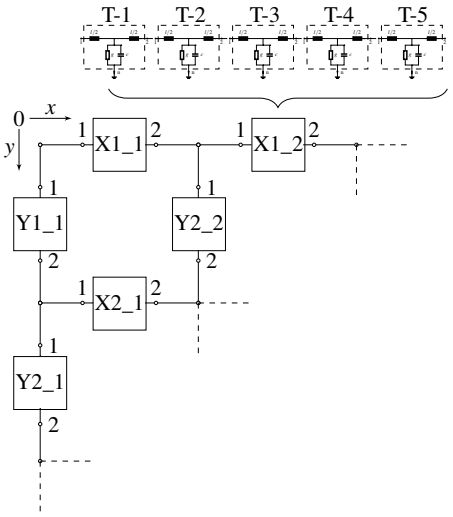

Figure 3.2: Grounding grid implementation strategy

From the per-unit length grounding wire in section 3.1.1, extension is made to form wire segments and eventually complex grounding system consisting of grids. The interconnection points (1 and 2) of the per-unit block element in fig. 3.1, gives the option for series chains of grounding wires segments. These segments, consisting of several per-unit block elements, are further interconnected in series and parallel to form grounding wire branches as grounding grids. The interconnection strategy with identification to form complex grounding grids are illustrated in fig. 3.2. The horizontal directional wire segments, x-direction, are defined with the prefix "X". Consequently, the vertical wire segments are defined with the prefix "Y". From the directional definitions, each wire segments identification is incremented both in x- and y-direction by prefixes of "X'y-dir'_'x-dir'" and "Y'y-dir'_'x-dir'" for horizontal and vertical wire segments, respectively, from the initial point (marked "0" in fig. 3.2).

There are defined two varieties in segment lengths which consist of five and ten per-unit block elements and follows in Appendix D.4.1. The intention of defining the segment lengths are to form interconnected quadratic grounding grids, as illustrated in fig. 3.2 where each segment consist of five per-unit block elements (T1 to T5). For the different segments lengths, there is developed complex grounding grid models of two sizes, 1600 m^2 and 3600 m^2, and are illustrated by fig. 3.3. These models can be found in Appendix D.4.2 for the 5×5 meter mesh size and D.4.3 for the 10×10 meter mesh size.

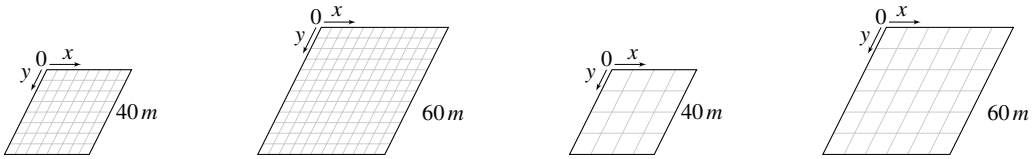

(a) 5×5 m, 1600 m^2 **(b)** 5×5 m, 3600 m^2 **(c)** 10×10 m, 1600 m^2 **(d)** 10×10 m, 3600 m^2

Figure 3.3: Implemented grounding grid models of 5×5 m and 10×10 m mesh size and total area of 1600 m^2 and 3600 m^2

3.1.3 Simulation Log Structure

Values from the implemented measurement nodes, for each grounding wire t-section as illustrated by section 3.1.1 and fig. 3.1, are stored in a simulation-log database. The simulation-log database is organized with value identifications from the t-section measurements definitions in addition to the grounding grid formation strategy, as described in section 3.1.2. An overview of notation to reference the entire simulation log values or time series per. measurement node are given in table 3.1. The logged values are implemented to follow the same integration time step defined by the overall simulation preferences, which gives a common reference for all the individual measurement series.

Node (fig. 3.1)	Log-file name	Grid Segment (fig. 3.2)	Element	Series selection
V_{l1}	simlog_scc_grounding_system.	X/Y'y-dir'_'x-dir'.	l1.v.	series.values/time
A_{l1}	simlog_scc_grounding_system.	X/Y'y-dir'_'x-dir'.	l1.i.	series.values/time
V_{l2}	simlog_scc_grounding_system.	X/Y'y-dir'_'x-dir'.	l2.v.	series.values/time
A_{l2}	simlog_scc_grounding_system.	X/Y'y-dir'_'x-dir'.	l2.i.	series.values/time
V_{1n}	simlog_scc_grounding_system.	X/Y'y-dir'_'x-dir'.	p1.v.	series.values/time
V_{2n}	simlog_scc_grounding_system.	X/Y'y-dir'_'x-dir'.	p2.v.	series.values/time
A_g	simlog_scc_grounding_system.	X/Y'y-dir'_'x-dir'.	g.i.	series.values/time
V_{gc}	simlog_scc_grounding_system.	X/Y'y-dir'_'x-dir'.	p.v.	series.values/time
A_c	simlog_scc_grounding_system.	X/Y'y-dir'_'x-dir'.	c.i.	series.values/time

Table 3.1: Simulation-log nodal measurement overview and grounding system variable definitions. Built on transmission line model implementation (section 3.1.1) and grounding grid formation strategy (section 3.1.2)

For the implemented grounding grid models (found in Appendix D.4.2 and D.4.3) the total number of required logged variables follows in table 3.2.

Grounding grid model	Area	Required number of logged variables
Appendix D.4.2	1600 m^2	6480
5 x 5 m mesh	3600 m^2	14040
Appendix D.4.3	1600 m^2	3600
10 x 10 m mesh	3600 m^2	7560

Table 3.2: Required number of logged variables to comply with nodal measurements for the transmission line implementation (section 3.1.1 and fig. 3.1) per grounding grid model

3.1.4 Nodal Measurements Mapped to Physical Properties

To connect the nodal measurements values in the complex grounding grid to physical properties (location in the plane) post-scripts was developed. These post-scripts are built on the definition of the grounding grid layout according to section 3.1.2 and simulation log definition in section 3.1.3. For the implemented grounding grid models, the associated load variable files are defined in section D.1.1.

3.1.4.1 Voltage Distribution

To perform ElectroMagnetic interference (EMI) analysis of the grounding grid area the developed voltage potential are of interest. For the grounding grid nodal voltage potential rise, at a given selection within the simulation-log, an overall distribution is given by the post-script found in Appendix D.3.2. The post-scripts collects the grounding grid voltage potentials, V_{1n} and V_{2n}, as illustrated by section 3.1.1 and fig. 3.1 to the grounding grid geometry. The overall data-set retrieved from this script is used to produce the three-dimensional representation of the grounding grid voltage distribution.

3.1.4.2 Leakage Current Distribution

The current leaked to the soil from an excited grounding system are given for each per-unit length grounding wire. To extract the overall leakage current distribution a post-script was developed which is found in Appendix D.3.3. The soil leaked current are the primary parameter in the evaluation of GPR and the electric field exerted on the soil. The post-scripts collects the soil current value leaked from the grounding grid, A_g, as illustrated by section 3.1.1 and fig. 3.1 to the grounding grid geometry. The overall data-set retrieved from this script are used for evaluation of the electric field strength exerted outwards in the soil from the grounding wire surface.

3.1.4.3 Electric Field Strength Distribution

From the overall leakage current distribution (section 3.1.4.2) the electric field strength is found, at the conductor surface, for each per-unit length grounding wire. By finding the soil exerted field strength, evaluation of soil ionization could be performed as described by section 2.4.4. An estimation of the exerted electric field is performed based on the soil leakage current, type of soil and grounding grid properties, from eq. (2.21), where the implementation are found in Appendix D.3.4. The overall representation, for the grounding grid, is used to produce the three-dimensional representation of the soil electric field strength close to the grounding wire surface.

3.1.5 Numeric Solver and Timing

From the formation of grounding grid structures, the required amount of measured values are highlighted in section 3.1.3 and table 3.2. With this in mind and solution of the fundamental transmission line model for relatively short wire segments, selection of numeric solver is the primary factor in reaching an acceptable level of accuracy which is weighted against computer resource needs. In isolated mode, Matlab®, the solution method of variable time step and integration engine ODE23t was selected [42]. The

ordinary differential equation solver is a powerful method to analyze the fundamental transmission line model, which are solved on a per-unit length level. The minimum integration step is set to cover nodal change on each per-unit length, which is dependent on maximum traveling wave speed in the grounding conductor. This led to a high detail level in the transient period of an injected surge current, which gives high computational effort. In reducing the computer, resource needs the variable time step solver are observing the per-unit length change, per simulation step, and consider a tolerance of difference which increases the time steep when the system is in temporary stationary conditions.

3.1.6 Double Exponential Lightning Current Source

In isolated mode, when the grounding system is simulated in Matlab®/Simulink®, there is implemented a current source of a double exponential waveform to simulate a surge according to section 2.1 and eq. (2.1). The source implementation is found in Appendix section D.4.4. Parameter defined as "A" and "B" describes the α and β, respectively. The surge magnitude, $\hat{I}$, are adjusted from the parameter "I_mag".

3.2 Transmission System Model in EMTP-RV

The implemented transmission system models represent a simplified 300 kV mains transformer connections to the grid. By utilizing the standard component library of EMTP-RV an overhead transmission line, surge arrester and a cable of variable length which connects a transformer is modeled as illustrated in fig. 3.4. Also, a lightning surge source is used which is designed to excite a CIGRE defined waveform of the standard lightning, as described in section 2.1. The full representation of implemented models are found in Appendix F. The variable cable length is given by two cases where the first case are characterized by a short cable of l_c=10 m between the transformer and surge arrester (Appendix F.1). In the second case the cable is prolonged to l_c=500 m and is characterized as a relatively long cable between the surge arrester and main transformer (Appendix F.2). The implemented transmission system models are inspired by [43, pp. 1-9].

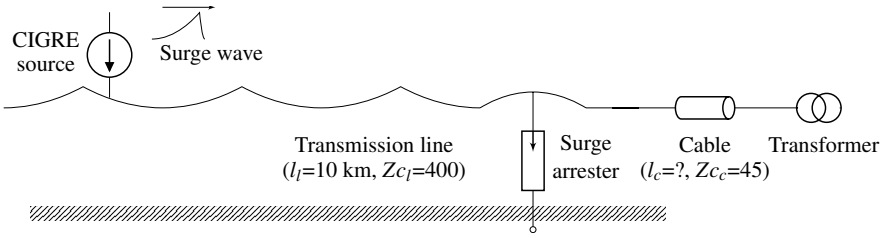

Figure 3.4: Simplified illustration of implemented transmission system in EMTP-RV

3.2.1 Transmission System

The minimal 300 kV transmission system models implemented is illustrated fig. 3.4. The model consists of line/cable block which is defined as TLM in the EMTP-RV library. This element is fully integrating the fundamental transmission line model, described in section 2.2, for surge wave propagation and losses. The transmission line and cable are parameterized as lossless and base the surge wave properties on the characteristic impedance Z_c and length l. The overhead transmission line (Z_{cl}=400) has a length of l_l=10 km to the substation. At the cable junction, between the transmission line and cable, there is placed a surge arrester. From the surge arrester, the transformer is connected through a cable (Z_{cc}=45) of variable length, l_c, according to implemented model (Appendix F.1 for l_c=10 m and F.2 for l_c=500 m).

3.2.2 Surge Arrester Parameters

For the grounding system, the most significant component is the surge arrester as the injection point. From the EMTP-RV library, the ZnO surge arrester with version number 865630 was selected. From the transmission network system voltage of 300 kV, the surge arrester breakdown V-I characteristics (section 2.3.1 and eq. (2.6)) were parameterized as follows in table 3.3. These parameters were adopted from [43, p. 9], which contains an example of a 300 kV transmission network.

Segment	k_{seg}	α_{arr}	U_{arr} (pu)
1	$4.23208099271728\times10^{9}$	$2.40279296219991\times10^{1}$	$2.98198270953446\times10^{-}1$
2	$2.81773645053899\times10^{10}$	$2.66219333383972\times10^{1}$	$4.81500000000002\times10^{-}1$
3	$4.15144087019289\times10^{8}$	$2.00870413085783\times10^{1}$	$5.24450368910346\times10^{-}1$
4	$2.63271405014350\times10^{12}$	$3.52906710089596\times10^{1}$	$5.62230840318764\times10^{-}1$
5	$3.21774149817822\times10^{6}$	$1.11310570543270\times10^{1}$	$5.69192036592734\times10^{-}1$
6	$1.93774621300766\times10^{5}$	5.36270125014300	$6.14408449804349\times10^{-}1$

Table 3.3: EMTP-RV ZnO surge arrester V-I parameters, adopted from [43, p. 9]

3.2.3 CIGRE Lightning Current Source

From the transmission line far-end, l_l=10 km from the substation (as shown in fig. 3.4), a lightning surge are injected from a CIGRE defined source (section 2.1). The source is selected from the EMTP-RV library, defined with name Icigre2, and parameterized as follows in table 3.4 to form a 1 kA, 1.2/50 μs stroke.

Description	Value	Unit
t_{start}	0	s
$\hat{I}$	1	kA
t_{rise}	1.2	μs
t_{half}	50	μs
Max steepens	0.9	kA/μs

Table 3.4: EMTP-RV CIGRE lightning current source parameters

3.3 Interfacing Matlab®/Simulink® and EMTP-RV

By taking advantage of two independent software application the developed grounding grid model was interfaced to perform combined system analysis, as illustrated by figs. 3.5 and 3.6. The vendor of EMTP-RV, Powersys, released in January 2018 an FMI software application toolbox which gives possibilities for co-simulation between Matlab®/Simulink® and EMTP-RV, where EMTP-RV is the master unit. The master unit is defined as FMI and the slave as Functional Mock-up Unit (FMU). When stating the that EMTP-RV is the master unit, this is a limitation by the released FMI software package. When running the simulation, synchronization and timing control are governed by EMTP-RV, and the Matlab®/Simulink® grounding grid models are acting as the slave. Each timestep iteration of the simulation are for this reason first made in EMTP-RV and secondly performed in Matlab®/Simulink® [41].

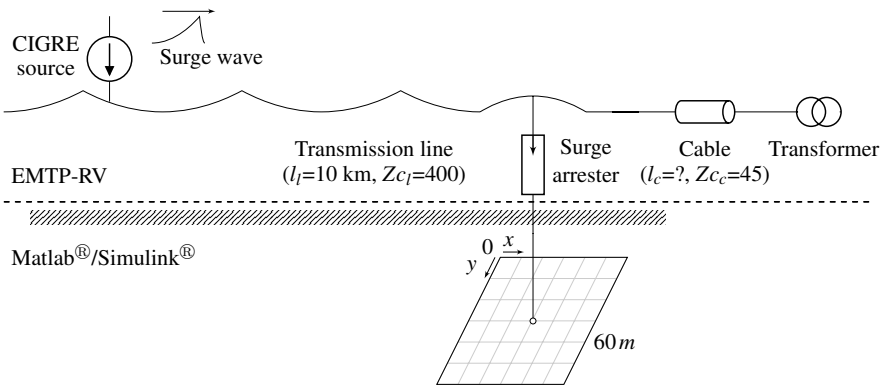

Figure 3.5: Simplified transmission system and grounding model interfaced. Illustrated with grounding grid of 10×10 meshes and a total area of 3600 m^2

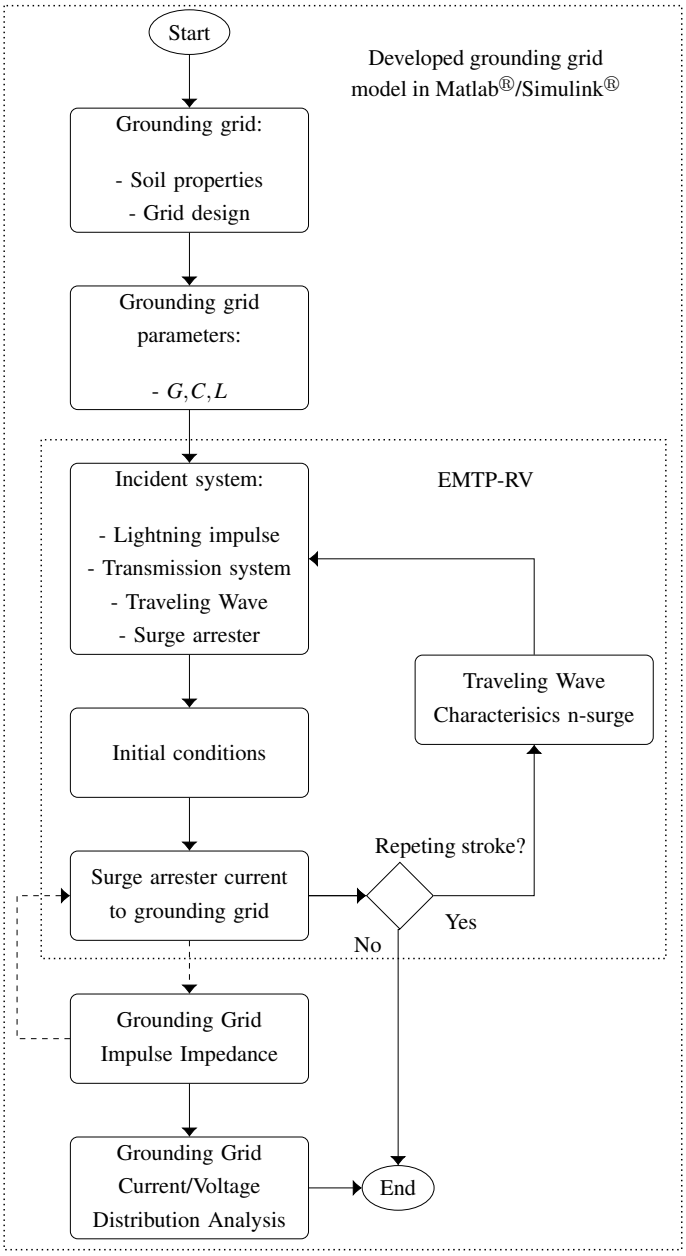

Figure 3.6: Orientation overview of the integrated model. Dashed lines indicate the integrated FMI signals exchange which dynamically effects both EMTP-RV and Matlab®/ Simulink®

3.3.1 Signals Selection

The amount of interfaced signals are implemented in mind of minimum data exchange of integrated signals to keep each separate model robust. A full description required by the surge arrester, as injection point, are the grounding system dynamic impedance when exerted to current injection. From the Matlab®/Simulink® developed grounding system model, the injection point impedance, and admittance are calculated based on the injected current, and induced voltage from eq. (2.12) and implementation could be found Appendix D.4.5. This gives the required integrated signals to be the source arrester

current from EMTP-RV to Matlab®/Simulink®. And the grounding grid injection point impedance/admittance from Matlab®/Simulink® to EMTP-RV. The integrated signals is indicated with dashed lines in fig. 3.6 and marked with "*" in table 3.5. Additional signals were interfaced to have a common overview of selected signals in one system. Due to the amount of signals required to build the grounding grid model, (section 3.1.3 and table 3.2), selected monitoring signals from the EMTP-RV models were exchanged to the Matlab®/Simulink® simulation log (section 3.1.3). The defined signal interface, with simulation log exchange, are given in table 3.5 and illustrated by the Simulink® implementation in Appendix E.

Signal	FMU-name	Description	Log-file name
Input*	i1CurrSurgeInject	Current from surge arrester	simlog_scc_grounding_system. I_EMTPCurrSurgeInject
Input	i2VoltCableEntry	Voltage at the cable entry	simlog_scc_grounding_system. I_EMTPVoltCableEntry
Input	i3VoltTrans	Voltage at the transformer	simlog_scc_grounding_system. I_EMTPVoltTrans
Input	i4VoltArrester	Voltage at the arrester output	simlog_scc_grounding_system. I_EMTPVoltArrester
Input	i5AdmReceive	Ground grid admittance check	simlog_scc_grounding_system. I_EMTPAdmReceive
Input	i6CurrSurgeSource	Current injected far-end	simlog_scc_grounding_system. I_EMTPCurrSurgeSource
Input	i7CurrCableEntry	Current trough cable entry	simlog_scc_grounding_system. I_EMTPCurrCableEntry
Input	i8CurrTrans	Current trough transformer	simlog_scc_grounding_system. I_EMTPCurrTrans
Output	o1CurrSurgeInject	Current surge arrester check	simlog_scc_grounding_system. I_EMTPCurrSurgeInject
Output	o2VoltSurgeInject	Voltage at injection point	simlog_scc_grounding_system. O_EMTPVoltInjectPoint
Output	o3ImpInjectPoint	Grounding grid impedance	simlog_scc_grounding_system. O_EMTPImpInjectPoint
Output*	o4AdmInjectPoint	Grounding grid admittance	simlog_scc_grounding_system. O_EMTPAdmInjectPoint

Table 3.5: FMU signal interface in Matlab®/Simulink® as slave unit to EMTP-RV FMI as master. Each signal are listed with a variable definition to the common simulation log (section 3.1.3). Integrated signals is identified by *

3.3.2 Simulation Time Step and Synchronization

With EMTP-RV as the master unit, a requirement from the FMI software package is a fixed time-step iteration when performing co-simulation [41]. The Matlab®/Simulink® solver, with variable time-step, described in section 3.1.5 are changed to for-fill this requirement and given a fixed time-step of 0.01 μs in performing co-simulation.

4 Results

This chapter presents results retrieved from simulations of the implemented models.
Firstly, the per-unit length grounding wire properties are extracted in the frequency domain to review the characteristic parameters. This is an evaluation based on the transmission line model and the basic parameters determined by different soil resistivity levels, with a specific wire configuration and one-meter length. The wire configuration and soil burial depth are kept constant during all simulations.
Secondly, the grounding system is simulated in time-domain in isolated mode. These simulations were carried out to show the characteristics of the total grounding system. With the simplicity of the external systems, only consisting of a current source of exponential form, the grounding system is treated under controlled conditions. Further, the results of per-unit length grounding wire from the center injection point in the grounding grid is shown, in time-domain, to review the characteristic properties from simulations.
Lastly, the grounding system is integrated into the transmission system. The complexity of the system is increased, both in regards to the transmission which conducts the surge and that the surge is injected through a surge arrester. Also, the current source is shifted to be of 1.2/50 μs CIGRE waveform. First, the short cable case is simulated and after that the design deviation with the long cable case. Also, the electric field distribution exerted on the soil is given for selected simulation performed in previous sections.

4.1 Per-Unit Length Characteristics

This section presents the characteristics results of a grounding wire of one meter buried in soil of various resistivity in the frequency domain. From estimating the soil parameters, section 2.4.3.1 and eqs. (2.15) and (2.16), the fundamental transmission line model is used to determine the characteristic parameters of the transmission line model, section 2.2 and eqs. (2.3) and (2.4), in a frequency span of lightning. The results are shown for a grounding system considering both the soil as frequency independent and also comparing the new research introduced by Alipio (section 2.4.2 and eq. (2.13)), as the soil medium itself as frequency dependent.
For all results presented in this chapter, the grounding wire burial depth and configuration is constant. Where the per-unit length, l=1 m, depth, d=0.6 m and wire radius of, a=0.004126 m.
The results in fig. 4.1 shows the per-unit length shunt admittance, Y, for both frequency

independent and dependent soil. The phase is added to highlight the capacitive contribution in the soil as a function of increased frequency.

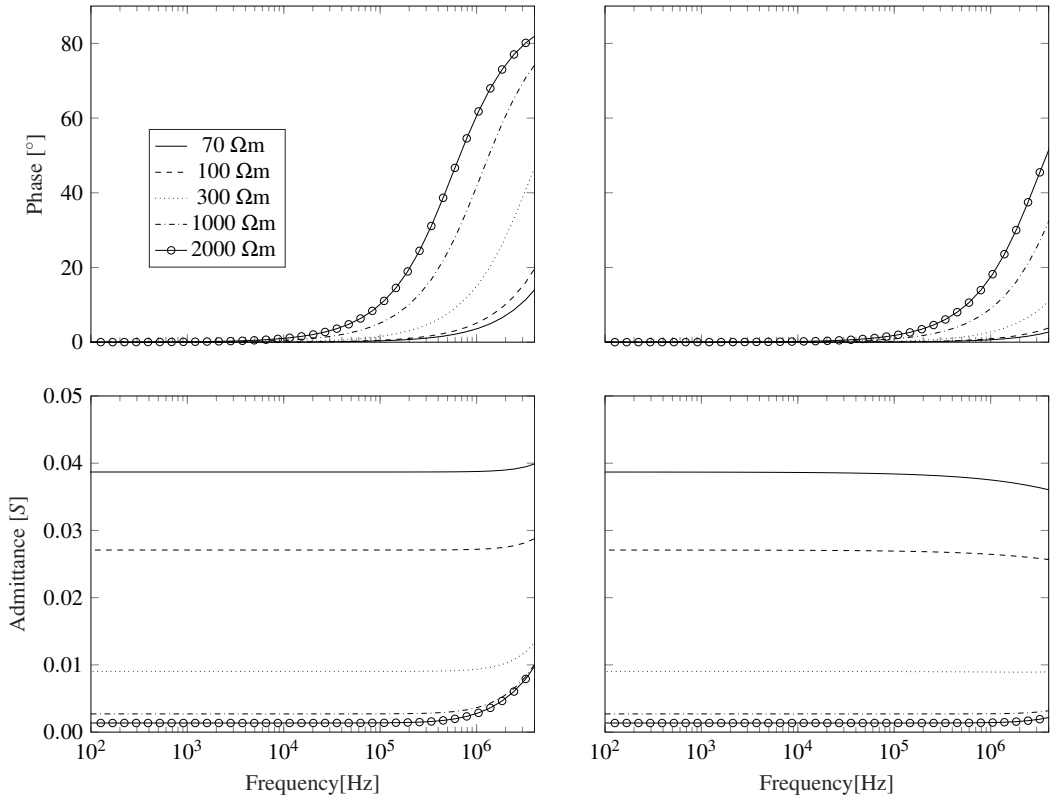

(a) Y in frequency independent soil **(b)** Y in frequency dependent soil

Figure 4.1: Effect on the shunt admittance (Y) for a per-unit length grounding grid wire in soil with different resistivity ρ_{soil}. Considering both frequency independent (fig. 4.1a) and dependent soil (fig. 4.1b)

The results in fig. 4.2 shows the per-unit length series impedance, Z. The series resistance is neglected, giving the simulated results as inductive. The series inductance is, as described in eq. (2.15), dependent on the geometry which is not affected by the soil properties.

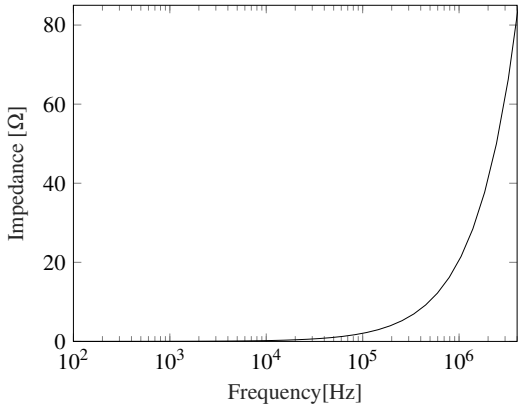

Figure 4.2: Per-unit length impedance (Z) considering lossless grounding wire

The results in fig. 4.3 shows the per-unit length propagation constant, γ. By giving the propagation constant in complex terms the attenuation and phase are shown for both frequency independent and dependent soil.

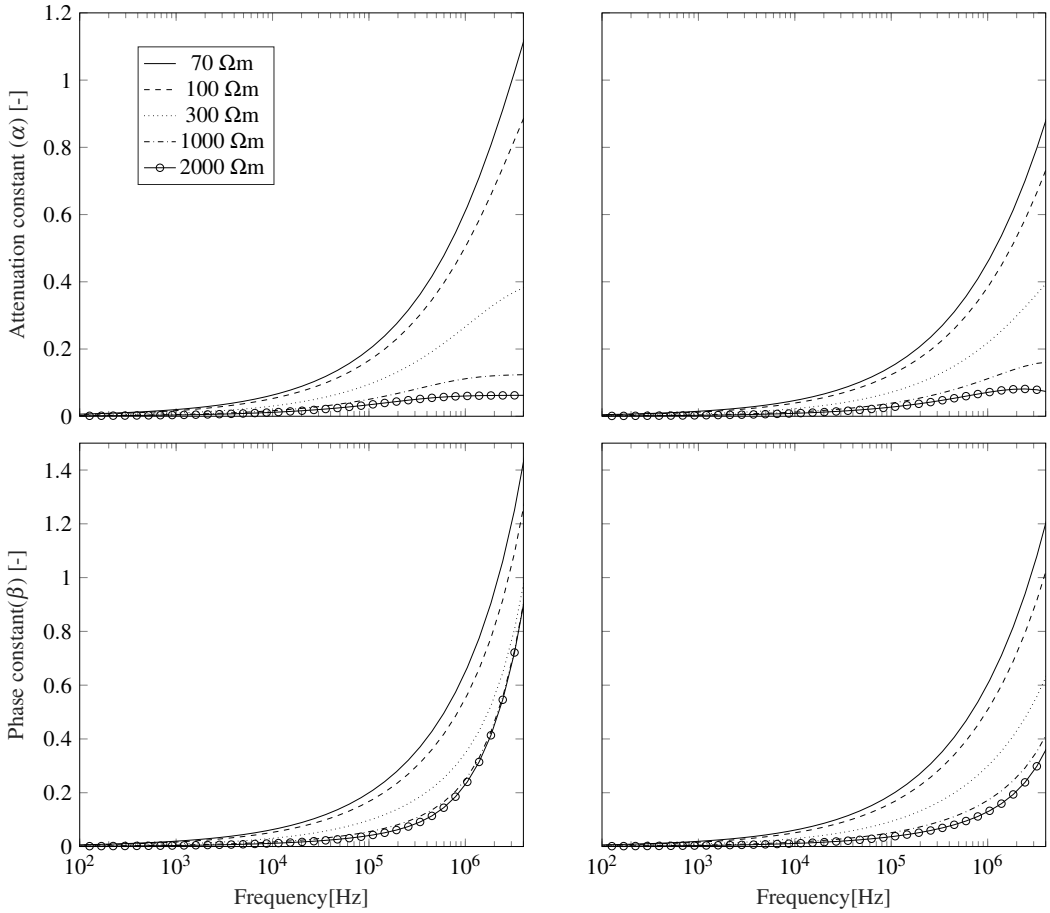

(a) γ in frequency independent soil **(b)** γ in frequency dependent soil

Figure 4.3: Effect on the propagation constant (γ) parameters for attenuation (α) and phase constant (β) for a per-unit length grounding grid wire in soil with different resistivity ρ_{soil}. Considering both frequency independent (fig. 4.3a) and dependent soil (fig. 4.3b)

The results in fig. 4.4 shows the per-unit length characteristic impedance, Z_c, for both frequency independent and dependent soil.

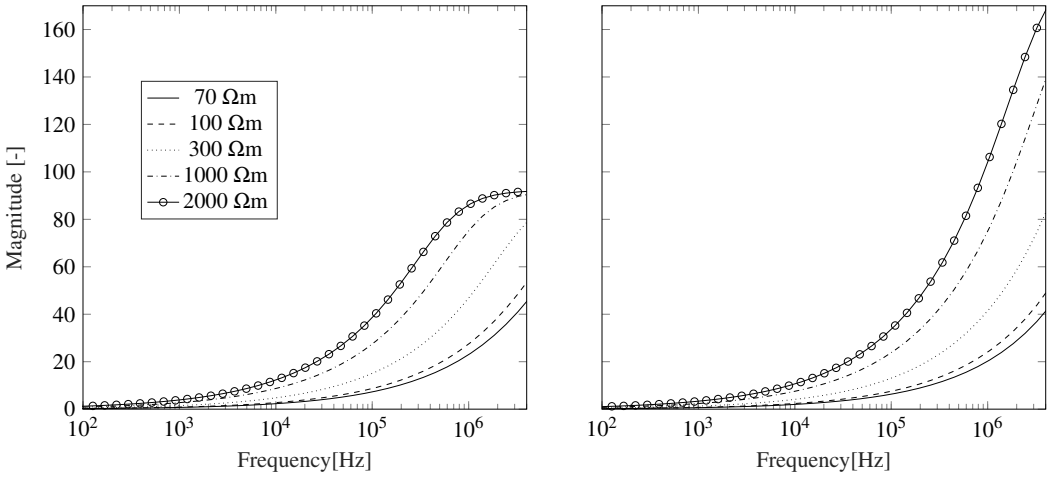

(a) Z_c in frequency independent soil

(b) Z_c in frequency dependent soil

Figure 4.4: Effect on the characteristic impedance (Z_c) for a per-unit length grounding grid wire in soil with different resistivity ρ_{soil}. Considering both frequency independent (fig. 4.4a) and dependent soil (fig. 4.4b)

4.2 Grounding Grid Model Isolated

In the following section grounding grid configurations of 10×10 m and 5×5 m mesh size are investigated when a single current stroke is injected. The grounding wire radius, a, and burial depth, d, is similar to the evaluation in section 4.1 and are summarized in table 4.1a. This similarity also applies to the injected current, which will be of same magnitude and waveform of a 1/20 μs stroke of double exponential form, giving constant values of α and β. The magnitude of the current source, $\hat{I}$, are adjusted for the grounding grid configurations to reach an approximate peak value of 1 kA at the injection point for all cases according to table 4.1. The simulations is performed based on the description given in section 3.1 where the system is isolated in Matlab®/Simulink®.

Wire depth, d	0.6	m
Wire radius, a	0.004126	m
Per-unit length, l	1	m
Current source decay constant, α	38×10^3	-
Current source crest constant, β	2.54×10^6	-

(a) Common values for simulation performed in section 4.2

Case	R_{soil} [Ωm]	$\hat{I}$ [kA]
6×6, 3600 m^2		
section 4.2.1.1	300	1.12
section 4.2.1.2	1000	1.12
sections 4.2.1.3 to 4.2.1.6	2000	1.14
4×4, 1600 m^2		
section 4.2.2.1	2000	1.36

(b) Applied for the 10×10 mesh size

Case	R_{soil} [Ωm]	$\hat{I}$ [kA]
12×12, 3600 m^2		
section 4.2.3.1	2000	1,11
8×8, 1600 m^2		
section 4.2.4.1	2000	1.40

(c) Applied for the 5×5 mesh size

Table 4.1: Parameter for simulation results in section 4.2. Common parameters used for both cases are given in table 4.1a while modified values of current magnitude, $\hat{I}$, is given in table 4.1b for 10 m and table 4.1c for 5 m mesh size

For each simulation case in section 4.2, the results are given by a figure which collects selected plots and overall grounding grid voltage distribution views. With reference to the individual subsections main figure, the grounding grid configuration is described in addition to soil properties and injected current.
The sub-figures are presenting:

- **(a)** Nodal measurements for selected points in the grounding grid, where each nodal point is marked on the illustration of the grounding grid area
- **(b)** Overall voltage distribution when the peak is reached
- **(c)** Overall voltage distribution when the entire grounding grid area is utilized
- **(d)** Overall voltage distribution at the peak current
- **(e)** Injected current in the grounding grid, with intersection markers for figs. b) to d).

4.2.1 6×6 Meshes, 3600 m^2

4.2.1.1 Soil Resistivity 300 Ωm and εr_{soil}=16, Fast Front

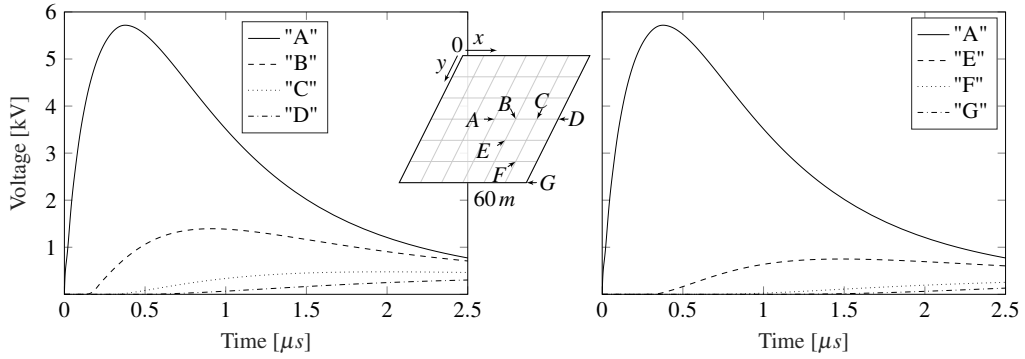

(a) Voltage distribution as function of time for selected points in the grounding grid

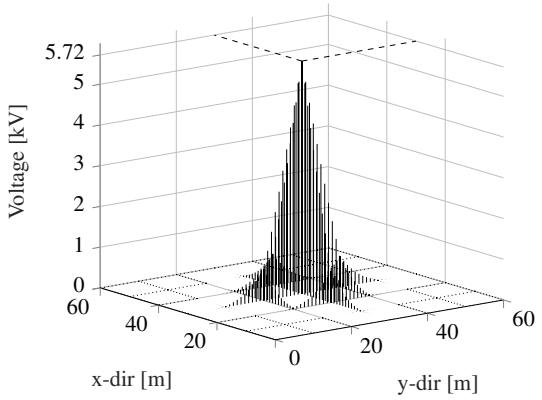

(b) t=0.38 μs, Peak voltage in the grid

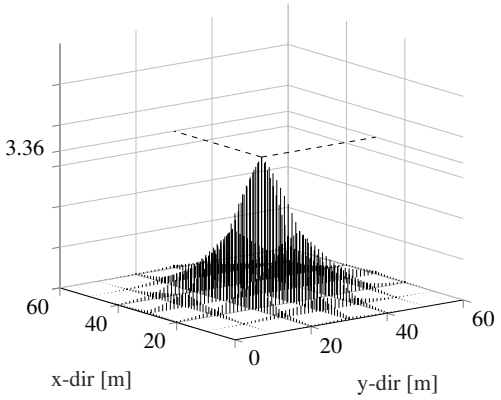

(c) t=1.04 μs, Surge reach corners

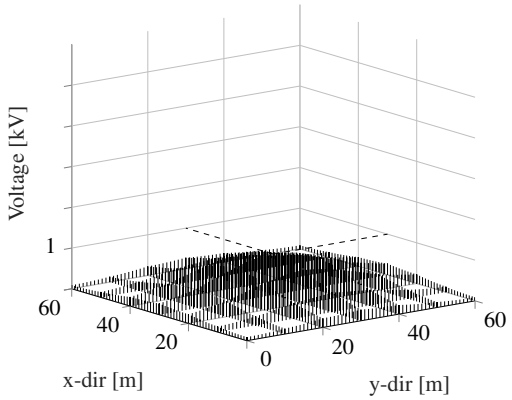

(d) t=2.2 μs, Peak current in the grid

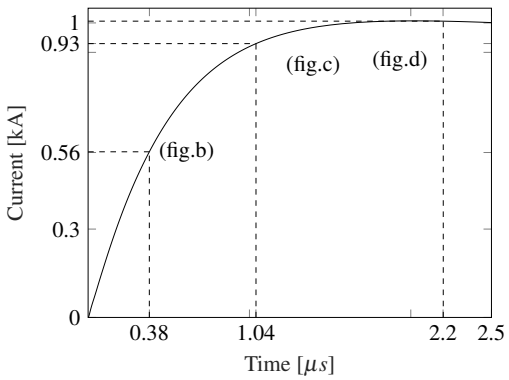

(e) Injected current in center of the grid("A")

Figure 4.5: Voltage distribution in a 6×6 grounding grid with mesh size of 10×10 m and ρ_{soil}=300 Ωm and εr_{soil}=16. Continuous voltage distribution for selected points are given in fig. 4.5a and overall distribution at chosen time steps in figs. 4.5b to 4.5d. Figure 4.5e gives the excitation current of an approximated 1 kA, 1/20 μs stroke of double exponential form in center of the grid (point "A" in fig. 4.5a). Parameters for the simulation are found in table 4.1

4.2.1.2 Soil Resistivity 1000 Ωm and εr_{soil}=16, Fast Front

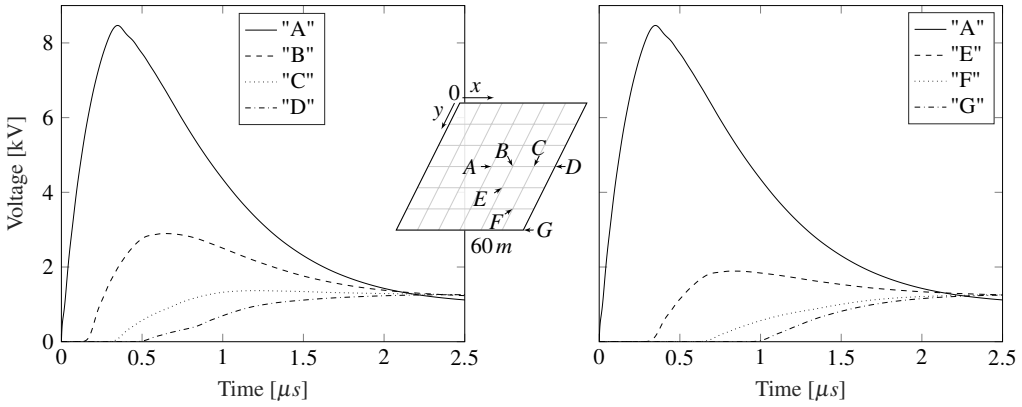

(a) Voltage distribution as function of time for selected points in the grounding grid

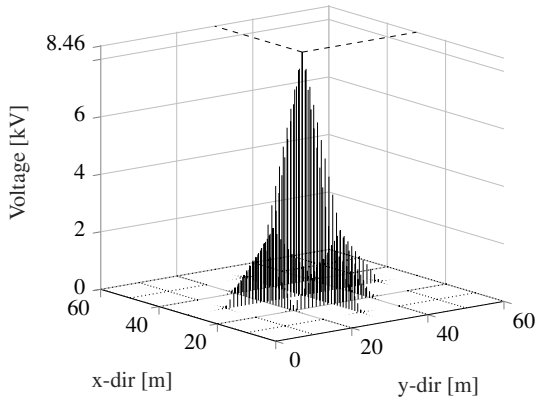

(b) t=0.35 μs, Peak voltage in the grid

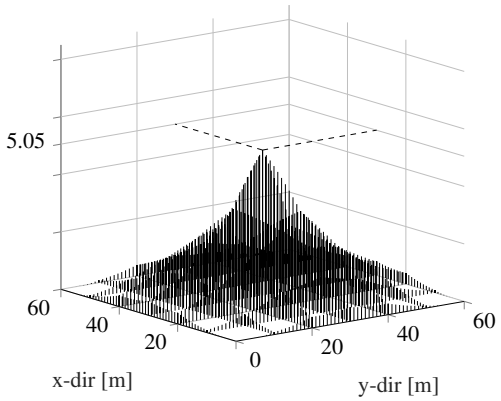

(c) t=0.88 μs, Surge reach corners

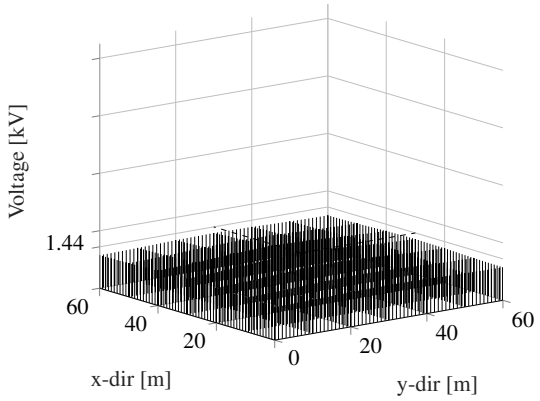

(d) t=2 μs, Peak current in the grid

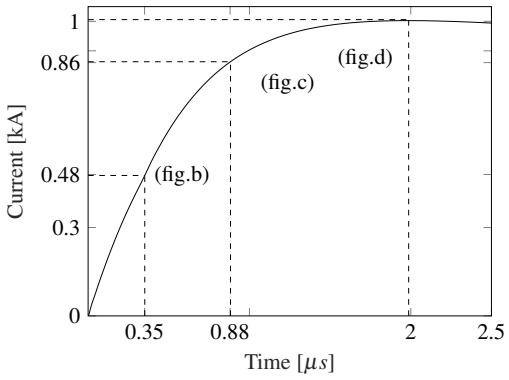

(e) Injected current in center of the grid("A")

Figure 4.6: Voltage distribution in a 6×6 grounding grid with mesh size of 10×10 m and ρ_{soil}=1000 Ωm and εr_{soil}=16. Continuous voltage distribution for selected points are given in fig. 4.6a and overall distribution at chosen time steps in figs. 4.6b to 4.6d. Figure 4.6e gives the excitation current of an approximated 1 kA, 1/20 μs stroke of double exponential form in center of the grid (point "A" in fig. 4.6a). Parameters for the simulation are found in table 4.1

4.2.1.3 Soil Resistivity 2000 Ωm and εr_{soil}=16, Fast Front

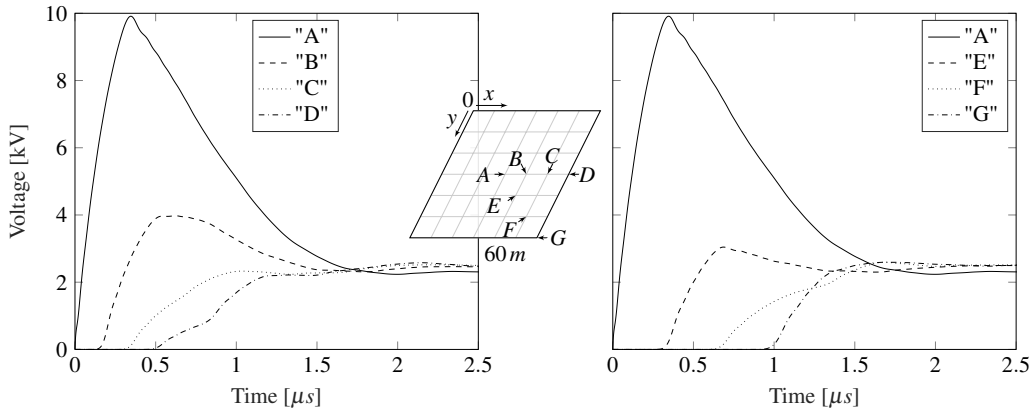

(a) Voltage distribution as function of time for selected points in the grounding grid

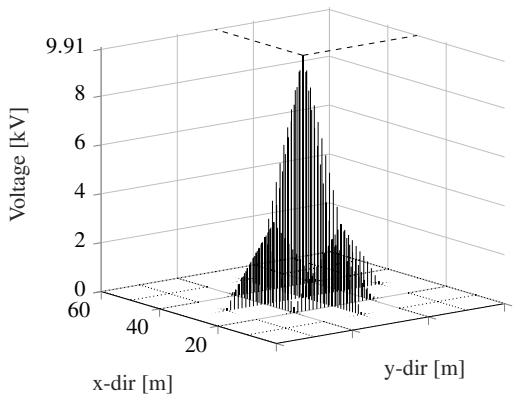

(b) t=0.35 μs, Peak voltage in the grid

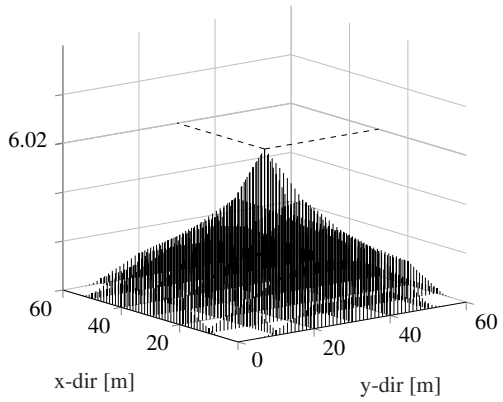

(c) t=0.86 μs, Surge reach corners

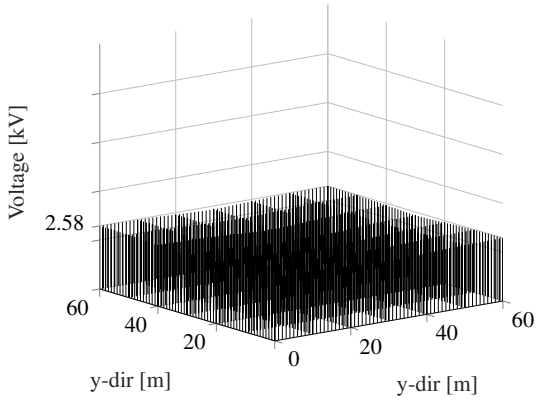

(d) t=1.83 μs, Peak current in the grid

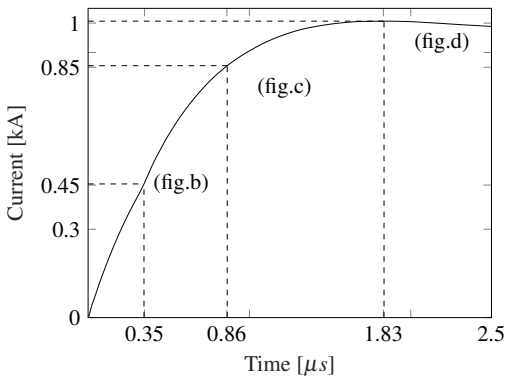

(e) Injected current in center of the grid("A")

Figure 4.7: Voltage distribution in a 6×6 grounding grid with mesh size of 10×10 m and ρ_{soil}=2000 Ωm and εr_{soil}=16. Continuous voltage distribution for selected points are given in fig. 4.7a and overall distribution at chosen time steps in figs. 4.7b to 4.7d. Figure 4.7e gives the excitation current of an approximated 1 kA, 1/20 μs stroke of double exponential form in center of the grid (point "A" in fig. 4.7a). Parameters for the simulation are found in table 4.1

4.2.1.4 Soil Resistivity 2000 Ωm and εr_{soil}=36, Fast Front

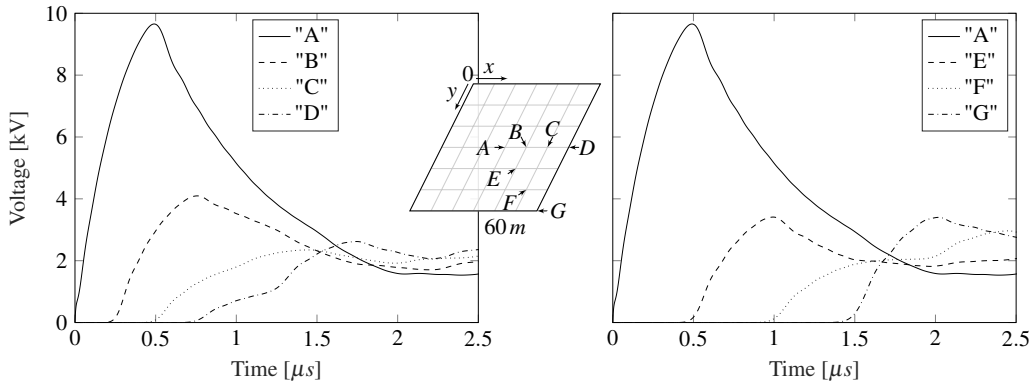

(a) Voltage distribution as function of time for selected points in the grounding grid

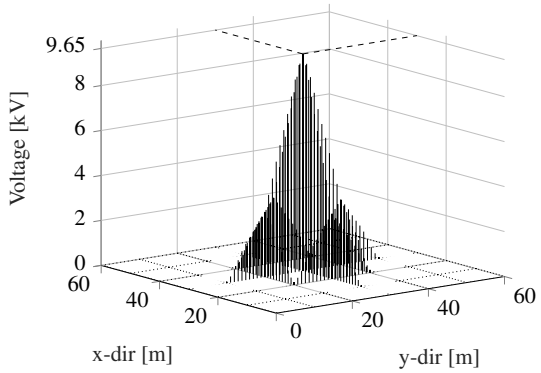

(b) t=0.49 μs, Peak voltage in the grid

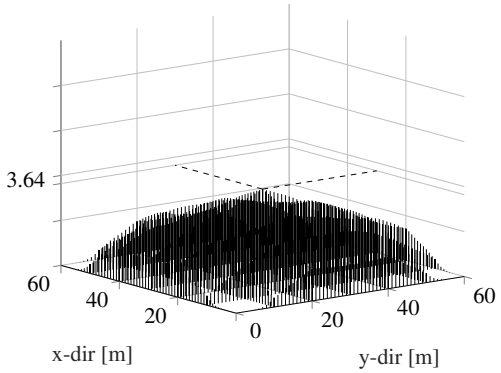

(c) t=1.30 μs, Surge reach corners

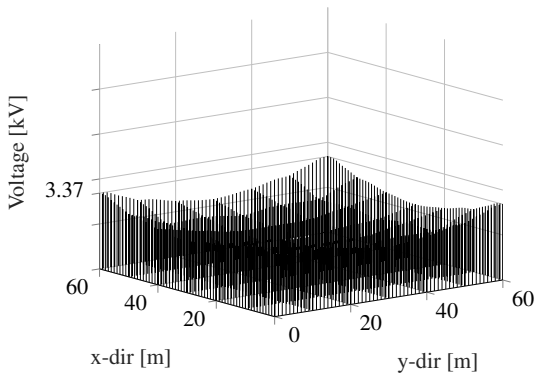

(d) t=1.98 μs, Peak current in the grid

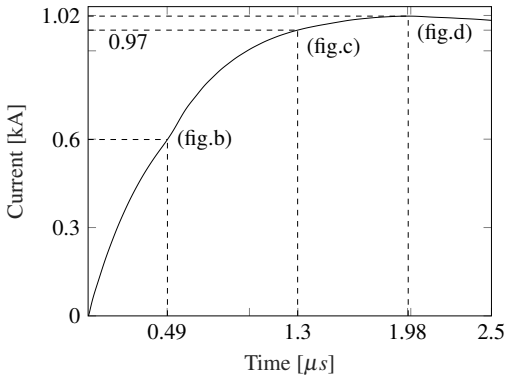

(e) Injected current in center of the grid("A")

Figure 4.8: Voltage distribution in a 6×6 grounding grid with mesh size of 10×10 m and ρ_{soil}=2000 Ωm and εr_{soil}=36. Continuous voltage distribution for selected points are given in fig. 4.8a and overall distribution at chosen time steps in figs. 4.8b to 4.8d. Figure 4.8e gives the excitation current of an approximated 1 kA, 1/20 μs stroke of double exponential form in center of the grid (point "A" in fig. 4.8a). Parameters for the simulation are found in table 4.1

4.2.1.5 Non Uniform Soil, Fast Front

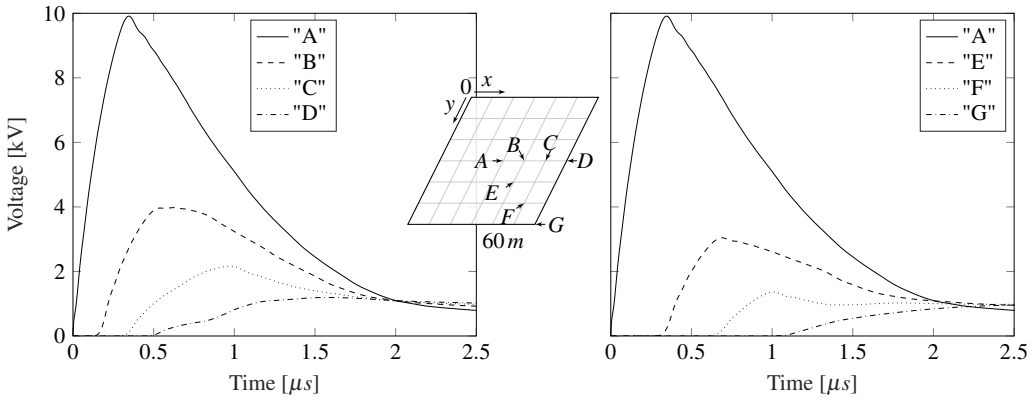

(a) Voltage distribution as function of time for selected points in the grounding grid

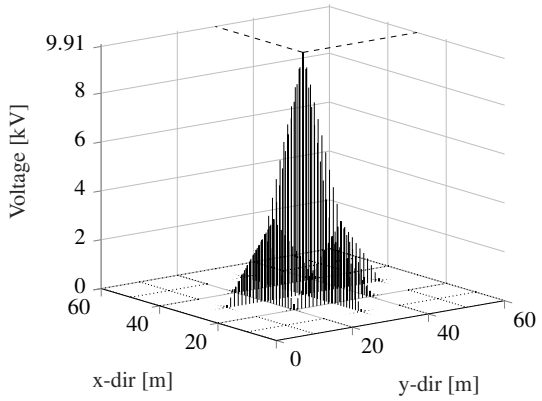

(b) t=0.35 μs, Peak voltage in the grid

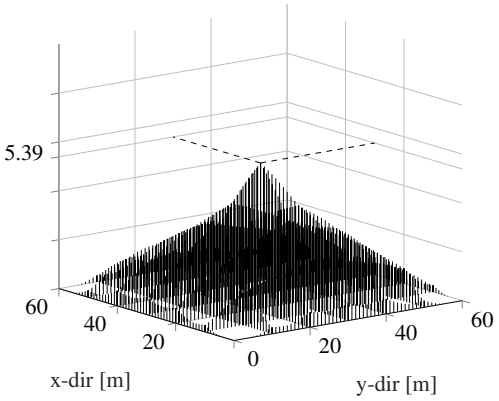

(c) t=0.95 μs, Surge reach corners

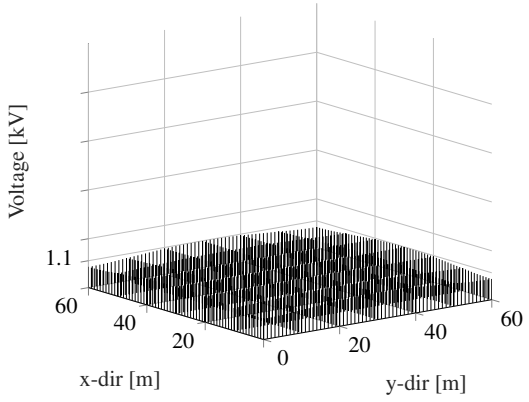

(d) t=2 μs, Peak current in the grid

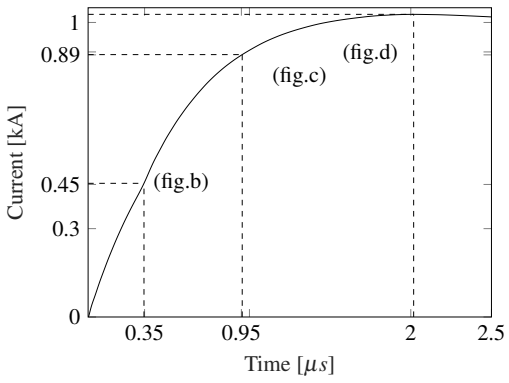

(e) Injected current in center of the grid("A")

Figure 4.9: Voltage distribution in a 6×6 grounding grid with mesh size of 10×10 m in non-uniform soil. Main grid area have soil parameters ρ_{soil}=2000 Ωm and εr_{soil}=16 while the outer conductors ring has ρ_{soil}=300 Ωm and εr_{soil}=36. Continuous voltage distribution for selected points are given in fig. 4.9a and overall distribution at chosen time steps in figs. 4.9b and 4.9d. Figure 4.9e gives the excitation current of an approximated 1 kA, 1/20 μs stroke of double exponential form in center of the grid (point "A" in fig. 4.9a). Parameters for the simulation are found in table 4.1

4.2.1.6 Soil Resistivity 2000 Ωm and εr_{soil}=16, Slow Front

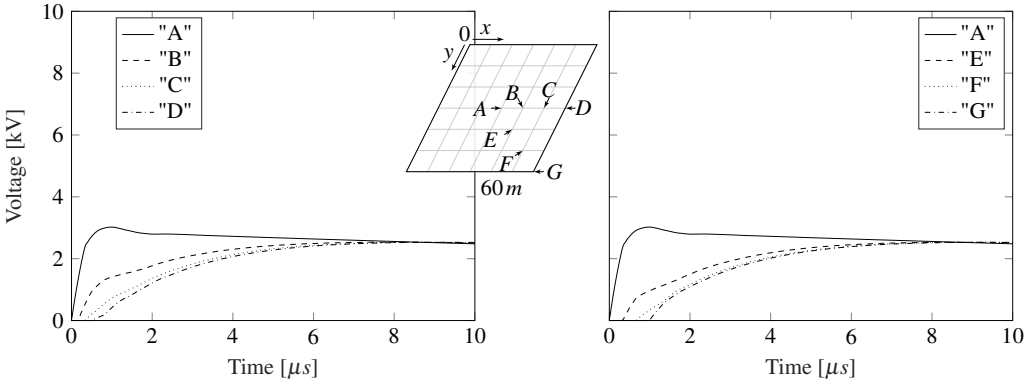

(a) Voltage distribution as function of time for selected points in the grounding grid

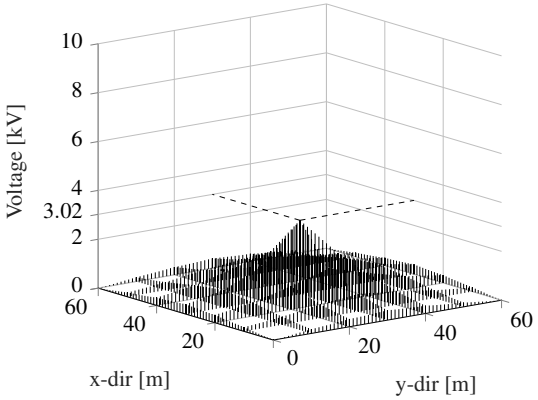

(b) t=0.88 μs, Peak voltage in the grid

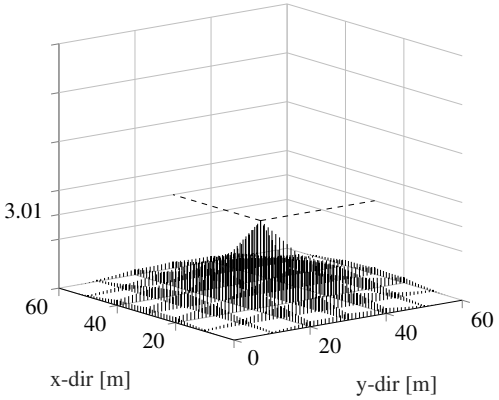

(c) t=0.99 μs, Surge reach corners

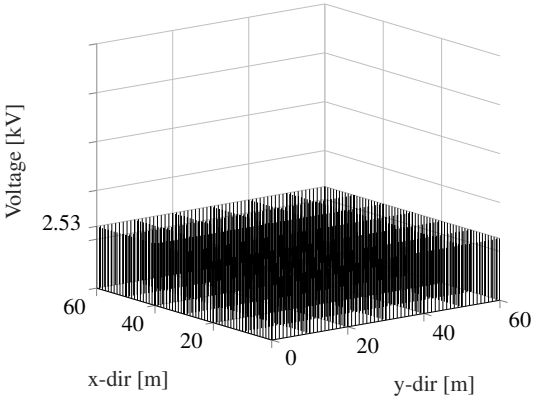

(d) t=8.6 μs, Peak current in the grid

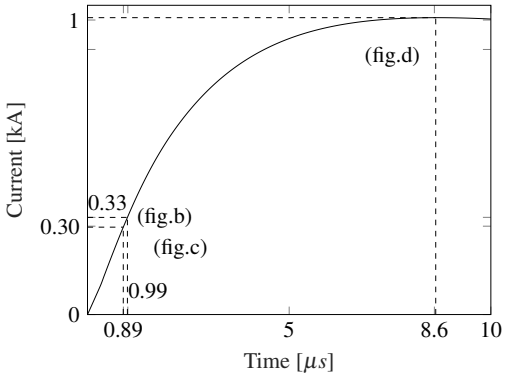

(e) Injected current in center of the grid("A")

Figure 4.10: Voltage distribution in a 6×6 grounding grid with mesh size of 10×10 m and ρ_{soil}=2000 Ωm and εr_{soil}=16. Continuous voltage distribution for selected points are given in fig. 4.10a and overall distribution at chosen time steps in figs. 4.10b to 4.10d. Figure 4.10e gives the excitation current of an approximated 1 kA, 5/20 μs stroke of double exponential form in center of the grid (point "A" in fig. 4.10a). Parameters for the simulation are found in table 4.1

4.2.2 4×4 Meshes, 1600 m^2

4.2.2.1 Soil Resistivity 2000 Ωm and εr_{soil}=16, Fast Front

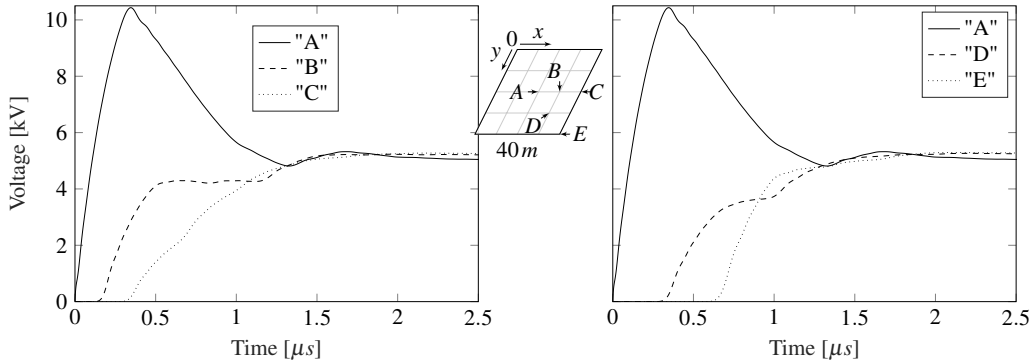

(a) Voltage distribution as function of time for selected points in the grounding grid

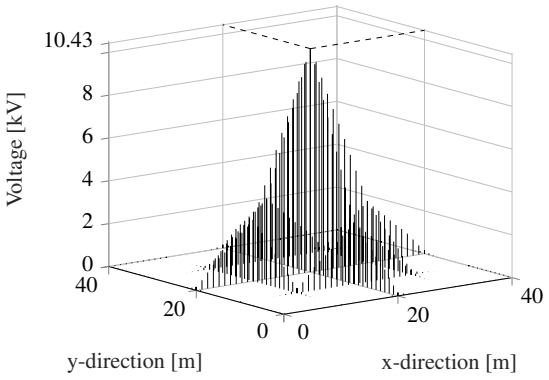

(b) t=0.35 μs, Peak voltage in the grid

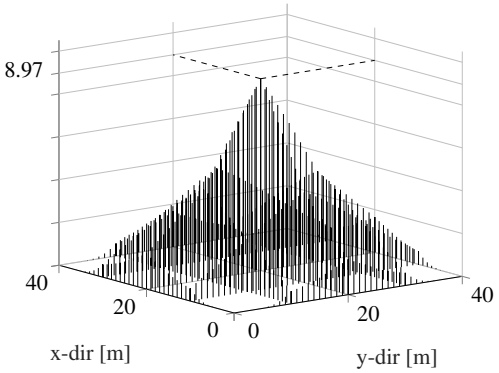

(c) t=0.54 μs, Surge reach corners

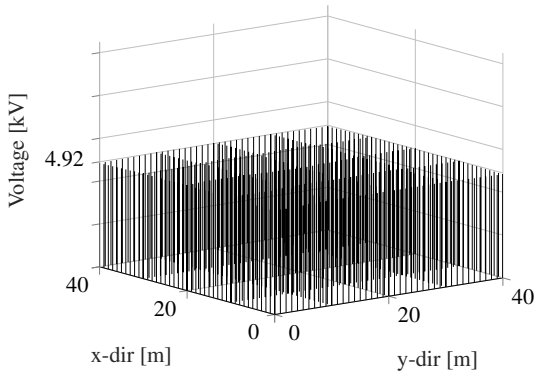

(d) t=1.37 μs, Peak current in the grid

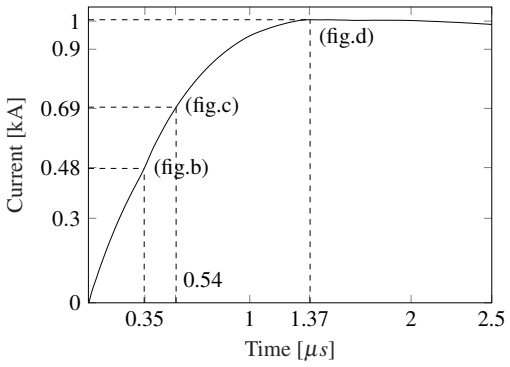

(e) Injected current in center of the grid("A")

Figure 4.11: Voltage distribution in a 4×4 grounding grid with mesh size of 10×10 m and ρ_{soil}=2000 Ωm and εr_{soil}=16. Continuous voltage distribution for selected points are given in fig. 4.11a and overall distribution at chosen time steps in figs. 4.11b to 4.11d. Figure 4.11e gives the excitation current of an approximated 1 kA, 1/20 μs stroke of double exponential form in center of the grid (point "A" in fig. 4.11a). Parameters for the simulation are found in table 4.1

4.2.3 12×12 Meshes, 3600 m^2

4.2.3.1 Soil Resistivity 2000 Ωm and εr_{soil}=16, Fast Front

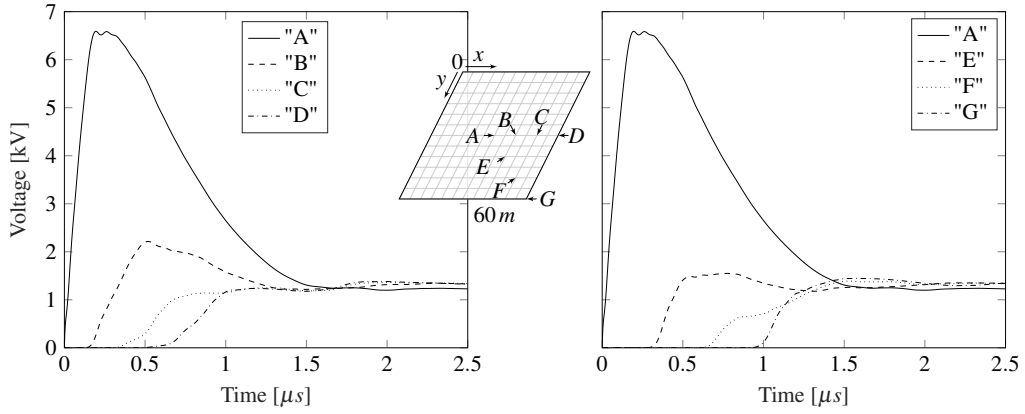

(a) Voltage distribution as function of time for selected points in the grounding grid

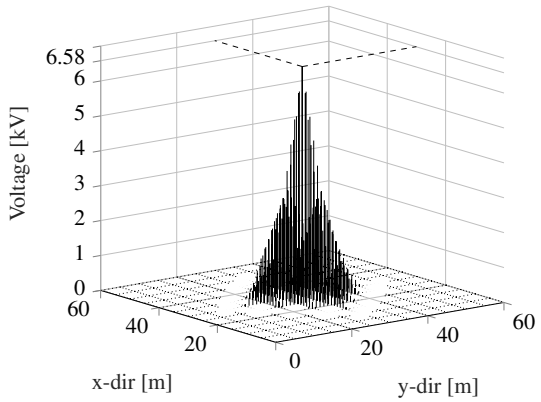

(b) t=0.26 μs, Peak voltage in the grid

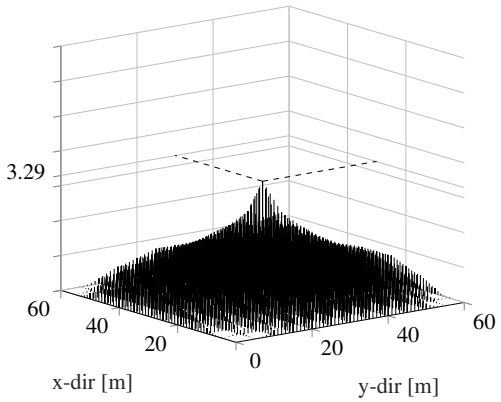

(c) t=0.87 μs, Surge reach corners

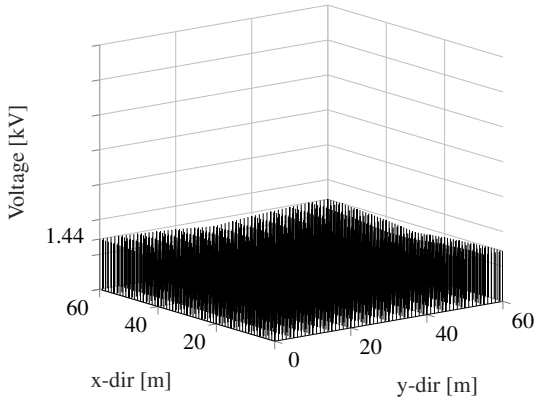

(d) t=1.68 μs, Peak current in the grid

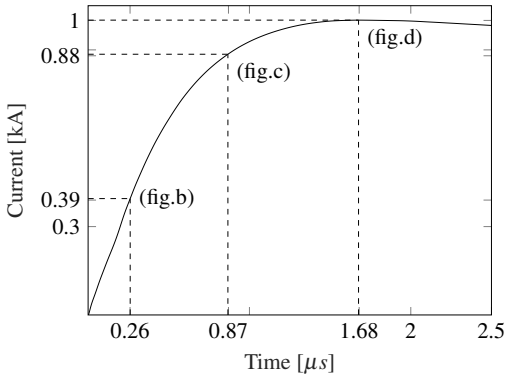

(e) Injected current in center of the grid("A")

Figure 4.12: Voltage distribution in a 12×12 grounding grid with mesh size of 5×5 m and ρ_{soil}=2000 Ωm and εr_{soil}=16. Continuous voltage distribution for selected points are given in fig. 4.12a and overall distribution at chosen time steps in figs. 4.12b to 4.12d. Figure 4.12e gives the excitation current of an approximated 1 kA, 1/20 μs stroke of double exponential form in center of the grid(point "A" in fig. 4.12a). Parameters for the simulation are found in table 4.1

4.2.4 8×8 Meshes, 1600 m^2

4.2.4.1 Soil Resistivity 2000 Ωm and εr_{soil}=16, Fast Front

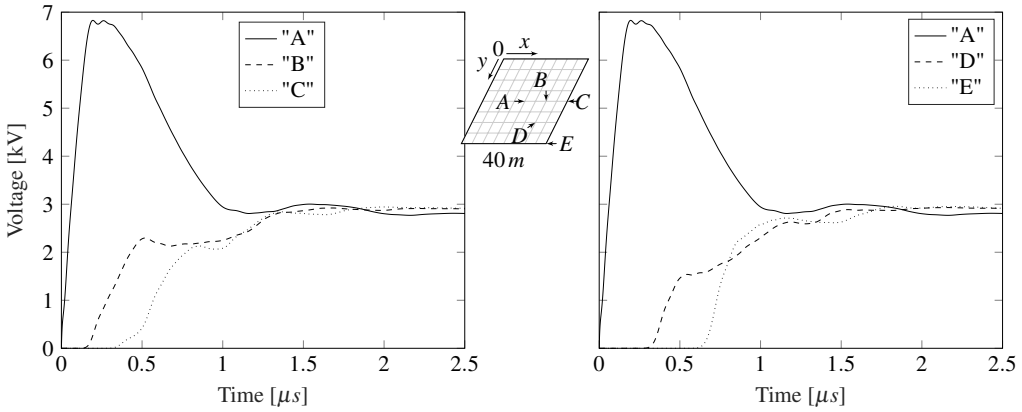

(a) Voltage distribution as function of time for selected points in the grounding grid

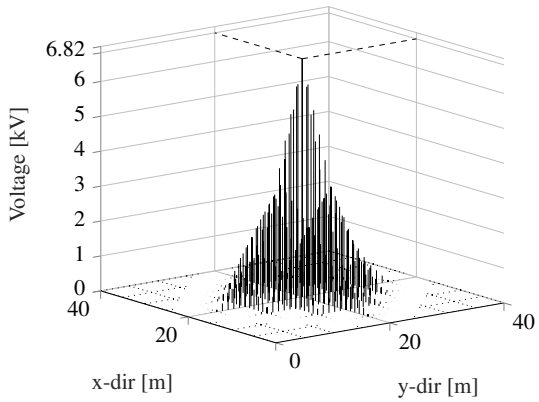

(b) t=0.26 μs, Peak voltage in the grid

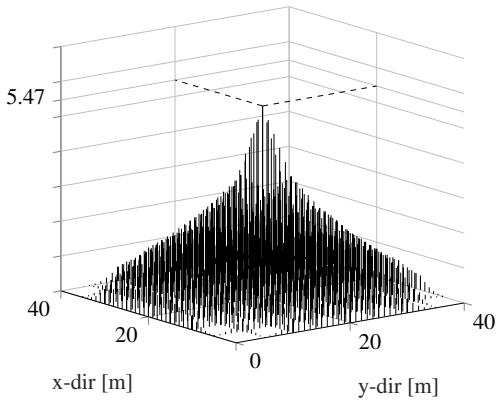

(c) t=0.55 μs, Surge reach corners

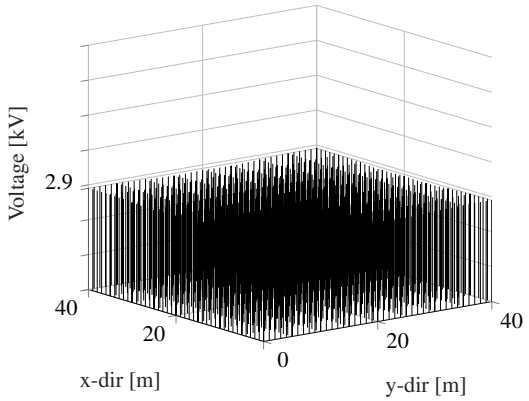

(d) t=1.74 μs, Peak current in the grid

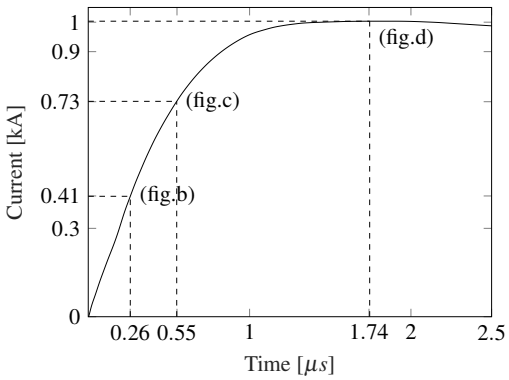

(e) Injected current in center of the grid("A")

Figure 4.13: Voltage distribution in a 8×8 grounding grid with mesh size of 5×5 m and ρ_{soil}=2000 Ωm and εr_{soil}=16. Continuous voltage distribution for selected points are given in fig. 4.13a and overall distribution at chosen time steps in figs. 4.13b to 4.13d. Figure 4.13e gives the excitation current of an approximated 1 kA, 1/20 μs stroke of double exponential form in center of the grid(point "A" in fig. 4.13a). Parameters for the simulation are found in table 4.1

4.3 First Segment from the Injection Point

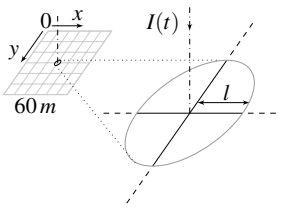

Figure 4.14: First wire segment from the injection point of length "l"

The first segment grounding wire after the injection point is studied with various soil resistivity and condition as in section 4.2. The selected results is presented by the simulation performed in section 4.2.1 and considers the 10 m mesh size 6×6 grounding grid configuration of 3600 m^2. From the implemented model in chapter 3 the per-unit length are set to one meter. This also applies for the first segment length, l, as illustrated in fig. 4.14. When considering the soil as uniform, the injected current is equally distributed from the center point of the first wire segment into the grounding grid system. The considered symmetry simplifies the present results current distribution, by only considering one of the four segments in the star point (circled area in fig. 4.14). Each segment of length l consist of basic fundamental electric elements in a t-section circuit form, as shown in section 3.1.1 and fig. 3.1, where measurement nodes for current and voltage is implemented.

In section 4.3.1 follows the results for the t-section measurement nodes during a fast front surge with sensitivity of soil resistivity. In section 4.3.2 the slow front simulation is considered.

The sub-figures are presenting:

- **(a)** Voltage potential over the first inductive element, V_{l1}
- **(b)** Current trough the first inductive element, A_{l1}
- **(c)** Voltage potential over the second inductive element, V_{l2}
- **(d)** Current trough the second inductive element, A_{l1}
- **(e)** Voltage potential from the t-section middle section to true ground, V_{gc}
- **(f)** Current leaked to the soil, A_g
- **(g)** Capacitive current to the soil, A_g

4.3.1 Fast Front Surge

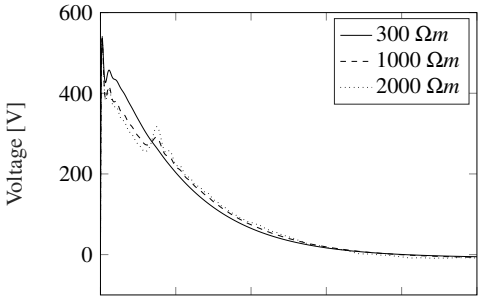

(a) Inductance voltage, V_{l1}

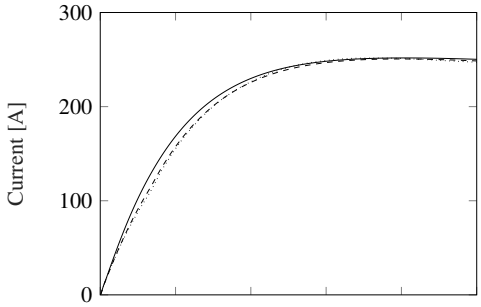

(b) Inductance current, A_{l1}

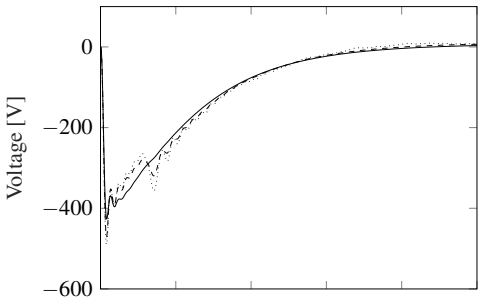

(c) Inductance voltage, V_{l2}

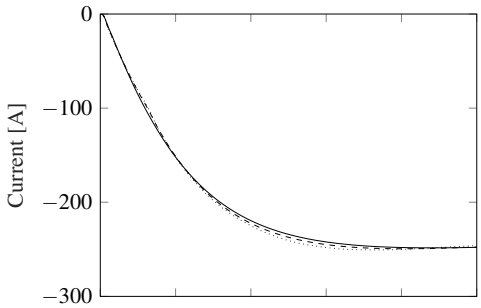

(d) Inductance current, A_{l2}

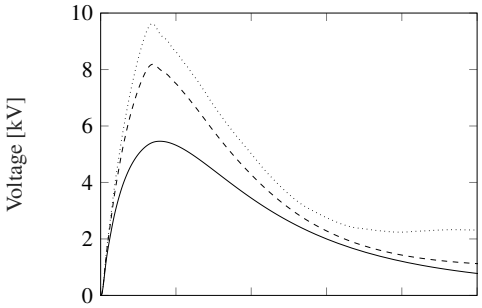

(e) Conductance and capacitance voltage to "true ground", V_{gc}

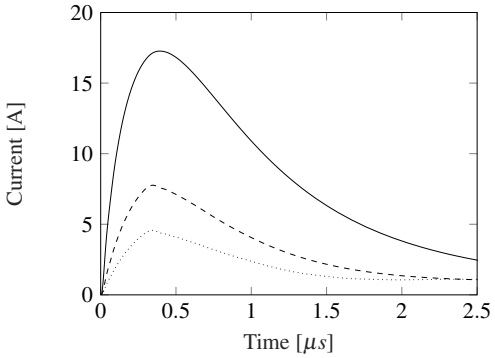

(f) Conductance current, A_g

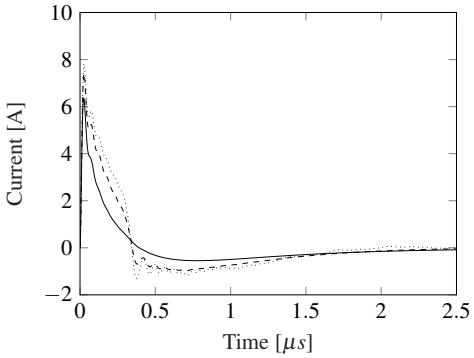

(g) Capacitance current, A_c

Figure 4.15: Voltage and current measurement of the first segment grounding wire of a 6×6 grounding grid with mesh size of 10×10 m, according to fig. 4.14. Measurement definitions are found in section 3.1.1 and fig. 3.1. Results evaluated from simulation performed in sections 4.2.1.1 to 4.2.1.3 for ρ_{soil} 300, 1000 and 2000 Ωm simulation, respectively

4.3.2 Slow Front Surge

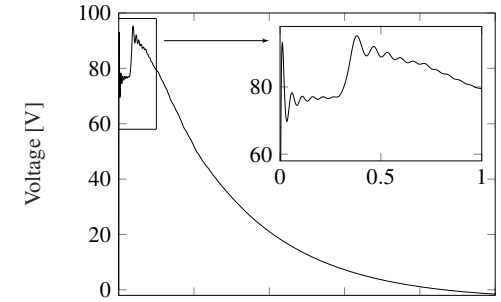

(a) Voltage over the inductance l1

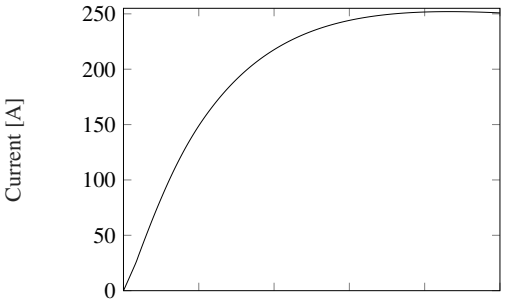

(b) Current trough the inductance l1

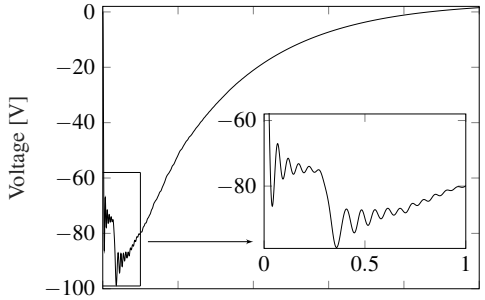

(c) Voltage over the inductance l2

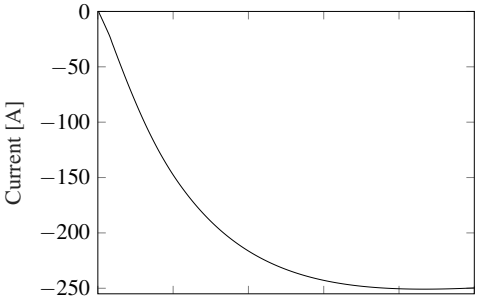

(d) Current trough the inductance l2

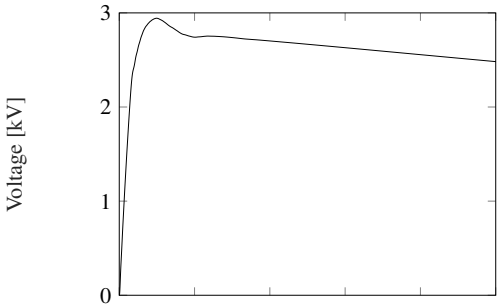

(e) Voltage over the conductance and capacitance to "true ground"

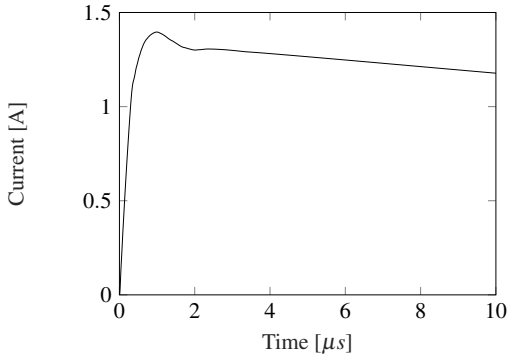

(f) Conductance current, leakage to soil

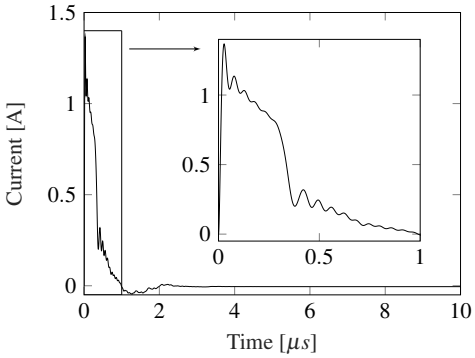

(g) Capacitance current

Figure 4.16: Voltage and current measurement of the first segment grounding wire of a 6×6 grounding grid with mesh size of 10×10 m, according to fig. 4.14. Measurement definitions are found in section 3.1.1 and fig. 3.1. Results evaluated from simulation performed in section 4.2.1.6 for ρ_{soil} 2000 Ωm simulation

4.4 Grounding Grid Model Integrated, Short Cable

As described in section 3.3 the grounding grid model in Matlab®/Simulink® and transmission system model in EMTP-RV is interfaced to perform co-simulation. With reference to section 3.3 and fig. 3.5 a lightning strikes the 300 kV overhead transmission line (Z_{cl}=400) at l_l=10 km distance from a substation. A shielding failure causes an injected current having a magnitude of 1 kA and 1.2/50 μs of CIGRE waveform stroke to flow towards the substation. In the substation, the cable is l_c=10 m (Z_{cc}=45) between the surge arrester and transformer.
Figure 4.17 shows the simulation results of the transmission system when the grounding system is ignored, setting the surge arrester discharge path to true ground.

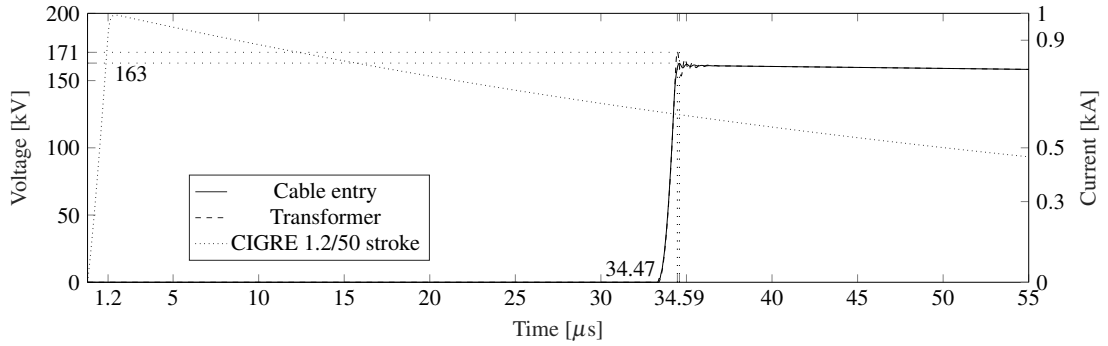

Figure 4.17: Ignoring grounding system and short cable case: transmission system nodal voltages and CIGRE 1.2/50 μs injected current stroke in far-end (l_l=10 km)

For each simulation case following in section 4.4 the results are given when a grounding system is added as the surge arrester injection point. The results are presented by a figure which collects selected plots and overall grounding grid voltage distribution views. With reference to the individual subsections main figure the grounding grid configuration is described in addition to soil properties and injected current.
The sub-figures are presenting:

- **(a)** Transmission system nodal voltages for the cable entry and transformer
- **(b)** Injection point voltage and current of the grounding system
- **(c)** Nodal measurements for selected points in the grounding grid, where each nodal point is marked on the illustration of the grounding grid area
- **(d)** Overall voltage distribution when the peak is reached
- **(e)** Overall voltage distribution when the corner peak is reached

4.4.1 6×6 Meshes, 3600 m^2

4.4.1.1 Soil resistivity 2000 Ωm and εr_{soil}=16

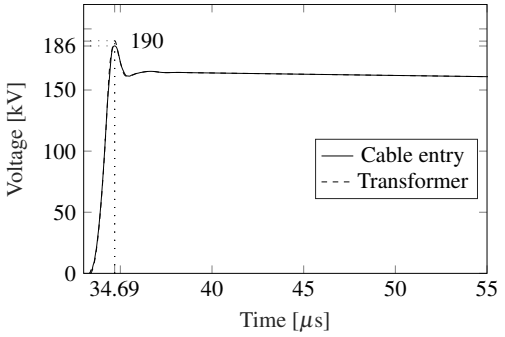

(a) Transmission system nodal voltages

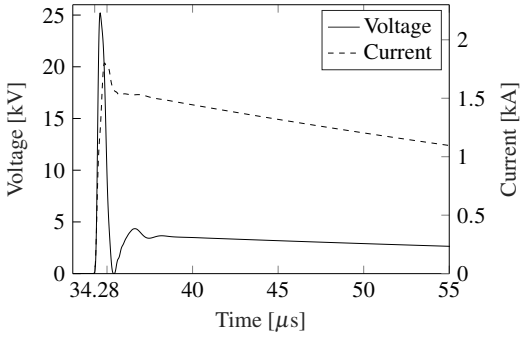

(b) Injection point current and voltage

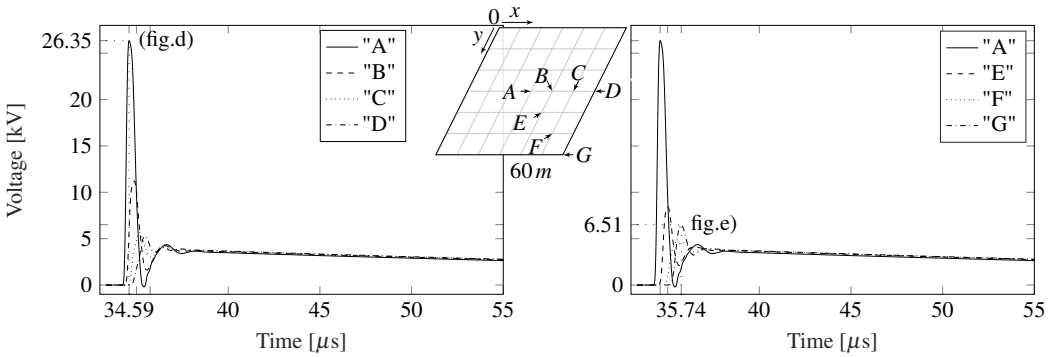

(c) Voltage distribution for selected points in the grounding grid

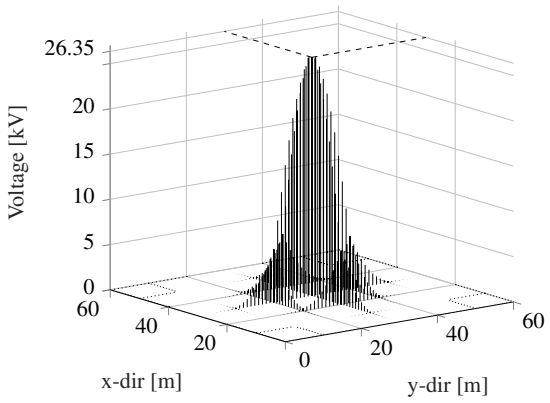

(d) t=34.59 μs, peak first stroke

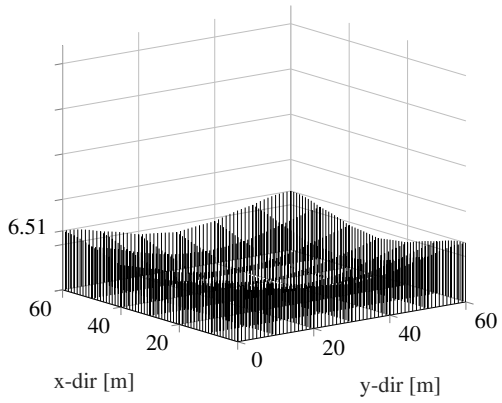

(e) t=35.74 μs, peak corner

Figure 4.18: Short cable case: integration of grounding model of 6×6 meshes of size 10×10 m, ρ_{soil}=2000 Ωm and εr_{soil}=16. Physical grounding grid properties are found in table 4.1a. Surge current, CIGRE 1.2/50 μs, impressed in far-end as shown in fig. 4.17. Nodal voltages at cable entry and transformer is shown in fig. 4.18a. From the surge arrester, placed at the cable entry, the injected point voltage and current to the grounding system are given in fig. 4.18b. Continuous voltage distribution for selected points are given in fig. 4.18c and overall distribution in figs. 4.18d and 4.18e at the peak voltage and the peak corner voltage, respectively

4.4.2 4×4 Meshes, 1600 m^2

4.4.2.1 Soil resistivity 2000 Ωm and εr_{soil}=16

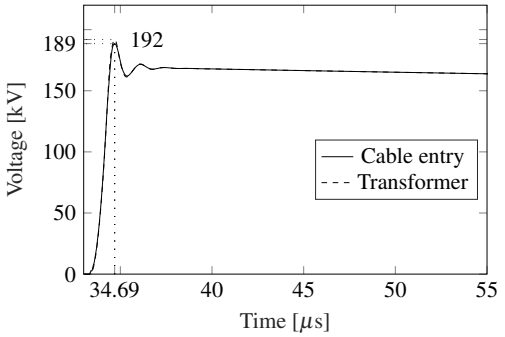

(a) Transmission system nodal voltages

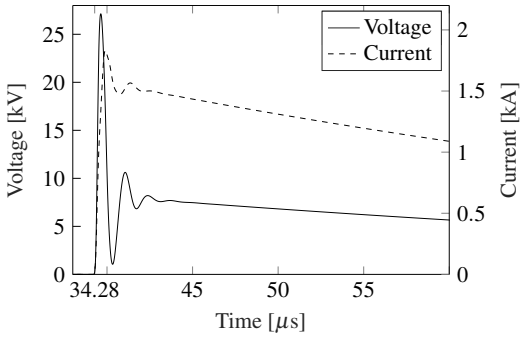

(b) Injection point current and voltage

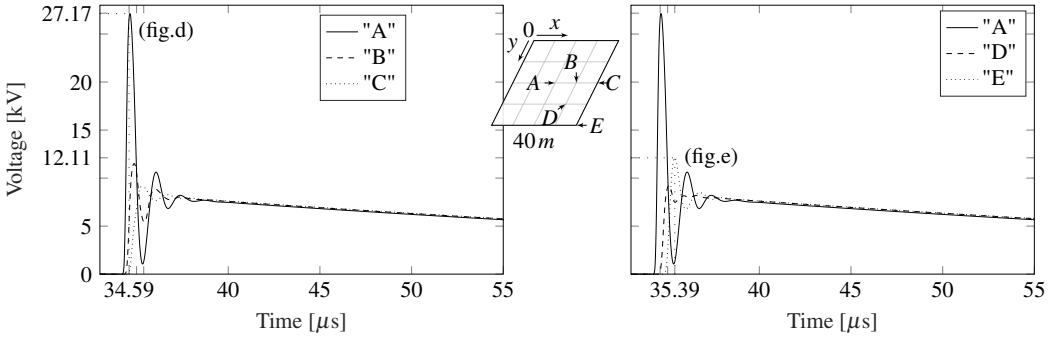

(c) Voltage distribution for selected points in the grounding grid

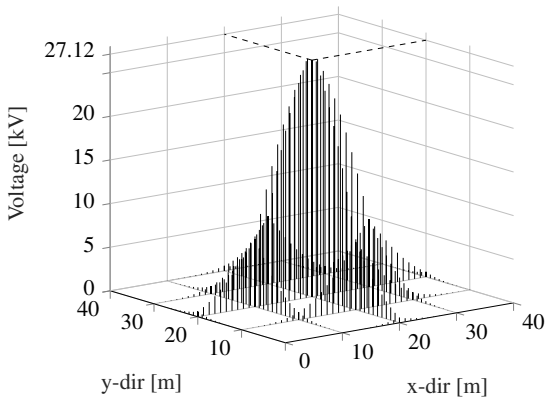

(d) t=34.59 μs, peak second stroke

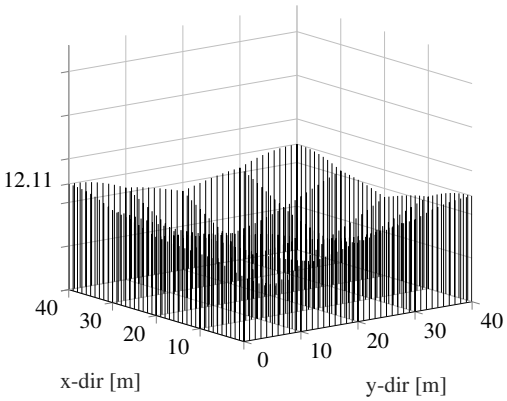

(e) t=35.39 μs, peak corner

Figure 4.19: Short cable case: integration of grounding model of 4×4 meshes of size 10×10 m, ρ_{soil}=2000 Ωm and εr_{soil}=16. Physical grounding grid properties are found in table 4.1a. Surge current, CIGRE 1.2/50 μs, impressed in far-end as shown in fig. 4.17. Nodal voltages at cable entry and transformer is shown in fig. 4.19a. From the surge arrester, placed at the cable entry, the injected point voltage and current to the grounding system are given in fig. 4.19b. Continuous voltage distribution for selected points are given in fig. 4.19c and overall distribution in figs. 4.19d and 4.19e at the peak voltage and the peak corner voltage, respectively

4.4.3 8×8 Meshes, 1600 m^2

4.4.3.1 Soil resistivity 2000 Ωm and εr_{soil}=16

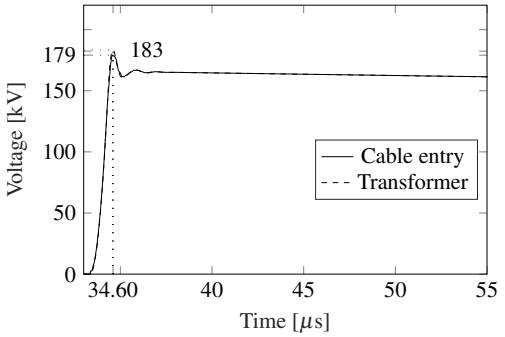

(a) Transmission system nodal voltages

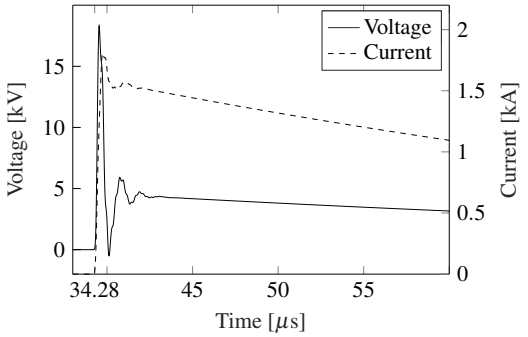

(b) Injection point current and voltage

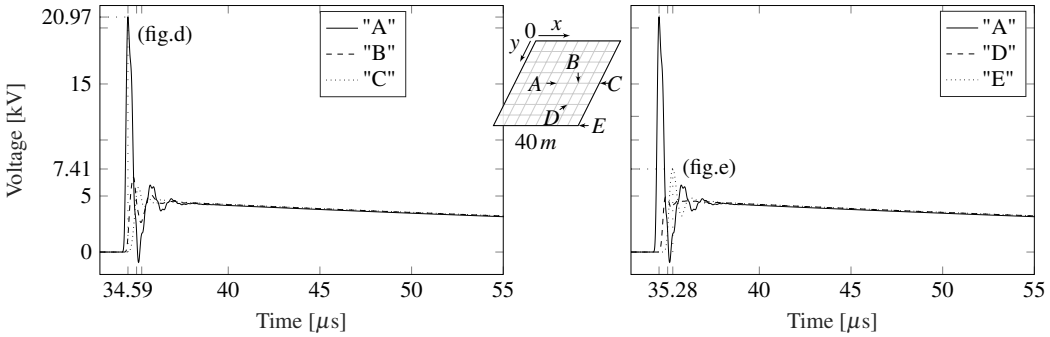

(c) Voltage distribution for selected points in the grounding grid

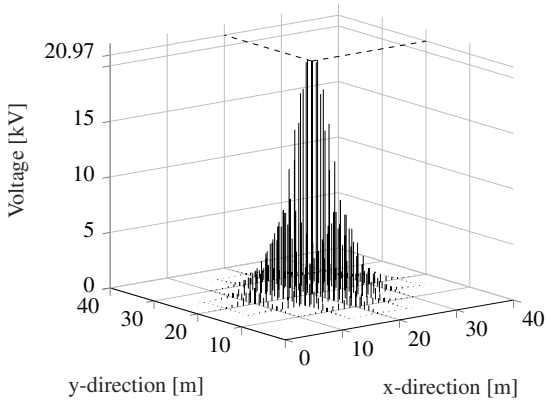

(d) t=34.59 μs, peak second stroke

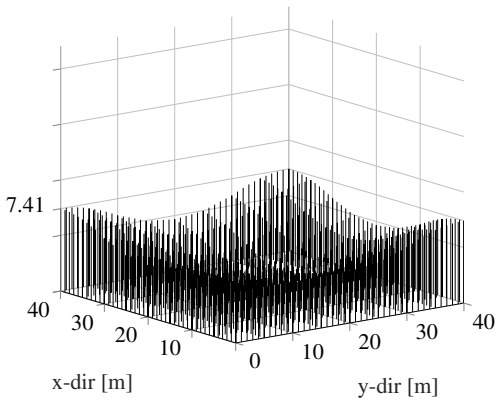

(e) t=35.28 μs, peak corner

Figure 4.20: Short cable case: integration of grounding model of 8×8 meshes of size 5×5 m, ρ_{soil}=2000 Ωm and εr_{soil}=16. Physical grounding grid properties are found in table 4.1a. Surge current, CIGRE 1.2/50 μs, impressed in far-end as shown in fig. 4.17. Nodal voltages at cable entry and transformer is shown in fig. 4.20a. From the surge arrester, placed at the cable entry, the injected point voltage and current to the grounding system are given in fig. 4.20b. Continuous voltage distribution for selected points are given in fig. 4.20c and overall distribution in figs. 4.20d and 4.20e at the peak voltage and the peak corner voltage, respectively

4.5 Grounding Grid Model Integrated, Long Cable

As for the short cable case in section 4.4 the grounding grid model in Matlab®/Simulink® and transmission system model in EMTP-RV is interfaced to perform co-simulation. With reference to section 3.3 and fig. 3.5 a lightning strikes the 300 kV overhead transmission line (Z_{cl}=400) at l_l=10 km distance from a substation. A shielding failure causes an injected current having a magnitude of 1 kA and 1.2/50 μs of CIGRE waveform stroke to flow towards the substation. In the long cable case l_c=500 m (Z_{cc}=45) between the surge arrester and transformer.
Figure 4.17 shows the simulation results of the transmission system when a relatively long cable is used between the surge arrester and transformer. The grounding system is ignored, setting the surge arrester discharge path to true ground.

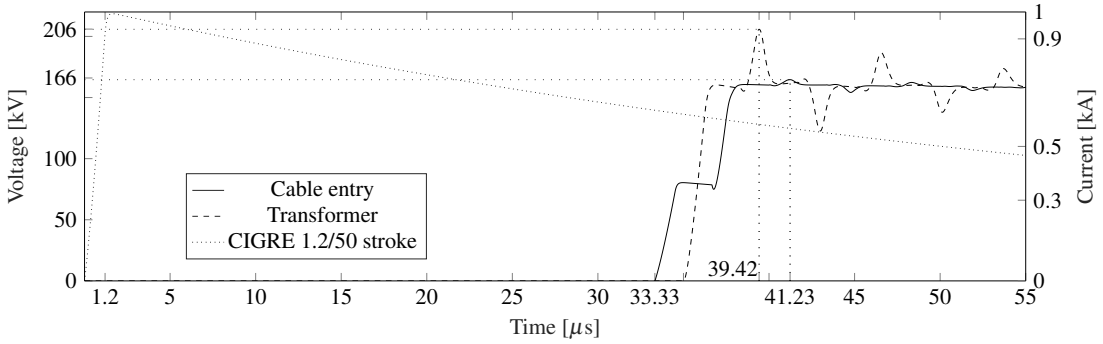

Figure 4.21: Ignoring grounding system and long cable case: transmission system nodal voltages and CIGRE 1.2/50 μs injected current stroke in far-end (l_l=10 km)

For each simulation case following in section 4.5 the results are given when a grounding system is added as the surge arrester injection point. The result is presented by a figure which collects selected plots and overall grounding grid voltage distribution views. With reference to the individual subsections main figure the grounding grid configuration is described in addition to soil properties and injected current.
The sub-figures are presenting:

- **(a)** Transmission system nodal voltages for the cable entry and transformer
- **(b)** Injection point voltage and current of the grounding system
- **(c)** Nodal measurements for selected points in the grounding grid, where each nodal point is marked on the illustration of the grounding grid area
- **(d)** Overall voltage distribution when the peak is reached
- **(e)** Overall voltage distribution when the corner peak is reached

4.5.1 6×6 Meshes and 3600 m^2

4.5.1.1 Soil resistivity 1000 Ωm and εr_{soil}=16

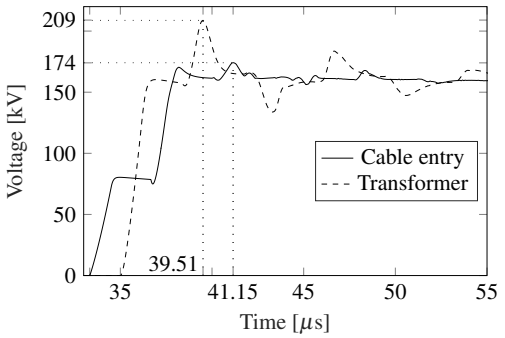

(a) Transmission system nodal voltages

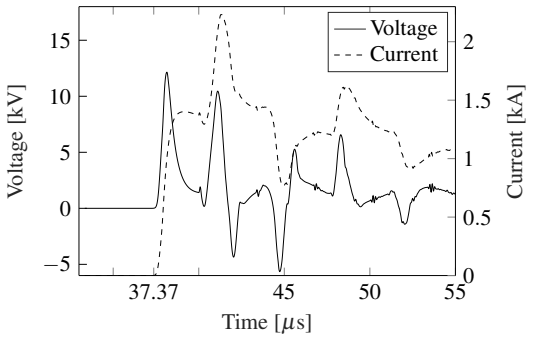

(b) Injection point current and voltage

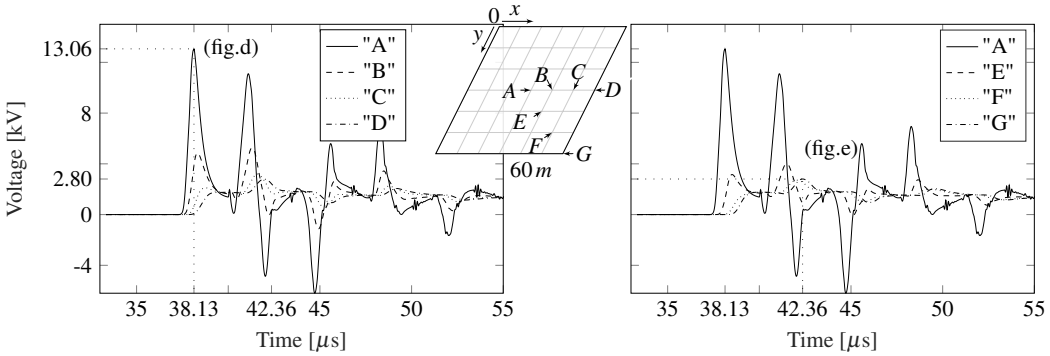

(c) Voltage distribution for selected points in the grounding grid

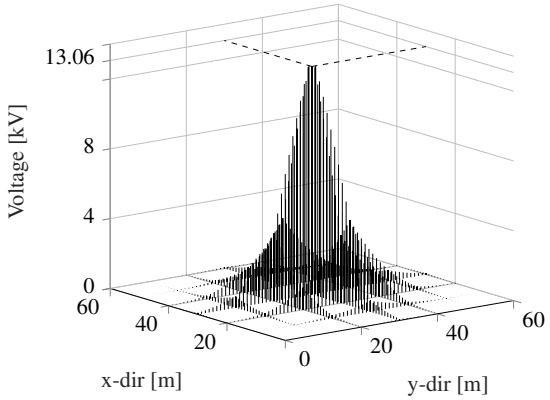

(d) t=38.13 μs, peak first stroke

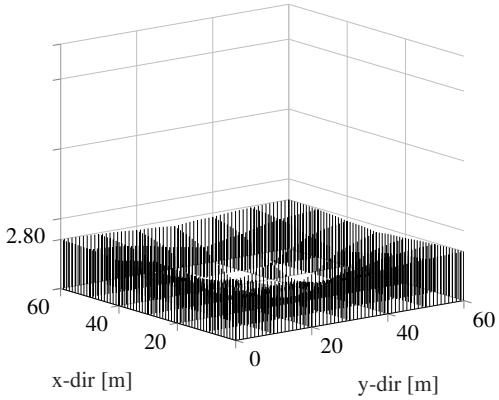

(e) t=42.36 μs, peak corner

Figure 4.22: Long cable case: integration of grounding model of 6×6 meshes of size 10×10 m, ρ_{soil}=1000 Ωm and εr_{soil}=16. Physical grounding grid properties are found in table 4.1a. Surge current, CIGRE 1.2/50 μs, impressed in far-end as shown in fig. 4.21. Nodal voltages at cable entry and transformer is shown in fig. 4.22a. From the surge arrester, placed at the cable entry, the injected point voltage and current to the grounding system are given in fig. 4.22b. Continuous voltage distribution for selected points are given in fig. 4.22c and overall distribution in figs. 4.22d and 4.22e at the peak voltage and the peak corner voltage, respectively

4.5.1.2 Soil resistivity 2000 Ωm and εr_{soil}=16

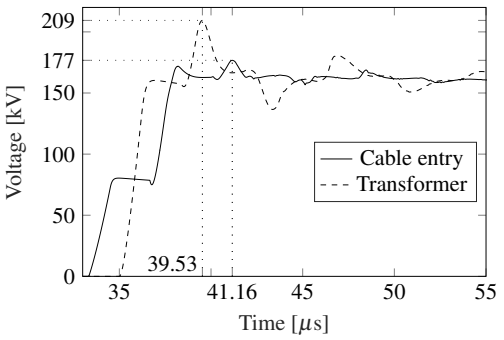

(a) Transmission system nodal voltages

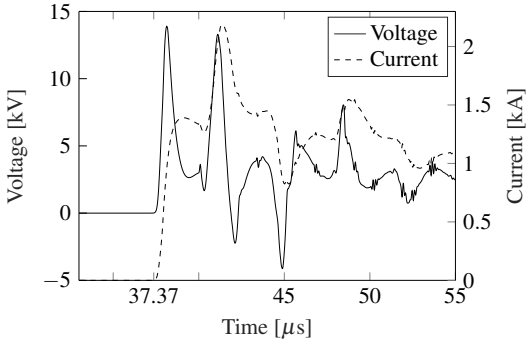

(b) Injection point current and voltage

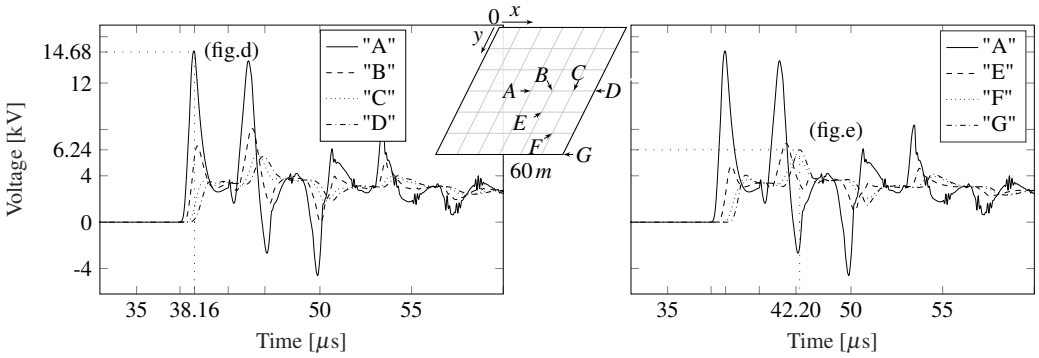

(c) Voltage distribution for selected points in the grounding grid

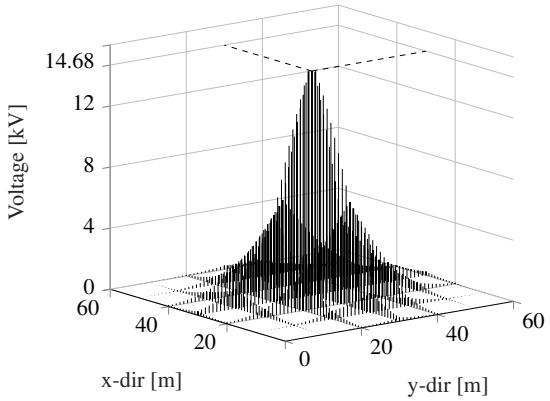

(d) t=38.16 μs, peak first stroke

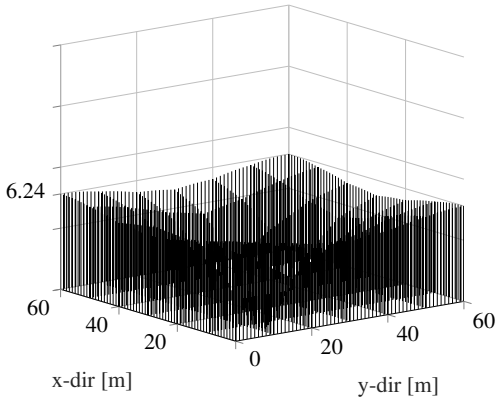

(e) t=42.20 μs, peak corner

Figure 4.23: Long cable case: integration of grounding model of 6×6 meshes of size 10×10 m, ρ_{soil}=2000 Ωm and εr_{soil}=16. Physical grounding grid properties are found in table 4.1a. Surge current, CIGRE 1.2/50 μs, impressed in far-end as shown in fig. 4.21. Nodal voltages at cable entry and transformer is shown in fig. 4.23a. From the surge arrester, placed at the cable entry, the injected point voltage and current to the grounding system are given in fig. 4.23b. Continuous voltage distribution for selected points are given in fig. 4.23c and overall distribution in figs. 4.23d and 4.23e at the peak voltage and the peak corner voltage, respectively

4.5.1.3 Soil resistivity 2000 Ωm and εr_{soil}=36

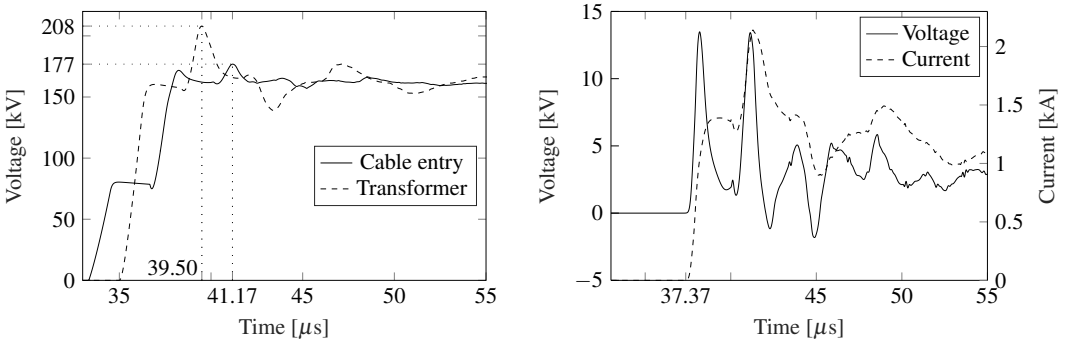

(a) Transmission system nodal voltages **(b)** Injection point current and voltage

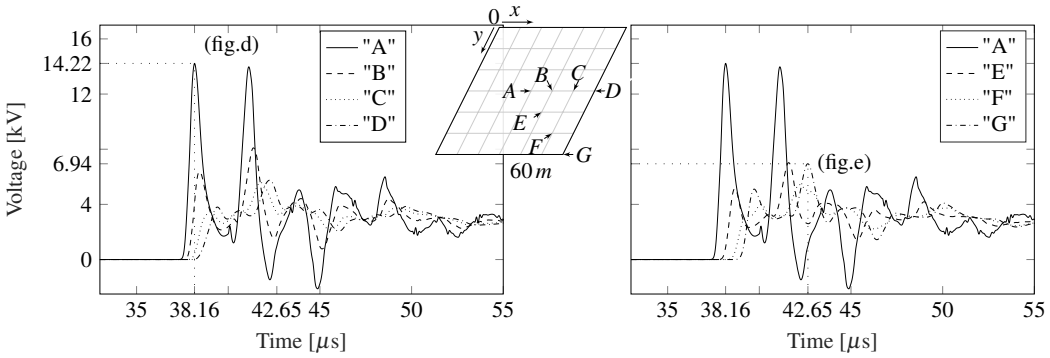

(c) Voltage distribution for selected points in the grounding grid

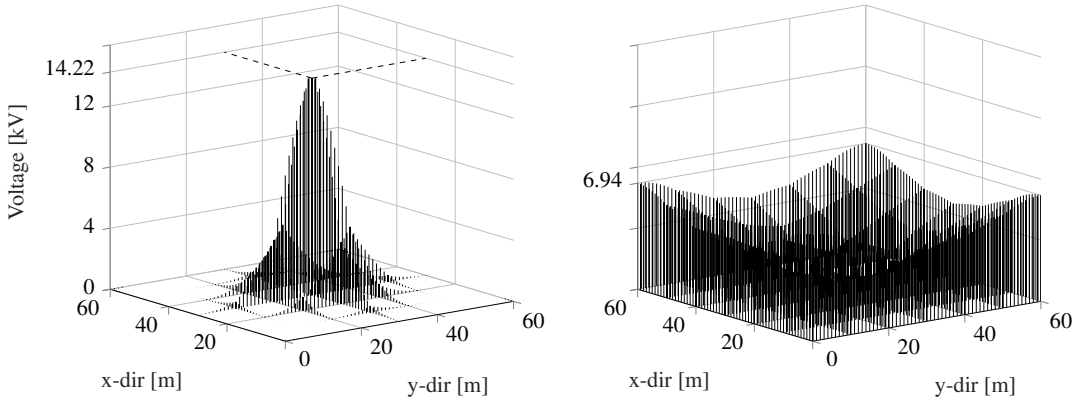

(d) t=38.16 μs, peak first stroke **(e)** t=42.65 μs, peak corner

Figure 4.24: Long cable case: integration of grounding model of 6×6 meshes of size 10×10 m, ρ_{soil}=2000 Ωm and εr_{soil}=36. Physical grounding grid properties are found in table 4.1a. Surge current, CIGRE 1.2/50 μs, impressed in far-end as shown in fig. 4.21. Nodal voltages at cable entry and transformer is shown in fig. 4.24a. From the surge arrester, placed at the cable entry, the injected point voltage and current to the grounding system are given in fig. 4.24b. Continuous voltage distribution for selected points are given in fig. 4.24c and overall distribution in figs. 4.24d and 4.24e at the peak voltage and the peak corner voltage, respectively

4.5.1.4 Non-Uniform Soil

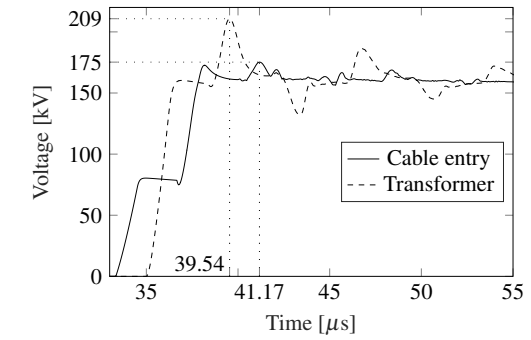

(a) Transmission system nodal voltages

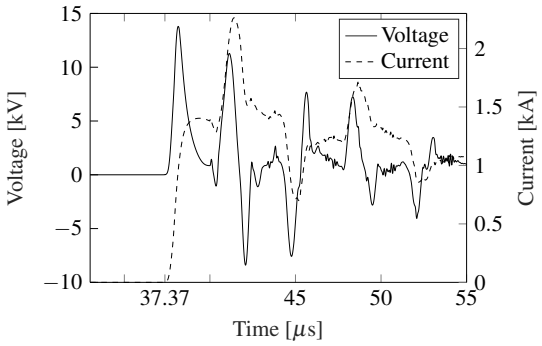

(b) Injection point current and voltage

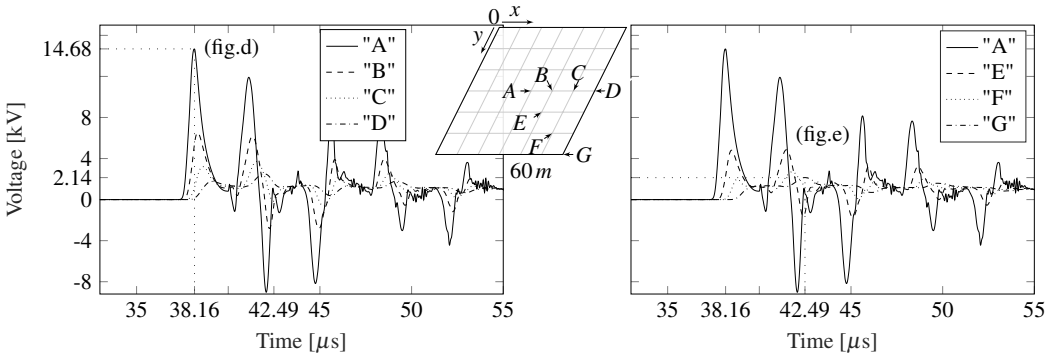

(c) Voltage distribution for selected points in the grounding grid

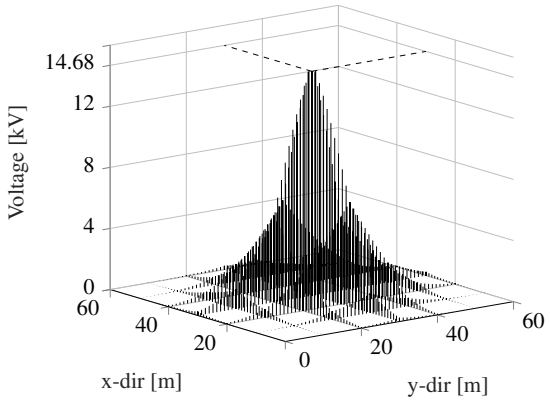

(d) t=38.16 μs, peak first stroke

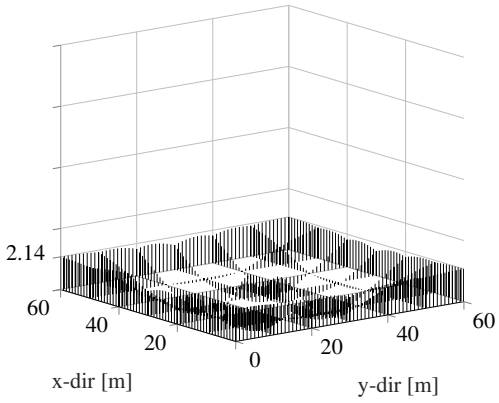

(e) t=42.49 μs, peak corner

Figure 4.25: Long cable case: integration of grounding model of 6×6 meshes of size 10×10 m, main area of ρ_{soil}=2000 Ωm and εr_{soil}=16 and outer ring of ρ_{soil}=300 Ωm and εr_{soil}=36. Physical grounding grid properties are found in table 4.1a. Surge current, CIGRE 1.2/50 μs, impressed in far-end as shown in fig. 4.21. Nodal voltages at cable entry and transformer is shown in fig. 4.25a. From the surge arrester, placed at the cable entry, the injected point voltage and current to the grounding system are given in fig. 4.25b. Continuous voltage distribution for selected points are given in fig. 4.25c and overall distribution in figs. 4.25d and 4.25e at the peak voltage and the peak corner voltage, respectively

4.5.2 4×4 Meshes and 1600 m^2

4.5.2.1 Soil resistivity 2000 Ωm and εr_{soil}=16

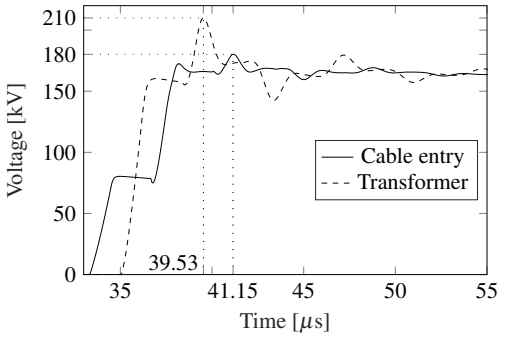

(a) Transmission system nodal voltages

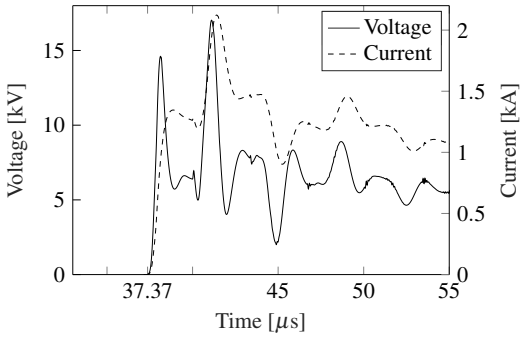

(b) Injection point current and voltage

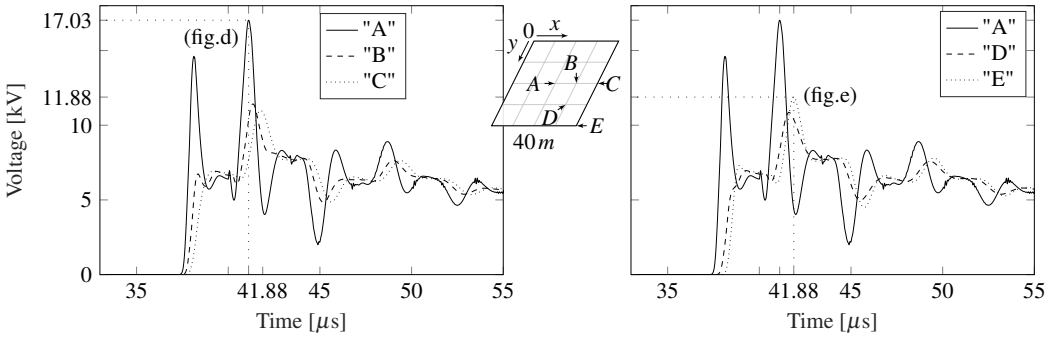

(c) Voltage distribution for selected points in the grounding grid

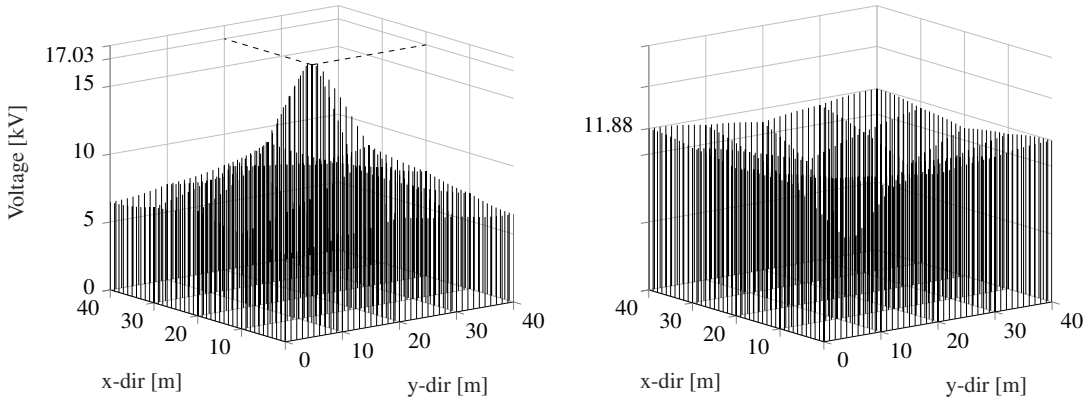

(d) t=41.11 μs, peak second stroke

(e) t=41.88 μs, peak corner

Figure 4.26: Long cable case: integration of grounding model of 4×4 meshes of size 10×10 m, ρ_{soil}=2000 Ωm and εr_{soil}=16. Physical grounding grid properties are found in table 4.1a. Surge current, CIGRE 1.2/50 μs, impressed in far-end as shown in fig. 4.21. Nodal voltages at cable entry and transformer is shown in fig. 4.26a. From the surge arrester, placed at the cable entry, the injected point voltage and current to the grounding system are given in fig. 4.26b. Continuous voltage distribution for selected points are given in fig. 4.26c and overall distribution in figs. 4.26d and 4.26e at the peak voltage and the peak corner voltage, respectively

4.5.3 8×8 Meshes and 1600 m^2

4.5.3.1 Soil resistivity 2000 Ωm and εr_{soil}=16

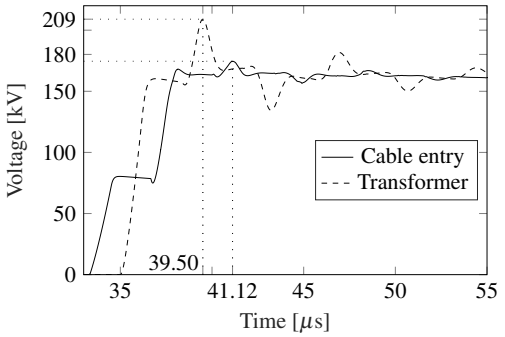

(a) Transmission system nodal voltages

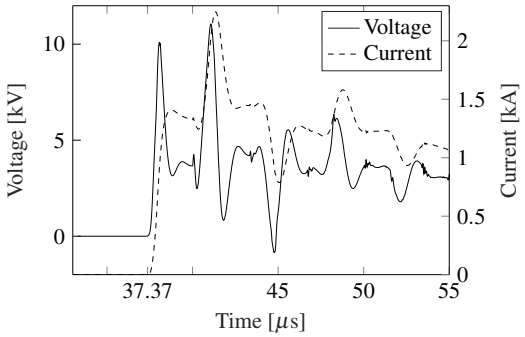

(b) Injection point current and voltage

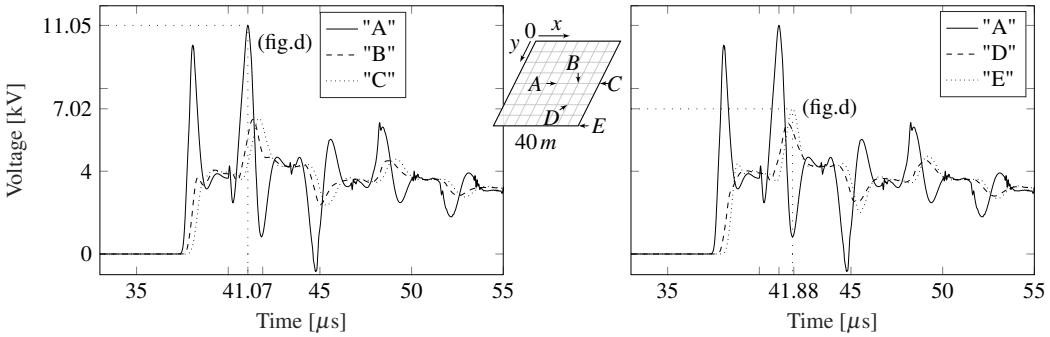

(c) Voltage distribution for selected points in the grounding grid

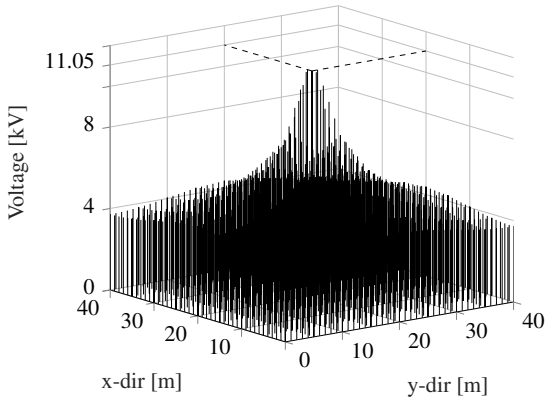

(d) t=41.07 μs, peak second stroke

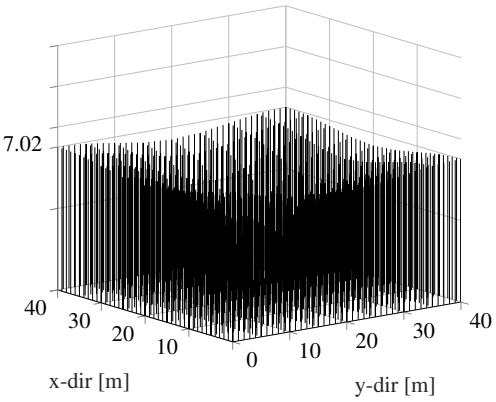

(e) t=41.81 μs, peak corner

Figure 4.27: Long cable case: integration of grounding model of 8×8 meshes of size 5×5 m, ρ_{soil}=2000 Ωm and εr_{soil}=16. Physical grounding grid properties are found in table 4.1a. Surge current, CIGRE 1.2/50 μs, impressed in far-end as shown in fig. 4.21. Nodal voltages at cable entry and transformer is shown in fig. 4.27a. From the surge arrester, placed at the cable entry, the injected point voltage and current to the grounding system are given in fig. 4.27b. Continuous voltage distribution for selected points are given in fig. 4.27c and overall distribution in figs. 4.27d and 4.27e at the peak voltage and the peak corner voltage, respectively

4.6 Electric Field Exerted to the Soil

This section presents results for electric field distribution exerted to the soil, E_{soil}, in selected grounding grids when integrated in EMTP-RV. With reference to the short cable case simulation section 4.4.1.1 and the long cable case in section 4.5.1.2, the corresponding electric field results is shown in figs. 4.28 and 4.29, respectively. Both cases has a grounding grid configuration of 6×6, 10 meter mesh size in uniform soil of ρ_{soil}=2000 Ωm and εr_{soil}=16. In fig. a) the electric field for selected points in the grounding grid is given. The nodal points are placed in the intersection of the grounding grid meshes, horizontally outwards from the center injection point as from the simulation cases (sections 4.4.1.1 and 4.5.1.2). In fig. b) the overall field distribution on the grounding wire surface is given at the peak value according to fig. a). Where the framed area indicates boundaries of electric field stronger than E_c= 400 kV/m.

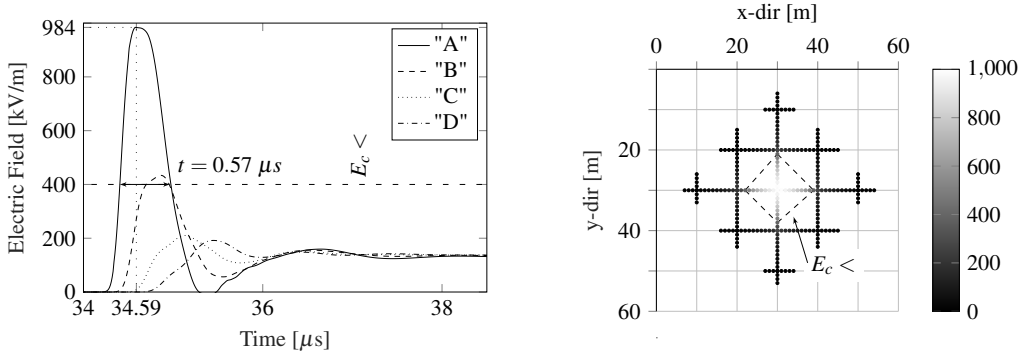

(a) Electric field for selected points **(b)** t=34.59 μs, Electric field distribution

Figure 4.28: Electric field distribution exerted on the soil, E_{soil}, at the grounding wire surface. Pre-processed from simulation in section 4.4.1.1 for the short cable case. Framed area indicates boundaries of electric field stronger than E_c= 400 kV/m

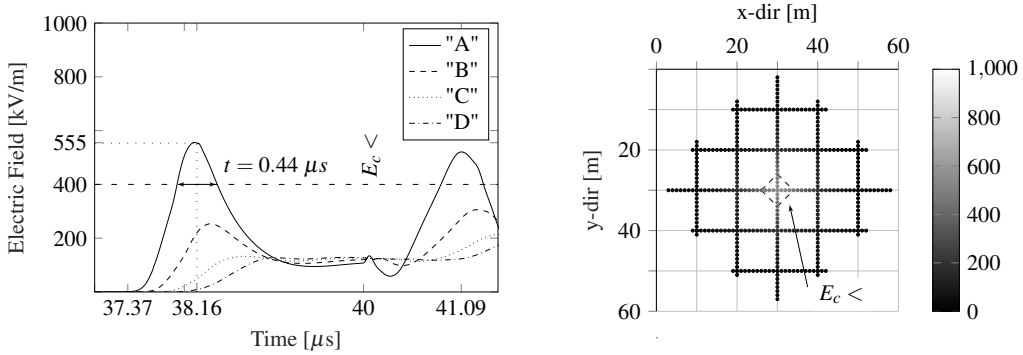

(a) Electric field for selected points **(b)** t=38.16 μs, Electric field distribution

Figure 4.29: Electric field distribution exerted on the soil, E_{soil}, at the grounding wire surface. Pre-processed from simulation in section 4.5.1.2 for the long cable case. Framed area indicates boundaries of electric field stronger than E_c= 400 kV/m

5 Discussion

The discussion chapter is divided into four parts. First, the results from the grounding system in isolated mode (sections 4.2 and 4.3) is treated to evaluate characteristics.
Secondly, the grounding models is integrated in a transmission system and the results from sections 4.4 and 4.5 discussed. The main objective of the thesis is concluded, comparing the short cable case with the design deviation of long cable between surge arrester and transformer.
Thirdly, common characteristics are discussed. Both regards to selected grounding grid configurations and soil properties. Also, an illustrative discussion, with practical outlines, is made to build an understanding of the EMI challenge in a substation.
Finally, model validation against previous work is presented in addition to a discussion of present uncertainties and model limitations.

5.1 Grounding Grid in Isolated Mode

The following section discusses the sensitivity of various grounding grid configurations and soil parameters. As the grounding system is considered in isolated mode, with a current source of double exponential form, simplicity applies to evaluate characteristics of the implemented grounding grid models. In addition, the powerful ODE solver with variable time-step, gives a high level of detail during the transient period.

5.1.1 Current Source

In section 4.2 all simulations of the grounding system has been excited by the double exponential source, according to section 3.1.6. These simulations have been performed solely in Matlab®/Simulink® where the soil parameters have varied while the excitation current has been attempted kept constant in magnitude and waveform. The easy nature of parameter adjustment gives the current source ideal properties for comparison purpose and fast implementation. In reviewed work, this current source is dominating in simulation cases. Moreover, a small change in the front time will have a great impact on the grounding system impulse characteristics. In examined work, the injected current has been attached to a limited extent, giving a source of uncertainty in the evaluation of results. With this consideration, the injected current has been attached for all simulation in addition to indicating selected key points of the corresponding voltage distribution.

5.1.2 Propagation Characteristics

From the results in section 4.2 the effect of changing the soil resistivity for a variety of grounding system configuration are presented individually. The grounding grid wire properties are constant, and an approximated 1/20 stroke of a double exponential waveform, with adjustment according to table 4.1, applies for the results. The simulation results give a peak voltage in the grounding grid, for all cases, in the first stage of the current injection. Due to the impulse are distributed as time and space dependent traveling wave in the grounding system, only parts of the grounding grid are utilized and contribute to the total impulse response. The limited utilization of the grounding grid during a fast front has been reported by several authors in the past and is a known characteristic reviewed in section 1.2. To further give insights of this phenomenon, with an application for domestic facilities, the sensitivity of soil parameters is simulated. Under these conditions, the effect of the traveling wave utilization is clearly illustrated in fig. 5.1. The figure is comparing the results from sections 4.2.3 and 4.2.4, where the soil is uniformly distributed with ρ_{soil}=2000 Ωm and εr_{soil}=16 for a mesh size of 5 m and grid area of 1600 m^2 and 3600 m^2. With a larger area, the characteristics of voltage distribution are similar. When considering the peak value, there are differences in the results which may be explained by the injected currents are slightly changed in magnitude (table 4.1). For the two grounding grid configurations, the peak value is reached for both at t=0.26 μs. Moreover, the corresponding injection point current is higher with a value of 0.41 and 0.39 kA for the 1600 m^2 and 3600 m^2, respectively. These results unveil the grounding system response sensitivity and strengthen the statement in section 5.1.1 of the importance by presenting the injected current as a part of the simulation results for validation and comparison. From this evaluation, all simulations performed in this thesis shows the voltage distribution in addition to the corresponding injected current.

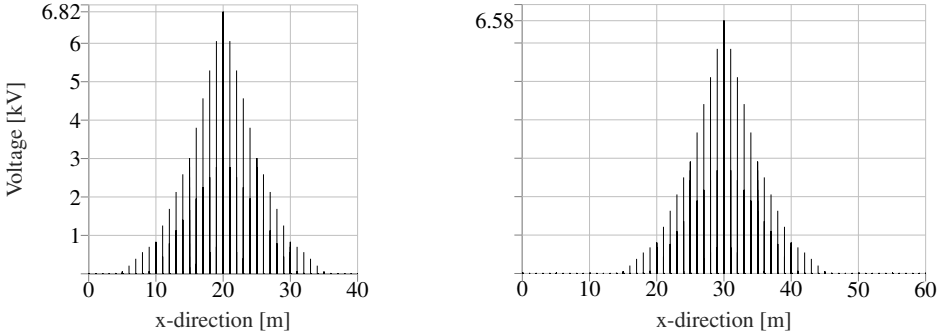

(a) Peak voltage in 8×8, 5 m mesh size **(b)** Peak voltage in 12×12, 5 m mesh size

Figure 5.1: Peak voltage in grounding grids of 5 m mesh size of configurations 8×8 and 12×12 in soil of ρ_{soil}=2000 Ωm and εr_{soil}=16. Evaluation with changed view of figs. 4.12b and 4.13b

The characteristic behavior of the traveling wave utilization of the grounding grid also applies for high resistivity soil and when the soil is non-uniform. A comparison of the peak values for mesh size of 10 m and grid area of 3600 m^2 in uniform soil from section 4.2.1.3 and the non-uniform from section 4.2.1.5 follows in fig. 5.2. The soil resistivity ρ_{soil}=2000 Ωm and εr_{soil}=16 in both cases, while the outer ring wire in fig. 5.2b are in soil of ρ_{soil}=300 Ωm and εr_{soil}=36. An interesting observation from this case evaluation shows that the overall grounding resistance in a facility is not contributing to the impulse performance of a grounding system. There are only the local soil properties, in the impulse effective region that is limiting the peak voltage. Contrary to discussion related to fig. 5.1, the injected current is similar for both cases, giving approximate similar peak voltage at the injection point as shown in fig. 5.2.

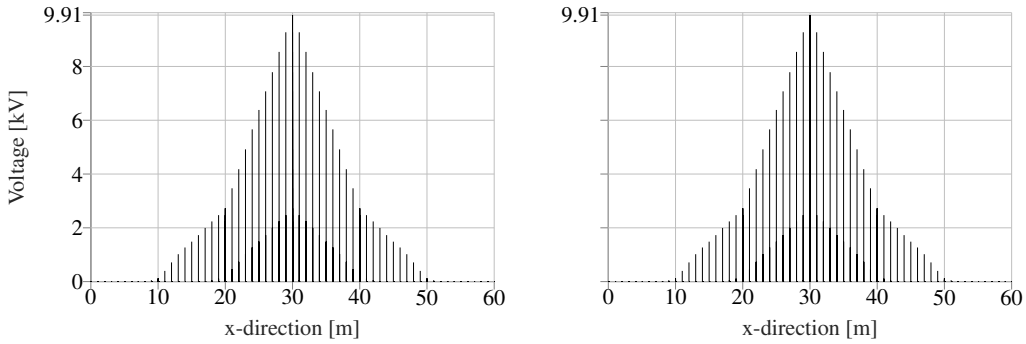

(a) Peak voltage in 6×6, 10 m mesh size grid, uniform soil

(b) Peak voltage in 6×6, 10 m mesh size grid, non-uniform soil

Figure 5.2: Peak voltage in grounding grids of 10 m of configurations 6×6 in uniform and non-uniform soil. Evaluation with changed view of figs. 4.7b and 4.9b

In further analysis of the impulse effective region, the grounding grid configuration of 6×6 and mesh size of 10 m are evaluated with a difference in the soil permittivity, εr_{soil}, in fig. 5.3. By comparing the results from sections 4.2.1.3 and 4.2.1.4 the grid area are of 3600 m^2, ρ_{soil}=2000 Ωm and the distinct factor of εr_{soil}=16 and 36. For the impulse effective area, the surge wave propagation speed is the main factor in describing the contribution and utilization of the grounding grid area, besides of inductive effect which limits the peak values outwards in the grounding grid. From the description of the propagation constant in section 2.2 and eq. (2.4a) the imaginary part is describing the phase of the traveling wave. When the value of soil permittivity, εr_{soil}, is changed the parameter modifies the capacitance element, eq. (2.16b), and further the connected behavior of the soil traveling wave propagation and distribution.

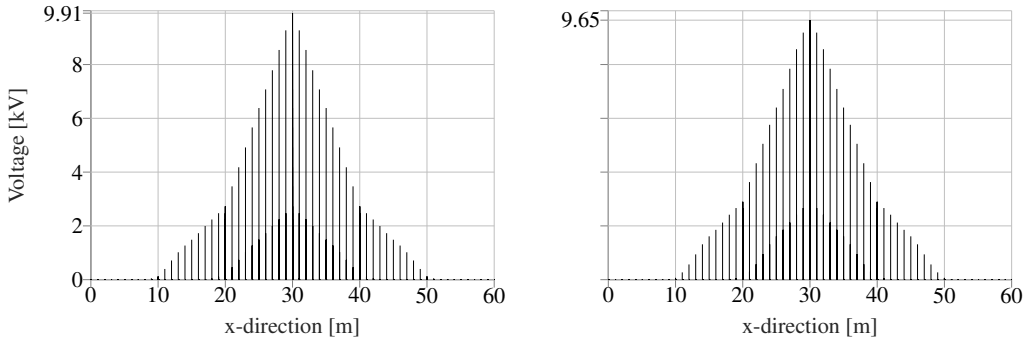

(a) Peak voltage in 6×6, 10 m mesh size grid, uniform soil for εr_{soil}=16 at t=0.35 μs

(b) Peak voltage in 6×6, 10 m mesh size grid, uniform soil for εr_{soil}=36 at t=0.60 μs

Figure 5.3: Peak voltage in grounding grids of 10 m mesh size of configurations 6×6 in uniform of εr_{soil}=16 and 36. Evaluation with changed view of figs. 4.7b and 4.8b

As observed from fig. 5.3 the peak value are reached at different time, where the maximum value are reached after t=0.35 μs for soil of εr_{soil}=16 and t=0.60 μs for soil of εr_{soil}=36. Another interesting observation from this comparison is that even though the traveling wave had a considerable difference in speed, the voltage distribution form and utilized grounding grid area are approximately similar when the peak voltage is reached. The considered results do have the similarity in grounding wire properties and excitation current of a 1/20 μs stroke. The selected excitation current is a steep surge front, in the lower front time range for what is considered in evaluated standards and previous work. To compare how the grounding system is performing with a stroke of the slower front, the peak value results from section 4.2.1.6 is presented in fig. 5.4 by the voltage distribution for a 5/20 μs stroke.

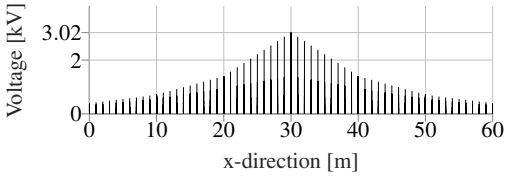

Figure 5.4: Peak voltage in 6×6, 10 m mesh size grid, uniform soil for εr_{soil}=16 at t=0.99 μs, current excitation of a approximated 5/20 of double exponential form. Evaluation with changed view of fig. 4.10b

The soil has same properties as in fig. 5.3a which gives similar surge wave propagation in the grounding system. However, the peak voltage in the grounding system is reached after approx 0.99 μs, whereas for the fast front surge are reached after 0.3 μs. This gives a larger area of the grounding grid to be utilized, and the peak voltage value is considerably lower in magnitude. An explanation of this behavior can be made by comparing the fast and slow front from the first grounding wire segment inductance after the injection point, evaluated in section 4.3. The results are compared, for the two cases of surge waves, in fig. 5.5. For the steep-fronted waveform, the opposing inductance force gives 5-6 times higher peak voltage than the for the slow fronted

waveform. This corresponds well with the characteristic behavior of the per-unit segment length impedance according to section 4.1 and fig. 4.2. This concludes that to provide design criteria for the impulse effective region and equipment, the most severe surge should be considered in the manner of expected steepest surge front time.

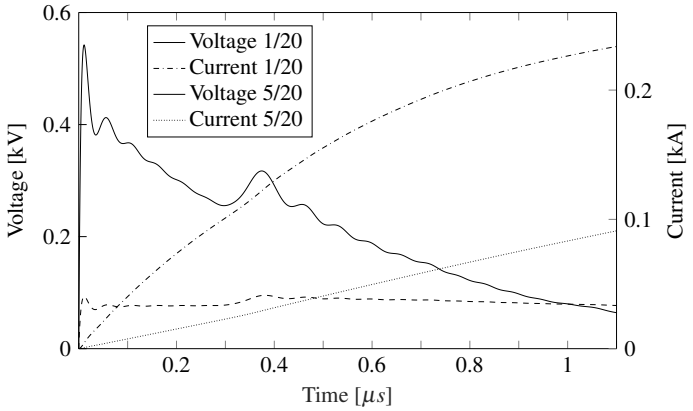

Figure 5.5: Comparing the inductive effects of the first segment at the injection points for a 1/20 and 5/20 μs stroke. Evaluation with changed view of figs. 4.15a and 4.15b where ρ_{soil}=2000 Ωm are selected and figs. 4.16a and 4.16b

5.2 Grounding System Integrated in Transmission System

To make use of the grounding system model in transient studies, Matlab®/Simulink® were interfaced with EMTP-RV trough FMI. The FMI solution was first released in January 2018 by Powersys EMTP-RV and acquired by Western Norway University of Applied Sciences (HVL) at the release date for the development in this project. Since HVL were the first customer of the new FMI package there has been close contact with Powersys developers to exchange user experience and to implement software improvements. Even though the FMI package are in the first release, the benefits of this close cooperation are weighted to compensate for the instabilities and required workarounds to carry out this work. Due to present software limitations(maximized allowed memory usage) the grounding grid model of 5×5 m mesh size and square footing of 3600 m^2 is not included in co-simulation.

In this work, a simplified 300 kV power transmission system has been integrated to demonstrate the substation grounding grid behavior during a current injection from a surge arrester, as illustrated in section 3.3 and fig. 3.5. It is expected that a lightning stroke is entering the phase wire due to a shielding failure of an overhead transmission line, and follows the line to the substation. The lightning stroke is of sufficiently low

magnitude to not break down air insulation or be discharged trough surge arresters on its path to the substation. When the traveling wave, originating from the stroke, are entering the substation mains transformer a reflected wave will arise of approximately doubled magnitude. For this study, a lightning stroke in the far-end of 1 kA amplitude was found sufficient, which follows the CIGRE defined waveform of a 1.2/50 stroke. The transmission system complexity will affect the lightning surge wave distribution, and the presented results are only valid for the implemented case. This also applies to the implemented surge arrester characteristics which have the most significant effect on the grounding system response as the source of current injection. Moreover, the present implementation of a dynamic model can be modified and readily adopted in EMTP-RV to perform a combined analysis of both the grounding and transmission system.

5.2.1 Surge Arrester

The surge arrester is implemented for a system voltage of 300 kV with corresponding V-I characteristics given in section 3.2.2 and table 3.3. When the transmission system discharge path to ground is through the surge arrester, it has a significant impact in the grounding system voltage distribution. In utilizing the standard library of EMTP-RV, and the given ZnO surge arrester, only the V-I parameters is possible to be adjusted. Loss factors, damping, and switching properties are some factors which are not available for the users. When investigating the surge arrester model user documentation there is given reference to the IEEE MOA implementation, represented by the equivalent circuit in section 2.3.1 and fig. 2.5. Most significant parameters for the grounding system, in addition to the V-I characteristics, are the damping and switching properties. As can be observed from the long cable case these properties are interacting when the surge arrester is suffering a pulsation motion form the transmission system in section 4.5 and fig. 4.21. If the surge arrester is changed or given other parameters, this may strongly affect the simulation results. In addition, a general weakness with commercial software is the hidden source code which is not possible to retrieve or document. Moreover, Powersys EMTP-RV has built a reputation over decades being a recognized provider of software to perform power transmission studies, both by industry and research institutions. This gives confidence that the surge arrester model presents realistic switching and damping interaction.

5.2.2 Propagation Velocity and Simulation Time-Step

When the grounding system was simulated in an isolated mode the solver was set with variable time-step as described in section 3.1.5. This is an effective method to keep sim-

ulation accuracy and reduce computer memory requirements and simulation time. In co-simulation, a software limitation of present FMI package solution requires EMTP-RV to be master unit and give a defined time-step iteration to keep both systems synchronized. In avoiding losing accuracy over the grounding wire segments, the propagation speed for the individual models is evaluated. From the results performed in isolated mode (section 4.2), each simulation gives the time when the surge is reaching the corners of the grounding grid. From this time, the overall surge wave velocity in the grounding system is estimated based on the time difference between the injection and the distance between injection point and corners. An overview of the surge wave velocity for selected grounding grid configurations is given in table 5.1. The characteristics of the propagation constant, section 4.1 and fig. 4.3, are confirmed where there is a minor difference in velocity between soil resistivity (ρ_{soil}) of 1000 and 2000 Ωm and soil of 300 Ωm gives a slower surge velocity. As can be observed from table 5.1 the maximum velocity are registered to v_s=74.07$\times 10^6$ m/s. To balance the computer requirements against accuracy in simulations, the fixed simulation time-step in co-simulation mode was set to 0.01 μs. A time-step of 0.01 μs gives a movement of the surge wave in the grounding system of 0.64 m when the velocity is maximum. Since the implemented per-unit length grounding wire are set to one meter, and each segment are set to five or ten meters, the time-step of 0.01 μs are found sufficient to perform co-simulation.

Grounding grid model	Soil parameter	Section ref.	Distance [m]	Time [μs]	Velocity v_s [m/s]
6×6, 10 m mesh size	ρ_{soil}=2000 Ωm, εr_{soil}=16	4.2.1.3	60	0.86	69.77$\times 10^6$
6×6, 10 m mesh size	ρ_{soil}=2000 Ωm, εr_{soil}=36	4.2.1.4	60	0.97	61.86$\times 10^6$
4×4, 10 m mesh size	ρ_{soil}=2000 Ωm, εr_{soil}=16	4.2.2.1	40	0.54	74.07$\times 10^6$
8×8, 5 m mesh size	ρ_{soil}=2000 Ωm, εr_{soil}=16	4.2.4.1	40	0.55	72.73$\times 10^6$

Table 5.1: Surge wave velocity in different grounding grids from results given in section 4.2

As described in section 3.3, another weakness of the FMI software tool in co-simulation are in the function of performing iteration between EMTP-RV and Matlab®/Simulink®. Each time-step iteration is performed individually, means that the master and the slave perform their calculation sequentially and not simultaneously. This gives a mismatch of one time-step between the systems and may be a source of error in the presented results in sections 4.4 and 4.5. This error will affect the entire simulation period while evaluated most significant in the stroke rise time, where the rate of change is highest. With a time-step at 0.01 μs and a surge rise time of t_{rise}=1.2 μs it gives 120 calculations per surge rise period. From this evaluation, the error is expected to be of minor importance while requiring computer demanding simulation. Since the grounding grid model are the most complex part of presented models in co-simulation, a more efficient solution would be to have Matlab®/Simulink® as the master unit. Unfortunately, at present a technical

solution is not available while is planned for a future release by Powersys.

5.2.3 Short Cable Between Transformer and Surge Arrester

The first case of evaluated substation design are following IEEE standards, and consist of a relatively short cable between the main transformer and surge arrester [23, p. 111]. The simulation results discussed are found with reference to section 4.4.

5.2.3.1 Effect on the Transmission System

If the grounding system is ignored, giving a direct connection to true ground, the resulting peak voltage at the cable entry and transformer are 163 kV and 171 kV, respectively as shown in section 4.4 and fig. 4.17. When the grounding system is included, there are minor deviations in peak voltages for grounding grid of same mesh size. With 6×6 meshes of size 10 m and soil resistivity ρ_{soil}=2000 Ωm and εr_{soil}=16 the cable entry and transformer voltage is increased to 186 kV and 190 kV, as shown in section 4.4.1 and fig. 4.18. From these values, the surge arrester performance is reduced by a factor of approx 1.12 when the grounding system is included for the transformer terminals peak voltage. With same grounding system properties, though reducing its size to 4×4 meshes of size 10 m, the peak voltage is increased to 189 kV and 192 kV for the cable entry and transformer terminals, respectively given by section 4.4.2 and fig. 4.19. An interesting observation shows that the mesh density has a more significant effect on the surge arrester performance than the grounding grid area. From the results given for the 8×8 meshes of size 5 m, 1600 m^2 grounding grid in section 4.4.3 and fig. 4.20 the cable entry and transformer voltage is increased to 179 kV and 183 kV. The reduction factor of surge arrester performance for the transformer terminal voltage is then approx 1.05. Such performance factor is strongly dependent on injected current, grounding system configuration and transmission system. Furthermore, conditions as transmission line system voltage level expected injected lightning surge, surge arrester characteristics, transmission system complexity and grounding system properties may vary from facilities. In reviewed work as [44] and [16], attempts to express the surge arrester performance relation empirically is proposed. Due to the many unknowns mentioned, a more practical method would be to use a modeling principle, as the present interfaced grounding grid model. This gives the present modeling approach as a useful tool in determining the surge arrester performance and the corresponding effect on the transmission system.

5.2.4 Long Cable Between Transformer and Surge Arrester

When deviation from the IEEE standards of recommended design, by placing the surge arrester at a relatively long distance from the transformer, the grounding system, and transmission network is exerted to a pulsation behavior due to traveling wave reflection in the transmission system. This is a typical design case found in larger domestic hydropower installation. The simulation results discussed are found with reference to the long cable case in section 4.5 and also comparing results from the short cable case in section 4.4.

5.2.4.1 Effect on the Transmission System

In presented results, a cable length between the transformer and surge arrester of l_c=500 m is defined as long. The chosen cable length is in a range which may be found in typical domestic hydropower plant of larger size, where the switchyard are placed outdoor, and the production generator and transformer are in a rock cavity. To evaluate the effect of the long cable case a comparison is made to the short cable case when the same conditions apply. From the short cable case in section 4.4 and fig. 4.17, the voltage peak at the cable entry is 163 kV when the grounding system is ignored, giving the surge arrester a path to true ground. While for the long cable case in section 4.5 and fig. 4.21 the peak voltage is only increased to 166 kV. For the selected source current and transmission system, this is a relative increase which is of minor importance to consider further. When comparing the same results for the peak voltage at the transformer terminals a more interesting observation is made. The present results show that the voltage is increased by a factor of 1.20, from 171 to 206 kV at peak for the short and long cable case, respectively. The increased peak voltage level at the transformer terminals are well known in selecting this design.
From the results given in section 4.5 the peak values at the cable entry and transformer are collected to give a common overview in table 5.2. From these results, with present current source and transmission network, the grounding system has a minor role in affecting the peak voltage for the selected points. Based on the presented results, ignoring the grounding system, setting the surge arrester path to true ground, will lead to an insignificant error when considering the overall insulation level. With this reflection and discussion made in section 5.2.3, the grounding system has a more significant effect on the transmission network for the short cable case in limiting the relative increase in peak voltage.

Grid configuration	Soil parameters	Results ref.	Cable entry peak	Transformer peak
Direct	-	fig. 4.21	166 kV	206 kV
3600 m^2, 10 × 10 m	ρ_{soil}=1000 Ωm, εr_{soil}=16	fig. 4.22a	174 kV	209 kV
3600 m^2, 10 × 10 m	ρ_{soil}=2000 Ωm, εr_{soil}=16	fig. 4.23a	177 kV	209 kV
3600 m^2, 10 × 10 m	ρ_{soil}=2000 Ωm, εr_{soil}=36	fig. 4.24a	177 kV	208 kV
3600 m^2, 10 × 10 m	ρ_{soil}=2000 Ωm, εr_{soil}=16 ρ_{soil}=300 Ωm, εr_{soil}=36	fig. 4.25a	175 kV	209 kV
1600 m^2, 10 × 10 m	ρ_{soil}=2000 Ωm, εr_{soil}=16	fig. 4.26a	180 kV	210 kV
1600 m^2, 5 × 5 m	ρ_{soil}=2000 Ωm, εr_{soil}=16	fig. 4.27a	180 kV	209 kV

Table 5.2: Peak voltage in the transmission system when the grounding system are included in the simulation case of long cable between surge arrester and transformer. Results collected from section 4.5

5.2.4.2 Effect on the Grounding System

The results in section 4.5 shows that the grounding system is suffering a more challenging behavior when a relatively long cable is used between the transformer and surge arrester. The transmission network surge traveling wave makes a pulsation surge arrester current to the grounding system which also accumulates potential of the individual strokes. With this behavior, the evaluation of characteristics related to the grounding system may be more complex. To identify if a design case with long cables are presenting an additional challenge to the overall substation grounding system in EMI evaluation, an comparison between to the short cable case (section 4.4) is collected in tables 5.3 and 5.4. The results show, for all cases of comparison, that the overall peak and the corner peak voltage has a lower order of magnitude for the long cable case. And in the further analysis, all point readings has a lower order of magnitude than for the short cable case during the simulation time. This statement even applies to the smaller grounding grid configurations where the overall peak and corner voltage is reached first after the second arrester stroke, as shown in sections 4.5.2 and 4.5.3.

		Short cable		Long cable	
Grid configuration	Soil parameters	Results ref.	Peak	Results ref.	Peak
3600 m^2, 10 × 10 m	ρ_{soil}=2000 Ωm, εr_{soil}=16	fig. 4.18d	26.35 kV	fig. 4.23d	14.68 kV
1600 m^2, 10 × 10 m	ρ_{soil}=2000 Ωm, εr_{soil}=16	fig. 4.19d	27.17 kV	fig. 4.26d	17.03 kV
1600 m^2, 5 × 5 m	ρ_{soil}=2000 Ωm, εr_{soil}=16	fig. 4.20d	20.97 kV	fig. 4.27d	11.05 kV

Table 5.3: Overall peak voltage in the grounding system. Comparison between results collected with reference to sections 4.4 and 4.5

From the results, it is clear that design deviation from IEEE with the long cables case between the surge arrester and transformer is not presenting additional challenges for the substation grounding system in EMI evaluation. The cable length is damping the injected current giving a positive effect on the grounding system voltage potential rise.

With this consideration and results evaluation, designing of a substation grounding system after present known factors in standards will be satisfactory also for the typical larger domestic hydropower plant arrangement with relatively long cable. As discussed in section 5.2.4.1 the peak voltage is increased, which is a known factor in insulation coordination studies, and will lead to the most strict requirement represented by selecting a long cable design.

		Short cable		Long cable	
Grid configuration	Soil parameters	Results ref.	Peak Corner	Results ref.	Peak Corner
3600 m^2, 10 × 10 m	ρ_{soil}=2000 Ωm, εr_{soil}=16	fig. 4.18e	6.51 kV	fig. 4.23e	6.24 kV
1600 m^2, 10 × 10 m	ρ_{soil}=2000 Ωm, εr_{soil}=16	fig. 4.19e	12.11 kV	fig. 4.26d	11.88 kV
1600 m^2, 5 × 5 m	ρ_{soil}=2000 Ωm, εr_{soil}=16	fig. 4.20e	7.41 kV	fig. 4.27e	7.02 kV

Table 5.4: Corner peak voltage in the grounding system. Comparison between results collected with reference to sections 4.4 and 4.5

5.3 Common Characteristics and Properties

5.3.1 Grounding Grid Properties

In this thesis, the grounding grid mesh size of 10×10 m and 5×5 m was selected due to the widespread application is given in current recommendations for high voltage substation up to 420 kV. For domestic facilities (in Norway) the described mesh size of 5×5 m is given by the TSO (Statnett) guidelines [25, p. 47]. This is an updated guideline, and still the weighted amount of facilities have larger ground grid meshes. To build an understanding of the lighting transient event, applicable for existing facilities, the grounding grid meshes size of 10 m were thoroughly investigated through simulations in section 4.2 to 4.5. For more general cases, the recommendation of 3 to 15 m between horizontal wires are established trough IEEE, where the spacing, in the given range, are mainly given attention to GPR when a power frequency fault occurs [23]. The chosen burial depth and grounding grid conductor sizes are also selected from the recommendation in [25, p. 47] which also was implemented in earlier standards.

5.3.2 Soil Parameters

From the simulation results in chapter 4, selected values of soil parameters is used to utilize the grounding system models in application cases for typical outdoor substations. The expected local soil mixture resistivity (ρ_{soil}) found in domestic substations lies in the range of 1000-2500 Ωm, which is defined as high resistivity soil in section 2.4 and table 2.1. During the project period, it was difficult to conduct physical measure-

ment of soil resistivity, according to the Wenner method described in section 2.4.1, due to a winter season with extraordinary snow conditions at the location of available substations. However, the soil mixture total resistivity based on the construction method is evaluated to give mean values in the high resistivity range [25]. This also applies to the soil relative permittivity level, where the expected values were set to εr_{soil} = 16 and 36. In reviewed literature, there is not found any source of information specifying expected values of relative permittivity for domestic substations. The value was chosen with a low and medium of the total range (section 2.4.2) to evaluate the sensitivity of this parameter trough simulations. As discussed in section 5.1.2 and supported by fig. 5.3 the results show that even though the permittivity is affecting the grounding system capacitance, the voltage distribution is of comparable character in the grounding grid. This support the easy and broadly known measurement technique of soil resistivity, by the Wenner method, to give the most significant input parameter to the simulation. This besides the grounding grid configuration itself with physical properties and burial depth.

5.3.3 Non-Uniform Soil

In practical application the grounding wires are buried in a soil which results in a variety of electrical properties, the soil is not uniform. In considering the effect of non-uniform electric properties two simulations were performed, one for the grounding grid in the isolated mode in section 4.2.1.5 and a second when the system was integrated for the long cable case in section 4.5.1.4. For this simplified case study the main area of the grounding grid are in high resistivity soil of ρ_{soil} = 2000 Ωm and εr_{soil}=16, where the grounding wire are buried in a mix of rocks, clay and moraine gravel. The outer boundary zone of the grid are connected to external grounding system and consist of lightly damped soil, giving a lower resistivity region of ρ_{soil} = 300 Ωm and εr_{soil}=36 for the grounding wires. This situation is intended to describe a typical high voltage outdoor substation for a domestic hydropower plant. Even though the construction method is similar for all cases of a substation, giving high resistivity soil of the buried grounding grid, the typical location is in remote areas. Usually, this gives the opportunity to utilize relatively large land area, interconnect external grounding systems and to use local soil material of low resistivity in the outer boundary zone. As shown in the discussion of surge propagation in section 5.1.2, there is a limited area of the grounding system contributing during the surge steep front. This is also the case for the simplified case study of non-uniform soil as shown in section 5.1.2 and fig. 5.2. Moreover, in the second period, the results from non-uniform soil shows how effective a lowered soil resistance value is on reducing the overall voltage distribution, for both the simulation in isolated mode and for the long cable case. When the grounding grid is in the isolated mode the

results are easy compared between the uniform soil case in section 4.2.1.3 and the non-uniform case in section 4.2.1.5. The peak value are similar after 0.35 μs for the injection point, and the stationary voltage after 2.5 μs is reduced, for all point in the grounding grid, from approx. 2.5 kV to 1 kV. For the long cable case, the voltage distribution over the simulation time is more complex. From the results in sections 4.5.1.2 and 4.5.1.4 the voltage readings at the injected point and grounding grid corners is selected from the uniform and non-uniform soil case, respectively as shown in fig. 5.6. As can be observed in fig. 5.6a the overall peak voltage is reached after 38.16 μs for both cases at the injection point ("A"), while the secondary stroke is giving a slightly lower order of magnitude for the grounding grid in the non-uniform soil. The more immediate effect of the non-uniform soil is observed for the grounding grid corners and are shown in fig. 5.6b. The corner voltage potential rise is of lower magnitude during the entire simulation, and the peak voltage is decreased from a value of 6.24 to 2.14 kV.

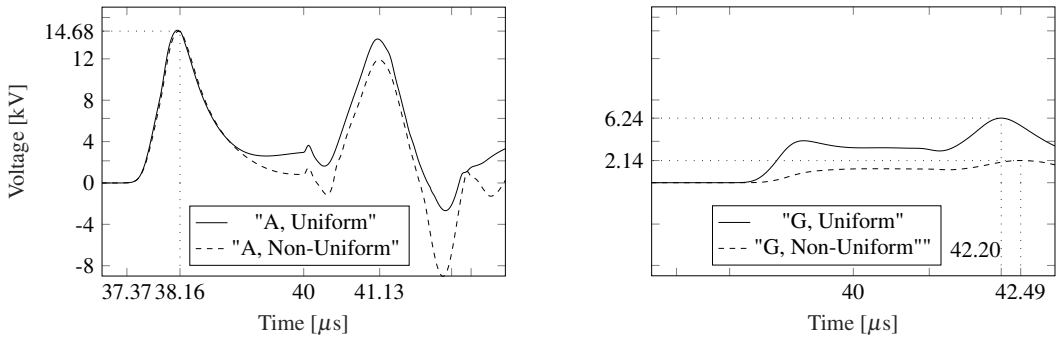

(a) Center and injection point ("A")

(b) Corner point ("G")

Figure 5.6: Comparison between the grounding grid in uniform and non-uniform soil when integrated in EMTP-RV. Given with changed and selective view of figs. 4.23c and 4.25c for the uniform and non-uniform soil, respectively

This consideration is given based on a current injected in the center of the grounding grid. If the injection point is shifted, and the non-uniform soil properties are kept similar, the surge wave will reach the outer boundary zone after a shorter time, and the more effective discharge will initiate earlier, lowering the overall voltage potential rise. With this consideration, the most severe voltage potential rise will exist with the center as the injection point for this case. Another important observation from these results is the capabilities of present model to consider the non-uniform properties in simulations. This gives the flexibility to evaluate local soil properties for any given location to adopt a realistic model.

5.3.4 Switchyard Layout and EMI

There exist limited available research considering the lightning transient voltage distribution in the grounding grid over the substation area. Much effort has been given for direct strikes, which represents higher currents, where the controlled discharge path is direct to a designed grounding system. For the substation grounding system, GPR is the design driver, with the aim of limiting the step and touch voltages at power frequency faults. By simulating different cases, the sensitivity of transmission system design, grounding grid configuration and soil parameters are given attention in this thesis to evaluate the potential rise in the grounding grid. There is expected that the surge current is entering through a transmission line with a sufficiently low magnitude to penetrate deep into the substation, reaching more sensitive equipment, and discharged true the surge arrester when interacting with transformer reflection. An typical example from an existing hydropower infeed arrangement is illustrated in fig. 5.7 where a possible EMI issue is present (picture in section 1.1 and fig. 1.3). From the mountain production hall, the power cable is connected to the air insulated switchyard through a surge arrester and circuit breaker. When investigating this illustration, we can observe that the control room is near the surge arrester. With present results in chapter 4, a voltage potential rise will be severe in the region around the injection point. For this case, the control room grounding system will suffer a potential rise if a fast front lightning surge wave is injected. Special concerns may be required to the control room grounding design. Alternatively, a modification of the substation layout, with a larger distance between the control room and surge arrester. With the implemented model, a tool exists to evaluate EMC in the grounding system to ensure reliable and safe operation.

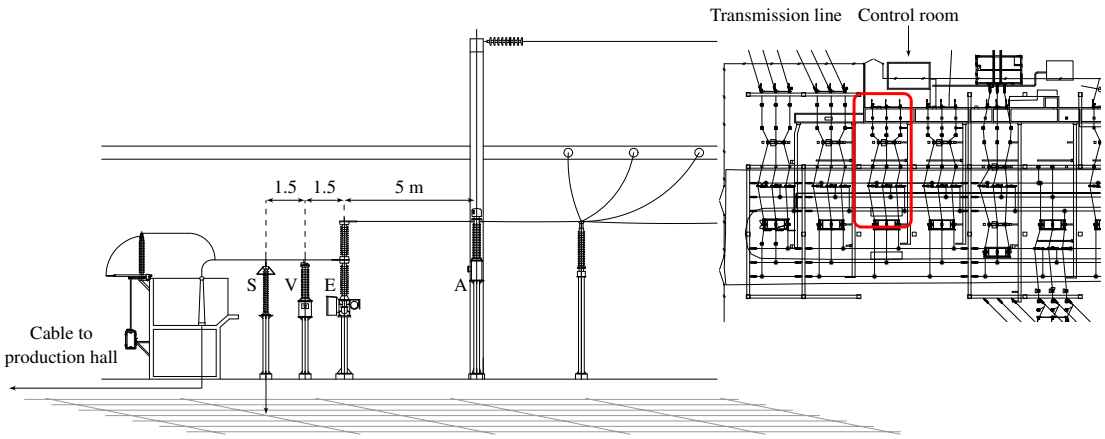

Figure 5.7: Typical arrangement for an air insulated infeed for a hydropower plant. "S", "V", "E" and "A" indicates surge arrester, voltage measurement, circuit breaker and current measurement, respectively. Illustrated with surge arrester injection point to a grounding grid with mesh size of 5×5 m. Framed area in upper right drawing illustrates the infeed position in a substation layout. Detailed schematics is found in Appendix H

5.4 Modeling Validation and Uncertainties

The present results in chapter 4 and discussion made in sections 5.1 to 5.3 is based on the implemented grounding system model and transmission system integration. As the grounding system still is given attention from researchers, new unknown factors is presently discovered and reported to improve the understanding during the transient event. In a complex field of research, this thesis is not intended to answer all unknowns or include all known factors. Although the grounding system model presented in this work is simple, it is flexible and features significant potential for further development so that the accuracy could be improved. Moreover, the grounding grid modeling approach described in section 3.1 and supported by Appendix D to E gives a powerful tool in simulation and pre-processing. With an open source code implementation, researchers may benefit of bringing the present development further. The innovation of grounding grid model in Matlab®/Simulink® and integration with EMTP-RV is therefore given as a contribution to IEEE ICHVE 2018 for further advance researcher in the field. The full conference contribution is found in Appendix B.
To bring insights in the modeling accuracy, the following sections will show a model validation. Secondly, known limitation and simplification, which are significant for the results, is discussed.

5.4.1 Model Validation

There exist limited available literature to verify the accuracy of implemented models. To bring further insights about the grounding system characteristics, during transient events, results given in section 4.2 presents cases changing the soil parameters and grounding grid configurations. Comparable work was identified for model verification. However, these results are given for low resistivity soil. Another weakens of this study is that all work have been performed by computer simulation. Laboratory experiments were not found feasible due to space requirements and equipment needs. The grounding system model is validated by comparing the implemented model against the EMF theory first performed by Grcev [45] and later by Jardines [46] who introduced a variant of the Multi-conductor Transmission Line (MTL) approach. In these cases of model verification, the current source of a double exponential waveform is used, and the simulation is performed in isolated mode (Matlab®/Simulink®).

5.4.1.1 Grounding Rod

A grounding rod of 15 m was simulated and measured by Grcev [45] and later evaluated by Jardines [46] as shown in fig. 5.8a. Using two independent modeling approaches and

relative similarities in results builds confidence for present modeling accuracy. The grounding rod is horizontally buried in soil of ρ_{soil}=70 Ωm and εr_{soil}=15, with a wire radius of a=0.012 m at depth d=0.6 m. The current source were set with the amplitude of $\hat{I}$=36 A and the stroke of 0.36/12 μs which lead to the new parameter values α=32$\times 10^3$ and β=7.6$\times 10^6$. The results from implemented model are given in fig. 5.8b. As can be observed from referenced work, the peak values at the injection point are approximate 560 V while by using more accurate readings, the implemented grounding model shows 569 V. The second point for comparison is at 7 m from the injection point where Grcev simulations show approximate 200 V while the results in this work gives 172 V after 0.7 μs. Besides the point value readings, the surge wave propagation along the grounding rod and voltage distribution are of similar character.

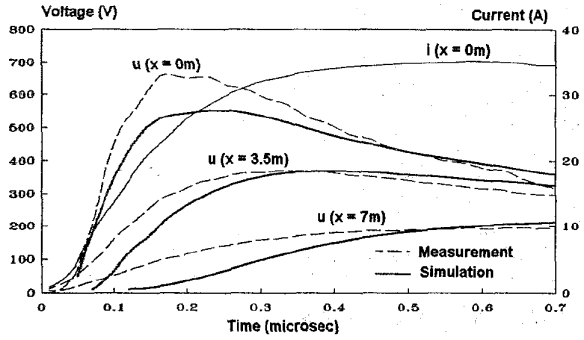

(a) Voltage response from [45, p. 818]

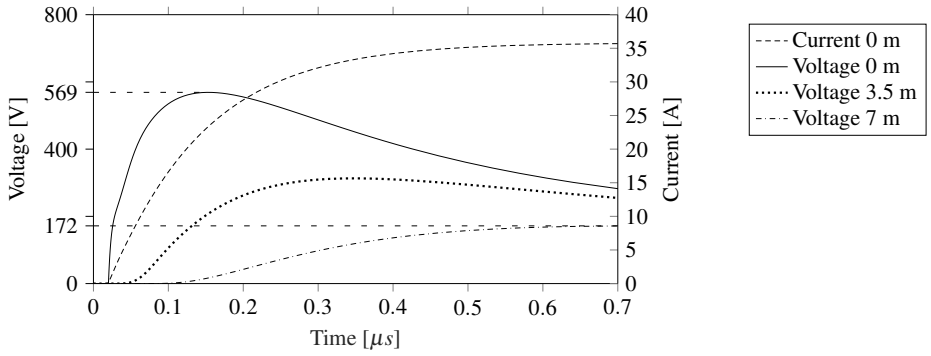

(b) Modeled and simulated voltage response

Figure 5.8: Voltage distribution along horizontal copper wire in ground (length l=15 m, conductor radius a= 0.012 m, at soil depth d=0.6 m) in soil of ρ_{soil}=70 Ωm and εr_{soil}=15. Results from implemented model is given by fig. 5.8b, with excitation current $\hat{I}$=36A double exponential waveform(α=32$\times 10^3$, β=7.6$\times 10^6$). Figure 5.8a gives result for comparison from research given in [45, p. 818].

5.4.1.2 Grounding Grid

A grounding system of 10 m mesh size and a total square footing of 3600 m^2 was simulated by Jardines [46] using a variant of the MTL approach, as shown in fig. 5.9a.

The grounding grid was buried in soil of ρ_{soil}=100 Ωm and εr_{soil}=36, with a wire radius of a=0.004126 m at depth d=0.6 m. The current source was set with amplitude of $\hat{I}$=1 kA and a 1/20 μs stroke with parameters α=38$\times$10^3 and β=2.54$\times$10^6. The results from the implemented model given in fig. 5.9b. As the injected current is not given in the referenced work, it is worth noting that a small deviation in the injected current will have a large impact on the grounding system response, especially for the region contributing to limiting the peak voltage (as discussed in section 5.1.2). As it can be observed, both the voltage distribution and the propagation characteristics correspond well. When comparing the simulation to Grcev [45] which was based on EMF against the simulation in the presented work, the peak value and the propagation characteristics are of comparable values. However, the distributed voltage at the given nodal points are more conservative with the transmission line approach, both the implemented model and based on Jardines work. This unveils a model accuracy difference compared to the EMF. As reviewed, Liu developed the non-uniform transmission line approach to compensate for the inaccuracy of this method and are treated in details in her work [9].

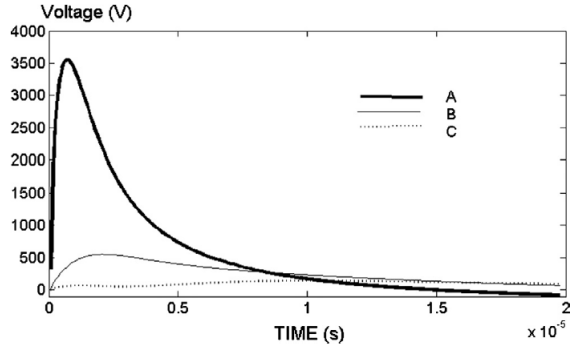

(a) Voltage response from [46, p. 31]

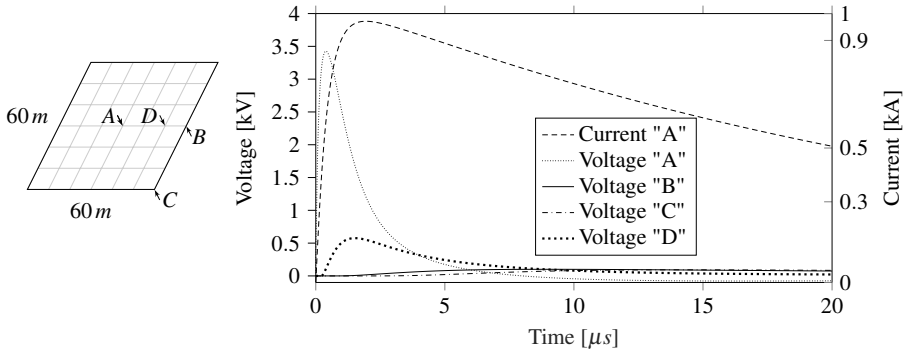

(b) Modeled and simulated voltage response

Figure 5.9: Voltage distribution in a grounding grid consistion of 6$\times$6 meshes of 10 m size. The grounding grid consist of conductors of American Wire Gauge (AWG) 2/0 $\approx$ a=0.004126 m, buried at d=0.6 m soil depth in soil of ρ_{soil}=100 Ωm and εr_{soil}=36. Results from implemented model in fig. 5.9b, with excitation current $\hat{I}$=1 kA double exponential waveform (α=38$\times$10^3, β=2.54$\times$10^6). Figure 5.9a gives result for comparison from research given in [46, p. 31].

5.4.2 Electric Field and Soil Ionization

In theory section 2.4.4 soil ionization is described as a factor that may introduce nonlinear discharge of the leaked current if the threshold value of electric field is exceeded. As described, the critical value of the electric field, E_c, is found in reviewed work with range from 400 to 1000 kV/m. However, the grain size and voids of air are strongly affecting the ionization level. Due to the construction method of the substations, with high water drainage, soil grains of larger size is expected. This concludes that the soil ionization level will fall in the lower range for this application. At present, the grounding system implementation is not capable of considering the nonlinear properties in the simulation. To evaluate this uncertainty in given results a manual check is performed based on section 2.4.4 and eq. (2.21). With a fixed grounding grid configuration it can be observed that the soil resistivity, ρ_{soil}, and leak current to the soil, I_{soil}, determine the electric field exerted on the soil close to the grounding grid conductor surface. Firstly, the grounding grid model in isolated mode is considered. With a controlled injection current through the double exponential source the exerted peak electric field, E_{soil}, is evaluated from the results in section 4.3 and is summarized in table 5.5. By considering the first length grounding wire after the injection point the highest voltage potential to true ground is considered, hence the maximum current leaked to the soil. This evaluation shows that the peak value for the grounding grid is below the lower level of the critical electric field for soil ionization, E_c = 400 kV/m. Which conclude that the results are given in sections 4.2 and 4.3 is simulated without this uncertainty.

Soil parameters	Peak leakage current	Conductor radius a	Peak electric field E_{soil}
300 Ωm, εr_{soil}=16	17.26 A	0.004126 m	200 kV/m
1000 Ωm, εr_{soil}=16	7.77 A	0.004126 m	300 kV/m
2000 Ωm, εr_{soil}=16	4.56 A	0.004126 m	352 kV/m

Table 5.5: Peak electric field, E_{soil}, in the grounding grid in isolated mode, according to section 4.2. Results collected from section 4.3.1 and fig. 4.15f and estimated by eq. (2.21)

For the cases when the grounding grid model is integrated as a part of the transmission system, the results are not as trivial. For both the long cable and short cable case, the results in section 4.6 shows electric field, E_{soil}, stronger than E_c = 400 kV/m, which may lead to soil ionization. For the long cable case, fig. 4.29a, E_c is exceeded in two separate time periods during the simulation due to reflection in the transmission system. However, the value is only exceeded for a limited time and with a low order of magnitude from E_c. This observation also applies to the short cable case in fig. 4.28a, while the duration is longer and the order of magnitude higher above the E_c.
As soil ionization is present, it will affect the results, for both the transmission and

the grounding system. For the transmission system, the results in sections 4.4 and 4.5 (with support from discussion in sections 5.2.3.1 and 5.2.4.1) shows that the grounding system variety of resistivity only shows a small effect on the transmission system. The soil ionization phenomena are therefore expected to present an insignificant error from these results. The ionization phenomena are expected to present a more significant impact on the voltage distribution in the grounding grid. Even though the time is short, and the electric field level exceed minor. Moreover, the grounding grid affected area of possible soil ionization is for both cases limited to the area close to the injection point as shown in figs. 4.28b and 4.29b for the long and short cable case, respectively. The area close to the injection point is the most critical area when considering the peak voltage in the grounding grid and overall system response. With the nature of soil ionization, the overall voltage distribution will be lowered if the critical field is exceeded. Even though the affected area of ionization is limited, the surge arrester as injection point will suffer on the nonlinear response in the grounding system. There is not found research describing the surge arrester discharge properties under these conditions which may be an interesting topic of investigation. A more present observation from these results lies in the limitations of implemented grounding grid models. If factors as higher currents are simulated, the soil ionization phenomena will act with a more significant impact on the results. Even if the grounding grid properties are modified, as higher resistivity soil or smaller grounding grid conductors, may have a substantial effect on the ionization activity. A method evaluated feasible to generalize the grounding system model for future implementation is described in section 2.4.4 by eq. (2.22).

5.4.3 Mutual Effects

The most significant limitation of present grounding system model, lies in ignoring the mutual effects. With the simplified method by Alipio and colleagues, they proposed in 2016 that the mutual coupling parameter in the grounding grid is estimated based on eq. (2.17) [13]. This simplification gives constant parameters of the mutual coupling. Also, it only considers the closest opposite wire segment as a contributor. As known from circuit theory, mutual coupling will only exist between wires which conduct current. This also applies to all grounding wires in the grounding grid, that any wire segment which is excited will contribute to the mutual coupling. To show a comparison, both for the grounding wires self parameters by eqs. (2.15) and (2.16) and the mutual coupling parameters values by eq. (2.17) is estimated and the results is given in table 5.6. The table shows that the mutual parameters have a significant contribution to the circuit when the parameters are treated as constants. As shown in the simulation results the surge wave propagation in the grounding system spreads out like time

and space traveling wave. There will be a time delay between the current is transferred between wire segments and excitation of the opposite grounding wire. If the mutual coupling parameters is fixed, the current between the wire segment should also be fixed to make the coupling parameters to interact. As the current injection rise time, with a steep front, is shown to be most critical in limiting the peak voltage, the grounding grid utilization will with fixed parameters for mutual coupling overestimate its contribution. Even when using smaller mesh sizes, a stronger mutual coupling is present; there is a time delay for the surge wave to reach the opposite conductor. However, when the grounding grid voltage distribution has reached stationary conditions, and an even current is flowing in all conductors, the constant parameters for mutual coupling has a more correct interacting in the grounding grid.

Parameter	Configuration	Soil parameters	Self ($_{ii}$)	Mutual ($_{ij}$)	Relative difference
L	10 m mesh size	2000 Ωm, εr_{soil}=16	2×10^{-6} H	1.2×10^{-6} H	0.6
G	10 m mesh size	2000 Ωm, εr_{soil}=16	4.7×10^{-4} S	8.8×10^{-4} S	1.9
C	10 m mesh size	2000 Ωm, εr_{soil}=16	1.3×10^{-10} F	2.5×10^{-10} F	1.9
L	5 m mesh size	2000 Ωm, εr_{soil}=16	2×10^{-6} H	1.54×10^{-6} H	0.8
G	5 m mesh size	2000 Ωm, εr_{soil}=16	4.7×10^{-4} S	7.2×10^{-4} S	1.5
C	5 m mesh size	2000 Ωm, εr_{soil}=16	1.3×10^{-10} F	2.0×10^{-10} F	1.5

Table 5.6: Grounding grid parameters estimated for comparison of self and mutual effects. Applicable for the simplified method presented by Alipio [13] (section 2.4.3.2)

With the integration of the grounding models in the transmission system, which may give pulsation currents into the soil, the method proposed by Alipio was evaluated to inaccurate. In 2004, Liu developed a non-uniform transmission line approach where each segment of mutual effects is interconnected by the actual conducted current. This method is described briefly in section 2.4.3.2. To make use of this advanced mathematical description in eqs. (2.18) to (2.20) of the transmission line model it required to solve the effective per-unit length parameters at each time step for each segment using Finite Difference Time Domain (FDTD). Even though the implementation is possible in present grounding system model, this task was evaluated unfeasible during the thesis project period. Liu reports a 20-30 % improvements in accuracy using the non-uniform transmission line approach for a single current injection compared to an implementation based on the EMF theory [9]. The improvements in simulation accuracy was observed in the stationary conditions area, where the mutual effects are strongest. When considering the impulse effective area and a fast front surge from a single injection pulse, the effect is less prominent. When the grounding system is interfaced in the transmission system, repeating stroke is observed from the results in section 4.5. The grounding system is already excited by a current when a second stroke is injected which leads to a stronger mutual coupling in the entire grounding grid. By the nature of the non-uniform

transmission line implementation, considering the per-unit mutual effects continuously, this approach is evaluated as beneficial when the grounding system is integrated with the transmission system. The non-uniform transmission line approach is therefore identified as a possible future implementation to improve the overall accuracy.

5.4.4 Frequency Dependent Soil

The frequency dependency of the soil is only considered when evaluating the per-unit length characteristics of the grounding wire in section 4.1. To model the frequency dependency was latest attempted quantified by Alipio and co-workers (section 2.4.2). The empirical formula (section 2.4.2 and eq. (2.13)) seems to be given without limitations to cover the soil behavior in the frequency range of lightning. While studying the results given in section 4.1 and fig. 4.1 for soil of ρ_{soil}= 70 and 100 Ωm the frequency dependent characteristics tends to give more conservative value (that the soil is more lossy). As shown in the modeling validation of a grounding grid (section 5.4.1.2), the simulated response is in comparison already more conservative than the reviewed work. By further reviewing the work of Alipio and co-works in [13] the only application given of the empirical formulation is to evaluate the GPR when built into a grounding system model. It seems like the empirical formula is not fitted generally to consider the soil as a medium, while the validity holds only when evaluating GPR. An interesting evaluation could be to evaluate the data developed by Alipio and co-workers to check the validity. If the validity is not applicable to assess the grounding system voltage potential rise (as in this thesis), the extended data-set could be used to fit new empirical formulas to cover this purpose.

5.4.5 Simplified Grounding Grid Geometry

The implemented models consist of grounding grids with 5×5 m and 10×10 meshes. For practical applications, such perfect geometric formation of the grounding conductor in the soil is unfeasible. At present, the modeling method is capable of implementing uneven distribution of the grounding grid meshes with one meter precision by the definition of the per-unit length grounding wire. This flexibility strengthens the selected modeling approach, by the implementation of a relatively short per-unit length. In addition, a simplification is made by only model the grounding grid elements. To improve performance, a standard practice is to supplement with vertical grounding rods, connected to the horizontally buried grounding grid, for selected points (section 2.4.1). For the future development, there is potential to include vertical grounding rods in the grounding system to perform more realistic simulations.

6 Conclusion

6.1 Conclusion

A new modeling approach which allows for integration of the grounding system when analyzing lightning surge performance of the transmission system is presented. By using the more detailed Matlab®/Simulink® model, large data-set are easier processed to extract overall measured values in EMC analysis and in addition processing different functions and parameters. Moreover, by taking advantage of the newly developed FMI interface, the grounding grid model itself is integrated as an element in the transmission system modeling and analysis by EMTP-RV.
The results show that a design deviation, with a long cable between the surge arrester and transformer, is not representing additional negative impact for the grounding system nor the transmission system. Instead, the long cable is shown to have a positive effect on the grounding system and are damping the overall peak voltage significantly. The increased voltage peak in the transmission system is evaluated insignificant on the overall insulation level.

6.2 Future work

Although the grounding system model presented in this work is simple, it is flexible and features significant potential for further development so that the accuracy could be improved.

- include mutual coupling between the grounding grid conductors by the non-uniform transmission line approach
- include soil ionization as an automated process
- implement and verify frequency dependency of the soil and dynamic parameter estimation
- fit new empirical formula for soil frequency dependency
- model verification through laboratory or field experiments
- investigate if soil ionization has a consequence on the surge arrester performance
- include a model of vertical grounding rods

References

[1] "Protection in an Unregulated Power Market - GPR and Lightning Protection – Risk Management," http://gpr-expert.com/protect-com.htm.

[2] "IEEE Application Guide for Surge Protection of Electric Generating Plants," *IEEE Std C62.23-1995*, 1995.

[3] *Statnett Earthing Guidelines, Part II. Implementation*. Statnett SF, 2010.

[4] K. Berger, "Novel observations on lightning discharges: Result of research on Mount San Salvatore," *Journal of the Franklin Institute*, vol. 283, pp. 478–525, 1967.

[5] L. V. Bewley, "Theory and tests of the counterpoise," *Electrical Engineering*, vol. 53, no. 8, pp. 1163–1172, Aug. 1934.

[6] P. L. Bellaschi, "Impulse and 60-cycle characteristics of driven grounds," *Electrical Engineering*, vol. 60, no. 3, pp. 123–127, Mar. 1941.

[7] E. D. Sunde, *Earth Conduction Effects in Transmission Systems*, 1st ed., ser. The Bell Telephone Laboratories. Dover Publications, 1949.

[8] B. R. Gupta and B. Thapar, "Impulse Impedance of Grounding Grids," *IEEE Transactions on Power Apparatus and Systems*, vol. PAS-99, no. 6, pp. 2357–2362, Nov. 1980.

[9] Y. Liu, "Transient Response of Grounding Systems Caused by Lightning: Modelling and Experiments," Ph.D., Uppsala University, Sweden, 2004.

[10] L. Grcev and F. Dawalibi, "An electromagnetic model for transients in grounding systems," *IEEE Transactions on Power Delivery*, vol. 5, no. 4, pp. 1773–1781, Oct. 1990.

[11] R. Velazquez and D. Mukhedkar, "Analytical Modelling of Grounding Electrodes Transient Behavior," *IEEE Transactions on Power Apparatus and Systems*, vol. PAS-103, no. 6, pp. 1314–1322, Jun. 1984.

[12] R. Alipio and S. Visacro, "A new model for the frequency dependence of soil parameters," in *2014 International Conference on Lightning Protection (ICLP)*, Oct. 2014, pp. 1432–1436.

[13] R. Alipio, R. M. Costa, R. N. Dias, A. D. Conti, and S. Visacro, "Grounding modeling using transmission line theory: Extension to arrangements composed of multiple electrodes," in *2016 33rd International Conference on Lightning Protection (ICLP)*, Sep. 2016, pp. 1–5.

[14] "Guide to Procedures for Estimating the Lightning Performance of Transmission Lines," *CIGRE WG C4.23*, 1991.

[15] *IEC Testing and Measurement Techniques - Surge Immunity Test*, 3rd ed., ser. 61000-4-5. International Electrotechnical Commission, 2014.

[16] V. Cooray, *Lightning Protection*, 1st ed., ser. Power and Energy. United Kingdom: The Institute of Engineering and Technology, 2010, no. 58.

[17] I. Djamel, F. H. Slaoui, and S. Georges, "Transient response of grounding systems under impulse lightning current," in *2016 Electric Power Quality and Supply Reliability (PQ)*, Aug. 2016, pp. 71–75.

[18] C. R. Paul, *Analysis of Multiconductor Transmission Lines*, 2nd ed. Hoboken, N.J: Wiley-IEEE Press, Oct. 2007.

[19] A. R. Bergen and V. Vittal, *Power System Analysis*, 2nd ed. New Jersey: Tom Robbins, 1999.

[20] A. Ametani, *Numerical Analysis of Power System Transients and Dynamics*, 1st ed., ser. Power and Energy. United Kingdom: The Institute of Engineering and Technology, 2015, no. 78.

[21] "IEEE Guide for the Application of Metal-Oxide Surge Arresters for Alternating-Current Systems," *IEEE Std C62.22-2009 (Revision of IEEE Std C62.22-1997)*, pp. 1–142, Jul. 2009.

[22] "Modeling of metal oxide surge arresters," *IEEE Transactions on Power Delivery*, vol. 7, no. 1, pp. 302–309, Jan. 1992.

[23] "IEEE Guide for Safety in AC Substation Grounding," *IEEE Std 80-2013 (Revision of IEEE Std 80-2000/ Incorporates IEEE Std 80-2013/Cor 1-2015)*, pp. 1–226, May 2015.

[24] "IEEE Guide for Measuring Earth Resistivity, Ground Impedance, and Earth Surface Potentials of a Grounding System," *IEEE Std 81-2012 (Revision of IEEE Std 81-1983)*, pp. 1–86, Dec. 2012.

[25] *Statnett Earthing Guidelines, Part I. Planning*. Statnett SF, 2010.

[26] *Forskrift om elektriske forsyningsanlegg med veiledning*, 2nd ed. Norway: Norsk Elektroteknisk Komite, 2006.

[27] A. Haddad and D. Warne, *Advances in High Voltage Engineering*, 1st ed., ser. Power and Energy. United Kingdom: The Institute of Engineering and Technology, 2009, no. 40.

[28] R. Alipio and S. Visacro, "Modeling the Frequency Dependence of Electrical Parameters of Soil," *IEEE Transactions on Electromagnetic Compatibility*, vol. 56, no. 5, pp. 1163–1171, Oct. 2014.

[29] R. Rüdenberg, "Grounding principles and practice I; Fundamental considerations on ground currents," *Electrical Engineering*, vol. 64, no. 1, pp. 1–13, Jan. 1945.

[30] J. He, R. Zeng, and B. Zhang, *Methodology and Technology for Power System Grounding*, 1st ed. Wiley, Nov. 2012.

[31] S. S. Pedersen, *Statnett Earthing Guidelines, Part III. Final Inspection*. Statnett SF, 2010.

[32] H. B. Dwight, "Calculation of Resistances to Ground," *Transactions of the American Institute of Electrical Engineers*, vol. 55, no. 12, pp. 1319–1328, Dec. 1936.

[33] S. Visacro, "A Comprehensive Approach to the Grounding Response to Lightning Currents," *IEEE Transactions on Power Delivery*, vol. 22, no. 1, pp. 381–386, Jan. 2007.

[34] Y. Liu, N. Theethayi, and R. Thottappillil, "An engineering model for transient analysis of grounding system under lightning strikes: Nonuniform transmission-line approach," *IEEE Transactions on Power Delivery*, vol. 20, no. 2, pp. 722–730, Apr. 2005.

[35] J. He, Y. Gao, R. Zeng, J. Zou, X. Liang, B. Zhang, J. Lee, and S. Chang, "Effective length of counterpoise wire under lightning current," *IEEE Transactions on Power Delivery*, vol. 20, no. 2, pp. 1585–1591, Apr. 2005.

[36] E. E. Oettle, "A new general estimation curve for predicting the impulse impedance of concentrated earth electrodes," *IEEE Transactions on Power Delivery*, vol. 3, no. 4, pp. 2020–2029, Oct. 1988.

[37] "Estimating lightning performance of transmission lines. II. Updates to analytical models," *IEEE Transactions on Power Delivery*, vol. 8, no. 3, pp. 1254–1267, Jul. 1993.

[38] J. He, B. Zhang, P. Kang, R. Zeng, and B. Zhang, "Lightning Impulse Breakdown Characteristics of Frozen Soil," *IEEE Transactions on Power Delivery*, vol. 23, no. 4, pp. 2216–2223, Oct. 2008.

[39] "IEEE Guide for the Application of Insulation Coordination," *IEEE Std 1313.2-1999*, 1999.

[40] Modelica Association c/o PELAB, "Functional Mock-up Interface," http://fmi-standard.org/, Mar. 2018.

[41] J. Cornau, *Guide EMTP-RV Matlab/Simulink FMI Export*. Powersys, Jan. 2018.

[42] MathWorks, "Solve moderately stiff ODEs and DAEs — trapezoidal rule - MATLAB ode23t - MathWorks Nordic," https://se.mathworks.com/help/matlab/ref/ode23t.html?s_tid=doc_ta, Feb. 2018.

[43] S. T. Hagen, *Lightning Strike Analysis*. Western Norway University of Applied Sciences, 2016.

[44] J. A. Martinez-Velasco, Ed., *Power System Transients: Parameter Determination*, 1st ed. Boca Raton, FL: CRC Press, Oct. 2009.

[45] L. D. Grcev, "Computer analysis of transient voltages in large grounding systems," *IEEE Transactions on Power Delivery*, vol. 11, no. 2, pp. 815–823, Apr. 1996.

[46] A. Jardines, J. L. Guardado, J. Torres, J. J. Chávez, and M. Hernández, "A multi-conductor transmission line model for grounding grids," *International Journal of Electrical Power & Energy Systems*, vol. 60, no. Supplement C, pp. 24–33, Sep. 2014.

Appendices

A Master Thesis Project Description

Faculty of Engineering
Department of Electrical Engineering
Date: 17.09.2017

HØGSKOLEN I BERGEN
BERGEN UNIVERSITY COLLEGE

Master degree project in *Energy – Energy Technology*

Project title: **Study of hydropower substation grounding performance under transient lightning surge conditions**

Description:

A typical arrangement for large hydropower stations compose of one or more generators and each generator with an associated step-up (main) transformer located in a rock cavity inside a mountain. The main transformers are connected to a switchyard (air insulated or insulated) via relatively long cables that differ not much in length; typically, several hundred meters long. The switchyard is connected to the grid via overhead transmission lines. Due to space restrictions and fire hazard, surge arresters have traditionally been installed only in the switchyard and not close to the transformer. The normal recommendation for surge arrester are placement close to the transformer to avoid high voltage build-up caused by voltage transient surge waves reflections.
With the present design for hydropower station and placement of the surge arrester, the overvoltage situation during lightning surge is well documented. However, the effect of a pulsating voltage surge wave into the grounding system needs investigation.
The design of switchyard grounding system has optimized properties for low-frequency faults, at power frequency (50 Hz). With a buried mesh layout it aims to give low resistance ground connection at any point over the switchyard area and secure low ground potential voltage rise in fault situations. This design is not optimized for high-frequency and fast front transient current injections, as characterised for lightning surge wave.

This study will investigate how the switchyard grounding system responds under direct lightning transient voltages and the effect of relatively long cables between surge arrester and transformer. The study will give practical outlines to Steinsland Kraftverk in Modalen that are in an upgrade phase raising the system voltage from 300 to 420 kV. A new switchyard is under construction following the latest standards for equipment and design.

Activity	Fall 2017					Spring 2018					
1. Field survey and literature search	■	■									
2. Define scope of work		■	■								
3. Develop method for investigation of ground system			■	■	■	■	■	■			
4. Simulation/modification and verification of method						■	■	■	■		
6. Reporting				■	■	■	■	■	■	■	■

Company Project Supervisors and Contact persons:

Technical manager power stations, Lars Søreide (lars.soreide@bkk.no)
Head of Section, Magne Harkestad (magne.harkestad@bkk.no)

University Project Supervisors and Contact persons:

Assistant professor, Lasse Sivertsen (Lasse.Hugo.Sivertsen@hvl.no)

Bergen University College
Phone: + 47 55 58 75 00
E-mail: post@hib.no

;

B IEEE ICHVE 2018 Conference Paper

The implemented model developed in this thesis is given as a contribution to IEEE International Conference on High Voltage Engineering and Application (ICHVE 2018), which is organized by National Technical University of Athens – Greece and endorsed by IEEE Dielectrics and Electrical Insulation Society. More information about the conference can be found on `http://ichve2018.ece.ntua.gr/`. All contributions presented at the conference September 10-13, 2018 will be transferred to IEEE Xplore digital library and can be found through the persistent link `https://ieeexplore.ieee.org/servlet/opac?punumber=1002613`. In the following two sections the full conference paper (4-page limitation) written during this thesis is attached in section B.1 and the one page summary in section B.2.

As defined in section 1.4, the thesis and conference paper should be treated as confidential with described limitations.

B.1 Full Conference Paper

A New Method to Include Complex Grounding System in Lightning Transient Studies and EMI Evaluations

V. Steinsland, L.H. Sivertsen, E. Cimpan, S. Zhang
Department of Electrical Engineering, Western Norway University of Applied Sciences
Inndalsveien 28, N-5063 Bergen, NO
v.steinsland@me.com

Abstract: **A new method of including complex grounding grids of electrical power transmission system in lightning transient studies is presented in this paper. The grounding system is modeled in Matlab/Simulink based on the transmission line theory. With a bottom-up approach, considering the properties of the fundamental elements a detail view of measurement values will be presented and analyzed. The Matlab/Simulink grounding system models are interfaced for co-simulation with EMTP-RV trough FMI 2.0. This modeling approach allows the use of the full component library and network design by EMTP-RV to evaluate and analyze the effects of the grounding system and transmission network simultaneously in Matlab/Simulink. The results presents a simplified transmission system where a surge is injected, CIGRE 1 kA 1.2/50, in far-end of a transmission line. When reaching a substation, the surge is injected into the grounding system through a surge arrester.**

I. Introduction

The grounding system that is essential in the manner of proper, reliable and safe operation of the power system can be accomplished by providing a true reference to the electrical system that controls the discharge path of high energy faults. The performance of the grounding system during power frequency faults is a present key driver in general design of substation grounding system [1]. The transient behavior of the grounding system during a lightning discharge is characterized by a steep front that induces inductive effects in the grounding system. Thus, a large short-term voltage rises within the grounding system region, close to the injection point.

The uneven voltage distribution can be explained in terms of current and voltage waves traveling along the grounding grid conductors that can be modeled by the telegrapher's equation. The computer models for analyzing the voltage distribution in grounding grids and associated equipment are used to carry out electromagnetic interference (EMI) studies.

The problematic lightning surge behavior has long been recognized by the industry and several models to describe these transient events, and related topics have been proposed in the relevant literature. However, an easy implementation method to evaluate the effect which is associated with lightning transient in the transmission system and the corresponding effect on the grounding system is not found publicly available.

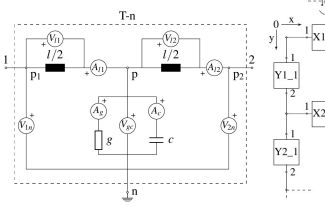

Figure 1a. Implemented per-unit length T-section

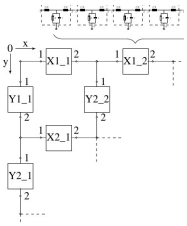

Figure 1b. Implementation strategy

II. Modeling the Grounding System

Based on the classic work by Sunde the grounding system in this work has been modelled as a lossy transmission line [2]. The soil medium characterized by electrical resistivity and permittivity surrounds the grounding wires that are characterized by their electrical parameters thus forming a unified system. The per-unit length grounding wire is implemented in Matlab as a T-section of the transmission line model, which represents the fundamental electric element (see Figure 1a). An appropriate number of T-sections and additional nodes implement the grounding system using Simulink graphical block elements as illustrated in Figure 1b. Thus, the grounding system electrical elements are connected to physical properties of the grounding system layout. To assure a smooth representation of the interconnection between elements and to possibly extend the model functionality of including mutual couplings the T-section represent one meter of ground wire (per unit length) [3]. Consequently, the model functionality can be extended to arbitrary lengths.

This consideration gives the total number of logged variables as an indication for selected grounding grid configurations of square sizes as shown in Table I.

TABLE I
Required number of logged variables per grounding grid size

Grounding Grid Configuration	Area	Logged variables
5 × 5 m meshes	1600 m^2	6480
	3600 m^2	14040
10 × 10 m meshes	1600 m^2	3600
	3600 m^2	7560

III. Parameters of the Grounding System

When selecting the transmission line model to represent the grounding wire and soil as a system the electrical parameters in per unit length are defined through eq. 1 and 2

$$y = (g + j\omega c)l_{unit} \tag{1}$$

$$z = (r + j\omega l)l_{unit} \tag{2}$$

Where g is defined as the grounding system conductance (S), c is the capacitance (F), r is the internal wire resistance (Ω), l is the inductance (H) and l_{unit} is the per-unit length (m).

Due to relatively short conductor length and large cross section the internal resistance (including the skin effect) and inductance are significantly smaller than the external self-inductance. With this consideration, a simplification to only include the self-inductance is made [4].

The connection between the soil properties and the grounding system elements defined above is represented by eq. (3) to (5) [2].

$$g = \frac{\pi}{\rho_{soil}\left(\ln\frac{2}{\sqrt{2ad)}} - 1\right)} \tag{3}$$

$$c = \frac{\pi\varepsilon_{soil}}{\ln\frac{2}{\sqrt{2ad)}} - 1} \tag{4}$$

$$l = \frac{\mu_0}{\pi}\left(\ln\frac{2}{\sqrt{2ad}} - 1\right) \tag{5}$$

Where ρ_{soil} is the soil resistivity (Ωm), ε_{soil} is the soil relative permittivity (-), a, is the conductor radius and d is the buried depth (m).

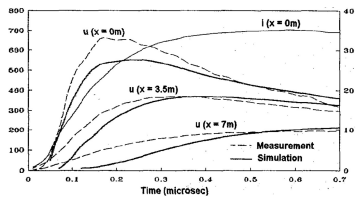

Figure 2a. Based on measurements and EMF theory, adopted from [5]

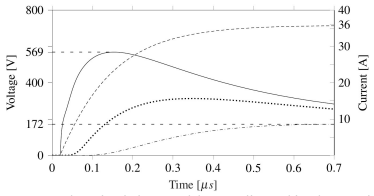

Figure 2b. Based on simulation: Matlab grounding rod implementation

IV. Model Verification

The grounding system model is validated by the work based on the electromagnetic field (EMF) theory first performed by Grcev [5] and later by Jardines [6] who introduced a variant of the multiconductor transmission line (MTL) approach. In these cases of model verifications, the current source is implemented using the double exponential waveform ($i(t) = I(e^{-\alpha t} - e^{-\beta t})$) and the source parameters where adjusted to fit the given stroke function.

A. Grounding rod of 15 m *length*

A grounding rod of 15 m was simulated and measured by Grcev [5] and later evaluated by Jardines [6] as shown in Figure 2a. Using two independent modeling approaches and relative similarities in results confers confidence with respect to model verification. The grounding rod is buried in soil of ρ_{soil} = 70 Ωm, ε_{soil}=15, with a wire radius of a = 0.012 m at depth d = 0.6 m. The current source where set with the amplitude of 36 A and the stroke of 0.36/12 μs which lead to the new parameter values $\alpha = 32\times10^3$ and $\beta = 7.6\times10^6$ The results from the implemented model are given in Figure 2b.

As it can be observed from the simulations, the peak values at the injection point are approximate 560 V while by using more accurate readings, the implemented grounding model gives 569 V [5]. The second point for comparison is at 7 m from the injection point where Grcev simulations [6] show approximate 200 V while the results in this work give 171 V after 0.7 μs. Besides the point value readings, the surge wave propagation along the grounding rod and voltage distribution are of similar character.

B. Grounding grid of 10 m meshes with total size 3600 m²

A grounding system of 10 × 10 m meshes size and a total square footing of 3600 m² where simulated by Jardines [7] using a variant of the multiconductor transmission line approach (see Figure 3a). The grounding grid was buried in soil of ρ_{soil} = 100 Ωm, ε_{soil} = 36, with a wire radius of a = 0.004126 m at depth d = 0.6 m. The current source was set with amplitude of 1 kA and a 1/20 μs stroke which gave adjusted parameters to $\alpha = 38\times10^3$ and $\beta = 2.54\times10^6$. The results from the implemented model in this work are given in Figure 3b. As the injected current is not given in the referenced work it is worth noting that a small deviation in the injected current will have a large impact on the grounding system response, especially for the region contributing to limiting the peak voltage. As it can be observed, both the voltage distribution and the propagation characteristics corresponds well. When comparing the simulation to Grcev [5] which was based on EMF the simulation in the presented work, the peak value and the propagation characteristics are of comparable values. However, the distributed voltage at the given nodal points are more conservative with the transmission line methods, both the implemented model and based on Jardines work. This may unveil differences in model accuracy based on the EMF theory and the transmission line approach.

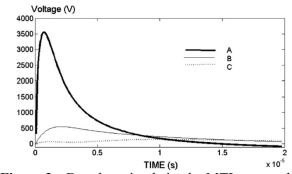

Figure 3a. Based on simulation by MTL approach, adopted from [6]

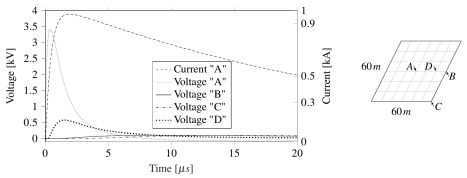

Figure 3b. Based on simulation of the grounding grid implementation

V. Integration of Grounding and Transmission System

The grounding system is of main attention in this presentation, given the transmission system as a secondary priority. Thus, the transmission system is simplified except the most important component of the grounding system, that is the stroke current source and the surge arrester at the injection point. The Matlab/Simulink developed grounding grid are integrated with EMTP-RV through a newly developed Functional Mock-Up Interface (FMI) [7], which was released by Powersys Solutions in early 2018. The FMI package gives possibilities for co-simulation with information exchange at a per simulation time-step interval (sequentially processed). From the transmission system surge arrester, the injection point impedance describes the grounding system response trough eq. (6).

$$Z(\omega) = \frac{U(\omega)}{I(\omega)} \tag{6}$$

When the transmission system surge arrester reaches the breakdown voltage a current surge is injected into the grounding system. The current injection value is exchanged from EMTP-RV to Matlab, which simulates the grounding system response. The grounding system initial impedance is set to the power frequency value, corresponding to the grounding system resistance [8]. From the injection point current and the induced voltage potential rise, the impulse impedance is calculated and exchanged from Matlab to EMTP-RV, which gives the dynamic response of the grounding system to the transmission system.

With a large number of logged variables required by the grounding system (see Table 1) and presented implementation strategy, the additional measured values of the transmission system were exchanged from EMTP-RV to Matlab to provide a common simulation log for pre-processing.

The advanced functionality offered by the Matlab/Simulink modeling of the per-unit length grounding wire (see Figure 1a) lies in the pre-processing of large data-sets.

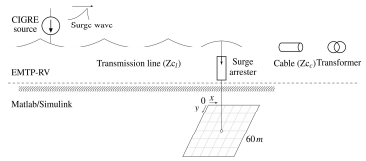

Figure 4. Simplified transmission system and grounding model interfaced

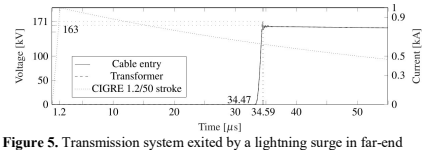

Figure 5. Transmission system exited by a lightning surge in far-end

VI. An Example of Results: Case Study

A simplified transmission system network is shown in Figure 4 with the grounding system model in Matlab interfaced. In EMTP-RV basic components available from the standard software library is used. At 10 km distance from a substation, a lightning strikes the 300 kV overhead transmission line (Zc_l = 400). A shielding failure causes an injected current having a magnitude of 1 kA and 1.2/50 μs of CIGRE waveform stroke to flow towards the substation. In the substation, the cable (Zc_c = 45) between the surge arrester (Appendix A) and transformer are 10 m. Figure 5 shows the simulation results of the transmission system when the grounding system is ignored, thus giving a peak voltage of 171 kV at the transformer.

A grounding system with 10 × 10 m mesh size are added and a total square footing of 3600 m^2 in soil of $\rho_{soil} = 2000$ Ωm, $\varepsilon_{soil} = 16$, with a wire radius of a = 0.04126 m at depth d = 0.6 m, the transmission system conditions are similar. The simulation results are given in Figure 6. As it can be observed the surge arrester performance is reduced to give a peak transformer voltage of 190 kV. Then, the EMI analysis of the substation is performed based on the overall distributions and presented here for selected key time steps in Figure 6c and 6d.

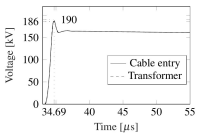

Figure 6a. Transmission system

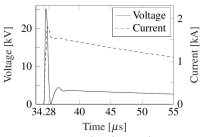

Figure 6b. Injection point

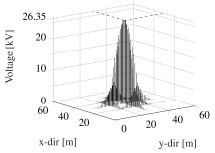

Figure 6c. t=34.59 μs: Peak

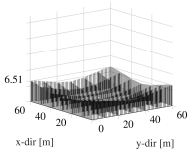

Figure 6d. t=35.74 μs: Peak corner

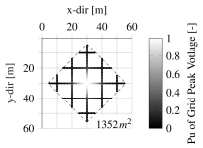

Figure 6e. t=34.59 µs: Impulse effective area

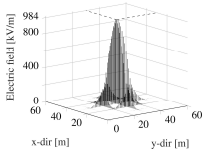

Figure 6f. t=34.59 µs: Peak Electric field

With the comprehensive log dataset further analysis is exemplified in Figure 6e and 6f.

The impulse effective area of the grounding grid defined in [9] is shown in Figure 6e. This is the total area of the grounding grid which limits the peak voltage in the grid. There exists several definitions and empirical formulas for estimating the effective length when optimizing the grounding grid design that was recently evaluated [10]. However, these approaches have not taken the transmission line network itself as an integrated element into consideration.

In addition, the electric field exerted on the soil close to the grounding wires that was based on the current density leaked to the soil is shown in Figure 6f. If the ionization level is reached the electric field in the soil has pronounced influence on the impulse peak voltage. Moreover, ionization has a positive effect by lowering the peak voltage due to arcing or puncturing in the soil [11].

VII. Conclusion

The new modeling approach allows easy integration of the grounding system when analyzing lightning surge performance of the transmission system. By using the more detailed Matlab/Simulink model presented in this work, large data-set are easier processed to extract overall measured values in EMI analysis and in addition processing different functions and parameters of the grounding system such as the effective length and the electric field distribution (Figure 6e and f). Moreover, by taking advantage of the newly developed FMI interface, the grounding grid model itself is integrated as an element in the transmission system modeling and analysis by EMTP-RV. Lastly, the surge arrester performance is given when including the grounding system and consequently, the corresponding effects of all parts in the transmission system could be more accurately analyzed.

Although the grounding system model presented in this work is simple, it is flexible and features significant potential for further development so that the accuracy could be improved.

VIII. References

[1] "IEEE Guide for Safety in AC Substation Grounding," *IEEE Std 80-2013 (Revision of IEEE Std 80-2000/ Incorporates IEEE Std 80-2013/Cor 1-2015)*, pp. 1–226, May 2015.

[2] E. D. Sunde, "Surge characteristics of a buried bare wire," *Electrical Engineering*, vol. 59, no. 12, pp. 987–991, Dec. 1940.

[3] Y. Liu, "Transient Response of Grounding Systems Caused by Lightning: Modelling and Experiments," Ph.D., Uppsala University, Sweden, 2004.

[4] Y. Liu, N. Theethayi, and R. Thottappillil, "An engineering model for transient analysis of grounding system under lightning strikes: nonuniform transmission-line approach," *IEEE Transactions on Power Delivery*, vol. 20, no. 2, pp. 722–730, Apr. 2005.

[5] L. D. Grcev, "Computer analysis of transient voltages in large grounding systems," *IEEE Transactions on Power Delivery*, vol. 11, no. 2, pp. 815–823, Apr. 1996.

[6] A. Jardines, J. L. Guardado, J. Torres, J. J. Chávez, and M. Hernández, "A multiconductor transmission line model for grounding grids," *International Journal of Electrical Power & Energy Systems*, vol. 60, no. Supplement C, pp. 24–33, Sep. 2014.

[7] "Functional Mock-up Interface." [Online]. Available: http://fmi-standard.org/. [Accessed: 20-Mar-2018].

[8] "IEEE Guide for Measuring Earth Resistivity, Ground Impedance, and Earth Surface Potentials of a Grounding System," *IEEE Std 81-2012 (Revision of IEEE Std 81-1983)*, pp. 1–86, Dec. 2012.

[9] B. R. Gupta and B. Thapar, "Impulse Impedance of Grounding Grids," *IEEE Transactions on Power Apparatus and Systems*, vol. PAS-99, no. 6, pp. 2357–2362, Nov. 1980.

[10] L. Grcev, "Lightning Surge Efficiency of Grounding Grids," *IEEE Transactions on Power Delivery*, vol. 26, no. 3, pp. 1692–1699, Jul. 2011.

[11] J. He *et al.*, "Effective length of counterpoise wire under lightning current," *IEEE Transactions on Power Delivery*, vol. 20, no. 2, pp. 1585–1591, Apr. 2005.

IX. Acknowledgment

The authors thank for the support given by Western Norway University of Applied Sciences and the University of Bergen to carry out this work.

X. Appendix

A. Surge Arrester V-I characteristics (EMTP-RV modelnr. 865630)

Nr.	k_{seg}	α_{arr}	U_{arr}(pu)
1	$4.2320809927173\times10^{9}$	24.027929621999	0.2981982709534
2	$2.817736450539\times10^{10}$	26.621933338397	0.4815000000000
3	$4.1514408701929\times10^{8}$	20.087041308578	0.5244503689103
4	$2.632714050144\times10^{12}$	35.290671008959	0.5622308403187
5	$3.2177414981782\times10^{6}$	11.131057054327	0.5691920365927
6	$1.9377462130077\times10^{5}$	5.3627012501430	0.6144084498043

B.2 One Page Summary of Conference Paper

A NEW METHOD TO INCLUDE COMPLEX GROUNDING SYSTEM IN LIGHTNING TRANSIENT STUDIES AND EMI EVALUATIONS

V. Steinsland, L.H. Sivertsen, E. Cimpan, S. Zhang
Department of Electrical Engineering, Western Norway University of Applied Sciences
Inndalsveien 28, N-5063 Bergen, NO
v.steinsland@me.com

Abstract: A new method of including complex grounding grids of electrical power transmission system in lightning transient studies is presented in this paper. The grounding system is modeled in Matlab/Simulink based on the transmission line theory. With a bottom-up approach, considering the properties of the fundamental elements, a detail view of measurement values will be presented and analyzed. The Matlab/Simulink grounding system models are interfaced for co-simulation with EMTP-RV trough FMI 2.0. This modeling approach allows the use of the full component library and network design by EMTP-RV to evaluate and analyze the effects of the grounding system and transmission network simultaneously in Matlab/Simulink.

1. INTRODUCTION

The grounding system that is essential in the manner of proper, reliable and safe operation of the power system can be accomplished by providing a true reference to the electrical system that controls the discharge path of high energy faults. The performance of the grounding system during power frequency faults is a present key driver in general design of substation grounding system [1]. The transient behavior of the grounding system during a lightning discharge is characterized by a steep front that induces inductive effects in the grounding system. Thus, a large short-term voltage rises within the grounding system region, close to the injection point.

2. RESULTS

Based on the classic work by Sunde the grounding system in this work has been modeled as a lossy transmission line in Matlab/Simulink [2]. The Matlab/Simulink developed grounding grid is integrated with EMTP-RV through a newly developed Functional Mock-Up Interface (FMI) [3], which was released by Powersys Solutions in early 2018.

A modeling case has been selected to present the simplified transmission network system interfaced with the grounding system as shown in Figure 1. In EMTP-RV basic components available from the standard software library is used. At 10 km distance from a substation, a lightning strikes the 300 kV overhead transmission line (Zc_l = 400). A shielding failure causes an injected current having a magnitude of 1 kA and 1.2/50 µs of CIGRE waveform stroke to flow towards the substation. In the substation, the cable (Zc_c = 45) between the surge arrester and transformer are 10 m.

To the transmission network system is added a grounding system with 10 × 10 m mesh size and total area of 3600 m^2 in soil of ρ_{soil} = 2000 Ωm, ε_{soil} = 16, with a wire radius of a = 0.04126 m at depth d = 0.6 m. Selected simulation results are given in Figure 2. The surge arrester performance is reduced to give a peak transformer voltage of 190 kV (171 kV ignoring the grounding system). A detailed EMI analysis of the substation grounding system can be performed as presented in Figure 2c and d.

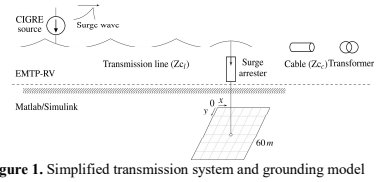

Figure 1. Simplified transmission system and grounding model

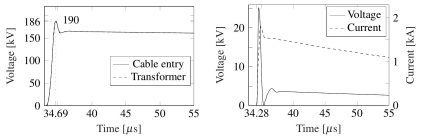

Figure 2a. Transmission system **Figure 2b.** Injection point

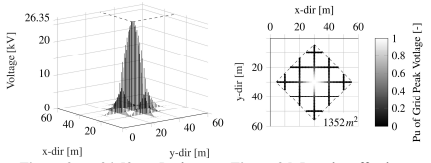

Figure 2c. t=34.59 µs: Peak **Figure 2d**. Impulse effective area

3. CONCLUSION

The new modeling approach allows easy integration of the grounding system when analyzing lightning surge performance of the transmission system. By using the more detailed Matlab/Simulink model presented in this work, large data-set are easier processed to extract overall measured values in EMI analysis and in addition processing different functions and parameters.

Moreover, by taking advantage of the newly developed FMI interface, the grounding grid model itself is integrated as an element in transmission system modeling by EMTP-RV.

4. REFERENCES

[1] "IEEE Guide for Safety in AC Substation Grounding," *IEEE Std 80-2013 (Revision of IEEE Std 80-2000/ Incorporates IEEE Std 80-2013/Cor 1-2015)*, pp. 1–226, May 2015.
[2] E. D. Sunde, "Surge characteristics of a buried bare wire," *Electrical Engineering*, vol. 59, no. 12, pp. 987–991, Dec. 1940.
[3] "Functional Mock-up Interface." [Online]. Available: http://fmi-standard.org/. [Accessed: 20-Mar-2018].

C CIGRE Lightning Surge Waveform

CIGRE Standard lightning impulse, 1.2/50-stroke, with definitions of rise (t_{rise}) and half time (t_{half}). Implemented according to [16, pp. 67-70]
Used to produce fig. 2.1 in section 2.1

```
trise=1.2;
thalv=50;


sn=0.9*(trise);
tn=0.6*(trise)*((3*sn^2)/(1+sn^2));
t1=((thalv-tn)/log(2));
t2=0.1/0.9;

I1=(((t1*t2)/(t1-t2)))*(0.9+0.9/t2);
I2=(((t1*t2)/(t1-t2)))*(0.9+0.9/t1);

exa=(1+(2*(sn-1)*(2+1/sn)));

A=(1/(exa-1))*(((0.9/tn)*exa)-0.9);
B=(1/(tn^(exa)*(exa-1)))*((0.9*tn)-0.9);

t3=0:0.03:trise;
t4=trise:0.03:4;
t5=4:1:400;

creest=A*t3+B*(t3.^(exa));
half=((I1*exp(-(t4-tn)/t1))-(I2*exp(-(t4-tn)/t2)));
half2=((I1*exp(-(t5-tn)/t1))-(I2*exp(-(t5-tn)/t2)));
plot(t3,creest,t4,half,t5,half2);
```

D Matlab® Implementation of Grounding Grid

A full representation of the implemented Matlab® m-code for the grounding system is given. This appendix is structured by load scripts, call functions, plot scripts, Simulink® models and developed equipment blocks with m-code. The listed m-code and models do not use similar notation/symbols as given in the report main content. Therefore, a reference to report content (e.g. sections, equations, tables) are implemented directly in the m-code in attempt to increase readability and raise the level of understanding. The code export from Matlab® to LaTeXwas made with the add-on package "M2TEX" version 1.0, distributed on the MathWorks® forum.

The following section is preferably viewed on screen or printed with colors.

D.1 Load Scripts

D.1.1 Definition of the Grounding Grid Geometric Properties

D.1.1.1 6×6, 10×10 m Meshes, 3600 m^2

```
% Definition of the grounding grid geometric properties
% for the simulation model "Sim10m_36MeshGrid.slx"
%
% Definition must be loaded, for the spesific grounding grid,
% infront of nodal data extraction from loaded simlog
%
nXWireRows=7;    % Number of horizontal wire segments
nXWireCol=6;     % Number of horizontal wire per segment

nYWireCol=7;     % Number of vertical wire per segment
nYWireRows=6;    % Number of vertical wire segments

%Geometry data for location data grounding grid
nlengthSegElement=10; % Number of lengths per wire segments
lengthSeg=1;     % length per segment[m]
nMeshes=36;      % number of Meshes
```

D.1.1.2 4×4, 10×10 m Meshes, 1600 m^2

```
% Definition of the grounding grid geometric properties
% for the simulation model "Sim10m_16MeshGrid.slx"
%
% Definition must be loaded, for the spesific grounding grid,
% infront of nodal data extraction from loaded simlog
%
nXWireRows=5;    % Number of horizontal wire segments
nXWireCol=4;     % Number of horizontal wire per segment
```

```
nYWireCol=5;     % Number of vertical wire per segment
nYWireRows=4;    % Number of vertical wire segments

%Geometry data for location data grounding grid
nlengthSegElement=10; % Number of lengths per wire segments
lengthSeg=1;     % length per segment[m]
nMeshes=16;      % number of Meshes
```

D.1.1.3 12×12, 5×5 m Meshes, 3600 m^2

```
% Definition of the grounding grid geometric properties
% for the simulation model "Sim5m_144MeshGrid.slx"
%
% Definition must be loaded, for the spesific grounding grid,
% infront of nodal data extraction from loaded simlog
%
nXWireRows=13;   % Number of horizontal wire segments
nXWireCol=12;    % Number of horizontal wire per segment

nYWireCol=13;    % Number of vertical wire per segment
nYWireRows=12;   % Number of vertical wire segments

%Geometry data for location data grounding grid
nlengthSegElement=5; %Number of lengths per wire segments
lengthSeg=1;     % length per segment[m]
nMeshes=144;     % number of Meshes
```

D.1.1.4 8×8, 5×5 m Meshes, 1600 m^2

```
% Definition of the grounding grid geometric properties
% for the simulation model "Sim5m_64MeshGrid.slx"
%
% Definition must be loaded, for the spesific grounding grid,
% infront of nodal data extraction from loaded simlog
%
nXWireRows=9;    % Number of horizontal wire segments
nXWireCol=8;     % Number of horizontal wire per segment

nYWireCol=9;     % Number of vertical wire per segment
nYWireRows=8;    % Number of vertical wire segments

%Geometry data for location data grounding grid
nlengthSegElement=5; % Number of lengths per wire segments
lengthSeg=1;     % length per segment[m]
nMeshes=64;      % number of Meshes
```

D.1.2 Grounding Grid Physical Properties

```
%%
% The grounding grid physical properties is defined in according to
% section 4.2 and table 4.1

% column 1-- conductor segment number [-]
% column 2-- lenght of conductor (m)
lenght = 1;          % Per unit lenght, set to 1 meter for all models
% column 3-- y position, depth in ground (m)
depth = 0.6;         % Burial depth in the soil, set to 0.6 meter for all
                     % models
% column 4-- radii of each conductor (m)
a = 0.004126;        % Ground conductor radi, set to 0.004126 meter for all
                     % models
```

```
% column 5-- conductor resistivity (Ohm-m)
Rcu = 1.68*1E-8;     % Ohm-m resistivity of the copper.
% column 6-- distance between conductors (m)
space = %;           % Set distance between conductors in ground
                     % (5 or 10 meter is implemented)

% Based on the above properties the grounding grid geometry is defined
Geom=[1 lenght depth a Rcu space];

%%
% Definition of universal constants
Mu = 4*pi*1E-7; % Permeability of vaccum [Henry/meters]
Eo = (1/(36*pi))*1E-9; % Permittivity of vaccum [Farads/meters]

%%
% Definition of parameters to perform frequency sweep in range of lightning
Ns = 50; % Number of samples
f = logspace(1,7,Ns); % Vector of log spaced Frequencies
w = 2*pi*f; % Vector of freqs in radian/sec.

%%
%Defines the soil parameters for the grounding grid area.
Rsu=%; % Soil resistivity [Ohm-m]
Ers=%; % Relative permittivity soil [-]
Er=Eo*Ers; %Soil spesific permittivity [Farads/meters]

%%

% Call of function script to define the per-unit length parameters in
% section D.2.1.
% The defined name must be aligned with variable definitions for the actual
% t-section which are defined in section D.1.3 and fig. D.1b


[y,z,yp,Zc,L,Lmut,Gsel,Gmut,C1,Cmut] = GroundSysPar...
    (lenght,Geom,Mu,Rsu,Er,Rcu,Ns,w);
[y,z,yp,Zc,L,Lmut,Gsel,Gmut,C1,Cmut] = GroundSysPar...
    (lenght,Geom,Mu,Rsu,Er,Rcu,Ns,w);


% If defined with non-uniform soil, several corresponding variables must be
% defined. As shown below for the second area of the grounding
% grid may be estimated. The t-section variable, for corresponing are must
% be defined accordingly
% (section D.1.3 and fig. D.1b)


Rsu2 = %; % Soil resistivity [Ohm-m]
Ers2= %; % Relative permittivity soil [-]
Er2=Eo*Ers2; %Soil spesific permittivity [Farads/meters]

[ys2,zs2,yps2,Zcs,L2,Lmut2,Gsel2,Gmut2,Csel2,Cmut2] = GroundSysPar...
    (lenght,Geom,Mu,Rsu2,Er2,Rcu,Ns,w);
```

D.1.3 Grounding Grid Per-Unit Length T-section

```
% Updated 10.02
% Updated 14.01
% Updated 28.12
% T-Section Transmission line, modelled as a per-unit
% length grounding wire. Please note the filetype of ssc, which utilize
% Simulink and Simscape libraries.

% Each per-unit length wire in the grounding grid must be defined
% according to wished grounding grid properties in loaded Simulink model
% and run of calulation load scripts in section D.1.2
```

```
import foundation.electrical.elements.*; % Electrical elements
import foundation.electrical.electrical; % Electrical domain
component t_section2

nodes
    p1 = electrical; % 1:top
    p2 = electrical; % 2:top
    n  = electrical; % n:bottom
end

% Initial parameters for one meter segment copper wire. Vaules are based
% on soil Er=16 and resitivity of 300 ohm/m, depth=0.6 m. Static and
% dynamic changes of the per unit segment values are handled by
% supporting scripts MainGroundGrid
parameters
    length = {1, 'm'}; % Segment length
    R = {0.00187, 'Ohm/m'}; % Resistance per-unit length
    L = {1.8620, 'uH/m'};  % Inductance per-unit length

    C = {31.935, 'pF/m'};   % Capacitance per-unit length
    G = {0.01, 'S/m'};  % Soil conductance per-unit length
end

% Defining the grounding system per-unit lenght parameters in a T-Section
% and connects the standard library of Simscape to utilize solver.
% Definition give measurment of current/voltage at each node by utilizing
% the Simulink Simcape enviorment.
components(Hidden=true)
% Per-unit length impedance
    r1 = resistor(R=R*length/2); % Grounding wire internal resistance,
    r2 = resistor(R=R*length/2); % are made available but set to zero in
                                 % in Simulation

    l1 = inductor(l=L*length/2); % Inductance of the grounding wire in the
                                 % soil
    l2 = inductor(l=L*length/2);

% Per-unit length shunt admittance
    c  = capacitor(c=C*length,r={0, 'Ohm'}); % Soil capacitance
    g  = resistor(R=1/(G*length)); % Soil admittance
end

% Defining the interconnection points and element to form a T-sections
% with measurment nodes.
connections
    connect(p1,r1.p)
    connect(r1.n,l1.p)
    connect(p2,r2.p)
    connect(r2.n,l2.p)
    connect(l1.n,l2.n,g.p,c.p)
    connect(n,g.n,c.n)
end

end

% Used Simulink v.9.0, Simscape v.4.3
```

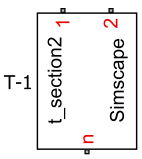

(a) Block Model

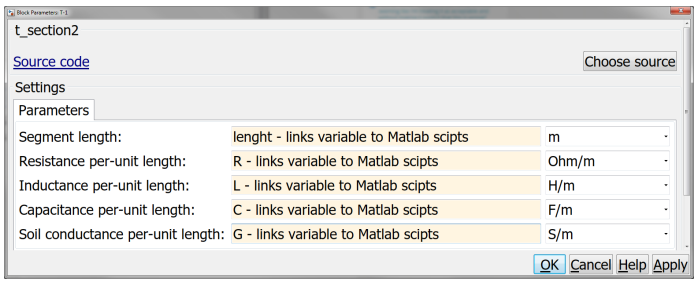

(b) Variable Interface

D.2 Function for Grounding Grid Geometric Parameters

D.2.1 Per-Unit Length Frequency Independent Parameters

```
%Updated 11.01
%Updated 13.01

% Function to calculate the characterisic electrical parameters for a
% per-unit length horizontal grounding wire over the
% frequenzy range of a lightning surge.
% The paramaters are calculated as function of frequency dependance of the
% soil, in range of lightning strikes, ref (section 2.4.2)
%
%
% Input
%
%    lengthSeg      ==> Length of wire segment [m]
%    Geom           ==> Grounding grid geometry matrix
%    Mu             ==> Permeability of vaccum [H/m]
%    Rsu            ==> Soil resistivity at power frequency [ohm-m]
%    Er             ==> Soil spesific permittivity [F/m]
%    Rcu            ==> Resistivity of copper [ohm-m]
%    Ns             ==> Number of samples
%    w              ==> Vector of freqs [rad/sec]
%
% Outputs
%
%    y              ==> Matrix of per unit length shunt admittance [S]
%    z              ==> Matrix of per unit length series impedance [ohm]
%    yp             ==> Matrix of per unit length propagation constant [-]
%    Zc             ==> Matrix of per unit length characteristic impendance [-]
%    Lsel           ==> Matrix of per unit length self inductance [H]
%    Lmut           ==> Matrix of per unit length mutual inductance [H]
%    Gsel           ==> Matrix of per unit length self inductance [S]
%    Gmut           ==> Matrix of per unit length mutual inductance [S]
%    Csel           ==> Matrix of per unit length self capacitance [C]
%    Cmut           ==> Matrix of per unit length mutual capacitance [C]
%
%%
function [y,z,yp,Zc,Lsel,Lmut,Gsel,Gmut,Csel,Cmut]=GroundSysPar(lengthSeg,...
    Geom,Mu,Rsu,Er,Rcu,Ns,w)

ymatrix= zeros(1,Ns);
zmatrix = zeros(1,Ns);

yres = zeros(1,Ns);
zres= zeros(1,Ns);

%Per-unit lenght self (ii) inductance(eq. (2.15)),
%conductance(eq. (2.16a)) and capacitance(eq. (2.16b))
Lsel=(Mu/(pi))*(log((2*lengthSeg)/(2*(Geom(1,3)*Geom(1,4))))-1);

Gsel=pi*(1/(Rsu*(log((2*lengthSeg)/(sqrt(2*Geom(1,4)*...
    Geom(1,3)))-1))));

Csel=Gsel*Rsu*Er;

%Per unit lenght mutual (ij) inductance, conductance and
%capacitance(eq. (2.17))
Lmut=(Mu/(pi))*(log((2*lengthSeg)/(2*(Geom(1,6)*Geom(1,4)))-1));

Gmut=pi*(1/(Rsu*(log((2*lengthSeg)/(sqrt(2*Geom(1,4)*...
    Geom(1,6)))-1))));

Cmut=Gmut*Rsu*Er;
```

```
kl=1;
ki=1;
kn=1;

% Loop to compute per-unit shunt admittance and
% impedance(eq. (2.3)) matrices for all frequencies

for kl=1:Ns

zmatrix(kl)=(j*w(kl)*Lsel)+(j*w(kl)*Lmut);
ymatrix(kl)=(Gsel+(j*w(kl)*Csel))+(Gmut+(j*w(kl)*Cmut));

end

%Per-unit shunt admittance and impedance matrix
y=ymatrix;
z=zmatrix;

%Per-unit propagation and surge impedance(eq. (2.4))
yp=sqrt(ymatrix.*zmatrix);
Zc=sqrt(zmatrix./ymatrix);
```

D.2.2 Per-Unit Length Frequency Dependent Parameters

```
%Updated 27.12
%Updated 11.01
%
% Function to calculate the characterisic electrical parameters for a
% per-unit length horizontal grounding wire over the
% frequency range of a lightning surge.
%
%
% Input
%
%    lengthSeg      ==> Length of wire segment [m]
%    Geom           ==> Grounding grid geometry matrix
%    Mu             ==> Permeability of vaccum [H/m]
%    Rsu            ==> Soil resistivity at power frequency [ohm-m]
%    Eo             ==> Permittivity of vaccum [F/m]
%    Rcu            ==> Resistivity of copper [ohm-m]
%    Ns             ==> Number of samples
%    w              ==> Vector of freqs [rad/sec]
%    f              ==> Vector of log spaced Frequencies [Hz]
%
% Outputs
%
%    y              ==> Matrix of per unit length shunt admittance [S]
%    z              ==> Matrix of per unit length series impedance [ohm]
%    yp             ==> Matrix of per unit length propagation constant [-]
%    Zc             ==> Matrix of per unit length characteristic impendance [-]
%    MFRsu          ==> Matrix of frequency dependant soil
%                       resitivity [ohm-m]
%    MEr            ==> Matrix of frequency dependant soil
%                       spesific permittivity [F/m]
%    Lsel           ==> Matrix of per unit length self inductance [H]
%    Lmut           ==> Matrix of per unit length mutual inductance [H]
%    Gsel           ==> Matrix of per unit length self inductance [S]
%    Gmut           ==> Matrix of per unit length mutual inductance [S]
%    Csel           ==> Matrix of per unit length self capacitance [C]
%    Cmut           ==> Matrix of per unit length mutual capacitance [C]
%
%%
function [y,z,yp,Zc,MFRsu,MEr]=GroundSysParFreq(lengthSeg,...
    Geom,Mu,Rsu,Eo,Rcu,Ns,w,f)
```

```
ymatrix= zeros(1,Ns);
zmatrix = zeros(1,Ns);

%Visacro frequency dependant formulation with mean results
%data table((table 2.2))
h1=(0.7*Rsu^(-0.73));
gamma=0.62;
EpsInfEpsZer=4;

%Per unit lenght self(segment ii) inductance(eq. (2.15))
%Lsel=(Mu/(2*pi))*(log((2*lenght)/(Geom(1,4))-1));
Lsel=(Mu/(pi))*(log((2*lengthSeg)/(2*(Geom(1,3)*Geom(1,4)))-1));

%Per unit lenght mutual(segment ij) inductance(eq. (2.17a))
Lmut=(Mu/(2*pi))*(log((2*lengthSeg)/(Geom(1,6))-1));

kl=1;
ki=1;
kn=1;

% Loop to compute per unit matrices for all frequencies
for kl=1:Ns
%Soil resitivity and permittivity as frequency
%dependant(eq. (2.13))
FRsu=Rsu+(Rsu*h1*((f(kl))/(10^6))^(gamma));
FErs=EpsInfEpsZer+(((tan((pi*gamma)/2)*(10^-3))/...
(2*pi*Eo*(10^6))^gamma)*(Rsu*h1*(f(kl))^(gamma-1)));
FEr=Eo*FErs;

%Per unit lenght self conductance(eq. (2.16a)) and
%capacitance(eq. (2.16b))

Gsel=pi*(1/(FRsu*(log((2*lengthSeg)/(sqrt(2*Geom(1,4)*...
    Geom(1,3)))-1))));

Csel=Gsel*FRsu*FEr;


%Per unit lenght mutual conductance(eq. (2.17b)) and
%capacitance(eq. (2.17c))
Gmut=pi*(1/(FRsu*(log((2*lengthSeg)/(sqrt(2*Geom(1,4)*...
    Geom(1,6)))-1))));
Cmut=Gsel*FRsu*FEr;

FRsumatrix(kl)=FRsu;
FErmatrix(kl)=FEr;

%per unit shunt admittance and impedance(eq. (2.3))
zmatrix(kl)=(j*w(kl)*Lsel)+(j*w(kl)*Lmut);
ymatrix(kl)=(Gsel+(j*w(kl)*Csel))+(Gmut+(j*w(kl)*Cmut));

end

%Soil resistivity and permittivity considering frequency
%dependendancy
MFRsu=FRsumatrix;
MEr=FErmatrix;

%Per-unit shunt admittance and impedance matrices
y=ymatrix;
z=zmatrix;

%Per unit propagation and surge
%impedance(eq. (2.4))
yp=sqrt(ymatrix.*zmatrix);
Zc=sqrt(zmatrix./ymatrix);
```

D.3 Nodal Measurements Mapped to Physical Properties

D.3.1 Definition for Series Selector

```
% Control of nodal measurment extractions and connect to physical
% properties of the grounding grid. Call of functions to generate plot
% memory (plotM) of selected dataset

% Outputs
%
%    plotMVoltPeak     ==> Matrix of nodal voltages for defined range
%                          of samples
%    plotMVCurrLeak    ==> Matrix of nodal leakage currents for
%                          defined range of samples
%    plotMElField      ==> Matrix of soil electric field distribution
%                          in the grounding grid for defined range of
%                          samples

%%
%For models in isolated mode.
% Verification of log-fil validity for defined simulation in isolated mode.

tempIcurrent(:,1)=eval(sprintf...
    ('simlog_ssc_grounding_system.CurrentSensor1.I.series.time'));
tempIcurrent(:,2)=eval(sprintf....
    ('simlog_ssc_grounding_system.CurrentSensor1.I.series.values'));
%%
% For models integrated in EMTP-RV.
% Verification of log-fil validity for defined simulation in integrated
% mode

tempIcurrent(:,1)=eval(sprintf...
    ('simlog_ssc_grounding_system.I_EMTPCurrSurgeInject.I.series.time'));
tempIcurrent(:,2)=eval(sprintf...
    ('simlog_ssc_grounding_system.I_EMTPCurrSurgeInject.I.series.values'));
%%
% Definition script of overall measrument loop control

nSamplScip=1;    %Loop constant to define scip in measurment series
nSamples=1;      %Loop constant to define end point of extraction
sSample=3469;    %Defines a point to specific extract. If single
                 %extraction are whished set nSamples=1 and nSampleScip=1.
                 %If range of samples set sSample=1

%%
% Call of function in section D.3.2

[plotMVoltPeak] = GroundGridNodalVoltage(simlog_ssc_grounding_system,...
    nXWireRows,nXWireCol,nYWireCol,nYWireRows,nlengthSegElement,...
    lengthSeg,nSamplScip,nSamples,sSample);
%%
% Call of function in section D.3.3

[plotMVCurrLeak] = GroundGridLeakageCurrent...
    (simlog_ssc_grounding_system,nXWireRows,nXWireCol,nYWireCol,...
    nYWireRows,nlengthSegElement,lengthSeg,nSamplScip,nSamples,sSample);
%%
% Call of function in section D.3.4
% plotMVCurrLeak must be loaded sequently

[plotMSoilElField]=SoilElectricFieldDist(plotMVCurrLeak, Rsu,Geom(1,4));
%%
```

D.3.2 Grounding Grid Nodal Voltage Extract and Map

```
% Function to map nodal voltages of the grounding grid to physical
% properties. Loop of function will establish series of grounding
% grid voltages in defined range
%
% Input
%
%    simlogGroundingGrid    ==> Load nodal solver from connected grounding
%                               grid model
%    nXWireRows     ==> Number of horizontal wire segments
%    nXWireCol      ==> Number of horizontal wire per segment
%    nYWireRows     ==> Number of vertical wire segments
%    nYWireCol      ==> Number of vertical wire per segment
%    nlengthSegElement      ==> Number of lengths per wire segments
%    lengthSeg      ==> Length of wire segment
%    nSamplScip     ==> Loop constant to define scip of measurment series
%    nSamples       ==> Loop constant to define end point of extraction
%    sSamples       ==> Defines a point to specific extract. If single
%                       extraction are whished set nSamples=1 and
%                       nSampleScip=1
% Outputs
%
%    plotM     ==> Matrix of nodal voltages for defined range of samples
%
%%
function [plotM] = GroundGridNodalVoltage(simlogGroundingGrid,...
    nXWireRows,nXWireCol,nYWireCol,nYWireRows,nlengthSegElement,...
    lengthSeg,nSamplScip,nSamples,sSample)
k=1;
m=1;
n=1;
o=1;
p=1;
q=1;

% Defines number of samples to be extraced
for k=1:nSamplScip:nSamples

if sSample==1
    elseif k==1
    k=sSample
    else
end

p=1;

%loop to extract nodal voltages for wires in horizontal(x) direction
for o=1:nXWireRows
%"%d" in function eval(sprintf(... search for variable, which give
%possibility to lookup Simscape node data refered to project name.
%inital length measures at incomming node of segment, p1.
tempo=eval(sprintf('simlogGroundingGrid.X%d_1.T_1.p1.v.series.values', o));
plotM(p,3,q)=tempo(k,1);
ydir=(nlengthSegElement*lengthSeg)*(o-1);
plotM(p,2,q)=ydir;

p=p+1;
xdir=0;
m=0;
n=1;

% Outer loop for number of horizontal grounding wire on "o" row and "m"
% column
for m=1:nXWireCol
```

```
xdir=(nlengthSegElement*lengthSeg)*(m-1);

%Inner loop to extract segment voltage
for n=1:1:nlengthSegElement

tempn=eval(sprintf...
    ('simlogGroundingGrid.X%d_%d.T_%d.p2.v.series.values',o,m,n));

plotM(p,3,q)=tempn(k,1);

%Increment physical grid locations per node
xdirn=xdir+lengthSeg*n;
plotM(p,1,q)=xdirn;
plotM(p,2,q)=ydir;

p=p+1;

end
m=m+1;
end
o=o+1;
end

m=1;
n=1;
o=1;

%loop to extract nodal voltages for wires in vertical(y) direction
for o=1:nYWireRows
%inital length measures at incomming node of segment, p1.
tempo=eval(sprintf...
    ('simlogGroundingGrid.Y%d_1.T_1.p1.v.series.values', o));
plotM(p,3,q)=tempo(k,1);
xdir=(nlengthSegElement*lengthSeg)*(o-1);
plotM(p,2,q)=xdir;

p=p+1;
ydir=0;
m=0;
n=1;

% Outer loop for number of horizontal grounding wire on "o" row and "m"
% column
for m=1:nYWireCol
xdir=(nlengthSegElement*lengthSeg)*(m-1);
ydir=(nlengthSegElement*lengthSeg)*(o-1);

tempm=eval(sprintf...
    ('simlogGroundingGrid.Y%d_%d.T_1.p1.v.series.values', o,m));

plotM(p,3,q)=tempm(k,1);
plotM(p,1,q)=xdir;
plotM(p,2,q)=ydir;

p=p+1;

%Inner loop to extract segment voltage
for n=1:1:nlengthSegElement

tempn=eval(sprintf...
    ('simlogGroundingGrid.Y%d_%d.T_%d.p2.v.series.values',o,m,n));

plotM(p,3,q)=tempn(k,1);

%Increment physical grid locations per node
ydirn=ydir+lengthSeg*n;
plotM(p,1,q)=xdir;
plotM(p,2,q)=ydirn;

p=p+1;
```

```
end
m=m+1;
end
o=o+1;
end
q=q+1
end

end
```

D.3.3 Soil Leakage Current Extract and Map

```
% Function to map nodal voltages of the grounding grid to physical
% properties. Loop of function will establish series of grounding
% grid leakage currents in defined range
%
% Input
%
%    simlogGroundingGrid    ==> Load nodal solver from connected grounding
%                               grid model
%    nXWireRows     ==> Number of horizontal wire segments
%    nXWireCol      ==> Number of horizontal wire per segment
%    nYWireRows     ==> Number of vertical wire segments
%    nYWireCol      ==> Number of vertical wire per segment
%    nlengthSegElement      ==> Number of lengths per wire segments
%    lengthSeg      ==> Length of wire segment
%    nSamplScip     ==> Loop constant to define scip of measurment series
%    nSamples       ==> Loop constant to define end point of extraction
%    sSamples       ==> Defines a point to specific extract. If single
%                       extraction are whished set nSamples=1 and
%                       nSampleScip=1
% Outputs
%
%    plotM     ==> Matrix of nodal leakage currents for defined range of
%                  samples
%
%%
function [plotM] = GroundGridLeakageCurrent(simlogGroundingGrid,...
    nXWireRows,nXWireCol,nYWireCol,nYWireRows,nlengthSegElement,...
    lengthSeg,nSamplScip,nSamples,sSample)
k=1;
m=1;
n=1;
o=1;
p=1;
q=1;

% Defines number of samples to be extraced
for k=1:nSamplScip:nSamples

if sSample==1
    elseif k==1
    k=sSample
    else
end

p=1;

%loop to extract leakage current for wires in horizontal(x) direction
for o=1:nXWireRows
%"%d" in function eval(sprintf(... search for variable, which give
%possibility to lookup Simscape node data refered to project name.
%inital length measures at incomming node of segment, p1.
tempo=eval(sprintf('simlogGroundingGrid.X%d_1.T_1.g.i.series.values', o));
plotM(p,3,q)=tempo(k,1);
ydir=(nlengthSegElement*lengthSeg)*(o-1);
plotM(p,2,q)=ydir;
```

```
p=p+1;
xdir=0;
m=0;
n=1;

% Outer loop for number of horizontal grounding wire on "o" row and "m"
% column
for m=1:nXWireCol

xdir=(nlengthSegElement*lengthSeg)*(m-1);

%Inner loop to extract segment leakage current
for n=1:1:nlengthSegElement

tempn=eval(sprintf...
    ('simlogGroundingGrid.X%d_%d.T_%d.g.i.series.values',o,m,n));

plotM(p,3,q)=tempn(k,1);

%Increment physical grid locations per node
xdirn=xdir+lengthSeg*n;
plotM(p,1,q)=xdirn;
plotM(p,2,q)=ydir;

p=p+1;

end
m=m+1;
end
o=o+1;
end

m=1;
n=1;
o=1;

%loop to extract leakage current for wires in vertical(y) direction
for o=1:nYWireRows
%inital length measures at incomming node of segment, p1.
tempo=eval(sprintf...
    ('simlogGroundingGrid.Y%d_1.T_1.g.i.series.values', o));
plotM(p,3,q)=tempo(k,1);
xdir=(nlengthSegElement*lengthSeg)*(o-1);
plotM(p,2,q)=xdir;

p=p+1;
ydir=0;
m=0;
n=1;

% Outer loop for number of horizontal grounding wire on "o" row and "m"
% column
for m=1:nYWireCol
xdir=(nlengthSegElement*lengthSeg)*(m-1);
ydir=(nlengthSegElement*lengthSeg)*(o-1);

tempm=eval(sprintf...
    ('simlogGroundingGrid.Y%d_%d.T_1.g.i.series.values', o,m));

plotM(p,3,q)=tempm(k,1);
plotM(p,1,q)=xdir;
plotM(p,2,q)=ydir;

p=p+1;

%Inner loop to extract segment leakage current
for n=1:1:nlengthSegElement

tempn=eval(sprintf...
    ('simlogGroundingGrid.Y%d_%d.T_%d.g.i.series.values',o,m,n));
```

```
plotM(p,3,q)=tempn(k,1);

%Increment physical grid locations per node
ydirn=ydir+lengthSeg*n;
plotM(p,1,q)=xdir;
plotM(p,2,q)=ydirn;

p=p+1;

end
m=m+1;
end
o=o+1;
end
q=q+1
end

end
```

D.3.4 Soil Electric Field Map

```
% Function to map the electric field exerted to the soil from the leakage
% current distribution of the grounding wire. The electric field distribution
% are maped to physical properties. Loop of function will establish
% series of the electric field in defined range
%
% Input
%
%    plotMCurrLeak  ==> Soil leakage current distribution matrix for one
%                         sample from the simulation
%    Rsoil          ==> Soil resitivity[Ohm/m]
%    rCond          ==> Grounding grid conductor radius [m]
%
% Outputs
%
%    plotMElField   ==> Matrix of soil electric field distribution in the
%                       grounding grid for one sample
%
%%
function [plotMSoilElField]=SoilElectricFieldDist(plotMCurrLeak,...
    Rsoil,rCond)

Msize=size(plotMCurrLeak,1);

k=1;
for k=1:1:Msize

    plotMSoilElField(k,1)=plotMCurrLeak(k,1);
    plotMSoilElField(k,2)=plotMCurrLeak(k,2);

    tempCurr=plotMCurrLeak(k,3);
    %The soil electric field from a leaked current
    %ref. ((eq. (2.21)))
    efield=(tempCurr/(2*pi*rCond))*Rsoil;
    plotMSoilElField(k,3)=efield;
end
```

D.4 Simulink® Implementation

D.4.1 Grounding Wires

D.4.1.1 Grounding Wire of 5 m Length Segment

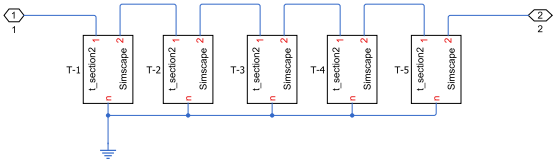

D.4.1.2 Grounding Wire of 10 m Length Segment

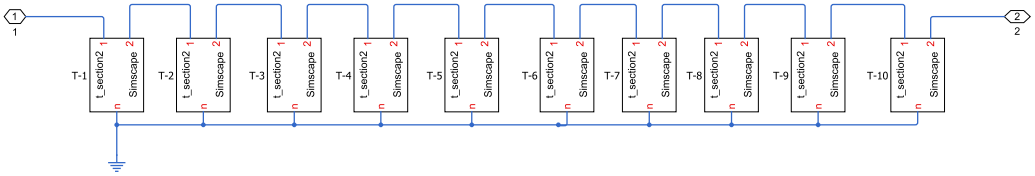

D.4.2 5×5 m Mesh Grounding Grid Models

D.4.2.1 12×12 Meshes, 3600 m^2

Implemented model is preferably viewed on screen or printed on minimum paper size A3 for detail review of grounding grid definitions.

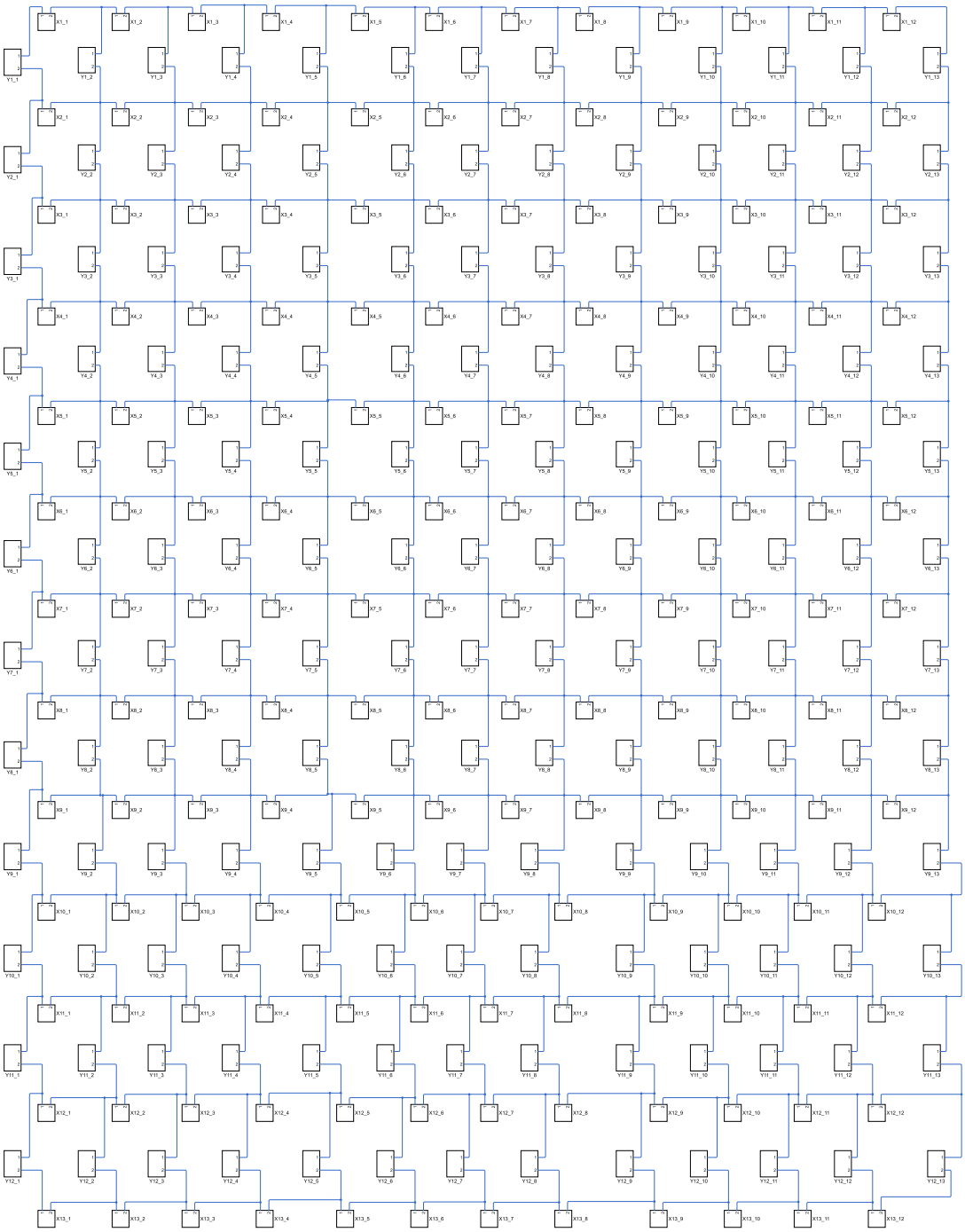

D.4.2.2 8×8 Meshes, 1600 m^2

Implemented model is preferably viewed on screen or printed on minimum paper size A3 for detail review of grounding grid definitions.

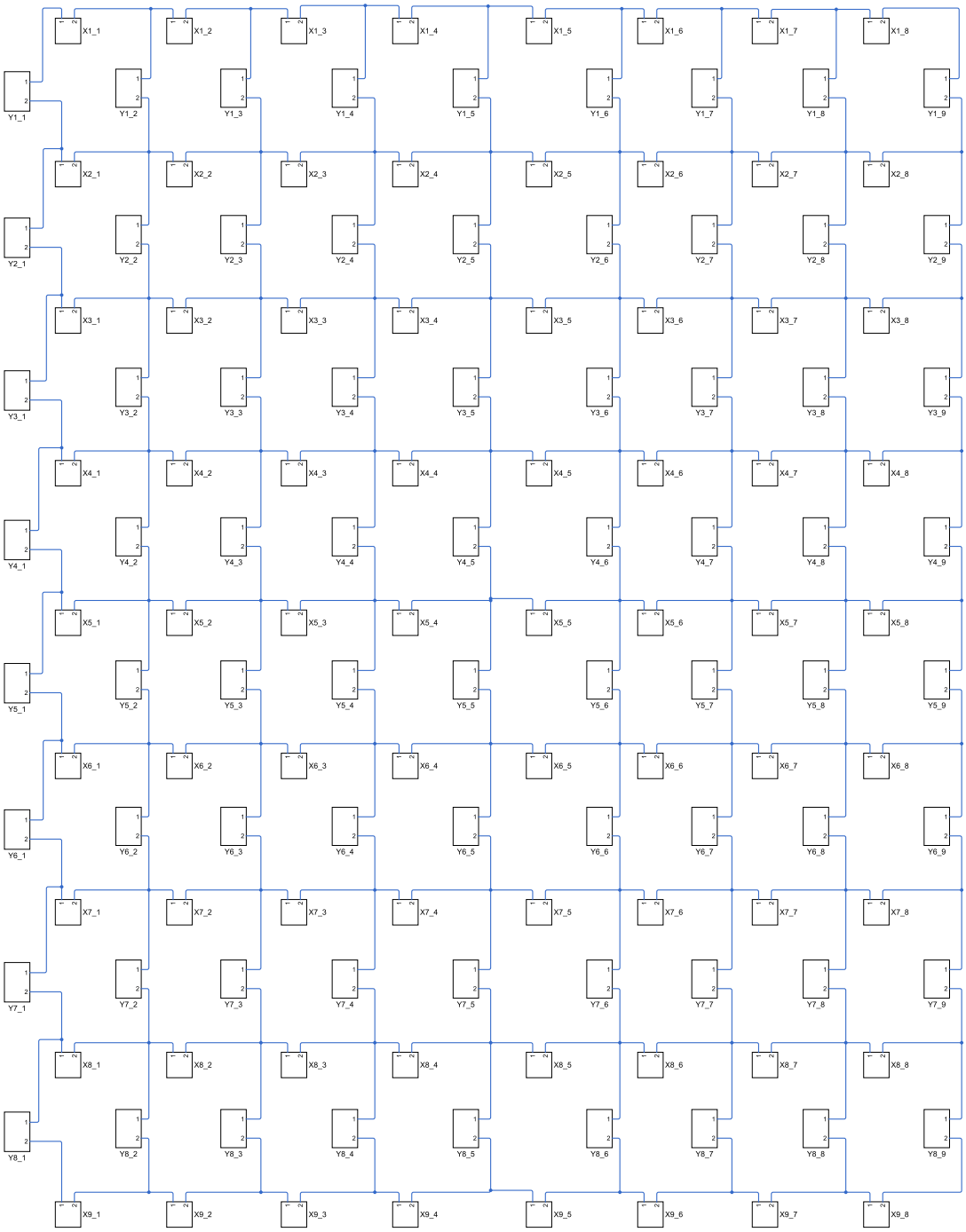

D.4.3 10×10 m Mesh Grounding Grid Models

D.4.3.1 6×6 Meshes, 3600 m^2

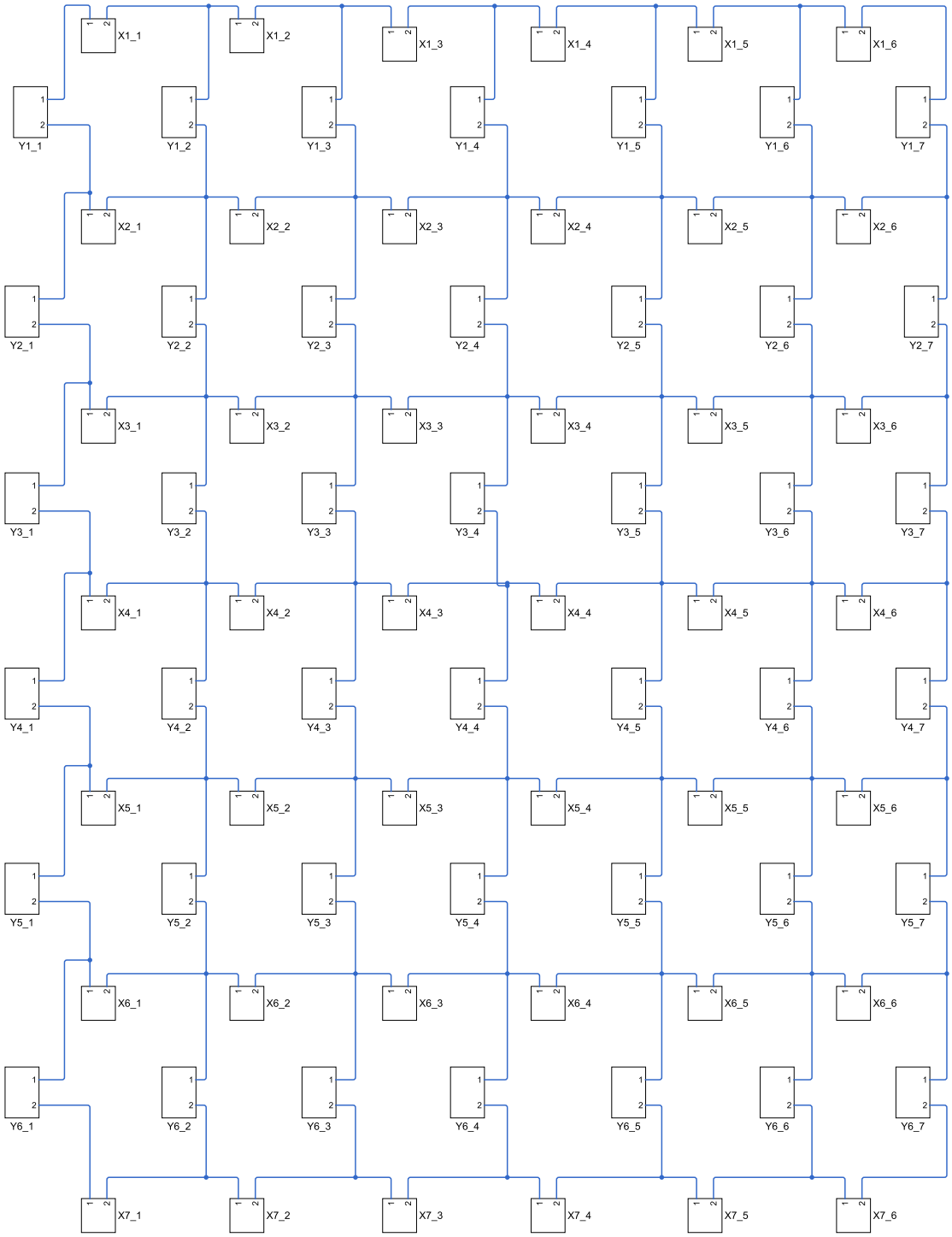

D.4.3.2 4×4 Meshes, 1600 m^2

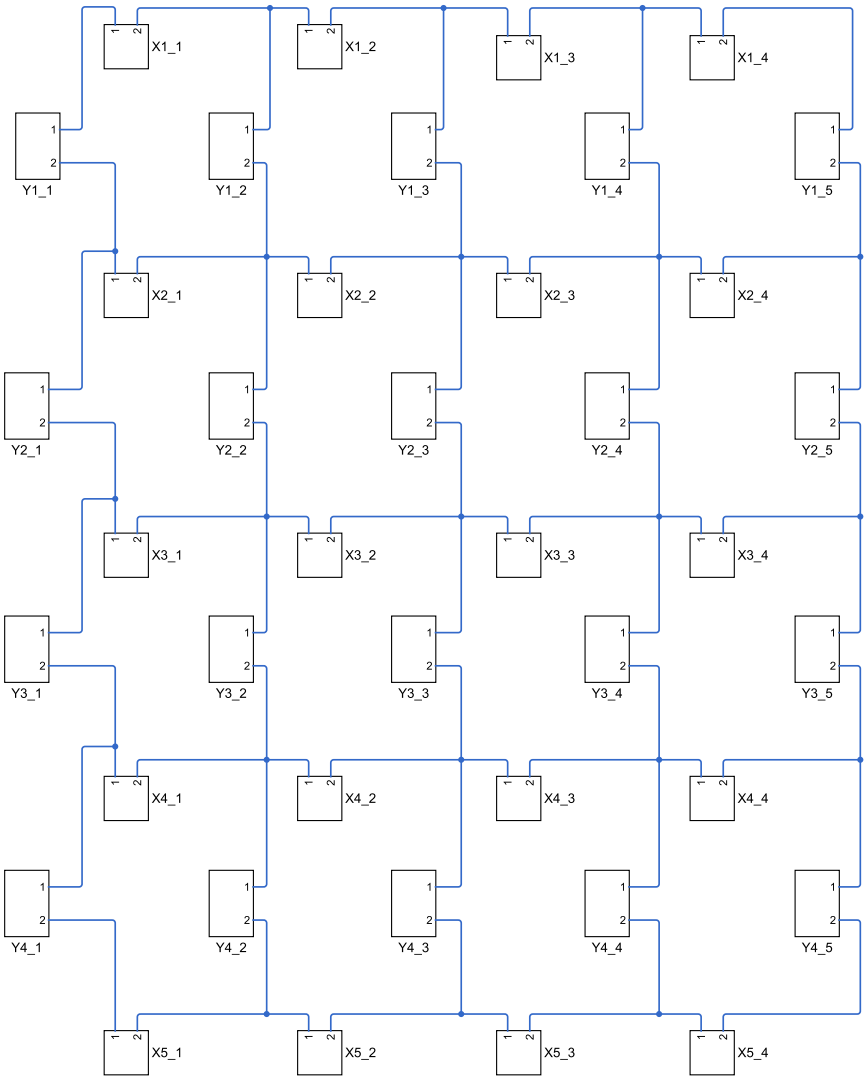

D.4.4 Current Source with Double Exponential Waveform

Current source of double exponential waveform is implemented according to eq. (2.1).

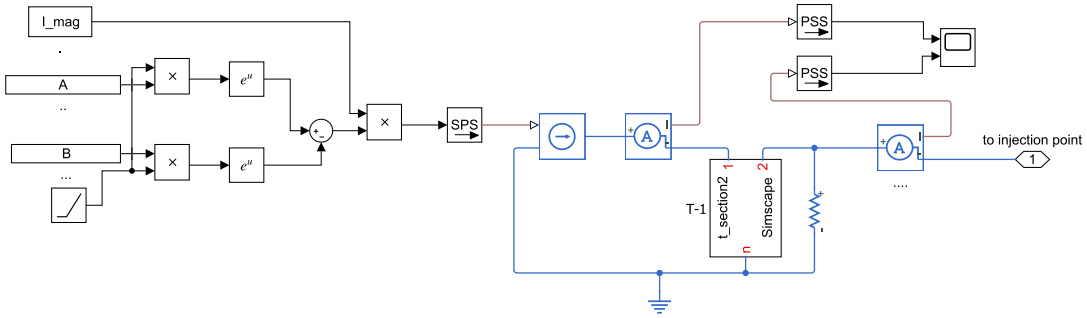

D.4.5 Impulse Impedance and Admittance of Grounding Grid

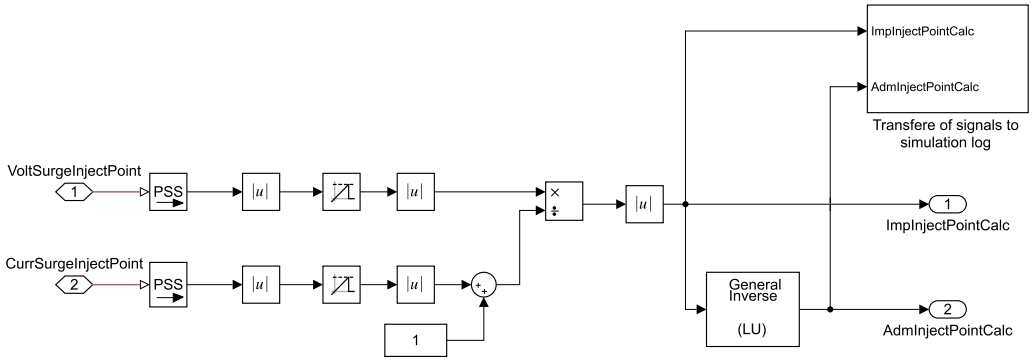

D.5 Plot Datasets of Presented Work

In this section manipulation of the datasets are given for the produced plot, with reference to report main content of use. Other changes made to the dataset, in transfer from Matlab® to LaTeX, are limited to layout and representation. The data was exchanged with the add-on package "matlab2tikz" version 1.1.0, developed by Nico Schlömer and maintained by Egon Geerardyn, in the developer forum GitHub and distributed on MathWorks® forum.

D.5.1 Per-Unit Length Parameters

```
% Updated 01.02
%
%additional data for plot with call of function for frequency
%independenant (section D.2.1) and
%depenant (section D.2.2) soil
[y1,z1,yp1,Zc1] = GroundSysPar(lenght,Geom,Mu,70,Er,Rcu,Ns,w);
[y2,z2,yp2,Zc2] = GroundSysPar(lenght,Geom,Mu,100,Er,Rcu,Ns,w);
[y3,z3,yp3,Zc3] = GroundSysPar(lenght,Geom,Mu,300,Er,Rcu,Ns,w);
[y4,z4,yp4,Zc4] = GroundSysPar(lenght,Geom,Mu,1000,Er,Rcu,Ns,w);
[y5,z5,yp5,Zc5] = GroundSysPar(lenght,Geom,Mu,2000,Er,Rcu,Ns,w);

[fy1,fz1,fyp1,fZc1,FRsu1,FEr1] = GroundSysParFreq(lenght...
    ,Geom,Mu,70,Eo,Rcu,Ns,w,f);
[fy2,fz2,fyp2,fZc2,FRsu2,FEr2] = GroundSysParFreq(lenght...
    ,Geom,Mu,100,Eo,Rcu,Ns,w,f);
[fy3,fz3,fyp3,fZc3,FRsu3,FEr3] = GroundSysParFreq(lenght...
    ,Geom,Mu,300,Eo,Rcu,Ns,w,f);
[fy4,fz4,fyp4,fZc4,FRsu4,FEr4] = GroundSysParFreq(lenght...
    ,Geom,Mu,1000,Eo,Rcu,Ns,w,f);
[fy5,fz5,fyp5,fZc5,FRsu5,FEr5] = GroundSysParFreq(lenght...
    ,Geom,Mu,2000,Eo,Rcu,Ns,w,f);

%%
%Dataplot for fig. 4.1
figure;
subplot(221),semilogx(f,angle(y1)*(180/pi),'k',f,angle(y2)*...
    (180/pi),'--k',f,angle(y3)*(180/pi),':k',f,angle(y4)*...
    (180/pi),'-.k',f,angle(y5)*(180/pi),'.k');
lgd = legend('70 ohm/m','100 ohm/m','300 ohm/m','1000 ohm/m'...
    , '2000 ohm/m');
```

```
ylabel('Angle[Degrees]')
axis([1E2 4E6 0 90])
title('Y in frequency independant soil');

subplot(223),semilogx(f,abs(y1),'k',f,abs(y2),'--k',f,abs(y3)...
    ,':k',f,abs(y4),'-.k',f,abs(y5),'.k');
xlabel('Frequency[Hz]')
ylabel('Impedance[ohm]')
axis([1E2 4E6 0 0.05]);

subplot(222),semilogx(f,angle(fy1)*(180/pi),'k',f,angle(fy2)*...
    (180/pi),'--k',f,angle(fy3)*(180/pi),':k',f,angle(fy4)*...
    (180/pi),'-.k',f,angle(fy5)*(180/pi),'.k');
axis([1E2 4E6 0 90]);
title('Y in frequency dependant soil');

subplot(224),semilogx(f,abs(fy1),'k',f,abs(fy2),'--k',f...
    ,abs(fy3),':k',f,abs(fy4),'-.k',f,abs(fy5),'.k');
xlabel('Frequency[Hz]')
axis([1E2 4E6 0 0.05]);


%%
%Dataplot for fig. 4.2
figure;
subplot(111),semilogx(f,abs(z));
axis([1E2 4E6 0 80])
title('z in frequency dependant soil');

%%
%Dataplot for fig. 4.3
figure;
subplot(221),semilogx(f,real(yp1),'k',f,real(yp2),'--k',f...
    ,real(yp3),':k',f,real(yp4),'-.k',f,real(yp5),'.k');
xlabel('Frequency[Hz]')
ylabel('Attenuation Constant')
axis([1E2 4E6 0 1.2]);

subplot(223),semilogx(f,imag(yp1),'k',f,imag(yp2),'--k',f...
    ,imag(yp3),':k',f,imag(yp4),'-.k',f,imag(yp5),'.k');
xlabel('Frequency[Hz]')
ylabel('Phase constant')
axis([1E2 4E6 0 1.5]);

subplot(222),semilogx(f,real(fyp1),'k',f,real(fyp2),'--k',f...
    ,real(fyp3),':k',f,real(fyp4),'-.k',f,real(fyp5),'.k');
xlabel('Frequency[Hz]')
ylabel('Attenuation Constant')
axis([1E2 4E6 0 1.2]);

subplot(224),semilogx(f,imag(fyp1),'k',f,imag(fyp2),'--k',f...
    ,imag(fyp3),':k',f,imag(fyp4),'-.k',f,imag(fyp5),'.k');
xlabel('Frequency[Hz]')
ylabel('Phase constant')
axis([1E2 4E6 0 1.5]);

%%
%Dataplot for fig. 4.4
figure;
subplot(221),semilogx(f,angle(Zc1)*(180/pi),'k',f,angle(Zc2)*...
    (180/pi),'--k',f,angle(Zc3)*(180/pi),':k',f,angle(Zc4)*...
    (180/pi),'-.k',f,angle(Zc5)*(180/pi),'.k');
ylabel('Angle[Degrees]')
axis([1E2 4E6 0 55])
title('Zc in frequency independant soil');

subplot(223),semilogx(f,abs(Zc1),'k',f,abs(Zc2),'--k',f...
    ,abs(Zc3),':k',f,abs(Zc4),'-.k',f,abs(Zc5),'.k');
xlabel('Frequency[Hz]')
ylabel('Magnitude')
axis([1E2 4E6 0 170]);
```

```
subplot(222),semilogx(f,angle(fZc1)*(180/pi),'k',f...
    ,angle(fZc2)*(180/pi),'--k',f,angle(fZc3)*(180/pi)...
    ,':k',f,angle(fZc4)*(180/pi),'-.k',f,angle(fZc5)*(180/pi)...
    ,'.k');
axis([1E2 4E6 0 55])
title('Zc in frequency dependant soil');

subplot(224),semilogx(f,abs(fZc1),'k',f,abs(fZc2),'--k'...
    ,f,abs(fZc3),':k',f,abs(fZc4),'-.k',f,abs(fZc5),'.k');
xlabel('Frequency[Hz]')
axis([1E2 4E6 0 170]);

%%
```

D.5.2 Isolated: Voltage and Current (2D)

D.5.2.1 6×6, 10×10 m Meshes, 3600 m^2

```
% Updated 22.01
%
% For the simulation model "Sim10m_36MeshGrid.slx"
% Nodal voltage for selected points, from center diagonaly and horizontaly
% at 1x meshes distance. Current plot for the injection point
%
% Simulation must be loaded, for the spesific grounding grid, infront
% of nodal data extraction from loaded simlog.
%
% Used to produce (figs. 4.5a, 4.5e, 4.6a, 4.6e, 4.7a, 4.7e, 4.8a, 4.8e, 4.9a, 4.9e, 4.10a and 4.10e)
% where fig X.a and X.e indicates voltage and current plot, respectivly
tempVDistDiag(:,1)=eval(sprintf...
    ('simlog_ssc_grounding_system.X4_3.T_10.p2.v.series.time'));
tempVDistDiag(:,2)=eval(sprintf...
    ('simlog_ssc_grounding_system.X4_3.T_10.p2.v.series.values'));
tempVDistDiag(:,3)=eval(sprintf...
    ('simlog_ssc_grounding_system.X5_4.T_10.p2.v.series.values'));
tempVDistDiag(:,4)=eval(sprintf...
    ('simlog_ssc_grounding_system.X6_5.T_10.p2.v.series.values'));
tempVDistDiag(:,5)=eval(sprintf...
    ('simlog_ssc_grounding_system.X7_6.T_10.p2.v.series.values'));
%%
tempVDistHoriz(:,1)=eval(sprintf...
    ('simlog_ssc_grounding_system.X4_3.T_10.p2.v.series.time'));
tempVDistHoriz(:,2)=eval(sprintf...
    ('simlog_ssc_grounding_system.X4_3.T_10.p2.v.series.values'));
tempVDistHoriz(:,3)=eval(sprintf...
    ('simlog_ssc_grounding_system.X4_4.T_10.p2.v.series.values'));
tempVDistHoriz(:,4)=eval(sprintf...
    ('simlog_ssc_grounding_system.X4_5.T_10.p2.v.series.values'));
tempVDistHoriz(:,5)=eval(sprintf...
    ('simlog_ssc_grounding_system.X4_6.T_10.p2.v.series.values'));
%%
%Current Distribution
tempIcurrent(:,1)=eval(sprintf...
    ('simlog_ssc_grounding_system.CurrentSensor1.I.series.time'));
tempIcurrent(:,2)=eval(sprintf...
    ('simlog_ssc_grounding_system.CurrentSensor1.I.series.values'));

%%
%2D plot of injected current: range from start to current 3D plot
figure();

subplot(3,1,1)
```

```
p2=plot(tempVDistHoriz(:,1)*1e6,tempVDistHoriz(:,2)/1e3,...
    tempVDistHoriz(:,1)*1e6,tempVDistHoriz(:,3)/1e3,...
    tempVDistHoriz(:,1)*1e6,tempVDistHoriz(:,4)/1e3,...
    tempVDistHoriz(:,1)*1e6,tempVDistHoriz(:,5)/1e3, 'Color','black');
%axis to be set in the range of actual model and wanted results
axis([0 2.5 0 12])
xlabel('Time [mu s]')
ylabel('Voltage [kV]')
title('Horizontal voltage distrbution from center');

subplot(3,1,2)
p1=plot(tempVDistDiag(:,1)*1e6,tempVDistDiag(:,2)/1e3,tempVDistDiag(:,1)...
    *1e6,tempVDistDiag(:,3)/1e3,tempVDistDiag(:,1)*1e6,...
    tempVDistDiag(:,4)/1e3,tempVDistDiag(:,1)*1e6,...
    tempVDistDiag(:,5)/1e3, 'Color','black');
%axis to be set in the range of actual model and wanted results
axis([0 2.5 0 12])
xlabel('Time [mu s]')
ylabel('Voltage [kV]')
title('Diagonal voltage distrbution from center');

subplot(3,1,3)
p3=plot(tempIcurrent(:,1)*1e6,tempIcurrent(:,2)/1e3,'Color','black');
%axis to be set in the range of actual model and wanted results
axis([0 2.5 0 1.05])
xlabel('Time [mu s]')
ylabel('Current [kA]')
title('Injected Current');
```

D.5.2.2 4×4, 10×10 m Meshes, 1600 m^2

```
% Updated 22.01
%
% For the simulation model "Sim10m_16MeshGrid.slx"
% Nodal voltage for selected points, from center diagonaly and horizontaly
% at 1x meshes distance. Current plot for the injection point
%
% Simulation must be loaded, for the spesific grounding grid, infront
% of nodal data extraction from loaded simlog.
%
% Used to produce (figs. 4.11a and 4.11e)
% where fig X.a and X.e indicates voltage and current plot, respectivly
tempVDistDiag(:,1)=eval(sprintf...
    ('simlog_ssc_grounding_system.X3_2.T_10.p2.v.series.time'));
tempVDistDiag(:,2)=eval(sprintf...
    ('simlog_ssc_grounding_system.X3_2.T_10.p2.v.series.values'));
tempVDistDiag(:,3)=eval(sprintf...
    ('simlog_ssc_grounding_system.X4_3.T_10.p2.v.series.values'));
tempVDistDiag(:,4)=eval(sprintf...
    ('simlog_ssc_grounding_system.X5_4.T_10.p2.v.series.values'));
%%
tempVDistHoriz(:,1)=eval(sprintf...
    ('simlog_ssc_grounding_system.X3_2.T_10.p2.v.series.time'));
tempVDistHoriz(:,2)=eval(sprintf...
    ('simlog_ssc_grounding_system.X3_2.T_10.p2.v.series.values'));
tempVDistHoriz(:,3)=eval(sprintf...
    ('simlog_ssc_grounding_system.X3_3.T_10.p2.v.series.values'));
tempVDistHoriz(:,4)=eval(sprintf...
    ('simlog_ssc_grounding_system.X3_4.T_10.p2.v.series.values'));
%%
%Current Distribution
tempIcurrent(:,1)=eval(sprintf...
    ('simlog_ssc_grounding_system.CurrentSensor1.I.series.time'));
tempIcurrent(:,2)=eval(sprintf...
    ('simlog_ssc_grounding_system.CurrentSensor1.I.series.values'));

%%
%2D plot of injected current: range from start to current 3D plot
```

```
figure();
subplot(3,1,1)
p2=plot(tempVDistHoriz(:,1)*1e6,tempVDistHoriz(:,2)/1e3,...
    tempVDistHoriz(:,1)*1e6,tempVDistHoriz(:,3)/1e3,...
    tempVDistHoriz(:,1)*1e6,tempVDistHoriz(:,4)/1e3, 'Color','black');
%axis to be set in the range of actual model and wanted results
axis([0 2.5 0 6])
xlabel('Time [mu s]')
ylabel('Voltage [kV]')
title('Horizontal voltage distrbution from center');

subplot(3,1,2)
p1=plot(tempVDistDiag(:,1)*1e6,tempVDistDiag(:,2)/1e3,tempVDistDiag(:,1)...
    *1e6,tempVDistDiag(:,3)/1e3,tempVDistDiag(:,1)*1e6,...
    tempVDistDiag(:,4)/1e3, 'Color','black');
%axis to be set in the range of actual model and wanted results
axis([0 2.5 0 6])
xlabel('Time [mu s]')
ylabel('Voltage [kV]')
title('Vertical voltage distrbution from center');

subplot(3,1,3)
p3=plot(tempIcurrent(:,1)*1e6,tempIcurrent(:,2)/1e3,'Color','black');
%axis to be set in the range of actual model and wanted results
axis([0 2.5 0 1.1])
xlabel('Time [mu s]')
ylabel('Current [kA]')
title('Injected Current');
```

D.5.2.3 12×12, 5×5 m Meshes, 3600 m^2

```
% Updated 22.01
%
% For the simulation model "Sim5m_144MeshGrid.slx"
% Nodal voltage for selected points, from center diagonaly and horizontaly
% at 2x meshes distance. Current plot for the injection point
%
% Simulation must be loaded, for the spesific grounding grid, infront
% of nodal data extraction from loaded simlog.
%
% Used to produce (figs. 4.12a and 4.12e)
% where fig X.a and X.e indicates voltage and current plot, respectivly
tempVDistDiag(:,1)=eval(sprintf...
    ('simlog_ssc_grounding_system.X7_6.T_5.p2.v.series.time'));
tempVDistDiag(:,2)=eval(sprintf...
    ('simlog_ssc_grounding_system.X7_6.T_5.p2.v.series.values'));
tempVDistDiag(:,3)=eval(sprintf...
    ('simlog_ssc_grounding_system.X9_8.T_5.p2.v.series.values'));
tempVDistDiag(:,4)=eval(sprintf...
    ('simlog_ssc_grounding_system.X11_10.T_5.p2.v.series.values'));
tempVDistDiag(:,5)=eval(sprintf...
    ('simlog_ssc_grounding_system.X13_12.T_5.p2.v.series.values'));
%%
tempVDistHoriz(:,1)=eval(sprintf...
    ('simlog_ssc_grounding_system.X7_6.T_5.p2.v.series.time'));
tempVDistHoriz(:,2)=eval(sprintf...
    ('simlog_ssc_grounding_system.X7_6.T_5.p2.v.series.values'));
tempVDistHoriz(:,3)=eval(sprintf...
    ('simlog_ssc_grounding_system.X7_8.T_5.p2.v.series.values'));
tempVDistHoriz(:,4)=eval(sprintf...
    ('simlog_ssc_grounding_system.X7_10.T_5.p2.v.series.values'));
tempVDistHoriz(:,5)=eval(sprintf...
    ('simlog_ssc_grounding_system.X7_12.T_5.p2.v.series.values'));

%%
%Current Distribution
tempIcurrent(:,1)=eval(sprintf...
```

```
    ('simlog_ssc_grounding_system.CurrentSensor1.I.series.time'));
tempIcurrent(:,2)=eval(sprintf...
    ('simlog_ssc_grounding_system.CurrentSensor1.I.series.values'));

%%
%2D plot of injected current: range from start to current 3D plot
figure();

subplot(3,1,1)
p2=plot(tempVDistHoriz(:,1)*1e6,tempVDistHoriz(:,2)/1e3,...
    tempVDistHoriz(:,1)*1e6,tempVDistHoriz(:,3)/1e3,...
    tempVDistHoriz(:,1)*1e6,tempVDistHoriz(:,4)/1e3,...
    tempVDistHoriz(:,1)*1e6,tempVDistHoriz(:,5)/1e3, 'Color','black');
%axis to be set in the range of actual model and wanted results
axis([0 2.5 0 9])
xlabel('Time [mu s]')
ylabel('Voltage [kV]')
title('Horizontal voltage distrbution from center');

subplot(3,1,2)
p1=plot(tempVDistDiag(:,1)*1e6,tempVDistDiag(:,2)/1e3,tempVDistDiag(:,1)...
    *1e6,tempVDistDiag(:,3)/1e3,tempVDistDiag(:,1)*1e6,...
    tempVDistDiag(:,4)/1e3,tempVDistDiag(:,1)*1e6,...
    tempVDistDiag(:,5)/1e3, 'Color','black');
%axis to be set in the range of actual model and wanted results
axis([0 2.5 0 9])
xlabel('Time [mu s]')
ylabel('Voltage [kV]')
title('Diagonal voltage distrbution from center');

subplot(3,1,3)
p3=plot(tempIcurrent(:,1)*1e6,tempIcurrent(:,2)/1e3,'Color','black');
%axis to be set in the range of actual model and wanted results
axis([0 2.5 0 1.05])
xlabel('Time [mu s]')
ylabel('Current [kA]')
title('Injected Current');
```

D.5.2.4 8×8, 5×5 m Meshes, 1600 m^2

```
% Updated 22.01
%
% For the simulation model "Sim5m_64MeshGrid.slx"
% Nodal voltage for selected points, from center diagonaly and horizontaly
% at 2x meshes distance. Current plot for the injection point
%
% Simulation must be loaded, for the spesific grounding grid, infront
% of nodal data extraction from loaded simlog.
%
% Used to produce (figs. 4.13a and 4.13e)
% where fig X.a and X.e indicates voltage and current plot, respectivly
tempVDistDiag(:,1)=eval(sprintf...
    ('simlog_ssc_grounding_system.X5_4.T_5.p2.v.series.time'));
tempVDistDiag(:,2)=eval(sprintf...
    ('simlog_ssc_grounding_system.X5_4.T_5.p2.v.series.values'));
tempVDistDiag(:,3)=eval(sprintf...
    ('simlog_ssc_grounding_system.X7_6.T_5.p2.v.series.values'));
tempVDistDiag(:,4)=eval(sprintf...
    ('simlog_ssc_grounding_system.X9_8.T_5.p2.v.series.values'));
%%
tempVDistHoriz(:,1)=eval(sprintf...
    ('simlog_ssc_grounding_system.X5_4.T_5.p2.v.series.time'));
tempVDistHoriz(:,2)=eval(sprintf...
    ('simlog_ssc_grounding_system.X5_4.T_5.p2.v.series.values'));
tempVDistHoriz(:,3)=eval(sprintf...
    ('simlog_ssc_grounding_system.X5_6.T_5.p2.v.series.values'));
tempVDistHoriz(:,4)=eval(sprintf...
    ('simlog_ssc_grounding_system.X5_8.T_5.p2.v.series.values'));
```

```
%%
%Current Distribution
tempIcurrent(:,1)=eval(sprintf...
    ('simlog_ssc_grounding_system.CurrentSensor1.I.series.time'));
tempIcurrent(:,2)=eval(sprintf...
    ('simlog_ssc_grounding_system.CurrentSensor1.I.series.values'));

%%
%2D plot of injected current: range from start to current 3D plot
figure();

subplot(3,1,1)
p2=plot(tempVDistHoriz(:,1)*1e6,tempVDistHoriz(:,2)/1e3,...
    tempVDistHoriz(:,1)*1e6,tempVDistHoriz(:,3)/1e3,...
    tempVDistHoriz(:,1)*1e6,tempVDistHoriz(:,4)/1e3, 'Color','black');
%axis to be set in the range of actual model and wanted results
axis([0 2.5 0 5])
xlabel('Time [mu s]')
ylabel('Voltage [kV]')
title('Horizontal voltage distrbution from center');

subplot(3,1,2)
p1=plot(tempVDistDiag(:,1)*1e6,tempVDistDiag(:,2)/1e3,tempVDistDiag(:,1)...
    *1e6,tempVDistDiag(:,3)/1e3,tempVDistDiag(:,1)*1e6,...
    tempVDistDiag(:,4)/1e3, 'Color','black');
%axis to be set in the range of actual model and wanted results
axis([0 2.5 0 5])
xlabel('Time [mu s]')
ylabel('Voltage [kV]')
title('Diagonal voltage distrbution from center');

subplot(3,1,3)
p3=plot(tempIcurrent(:,1)*1e6,tempIcurrent(:,2)/1e3,'Color','black');
%axis to be set in the range of actual model and wanted results
axis([0 2.5 0 1.05])
xlabel('Time [mu s]')
ylabel('Current [kA]')
title('Injected Current');
```

D.5.3 Isolated: First Segment Grounding Wire (2D)

D.5.3.1 Fast Front

```
% Evaluated with simlog for the 6x6, 10x10m meshes under same conditions as
% in (section 4.2.1) for the 300, 1000 and 2000 ohm m
% soil resistivity.
% The nodal measurments are retrived from the first wire segment from the
% injection point.
%
% Used to produce plots in section 4.3.1
%
%%
% Retrive data for 300 ohm m

% l1 - incomming inductor
FirstSeg300_l1(:,1)=eval(sprintf...
    ('simlog_ssc_grounding_system300.X4_4.T_1.l1.i.series.time'));
FirstSeg300_l1(:,2)=eval(sprintf...
    ('simlog_ssc_grounding_system300.X4_4.T_1.l1.i.series.values'));
FirstSeg300_l1(:,3)=eval(sprintf...
    ('simlog_ssc_grounding_system300.X4_4.T_1.l1.v.series.values'));
% l2 - incomming inductor
FirstSeg300_l2(:,1)=eval(sprintf...
    ('simlog_ssc_grounding_system300.X4_4.T_1.l2.i.series.time'));
FirstSeg300_l2(:,2)=eval(sprintf...
```

```
    ('simlog_ssc_grounding_system300.X4_4.T_1.l2.i.series.values'));
FirstSeg300_l2(:,3)=eval(sprintf...
    ('simlog_ssc_grounding_system300.X4_4.T_1.l2.v.series.values'));
% c - capacitance
FirstSeg300_c(:,1)=eval(sprintf...
    ('simlog_ssc_grounding_system300.X4_4.T_1.c.i.series.time'));
FirstSeg300_c(:,2)=eval(sprintf...
    ('simlog_ssc_grounding_system300.X4_4.T_1.c.i.series.values'));
FirstSeg300_c(:,3)=eval(sprintf...
    ('simlog_ssc_grounding_system300.X4_4.T_1.c.v.series.values'));
% g - conductance
FirstSeg300_g(:,1)=eval(sprintf...
    ('simlog_ssc_grounding_system300.X4_4.T_1.g.i.series.time'));
FirstSeg300_g(:,2)=eval(sprintf...
    ('simlog_ssc_grounding_system300.X4_4.T_1.g.i.series.values'));
FirstSeg300_g(:,3)=eval(sprintf...
    ('simlog_ssc_grounding_system300.X4_4.T_1.g.v.series.values'));
%%
% Retrive data for 1000 ohm m

% l1 - incomming inductor
FirstSeg1000_l1(:,1)=eval(sprintf...
    ('simlog_ssc_grounding_system1000.X4_4.T_1.l1.i.series.time'));
FirstSeg1000_l1(:,2)=eval(sprintf...
    ('simlog_ssc_grounding_system1000.X4_4.T_1.l1.i.series.values'));
FirstSeg1000_l1(:,3)=eval(sprintf...
    ('simlog_ssc_grounding_system1000.X4_4.T_1.l1.v.series.values'));
% l2 - incomming inductor
FirstSeg1000_l2(:,1)=eval(sprintf...
    ('simlog_ssc_grounding_system1000.X4_4.T_1.l2.i.series.time'));
FirstSeg1000_l2(:,2)=eval(sprintf...
    ('simlog_ssc_grounding_system1000.X4_4.T_1.l2.i.series.values'));
FirstSeg1000_l2(:,3)=eval(sprintf...
    ('simlog_ssc_grounding_system1000.X4_4.T_1.l2.v.series.values'));
% c - capacitance
FirstSeg1000_c(:,1)=eval(sprintf...
    ('simlog_ssc_grounding_system1000.X4_4.T_1.c.i.series.time'));
FirstSeg1000_c(:,2)=eval(sprintf...
    ('simlog_ssc_grounding_system1000.X4_4.T_1.c.i.series.values'));
FirstSeg1000_c(:,3)=eval(sprintf...
    ('simlog_ssc_grounding_system1000.X4_4.T_1.c.v.series.values'));
% g - conductance
FirstSeg1000_g(:,1)=eval(sprintf...
    ('simlog_ssc_grounding_system1000.X4_4.T_1.g.i.series.time'));
FirstSeg1000_g(:,2)=eval(sprintf...
    ('simlog_ssc_grounding_system1000.X4_4.T_1.g.i.series.values'));
FirstSeg1000_g(:,3)=eval(sprintf...
    ('simlog_ssc_grounding_system1000.X4_4.T_1.g.v.series.values'));
%%
% Retrive data for 2000 ohm m

% l1 - incomming inductor
FirstSeg2000_l1(:,1)=eval(sprintf...
    ('simlog_ssc_grounding_system2000.X4_4.T_1.l1.i.series.time'));
FirstSeg2000_l1(:,2)=eval(sprintf...
    ('simlog_ssc_grounding_system2000.X4_4.T_1.l1.i.series.values'));
FirstSeg2000_l1(:,3)=eval(sprintf...
    ('simlog_ssc_grounding_system2000.X4_4.T_1.l1.v.series.values'));
% l2 - incomming inductor
FirstSeg2000_l2(:,1)=eval(sprintf...
    ('simlog_ssc_grounding_system2000.X4_4.T_1.l2.i.series.time'));
FirstSeg2000_l2(:,2)=eval(sprintf...
    ('simlog_ssc_grounding_system2000.X4_4.T_1.l2.i.series.values'));
FirstSeg2000_l2(:,3)=eval(sprintf...
    ('simlog_ssc_grounding_system2000.X4_4.T_1.l2.v.series.values'));
% c - capacitance
FirstSeg2000_c(:,1)=eval(sprintf...
    ('simlog_ssc_grounding_system2000.X4_4.T_1.c.i.series.time'));
FirstSeg2000_c(:,2)=eval(sprintf...
    ('simlog_ssc_grounding_system2000.X4_4.T_1.c.i.series.values'));
FirstSeg2000_c(:,3)=eval(sprintf...
```

```
    ('simlog_ssc_grounding_system2000.X4_4.T_1.c.v.series.values'));
% g - conductance
FirstSeg2000_g(:,1)=eval(sprintf...
    ('simlog_ssc_grounding_system2000.X4_4.T_1.g.i.series.time'));
FirstSeg2000_g(:,2)=eval(sprintf...
    ('simlog_ssc_grounding_system2000.X4_4.T_1.g.i.series.values'));
FirstSeg2000_g(:,3)=eval(sprintf...
    ('simlog_ssc_grounding_system2000.X4_4.T_1.g.v.series.values'));

%%
figure();
subplot(3,1,1)
p2=plot(FirstSeg300_g(:,1)*10^6,FirstSeg300_g(:,3)/10^3,...
    FirstSeg1000_g(:,1)*10^6,FirstSeg1000_g(:,3)/10^3,...
    FirstSeg2000_g(:,1)*10^6,FirstSeg2000_g(:,3)/10^3, 'Color','black');
%axis to be set in the range of actual model and wanted results
axis([0 2.5 0 10])
xlabel('Time [mu s]')
ylabel('Voltage [kV]')
title('Midle section voltage(C and G to "true" ground)');

subplot(3,1,2)
p2=plot(FirstSeg300_g(:,1)*10^6,FirstSeg300_g(:,2),...
    FirstSeg1000_g(:,1)*10^6,FirstSeg1000_g(:,2),...
    FirstSeg2000_g(:,1)*10^6,FirstSeg2000_g(:,2), 'Color','black');
%axis to be set in the range of actual model and wanted results
axis([0 2.5 0 20])
xlabel('Time [mu s]')
ylabel('Current [A]')
title('Conductance Current(leakage current to ground)');

subplot(3,1,3)
p2=plot(FirstSeg300_c(:,1)*10^6,FirstSeg300_c(:,2),...
    FirstSeg1000_c(:,1)*10^6,FirstSeg1000_c(:,2),...
    FirstSeg2000_c(:,1)*10^6,FirstSeg2000_c(:,2), 'Color','black');
%axis to be set in the range of actual model and wanted results
axis([0 2.5 -6 14])
xlabel('Time [mu s]')
ylabel('Current [A]')
title('Capacitor Current');

%%
figure();
subplot(2,1,1)
p2=plot(FirstSeg300_l1(:,1)*10^6,FirstSeg300_l1(:,2),...
    FirstSeg1000_l1(:,1)*10^6,FirstSeg1000_l1(:,2),...
    FirstSeg2000_l1(:,1)*10^6,FirstSeg2000_l1(:,2), 'Color','black');
%axis to be set in the range of actual model and wanted results
axis([0 2.5 0 300])
xlabel('Time [mu s]')
ylabel('Current [A]')
title('Current from injection point to L1');

subplot(2,1,2)
p1=plot(FirstSeg300_l1(:,1)*10^6,FirstSeg300_l1(:,3),...
    FirstSeg1000_l1(:,1)*10^6,FirstSeg1000_l1(:,3),...
    FirstSeg2000_l1(:,1)*10^6,FirstSeg2000_l1(:,3), 'Color','black');
%axis to be set in the range of actual model and wanted results
axis([0 2.5 -100 600])
xlabel('Time [mu s]')
ylabel('Voltage [V]')
title('Voltage over L1');

%%
figure();
subplot(2,1,1)
p2=plot(FirstSeg300_l2(:,1)*10^6,FirstSeg300_l2(:,2),...
    FirstSeg1000_l2(:,1)*10^6,FirstSeg1000_l2(:,2),...
    FirstSeg2000_l2(:,1)*10^6,FirstSeg2000_l2(:,2), 'Color','black');
%axis to be set in the range of actual model and wanted results
axis([0 2.5 -300 0])
```

```
xlabel('Time [mu s]')
ylabel('Current [A]')
title('Current from first wire segment trough L2');

subplot(2,1,2)
p2=plot(FirstSeg300_l2(:,1)*10^6,FirstSeg300_l2(:,3),...
    FirstSeg1000_l2(:,1)*10^6,FirstSeg1000_l2(:,3),...
    FirstSeg2000_l2(:,1)*10^6,FirstSeg2000_l2(:,3), 'Color','black');
%axis to be set in the range of actual model and wanted results
axis([0 2.5 -600 100])
xlabel('Time [mu s]')
ylabel('Voltage [V]')
title('Voltage over L2');
```

D.5.3.2 Slow Front

```
% Evaluated with simlog for the 6x6, 10x10m meshes under same conditions as
% in (section 4.2.1) for soil
% resistivity2000 ohm m and Er=16 with a slow front surge wave
% The nodal measurments are retrived from the first wire segment from the
% injection point.
%
% Used to produce plots in section 4.3.2
%%
% Retrive data for 2000 ohm m and slow front surge wave

% l1 - incomming inductor
FirstSeg2000_l1(:,1)=eval(sprintf...
('simlog_ssc_grounding_system2000SlowFront.X4_4.T_1.l1.i.series.time'));
FirstSeg2000_l1(:,2)=eval(sprintf...
('simlog_ssc_grounding_system2000SlowFront.X4_4.T_1.l1.i.series.values'));
FirstSeg2000_l1(:,3)=eval(sprintf...
('simlog_ssc_grounding_system2000SlowFront.X4_4.T_1.l1.v.series.values'));
% l2 - incomming inductor
FirstSeg2000_l2(:,1)=eval(sprintf...
('simlog_ssc_grounding_system2000SlowFront.X4_4.T_1.l2.i.series.time'));
FirstSeg2000_l2(:,2)=eval(sprintf...
('simlog_ssc_grounding_system2000SlowFront.X4_4.T_1.l2.i.series.values'));
FirstSeg2000_l2(:,3)=eval(sprintf...
('simlog_ssc_grounding_system2000SlowFront.X4_4.T_1.l2.v.series.values'));
% c - capacitance
FirstSeg2000_c(:,1)=eval(sprintf...
('simlog_ssc_grounding_system2000SlowFront.X4_4.T_1.c.i.series.time'));
FirstSeg2000_c(:,2)=eval(sprintf...
('simlog_ssc_grounding_system2000SlowFront.X4_4.T_1.c.i.series.values'));
FirstSeg2000_c(:,3)=eval(sprintf...
('simlog_ssc_grounding_system2000SlowFront.X4_4.T_1.c.v.series.values'));
% g - conductance
FirstSeg2000_g(:,1)=eval(sprintf...
('simlog_ssc_grounding_system2000SlowFront.X4_4.T_1.g.i.series.time'));
FirstSeg2000_g(:,2)=eval(sprintf...
('simlog_ssc_grounding_system2000SlowFront.X4_4.T_1.g.i.series.values'));
FirstSeg2000_g(:,3)=eval(sprintf...
('simlog_ssc_grounding_system2000SlowFront.X4_4.T_1.g.v.series.values'));


%%
figure();
subplot(3,1,1)
p2=plot(FirstSeg2000_g(:,1)*10^6,FirstSeg2000_g(:,3)/10^3,...
    'Color','black');
%axis to be set in the range of actual model and wanted results
axis([0 10 0 3])
xlabel('Time [mu s]')
ylabel('Voltage [kV]')
title('Midle section voltage(C and G to "true" ground)');

subplot(3,1,2)
```

```
p2=plot(FirstSeg2000_g(:,1)*10^6,FirstSeg2000_g(:,2), 'Color','black');
%axis to be set in the range of actual model and wanted results
axis([0 10 0 2])
xlabel('Time [mu s]')
ylabel('Current [A]')
title('Conductance Current(leakage current to ground)');

subplot(3,1,3)
p2=plot(FirstSeg2000_c(:,1)*10^6,FirstSeg2000_c(:,2), 'Color','black');
%axis to be set in the range of actual model and wanted results
axis([0 10 -1 2])
xlabel('Time [mu s]')
ylabel('Current [A]')
title('Capacitor Current');

matlab2tikz;
%%
figure();
subplot(2,1,1)
p2=plot(FirstSeg2000_l1(:,1)*10^6,FirstSeg2000_l1(:,2), 'Color','black');
%axis to be set in the range of actual model and wanted results
axis([0 10 0 300])
xlabel('Time [mu s]')
ylabel('Current [A]')
title('Current from injection point to L1');

subplot(2,1,2)
p1=plot(FirstSeg2000_l1(:,1)*10^6,FirstSeg2000_l1(:,3), 'Color','black');
%axis to be set in the range of actual model and wanted results
axis([0 10 -10 100])
xlabel('Time [mu s]')
ylabel('Voltage [V]')
title('Voltage over L1');

matlab2tikz;
%%
figure();
subplot(2,1,1)
p2=plot(FirstSeg2000_l2(:,1)*10^6,FirstSeg2000_l2(:,2), 'Color','black');
%axis to be set in the range of actual model and wanted results
axis([0 10 -300 0])
xlabel('Time [mu s]')
ylabel('Current [A]')
title('Current from first wire segment trough L2');

subplot(2,1,2)
p2=plot(FirstSeg2000_l2(:,1)*10^6,FirstSeg2000_l2(:,3), 'Color','black');
%axis to be set in the range of actual model and wanted results
axis([0 10 -100 10])
xlabel('Time [mu s]')
ylabel('Voltage [V]')
title('Voltage over L2');

matlab2tikz;
```

D.5.4 Integrated: Voltage and Current (2D)

D.5.4.1 6×6, 10×10 m Meshes, 3600 m^2

```
% Updated 02.04
%
% From simulation of EMTP-RV model file "EMTPSim10m_36MeshGrid.slx"
% Nodal voltage for selected points, from center diagonaly and horizontaly
% at 1x meshes distance. Current plot for the injection point
%
% Simulation must be loaded, for the spesific grounding grid, infront
```

```
% of nodal data extraction from loaded simlog.
%
%%
% Limitiation of FMI interface are that simulation log
% needs to be manualy stored by command:
% "simscape.logging.export(simlog_ssc_grounding_system...
%    ,'local path on disk.h5')"
% And loaded to Matlab for pre-prosessing by command
% simlog_ssc_grounding_system=simscape.logging.import...
%   (simlog_ssc_grounding_system,'local path on disk.h5')"
%
%%
% Used to produce figs. 4.18a to 4.18c, 4.22a to 4.22c, 4.23a to 4.23c, 4.24a to 4.24c and 4.25a to 4.25c
%
%%
tempVDistDiag(:,1)=eval(sprintf...
    ('simlog_ssc_grounding_system.X4_3.T_9.p2.v.series.time'));
tempVDistDiag(:,2)=eval(sprintf...
    ('simlog_ssc_grounding_system.X4_3.T_9.p2.v.series.values'));
tempVDistDiag(:,3)=eval(sprintf...
    ('simlog_ssc_grounding_system.X5_4.T_10.p2.v.series.values'));
tempVDistDiag(:,4)=eval(sprintf...
    ('simlog_ssc_grounding_system.X6_5.T_10.p2.v.series.values'));
tempVDistDiag(:,5)=eval(sprintf...
    ('simlog_ssc_grounding_system.X7_6.T_10.p2.v.series.values'));
%%
tempVDistHoriz(:,1)=eval(sprintf...
    ('simlog_ssc_grounding_system.X4_3.T_9.p2.v.series.time'));
tempVDistHoriz(:,2)=eval(sprintf...
    ('simlog_ssc_grounding_system.X4_3.T_9.p2.v.series.values'));
tempVDistHoriz(:,3)=eval(sprintf...
    ('simlog_ssc_grounding_system.X4_4.T_10.p2.v.series.values'));
tempVDistHoriz(:,4)=eval(sprintf...
    ('simlog_ssc_grounding_system.X4_5.T_10.p2.v.series.values'));
tempVDistHoriz(:,5)=eval(sprintf...
    ('simlog_ssc_grounding_system.X4_6.T_10.p2.v.series.values'));
%%
%Current Distribution
tempIcurrent(:,1)=eval(sprintf...
    ('simlog_ssc_grounding_system.I_EMTPCurrSurgeInject.I.series.time'));
tempIcurrent(:,2)=eval(sprintf...
    ('simlog_ssc_grounding_system.I_EMTPCurrSurgeInject.I.series.values'));

%%
%Current Injected
tempIcurrent(:,1)=eval(sprintf...
    ('simlog_ssc_grounding_system.I_EMTPCurrSurgeInject.I.series.time'));
tempIcurrent(:,2)=eval(sprintf...
    ('simlog_ssc_grounding_system.I_EMTPCurrSurgeInject.I.series.values'));

%%
%Nodal Voltage at cable junction and transformer
tempUNettworkVolt(:,1)=eval(sprintf...
    ('simlog_ssc_grounding_system.O_EMTPVoltCableEntry.V.series.time'));
tempUNettworkVolt(:,2)=eval(sprintf...
    ('simlog_ssc_grounding_system.O_EMTPVoltCableEntry.V.series.values'));
tempUNettworkVolt(:,3)=eval(sprintf...
    ('simlog_ssc_grounding_system.O_EMTPVoltTrans.V.series.values'));
tempUNettworkVolt(:,4)=eval(sprintf...
    ('simlog_ssc_grounding_system.O_EMTPVoltArrester.V.series.values'));
tempUNettworkVolt(:,5)=eval(sprintf...
    ('simlog_ssc_grounding_system.O_EMTPCurrSurgeSource.V.series.values'));

%%
%Grounding grid injection point, current voltage and impedance
tempInjectPointI(:,1)=eval(sprintf...
    ('simlog_ssc_grounding_system.I_EMTPCurrSurgeInject.I.series.time'));
tempInjectPointI(:,2)=eval(sprintf...
    ('simlog_ssc_grounding_system.I_EMTPCurrSurgeInject.I.series.values'));

tempInjectPointV(:,1)=eval(sprintf...
```

```
    ('simlog_ssc_grounding_system.X4_3.VoltInjectPoint.V.series.time'));
tempInjectPointV(:,2)=eval(sprintf...
    ('simlog_ssc_grounding_system.X4_3.VoltInjectPoint.V.series.values'));

tempInjectPointImp(:,1)=eval(sprintf...
    ('simlog_ssc_grounding_system.ImpInjectPoint.V.series.time'));
tempInjectPointImp(:,2)=eval(sprintf...
    ('simlog_ssc_grounding_system.ImpInjectPoint.V.series.values'));


%%
%
figure();
subplot(3,1,1)
p2=plot(tempVDistHoriz(:,1)*1e6,tempVDistHoriz(:,2)/1e3,...
    tempVDistHoriz(:,1)*1e6,tempVDistHoriz(:,3)/1e3,...
    tempVDistHoriz(:,1)*1e6,tempVDistHoriz(:,4)/1e3,...
    tempVDistHoriz(:,1)*1e6,tempVDistHoriz(:,5)/1e3, 'Color','black');
%axis to be set in the range of actual model and wanted results
axis([0 56 -10 15])
xlabel('Time [mu s]')
ylabel('Voltage [kV]')
title('Horizontal voltage distrbution from center');

subplot(3,1,2)
p1=plot(tempVDistDiag(:,1)*1e6,tempVDistDiag(:,2)/1e3,tempVDistDiag(:,1)...
    *1e6,tempVDistDiag(:,3)/1e3,tempVDistDiag(:,1)*1e6,...
    tempVDistDiag(:,4)/1e3,tempVDistDiag(:,1)*1e6,...
    tempVDistDiag(:,5)/1e3, 'Color','black');
%axis to be set in the range of actual model and wanted results
axis([0 56 -10 15])
xlabel('Time [mu s]')
ylabel('Voltage [kV]')
title('Diagonal voltage distrbution from center');

%%

%2D plot of nettwork nodal voltages and injected current in far-end

figure();
p4=plot(tempUNettworkVolt(:,1)*1e6,tempUNettworkVolt(:,2)/1e3,...
    tempUNettworkVolt(:,1)*1e6,tempUNettworkVolt(:,3)/1e3,...
    tempUNettworkVolt(:,1)*1e6,tempUNettworkVolt(:,4)/1e3,'Color','black');
axis([0 60 0 250])
xlabel('Time [mu s]')
ylabel('Voltage [kV]')
title('Nettwork nodal voltage');
%axis to be set in the range of actual model and wanted result

%%
figure();
p5=plot(tempUNettworkVolt(:,1)*1e6,tempUNettworkVolt(:,5)/1e3,'Color','black');
axis([0 65 0 1])
xlabel('Time [mu s]')
ylabel('Current [kA]')
title('Nettwork current injected in far-end');

%%
%2D plot of injectpointVoltage

figure();
p6=plot(tempInjectPointV(:,1)*1e6,tempInjectPointV(:,2)/1e3,'Color','black');
axis([33 55 -10 15])
xlabel('Time [mu s]')
ylabel('Voltage [kV]')
title('Injection point voltage');
%axis to be set in the range of actual model and wanted result

%%
%2D plot of injectpointCurrent
figure();
```

```
p7=plot(tempInjectPointI(:,1)*1e6,tempInjectPointI(:,2)/1e3);
axis([33 55 0 2.5])
xlabel('Time [mu s]')
ylabel('Current [kA]')
title('Injection point current');

%%
figure();
p8=plot(tempInjectPointImp(:,1)*1e6,tempInjectPointImp(:,2)...
    ,'Color','black');
%axis to be set in the range of actual model and wanted results
axis([33 65 0 23])
xlabel('Time [mu s]')
ylabel('Impedance [ohm]')
title('Grounding grid impulse impedance from injection point');
```

D.5.4.2 4×4, 10×10 m Meshes, 1600 m^2

```
% Updated 26.03
%
% From simulation of EMTP-RV model file "EMTPSim10m_16MeshGrid.slx"
% Nodal voltage for selected points, from center diagonaly and horizontaly
% at 1x meshes distance. Current plot for the injection point
%
% Simulation must be loaded, for the spesific grounding grid, infront
% of nodal data extraction from loaded simlog.
%
%%
% Limitiation of FMI interface are that simulation log
% needs to be manualy stored by command:
% "simscape.logging.export(simlog_ssc_grounding_system...
%    ,'local path on disk.h5')"
% And loaded to Matlab for pre-prosessing by command
% simlog_ssc_grounding_system=simscape.logging.import...
%   (simlog_ssc_grounding_system,'local path on disk.h5')"
%
%%
% Used to produce figs. 4.17, 4.19a to 4.19c and 4.26a to 4.26c
%
%%
tempVDistDiag(:,1)=eval(sprintf...
    ('simlog_ssc_grounding_system.X3_2.T_10.p1.v.series.time'));
tempVDistDiag(:,2)=eval(sprintf...
    ('simlog_ssc_grounding_system.X3_2.T_10.p1.v.series.values'));
tempVDistDiag(:,3)=eval(sprintf...
    ('simlog_ssc_grounding_system.X4_3.T_10.p2.v.series.values'));
tempVDistDiag(:,4)=eval(sprintf...
    ('simlog_ssc_grounding_system.X5_4.T_10.p2.v.series.values'));
%%
tempVDistHoriz(:,1)=eval(sprintf...
    ('simlog_ssc_grounding_system.X3_2.T_10.p1.v.series.time'));
tempVDistHoriz(:,2)=eval(sprintf...
    ('simlog_ssc_grounding_system.X3_2.T_10.p1.v.series.values'));
tempVDistHoriz(:,3)=eval(sprintf...
    ('simlog_ssc_grounding_system.X3_3.T_10.p2.v.series.values'));
tempVDistHoriz(:,4)=eval(sprintf...
    ('simlog_ssc_grounding_system.X3_4.T_10.p2.v.series.values'));
%%
%Current Injected
tempIcurrent(:,1)=eval(sprintf...
    ('simlog_ssc_grounding_system.I_EMTPCurrSurgeInject.I.series.time'));
tempIcurrent(:,2)=eval(sprintf...
    ('simlog_ssc_grounding_system.I_EMTPCurrSurgeInject.I.series.values'));

%%
%Nodal Voltage at cable junction and transformer
tempUNettworkVolt(:,1)=eval(sprintf...
    ('simlog_ssc_grounding_system.O_EMTPVoltCableEntry.V.series.time'));
```

```
tempUNettworkVolt(:,2)=eval(sprintf...
    ('simlog_ssc_grounding_system.O_EMTPVoltCableEntry.V.series.values'));
tempUNettworkVolt(:,3)=eval(sprintf...
    ('simlog_ssc_grounding_system.O_EMTPVoltTrans.V.series.values'));
tempUNettworkVolt(:,4)=eval(sprintf...
    ('simlog_ssc_grounding_system.O_EMTPVoltArrester.V.series.values'));
tempUNettworkVolt(:,5)=eval(sprintf...
    ('simlog_ssc_grounding_system.O_EMTPCurrSurgeSource.V.series.values'));

%%
%Grounding grid injection point, current voltage and impedance
tempInjectPointI(:,1)=eval(sprintf...
    ('simlog_ssc_grounding_system.I_EMTPCurrSurgeInject.I.series.time'));
tempInjectPointI(:,2)=eval(sprintf...
    ('simlog_ssc_grounding_system.I_EMTPCurrSurgeInject.I.series.values'));

tempInjectPointV(:,1)=eval(sprintf...
    ('simlog_ssc_grounding_system.X3_2.VoltInjectPoint.V.series.time'));
tempInjectPointV(:,2)=eval(sprintf...
    ('simlog_ssc_grounding_system.X3_2.VoltInjectPoint.V.series.values'));

tempInjectPointImp(:,1)=eval(sprintf...
    ('simlog_ssc_grounding_system.ImpInjectPoint.V.series.time'));
tempInjectPointImp(:,2)=eval(sprintf...
    ('simlog_ssc_grounding_system.ImpInjectPoint.V.series.values'));

%%

%2D plot of injected current: range from start to current 3D plot

figure();
subplot(3,1,1)
p1=plot(tempVDistHoriz(:,1)*1e6,tempVDistHoriz(:,2)/1e3,...
    tempVDistHoriz(:,1)*1e6,tempVDistHoriz(:,3)/1e3,...
    tempVDistHoriz(:,1)*1e6,tempVDistHoriz(:,4)/1e3, 'Color','black');
%axis to be set in the range of actual model and wanted results
axis([33 65 0 28])
xlabel('Time [mu s]')
ylabel('Voltage [kV]')
title('Horizontal voltage distrbution from center');

subplot(3,1,2)
p2=plot(tempVDistDiag(:,1)*1e6,tempVDistDiag(:,2)/1e3,tempVDistDiag(:,1)...
    *1e6,tempVDistDiag(:,3)/1e3,tempVDistDiag(:,1)*1e6,...
    tempVDistDiag(:,4)/1e3, 'Color','black');
%axis to be set in the range of actual model and wanted results
axis([33 65 0 28])
xlabel('Time [mu s]')
ylabel('Voltage [kV]')
title('Vertical voltage distrbution from center');

%%
%2D plot of nettwork nodal voltages and injected current in far-end

figure();
p4=plot(tempUNettworkVolt(:,1)*1e6,tempUNettworkVolt(:,2)/1e3,...
    tempUNettworkVolt(:,1)*1e6,tempUNettworkVolt(:,3)/1e3,...
    tempUNettworkVolt(:,1)*1e6,tempUNettworkVolt(:,4)/1e3,'Color','black');
axis([0 65 0 200])
xlabel('Time [mu s]')
ylabel('Voltage [kV]')
title('Nettwork nodal voltage');
%axis to be set in the range of actual model and wanted result

%%
figure();
p5=plot(tempUNettworkVolt(:,1)*1e6,tempUNettworkVolt(:,5)/1e3,'Color','black');
axis([0 65 0 1])
xlabel('Time [mu s]')
ylabel('Current [kA]')
title('Nettwork current injected in far-end');
```

```
%%
%2D plot of injectpointVoltage

figure();
p6=plot(tempInjectPointV(:,1)*1e6,tempInjectPointV(:,2)/1e3,'Color','black');
axis([33 55 -10 30])
xlabel('Time [mu s]')
ylabel('Voltage [kV]')
title('Injection point voltage');
%axis to be set in the range of actual model and wanted result

%%
%2D plot of injectpointCurrent
figure();
p7=plot(tempInjectPointI(:,1)*1e6,tempInjectPointI(:,2)/1e3);
axis([33 75 0 2.5])
xlabel('Time [mu s]')
ylabel('Current [kA]')
title('Injection point current');

%%
figure();
p8=plot(tempInjectPointImp(:,1)*1e6,tempInjectPointImp(:,2)...
    ,'Color','black');
%axis to be set in the range of actual model and wanted results
axis([33 65 0 23])
xlabel('Time [mu s]')
ylabel('Impedance [ohm]')
title('Grounding grid impulse impedance from injection point');
```

D.5.4.3 8×8, 5×5 m Meshes, 1600 m^2

```
% Updated 29.03
%
% From simulation of EMTP-RV model file "EMTPSim5m_64MeshGrid.slx"
% Nodal voltage for selected points, from center diagonaly and horizontaly
% at 2x meshes distance. Current plot for the injection point
%
%
%%
% Simulation must be loaded, for the spesific grounding grid, infront
% of nodal data extraction from loaded simlog.
%%
%
% Limitiation of FMI interface are that simulation log
% needs to be manualy stored by command:
% "simscape.logging.export(simlog_ssc_grounding_system...
%    ,'local path on disk.h5')"
% And loaded to Matlab for pre-prosessing by command
% simlog_ssc_grounding_system=simscape.logging.import...
%   (simlog_ssc_grounding_system,'local path on disk.h5')"
%
%%
% Used to produce figs. 4.20a to 4.20c and 4.27a to 4.27c
%
%%
tempVDistDiag(:,1)=eval(sprintf...
    ('simlog_ssc_grounding_system.X5_4.T_4.p2.v.series.time'));
tempVDistDiag(:,2)=eval(sprintf...
    ('simlog_ssc_grounding_system.X5_4.T_4.p2.v.series.values'));
tempVDistDiag(:,3)=eval(sprintf...
    ('simlog_ssc_grounding_system.X7_6.T_5.p2.v.series.values'));
tempVDistDiag(:,4)=eval(sprintf...
    ('simlog_ssc_grounding_system.X9_8.T_5.p2.v.series.values'));
%%
tempVDistHoriz(:,1)=eval(sprintf...
    ('simlog_ssc_grounding_system.X5_4.T_4.p2.v.series.time'));
```

```
tempVDistHoriz(:,2)=eval(sprintf...
    ('simlog_ssc_grounding_system.X5_4.T_4.p2.v.series.values'));
tempVDistHoriz(:,3)=eval(sprintf...
    ('simlog_ssc_grounding_system.X5_6.T_5.p2.v.series.values'));
tempVDistHoriz(:,4)=eval(sprintf...
    ('simlog_ssc_grounding_system.X5_8.T_5.p2.v.series.values'));

%%
%Current Injected
tempIcurrent(:,1)=eval(sprintf...
    ('simlog_ssc_grounding_system.I_EMTPCurrSurgeInject.I.series.time'));
tempIcurrent(:,2)=eval(sprintf...
    ('simlog_ssc_grounding_system.I_EMTPCurrSurgeInject.I.series.values'));

%%
%Nodal Voltage at cable junction and transformer
tempUNettworkVolt(:,1)=eval(sprintf...
    ('simlog_ssc_grounding_system.O_EMTPVoltCableEntry.V.series.time'));
tempUNettworkVolt(:,2)=eval(sprintf...
    ('simlog_ssc_grounding_system.O_EMTPVoltCableEntry.V.series.values'));
tempUNettworkVolt(:,3)=eval(sprintf...
    ('simlog_ssc_grounding_system.O_EMTPVoltTrans.V.series.values'));
tempUNettworkVolt(:,4)=eval(sprintf...
    ('simlog_ssc_grounding_system.O_EMTPVoltArrester.V.series.values'));
tempUNettworkVolt(:,5)=eval(sprintf...
    ('simlog_ssc_grounding_system.O_EMTPCurrSurgeSource.V.series.values'));

%%
%Grounding grid injection point, current voltage and impedance
tempInjectPointI(:,1)=eval(sprintf...
    ('simlog_ssc_grounding_system.I_EMTPCurrSurgeInject.I.series.time'));
tempInjectPointI(:,2)=eval(sprintf...
    ('simlog_ssc_grounding_system.I_EMTPCurrSurgeInject.I.series.values'));

tempInjectPointV(:,1)=eval(sprintf...
    ('simlog_ssc_grounding_system.X5_4.VoltInjectPoint.V.series.time'));
tempInjectPointV(:,2)=eval(sprintf...
    ('simlog_ssc_grounding_system.X5_4.VoltInjectPoint.V.series.values'));

tempInjectPointImp(:,1)=eval(sprintf...
    ('simlog_ssc_grounding_system.ImpInjectPoint.V.series.time'));
tempInjectPointImp(:,2)=eval(sprintf...
    ('simlog_ssc_grounding_system.ImpInjectPoint.V.series.values'));

%%
figure();

subplot(3,1,1)
p2=plot(tempVDistHoriz(:,1)*1e6,tempVDistHoriz(:,2)/1e3,...
    tempVDistHoriz(:,1)*1e6,tempVDistHoriz(:,3)/1e3,...
    tempVDistHoriz(:,1)*1e6,tempVDistHoriz(:,4)/1e3, 'Color','black');
%axis to be set in the range of actual model and wanted results
axis([0 56 -10 30])
xlabel('Time [mu s]')
ylabel('Voltage [kV]')
title('Horizontal voltage distrbution from center');

subplot(3,1,2)
p1=plot(tempVDistDiag(:,1)*1e6,tempVDistDiag(:,2)/1e3,...
    tempVDistDiag(:,1)*1e6,tempVDistDiag(:,3)/1e3,...
    tempVDistDiag(:,1)*1e6,tempVDistDiag(:,4)/1e3, 'Color','black');
%axis to be set in the range of actual model and wanted results
axis([0 56 -10 30])
xlabel('Time [mu s]')
ylabel('Voltage [kV]')
title('Diagonal voltage distrbution from center');


%%

%2D plot of nettwork nodal voltages and injected current in far-end
```

```
figure();
p4=plot(tempUNettworkVolt(:,1)*1e6,tempUNettworkVolt(:,2)/1e3,...
    tempUNettworkVolt(:,1)*1e6,tempUNettworkVolt(:,3)/1e3,'Color','black');
axis([0 60 0 250])
xlabel('Time [mu s]')
ylabel('Voltage [kV]')
title('Nettwork nodal voltage');
%axis to be set in the range of actual model and wanted result

%%
figure();
p5=plot(tempUNettworkVolt(:,1)*1e6,tempUNettworkVolt(:,5)/1e3,'Color','black');
axis([0 65 0 1])
xlabel('Time [mu s]')
ylabel('Current [kA]')
title('Nettwork current injected in far-end');

%%
%2D plot of injectpointVoltage

figure();
p6=plot(tempInjectPointV(:,1)*1e6,tempInjectPointV(:,2)/1e3,'Color','black');
axis([33 55 -10 28])
xlabel('Time [mu s]')
ylabel('Voltage [kV]')
title('Injection point voltage');
%axis to be set in the range of actual model and wanted result


%%
%2D plot of injectpointCurrent
figure();
p7=plot(tempInjectPointI(:,1)*1e6,tempInjectPointI(:,2)/1e3);
axis([33 55 0 2.5])
xlabel('Time [mu s]')
ylabel('Current [kA]')
title('Injection point current');

%%
figure();
p8=plot(tempInjectPointImp(:,1)*1e6,tempInjectPointImp(:,2)...
    ,'Color','black');
%axis to be set in the range of actual model and wanted results
axis([33 65 0 23])
xlabel('Time [mu s]')
ylabel('Impedance [ohm]')
title('Grounding grid impulse impedance from injection point');

%%
figure();
p8=plot(tempUNettworkVolt(:,1)*1e6,tempUNettworkVolt(:,5)/1e3...
    ,'Color','black');
%axis to be set in the range of actual model and wanted results
axis([0 65 0 1])
xlabel('Time [mu s]')
ylabel('Current')
title('Injected current source, far-end');
```

D.5.5 Isolated/Integrated: Voltage Distribution (3D)

```
% Updated 13.04
%
% From simulation for both Isolated and EMTP-RV model files. Definition of
% plot is generic and will fit all models.
%
% Simulation must be loaded, for the spesific grounding grid, infront
```

```
% of nodal data extraction from loaded simlog.
% Preconditions:
% 1. Definition of current grounding grid physical properties according
%       chapter D for selected model
% 2. Define distribution sample according to for selected time within
% log series
%       section D.3.1
% 3. Generate plot memory by running function
%       - section D.3.2
%%
% Limitiation of FMI interface are that simulation log
% needs to be manualy stored by command:
% "simscape.logging.export(simlog_ssc_grounding_system...
%    ,'local path on disk.h5')"
% And loaded to Matlab for pre-prosessing by command
% simlog_ssc_grounding_system=simscape.logging.import...
%   (simlog_ssc_grounding_system,'local path on disk.h5')"
%%
% Simulation log in isolated mode can be imported directly from file or
% current simulation
%
%
%%
% Used to produce all 3D plots sections 4.2, 4.4 and 4.5
%
%%
% Voltage distribution in the grounding grid

h4 = figure();
%subplot(3,2,1)
p3=stem3(plotMVoltPeak(:,1),plotMVoltPeak(:,2),...
    (plotMVoltPeak(:,3)/1e3),'.','fill','black');
set(gca,'FontSize',20)
xlabel('Grid x-direction [m]')
ylabel('Grid y-direction [m]')
zlabel('Voltage [kV]')
title('Voltage distribution')
tickValues = min(plotMVoltPeak(:,1)):10:max(plotMVoltPeak(:,1));
set(gca,'XTick',tickValues)
tickValues = min(plotMVoltPeak(:,2)):10:max(plotMVoltPeak(:,2));
set(gca,'YTick',tickValues)
tickValues = 0:5:30;
set(gca,'ZTick',tickValues)
zlim([0 30])
```

D.5.6 Integrated: Electric Field (2D)

```
% Updated 02.05
%
% From simulation of EMTP-RV model file "EMTPSim10m_16MeshGrid.slx"
% Nodal electric field for selected points, from center diagonaly and
% horizontaly % at 1x meshes distance.
%
% Simulation must be loaded, for the spesific grounding grid, infront
% of nodal data extraction from loaded simlog.
%
%%
% Limitiation of FMI interface are that simulation log
% needs to be manualy stored by command:
% "simscape.logging.export(simlog_ssc_grounding_system...
%    ,'local path on disk.h5')"
% And loaded to Matlab for pre-prosessing by command
% simlog_ssc_grounding_system=simscape.logging.import...
%   (simlog_ssc_grounding_system,'local path on disk.h5')"
%
```

```
%%
% Used to produce figs. 4.28a and 4.29a
%
%%
% Leakage current distribution
tempLekageCurrentDiag(:,1)=eval(sprintf...
    ('simlog_ssc_grounding_system.X4_3.T_10.g.i.series.time'));
tempLekageCurrentDiag(:,2)=eval(sprintf...
    ('simlog_ssc_grounding_system.X4_3.T_10.g.i.series.values'));
tempLekageCurrentDiag(:,3)=eval(sprintf...
    ('simlog_ssc_grounding_system.X5_4.T_10.g.i.series.values'));
tempLekageCurrentDiag(:,4)=eval(sprintf...
    ('simlog_ssc_grounding_system.X6_5.T_10.g.i.series.values'));
tempLekageCurrentDiag(:,5)=eval(sprintf...
    ('simlog_ssc_grounding_system.X7_6.T_10.g.i.series.values'));
%%
tempLekageCurrenHoriz(:,1)=eval(sprintf...
    ('simlog_ssc_grounding_system.X4_3.T_10.g.i.series.time'));
tempLekageCurrenHoriz(:,2)=eval(sprintf...
    ('simlog_ssc_grounding_system.X4_3.T_10.g.i.series.values'));
tempLekageCurrenHoriz(:,3)=eval(sprintf...
    ('simlog_ssc_grounding_system.X4_4.T_10.g.i.series.values'));
tempLekageCurrenHoriz(:,4)=eval(sprintf...
    ('simlog_ssc_grounding_system.X4_5.T_10.g.i.series.values'));
tempLekageCurrenHoriz(:,5)=eval(sprintf...
    ('simlog_ssc_grounding_system.X4_6.T_10.g.i.series.values'));
%%

% manualy set parameters which are dependant on simlog origin
% soil leakage Current must be loaded from simlog first. Calculation of
% electric field is made based on section 2.4.4 and eq. (2.21)
rCond=a;
Rsoil=Rsu;

tempSoilElFieldDiag(:,1)=tempLekageCurrentDiag(:,1);
tempSoilElFieldDiag(:,2)=(tempLekageCurrentDiag(:,2)/(2*pi*rCond))*Rsoil;
tempSoilElFieldDiag(:,3)=(tempLekageCurrentDiag(:,3)/(2*pi*rCond))*Rsoil;
tempSoilElFieldDiag(:,4)=(tempLekageCurrentDiag(:,4)/(2*pi*rCond))*Rsoil;
tempSoilElFieldDiag(:,5)=(tempLekageCurrentDiag(:,5)/(2*pi*rCond))*Rsoil;
%%
tempSoilElFieldHoriz(:,1)=tempLekageCurrenHoriz(:,1);
tempSoilElFieldHoriz(:,2)=(tempLekageCurrenHoriz(:,2)/(2*pi*rCond))*Rsoil;
tempSoilElFieldHoriz(:,3)=(tempLekageCurrenHoriz(:,3)/(2*pi*rCond))*Rsoil;
tempSoilElFieldHoriz(:,4)=(tempLekageCurrenHoriz(:,4)/(2*pi*rCond))*Rsoil;
tempSoilElFieldHoriz(:,5)=(tempLekageCurrenHoriz(:,5)/(2*pi*rCond))*Rsoil;

%%
subplot(2,1,1)
p2=plot(tempSoilElFieldDiag(:,1)*1e6,tempSoilElFieldDiag(:,2)/1e3,...
    tempSoilElFieldDiag(:,1)*1e6,tempSoilElFieldDiag(:,3)/1e3,...
    tempSoilElFieldDiag(:,1)*1e6,tempSoilElFieldDiag(:,4)/1e3,...
    tempSoilElFieldDiag(:,1)*1e6,tempSoilElFieldDiag(:,5)/1e3,...
    'Color','black');
%axis to be set in the range of actual model and wanted results
axis([0 56 -200 1000])
xlabel('Time [mu s]')
ylabel('Electric Field [kV/m]')
title('Diagonal electric field distrbution from center');

subplot(2,1,2)
p1=plot(tempSoilElFieldHoriz(:,1)*1e6,tempSoilElFieldHoriz(:,2)/1e3,...
    tempSoilElFieldHoriz(:,1)*1e6,tempSoilElFieldHoriz(:,3)/1e3,...
    tempSoilElFieldHoriz(:,1)*1e6,tempSoilElFieldHoriz(:,4)/1e3,...
    tempSoilElFieldHoriz(:,1)*1e6,tempSoilElFieldHoriz(:,5)/1e3, 'Color','black');
%axis to be set in the range of actual model and wanted results
axis([0 56 -200 1000])
xlabel('Time [mu s]')
ylabel('Electric Field [kV/m]')
title('Horizontal electric field distrbution from center');
```

D.5.7 Integrated: Electric Field Distribution (3D)

```
% Updated 02.05
%
% From simulation for both Isolated and EMTP-RV model files. Definition of
% plot is generic and will fit all models.
%
% Simulation must be loaded, for the spesific grounding grid, infront
% of nodal data extraction from loaded simlog.
% Preconditions:
% 1. Definition of current grounding grid physical properties according
%       chapter D for selected model
% 2. Define distribution sample according to
%       section D.3.1
% 3. Generate plot memory by running function
%       - section D.3.3
%       - section D.3.4
%%
% Limitiation of FMI interface are that simulation log
% needs to be manualy stored by command:
% "simscape.logging.export(simlog_ssc_grounding_system...
%    ,'local path on disk.h5')"
% And loaded to Matlab for pre-prosessing by command
% simlog_ssc_grounding_system=simscape.logging.import...
%   (simlog_ssc_grounding_system,'local path on disk.h5')"
%%
% Simulationlog in isolated mode can be imported directly or file
% use of current simulation in Matlab Simulink
%
%
%%
% Used to produce figs. 4.28b and 4.29b
%
%%
% Leakage current distribution

h4 = figure();
%subplot(3,2,1)
p3=stem3(plotMSoilElField(:,1),plotMSoilElField(:,2),...
    plotMSoilElField(:,3)/1e3,'.','fill','black');
set(gca,'FontSize',20)
xlabel('Grid x-direction [m]')
ylabel('Grid y-direction [m]')
zlabel('Electric field [kV/m]')
title('Soil electric field distribution')
tickValues = min(plotMSoilElField(:,1)):10:max(plotMSoilElField(:,1));
set(gca,'XTick',tickValues)
tickValues = min(plotMSoilElField(:,2)):10:max(plotMSoilElField(:,2));
set(gca,'YTick',tickValues)
tickValues = 0:200:1000;
set(gca,'ZTick',tickValues)
zlim([0 1000])
```

E Matlab®/Simulink® FMU Interface

Interfaced signals which are defined after section 3.3.1 and table 3.5 for Matlab®/Simulink® as FMU.

The signal interface is preferably viewed on screen or printed with colors.

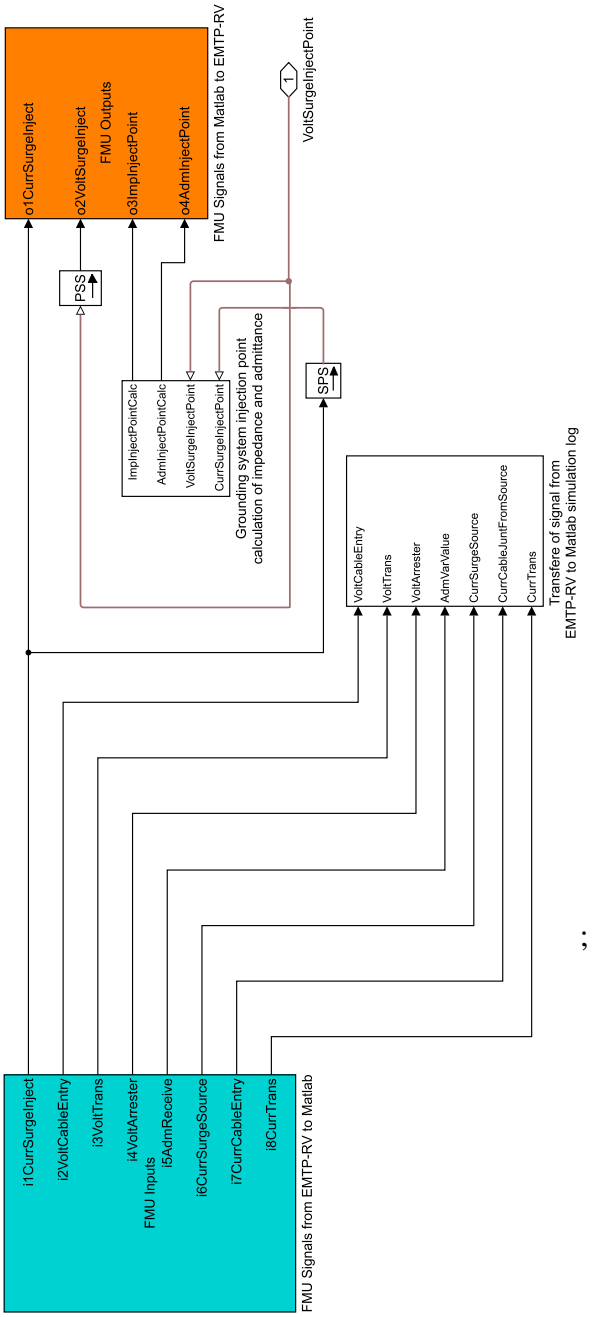

;

F EMTP-RV Models with FMI

The following Powersys EMTP-RV models are given for two cable lengths between the transformer and surge arrester, the short cable case in section 4.4 and the long cable case in section 4.5.

Several integrated models were developed based on these two models while changing the FMI-block to correspond the different grounding grid models (FMU-export) used in simulations.

F.1 Short Cable Between Switchyard and Transformer

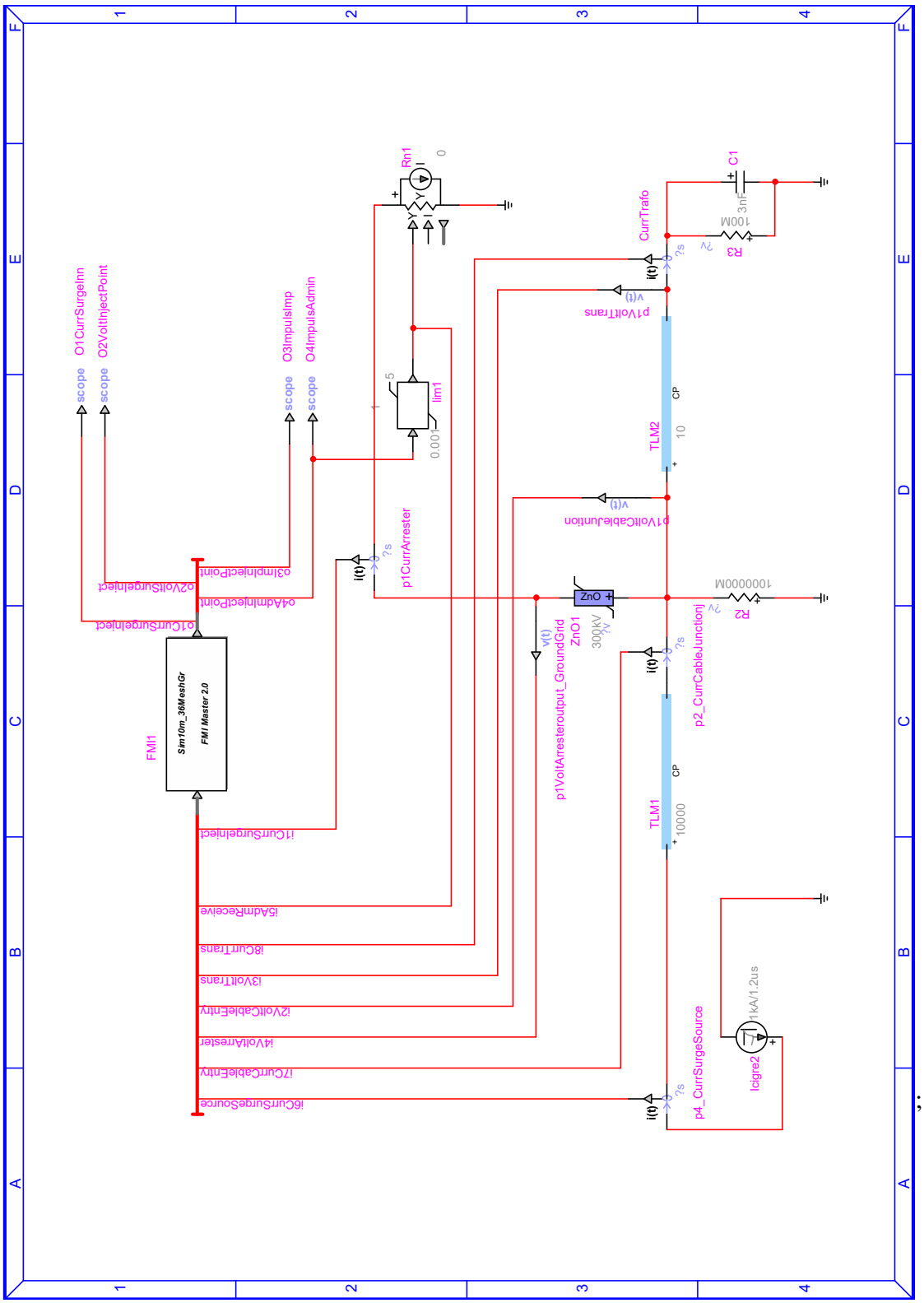

F.2 Long Cable Between Switchyard and Transformer

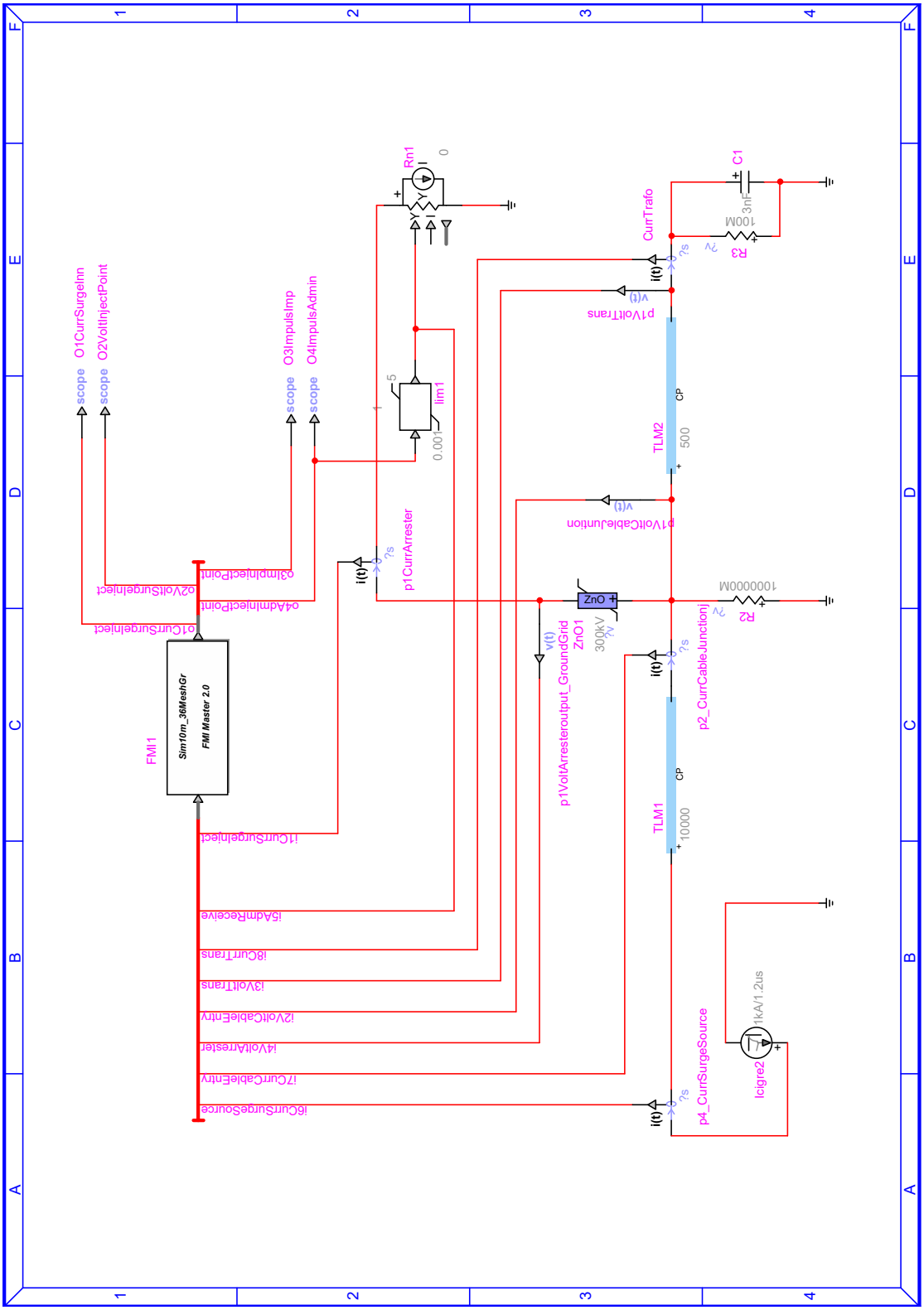

G Computer and Software Specifications

G.1 Computer Hardware and OS

All simulations were performed on a standard consumer laptop computer with Intel Core I7-2640M (dual-core, 2.70GHz, 4MB Cache) CPU and 8 GB (1333 MHz) RAM. The Matlab®/Simulink® grounding grid models was developed and tested on 64-bit systems of both Microsoft Windows 10 Pro version 1709 and Canonical Ubuntu 16.04.03 LTS. In co-simulation (Matlab®/Simulink® and EMTP-RV) Windows 10 Pro were used due to software support limitations of Powersys EMTP-RV.

G.2 Software

G.2.1 Matlab®/Simulink®

Windows version

- MathWorks Matlab® version 9.3, R2017b, 64-bit (September 14, 2017)
- MathWorks Simulink® version 9.0, R2017b, 64-bit (July 24, 2017)
- MathWorks Simscape version 4.3 (November 18, 2017)

G.2.2 Powersys EMTP-RV

- Powersys EMTP-RV 3.5 32-bit (January 17, 2017)
- Powersys FMI Add-On for Matlab®/Simulink® (March 15, 2018)

H Substation Arrangement Drawings

The refereed schematics is attached for a detailed review of a typical hydropower outdoor switchyard. Same facility is used for the picture in section 1.1 and fig. 1.3 and the highlighted extraction in the EMI discussion in section 5.3.4 and fig. 5.7.

Due to confidentiality restrictions described in section 1.4, the schematics is modified to hide plant-specific sensitive information (black areas).

The schematics are preferably viewed on screen or printed on minimum paper size A3.

H.1 Layout

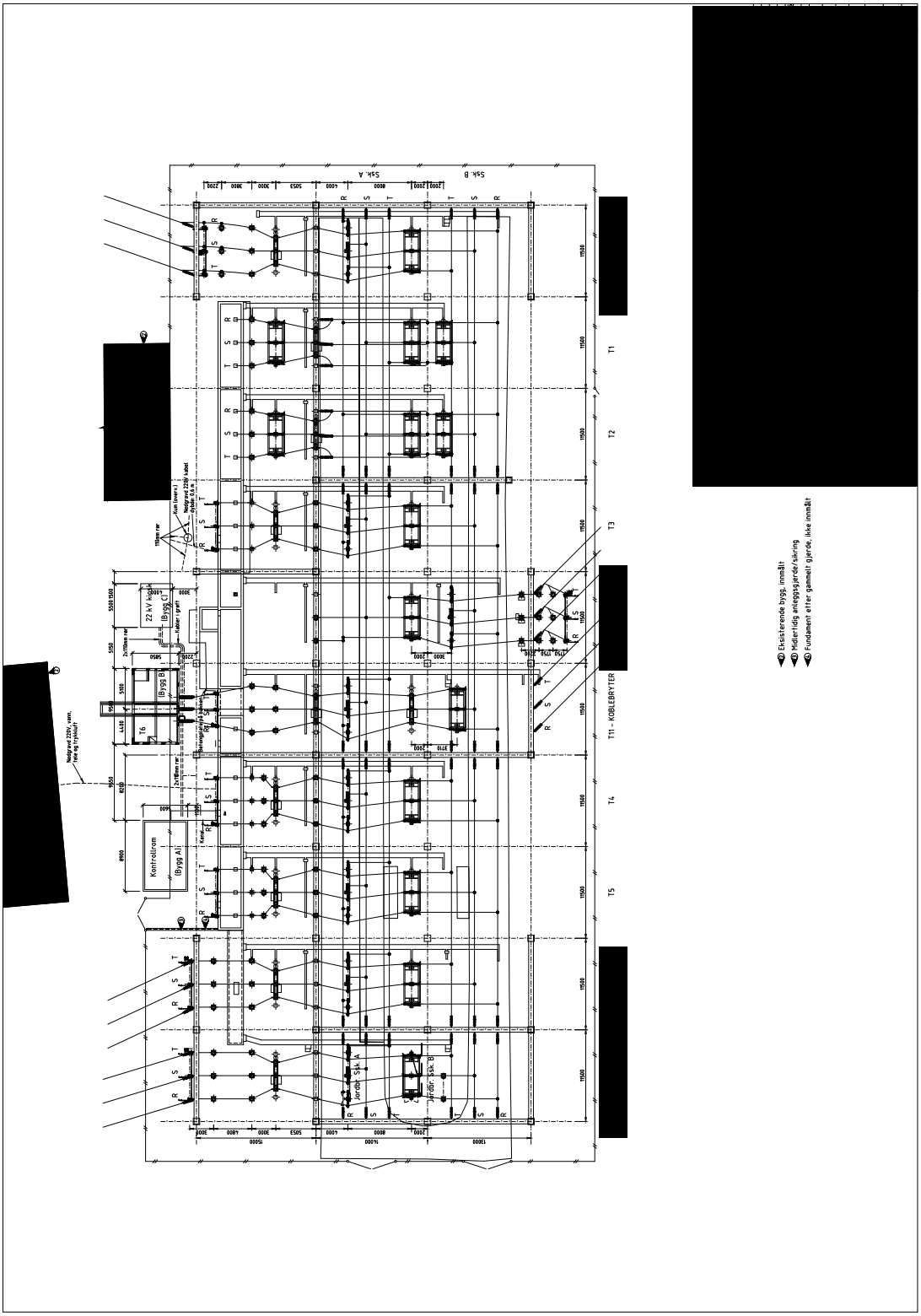
Snitt A
Snitt B
T1
T2
T3
T4
T5
T11 - KOBLEBRYTER
Bygg B
Bygg C
Kontrollrom
(Bygg A)
Nordre Sikt A
Nordre Sikt B
Eksisterende bygg, innmålt
Midlertidig anleggsgjerde/sikring
Fundament etter gammelt gjerde, ikke innmålt

H.2 Feeder

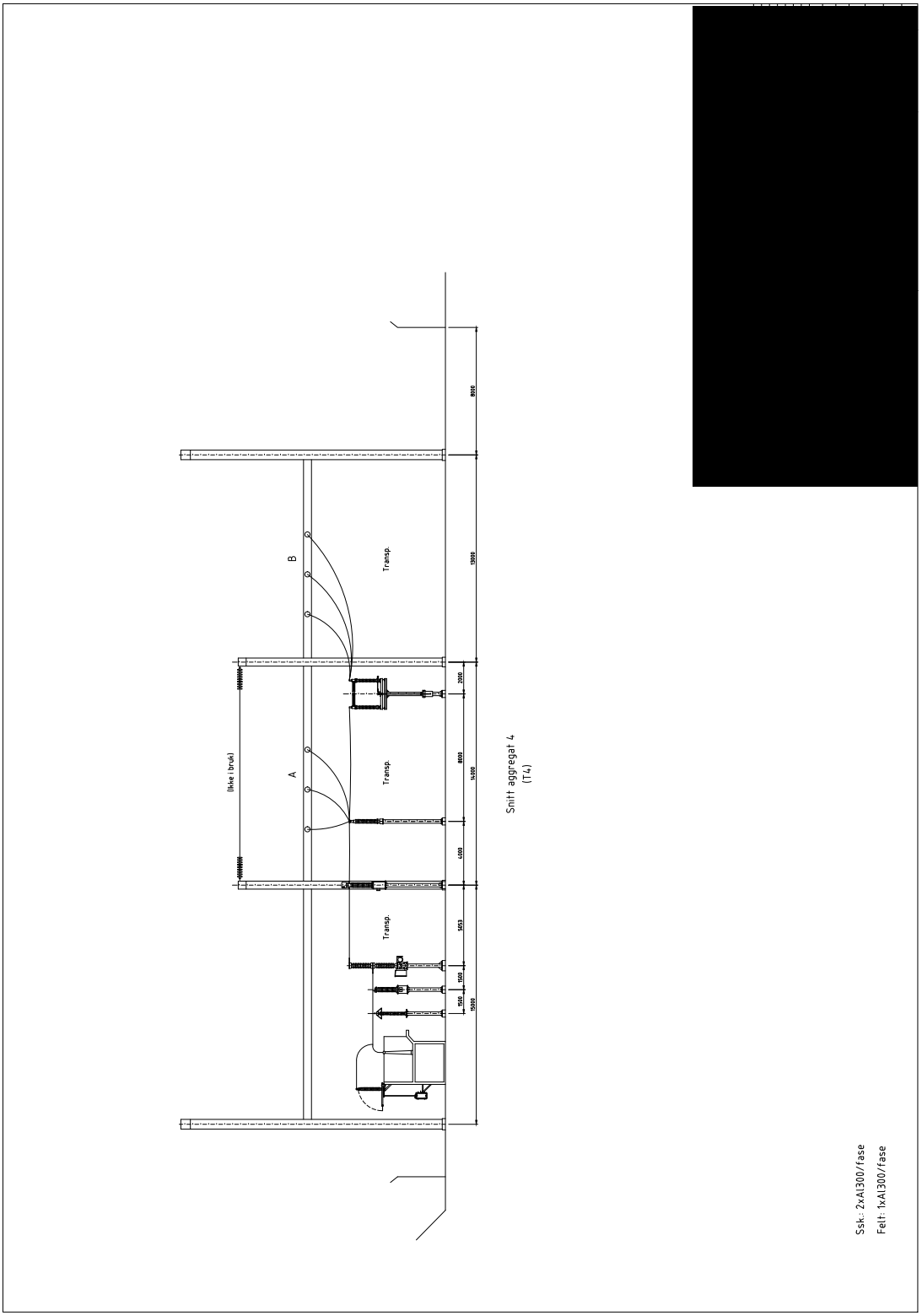
B
Transp.
A
Transp.
Transp.
(ikke i bruk)
Snitt aggregat 4
(T4)
Ssk: 2xAl300/fase
Felt: 1xAl300/fase